

**DESIGN AND DEVELOPMENT OF A HYPHENATED  
TECHNIQUE FOR MONITORING THE CURE OF  
EPOXY-AMINE RESIN SYSTEMS**

DEE HARRIS (BSc MRes)

A thesis submitted to the  
University of Birmingham  
for the degree of  
DOCTOR OF PHILOSOPHY



School of Metallurgy and Materials  
College of Engineering and Physical Sciences  
University of Birmingham  
April 2011

UNIVERSITY OF  
BIRMINGHAM

**University of Birmingham Research Archive**

**e-theses repository**

This unpublished thesis/dissertation is copyright of the author and/or third parties. The intellectual property rights of the author or third parties in respect of this work are as defined by The Copyright Designs and Patents Act 1988 or as modified by any successor legislation.

Any use made of information contained in this thesis/dissertation must be in accordance with that legislation and must be properly acknowledged. Further distribution or reproduction in any format is prohibited without the permission of the copyright holder.

## ABSTRACT

Previous researchers have demonstrated the use of optical fibre sensors for cure monitoring of thermosetting resin systems. The main parameters which have been investigated include: (i) refractive index; (ii) cross-linking kinetics; (iii) strain; and (iv) temperature. However, the majority of these studies have involved single parameter-based experiments. Therefore, the cross-correlation of the data obtained on different parameters is difficult. The main reasons for this are: (i) the heating rates and thermal gradients within the different reaction vessels are variable; (ii) the substrate containing the resin can be dissimilar; and (iii) the experiments are conducted using individual samples and therefore the stoichiometry and homogeneity may not be the same.

The ability to monitor the curing of thermosetting resins using multiple sensors in one environment will alleviate some of the above-mentioned concerns. The main focus of the current study was to design, construct and evaluate a common platform to enable the integration of multiple sensing systems. In the current study, an Abbe refractometer was selected to house a custom-made cell which accommodated the following optical sensors: (i) Fresnel reflection sensor; (ii) near-infrared transmission sensor; (iii) evanescent wave sensor; and (iv) fibre Bragg grating sensor. The cell was designed such that it was also possible to simultaneously acquire conventional refractive index data during the cross-linking process. In addition, a k-type thermocouple was used in all of the experiments. Thus, the cross-correlation of data on refractive index, cross-linking kinetics, strain and temperature was facilitated.

The overall cost of the sensing system is a determining factor with regard to its implementation for routine process monitoring of thermosetting resins and composites. Of the sensors mentioned above, the Fresnel reflection sensor offers a simple and low-cost route to monitor changes in refractive index during cross-linking. If the data from the Fresnel reflection sensor can be cross-correlated to an established quantitative cure monitoring technique such as Fourier transform infrared (FTIR) spectroscopy, the cost-savings with regard to its implementation for routine monitoring can be significant.

In the current study it was found that the trends observed in the qualitative (intensity-based refractive index monitoring via the Fresnel reflection sensor) and quantitative (optical fibre-based transmission FTIR spectroscopy) approaches were similar during the cure of common thermosetting resin systems. Furthermore, for the first time, S-2 glass<sup>®</sup> fibres were used to obtain evanescent wave spectra during cross-linking, and excellent correlation was observed with the transmission FTIR spectral data. Fibre Bragg grating sensors were used to infer the magnitude of the residual fabrication strain; the shrinkage strain was also calculated at specified points during the evolution of the refractive index profile. Excellent correlation was observed between the refractive index data generated using the Abbe refractometer and Fresnel reflection sensor.

Given the good cross-correlation between the various sensing systems, it can be concluded that the low-cost Fresnel reflection sensor can be employed for routine process monitoring. This was made possible by the design and deployment of the custom-made cell which enabled the sensors to be operated under near-identical conditions.

*This thesis is dedicated to the memory of Nanny May.*

*Devoted family member, gifted cook*

*and victim of Alzheimer's Disease during the writing of this thesis.*

## **ACKNOWLEDGEMENTS**

I would like to thank my supervisor Professor Gerard Fernando for giving me the opportunity to initiate this project, and the confidence to complete it. Without his enthusiasm, kindness, knowledge, guidance and time this work would not have been possible. I owe him sincere appreciation for his optimism and for always believing in me.

I am also grateful for the advice offered by my secondary supervisor, Dr Mike Jenkins. I would like to thank Dr Liwei Wang for her guidance, particularly during the start of my research programme. Appreciation is due to my colleagues in the Sensors and Composites Group for their help and support. I am grateful for the technical support and valuable assistance offered by John Lane, Frank Biddlestone, Anne Cabezas and Warren Hay. I am very grateful for the funding and support given by the Engineering and Physical Sciences Research Council (EPSRC), and the industrial partners involved in my work.

My gratefulness extends to my two older brothers, Ross and Glen, for their limitless patience and moral support. I am thankful to all of my family and friends for their understanding.

Finally, I am indebted to my parents for their physical, emotional and financial support, but most of all for their unconditional love. I can never re-pay their dedication and the sacrifices they have made for me.

# LIST OF PUBLICATIONS

## Journal paper

1. Wang, L., Pandita, S.D., Machavaram, V. R., Malik, S., Harris, D., Fernando, G. F. “Characterisation of the cross-linking process in an E-glass fibre/epoxy composite using evanescent wave spectroscopy”, *Composites Science and Technology*, 69 (13), 2069-2074. (2009).

## Journal papers in preparation

1. Harris, D., Fernando, G. F. “The development of a hyphenated analytical technique for the measurement of refractive index, strain, temperature and cross-linking kinetics”. To be submitted to *Journal of Applied Polymer Science*.
2. Harris, D., Wang, L., Machavaram, V. R., Fernando, G. F. “Process monitoring of thermosetting resin systems using low-cost optical fibre sensor systems”. To be submitted to *Composites Part A*.
3. Machavaram, V. R., Wang, L., Harris, D., Hellmann, S., Mahendran, R. S., Biddlestone, F., Fernando, G. F. “Multiplexed Fresnel reflection sensing for monitoring cross-linking reactions”. To be submitted to *Journal of Applied Optics*.
4. Malik, S., Wang, L., Harris, D., Mahendran, R., Paget, M., Pandita, S. D., Machavaram, V. R., Ojo, S., Collins, D., Fernando, G. F. "In-situ damage detection using self-sensing composites". To be submitted to *Composites Science and Technology*.
5. Irfan, M. S., Machavaram, V. R., Pandita, S. D., Shotton-Gale, N., Mahendran, R. S., Wait, C. F., Harris, D., Paget, M. A., Fernando, G. F. “Clean wet-filament winding – Part 1: Design concept and simulations”. To be submitted to *Polymer Composites*.

## **Book Chapters**

1. Harris, D., Machavaram, V. R., Fernando, G. F. “Process monitoring and damage detection using optical fibre sensors”, Chapter 14 in Management, Recycling and Reuse of Waste Composites, 369-424. Goodship, V. (Editor). Woodhead Publishing Ltd., Cambridge, UK. (2010).
2. Shotton-Gale, N., Harris, D., Pandita, S. D., Paget, M., Allen, J. A., Fernando, G. F. “Clean and environmentally friendly wet-filament winding”, Chapter 13 in Management, Recycling and Reuse of Waste Composites, 331-368. Goodship, V. (Editor). Woodhead Publishing Ltd., Cambridge, UK. (2010).

## **Conference papers**

1. Mahendran, R., Harris, D., Wang, L., Machavaram, V. R., Chen, R., Kukureka, S. N., Fernando, G. F. “Fibre optic sensor design for chemical process and environmental monitoring”, International Conference on Smart Materials and Nanotechnology in Engineering. Proceedings of SPIE, Vol. 6423, 64232S. Harbin, China (July 2007).
2. Wang, L., Malik, S. A., Harris, D., Fernando, G. F. “Self-sensing composites: in-situ cure monitoring”, International Conference on Smart Materials and Nanotechnology in Engineering. Proceedings of SPIE, Vol. 6423, 64231F. Harbin, China. (July 2007).
3. Wang, L., Malik, S. A., Pandita, S. D., Harris, D., Fernando, G. F. “Self-sensing composites: cure monitoring”, 9<sup>th</sup> International Conference on Optical Chemical Sensors and Biosensors. Dublin, Ireland. (March/April 2008).
4. Mahendran, R. S., Machavaram, V. R., Wang, L., Burns, J. M., Harris, D., Kukureka, S. N., Fernando, G. F. “A novel multi-functional fibre optic sensor”, 16<sup>th</sup> Annual

- International Symposium Smart Structures/NDE. Proceedings of SPIE, Vol. 7293, 729204. San Diego, CA. USA. (March 2009).
5. Harris, D., Mahendran, R. S., Brooks, D., Al-Khodairi, F. A. A., Machavaram, V. R., Reynolds, P., Wang, L., Pandita, S. D., Paget, M., Wedderburn, J., Malik, S. A., Ojo, S. O., Kukureka, S. N., Fernando, G. F. "Self-sensing, self-healing and crack-arrestor composites", 16<sup>th</sup> Annual International Symposium Smart Structures/NDE. Proceedings of SPIE, Vol. 7293, 729204. San Diego, CA. USA. (March 2009).
  6. Malik, S. A., Wang, L., Mahendran, R. S., Harris, D., Ojo, S. O., Collins, D., Paget, M., Pandita, S. D., Machavaram, V. R., Fernando, G. F. "In-situ damage detection using self-sensing composites", 16<sup>th</sup> Annual International Symposium Smart Structures/NDE. Proceedings of SPIE, Vol. 7292, 729204. San Diego, CA. USA. (March 2009).
  7. Malik, S. A., Mahendran, R. S., Harris, D., Paget, M., Pandita, S. D., Machavaram, V. R., Collins, D., Burns, J. M., Wang, L., Fernando, G. F. "Finite element modelling of fibre Bragg grating sensors and experimental validation", 16<sup>th</sup> Annual International Symposium Smart Structures/NDE. Proceedings of SPIE, Vol. 7292, 72921V. San Diego, CA. USA. (March 2009).
  8. Wang, L., Machavaram, V. R., Mahendran, R. S., Harris, D., Pandita, S. D., Tomlin, A., Redmore, E., Malik, S. A., Fernando, G. F. "A comparison of cure monitoring techniques", 16<sup>th</sup> Annual International Symposium Smart Structures/NDE. Proceedings of SPIE, Vol. 7292, 729213. San Diego, CA. USA. (March 2009).
  9. Burns, J. M., Chen, R., Harris, D., Gower, M., Bryce, G., Fernando, G. F. "A fibre optic sensor for acoustic emission detection in fibre reinforced composites", International Conference on Composite Structures, ICCS, Porto, Portugal, (2009).

10. Harris, D., Fernando, G. F. "Simultaneous acquisition of data on refractive index, strain, temperature and cross-linking kinetics", International Conference on Composite Materials, ICCM-17, Edinburgh July 27-31, (2009).
11. Shotton-Gale, N., Pandita, S. D., Paget, M., Wait, C., Allen, J. A., Harris, D., Fernando, G. F. "An environmentally friendly modified wet-filament winding process", International Conference on Composite Materials, ICCM-17, Edinburgh July 27-31, (2009).
12. Malik, S., Wang, L., Harris, D., Paget, M., Pandita, S. D., Ojo, S., Collins, D., Fernando, G. F. "In-situ damage detection in glass fibre composites", International Conference on Composite Materials, ICCM-17, Edinburgh July 27-31, (2009).
13. Harris, D., Wang, L., Machavaram, V. R., Fernando, G. F. "Process monitoring of thermosetting resins using low-cost optical fibre sensor systems", Composites CRC Conference, Adelaide, Australia. April 2010.
14. Harris, D., Rowbotham, L., Wang, L., Machavaram, V. R., Fernando, G. F. "Self-sensing composites", Composites CRC Conference, Adelaide, Australia. April 2010.

# TABLE OF CONTENTS

<b>1. INTRODUCTION</b> .....	<b>- 1 -</b>
1.1. AIMS OF THIS STUDY.....	- 4 -
1.2. STRUCTURE OF THIS THESIS .....	- 5 -
<b>2. LITERATURE REVIEW</b> .....	<b>- 6 -</b>
2.1. RESINS .....	- 6 -
2.1.1. Epoxy resins .....	- 6 -
2.1.2. Curing of epoxy resins.....	- 7 -
2.2. OPTICAL FIBRES.....	- 11 -
2.2.1. Silica-based optical fibres .....	- 11 -
2.2.2. Light propagation.....	- 14 -
2.2.3. Light attenuation .....	- 16 -
2.2.4. Evanescent waves.....	- 18 -
2.3. PROCESS MONITORING .....	- 20 -
2.3.1. Conventional methods of process monitoring.....	- 22 -
2.3.1.1. Infrared spectroscopy .....	- 22 -
2.3.2. Optical fibre-based methods of process monitoring.....	- 26 -
2.3.2.1. Optical fibre-based infrared spectroscopy .....	- 27 -
2.3.2.2. Optical fibre-based evanescent wave spectroscopy.....	- 33 -
2.3.2.2.1. Reinforcing fibre-based evanescent wave spectroscopy .....	- 35 -
2.3.2.3. Optical fibre-based refractive index monitoring .....	- 38 -
2.3.2.4. Optical fibre-based strain monitoring.....	- 43 -

2.3.3. Cure monitoring using an Abbe refractometer .....	- 48 -
2.3.4. Hyphenated cure monitoring techniques .....	- 49 -
<b>3. EXPERIMENTAL PROCEDURES.....</b>	<b>- 56 -</b>
3.1. MATERIALS .....	- 56 -
3.1.1. Resin systems .....	- 56 -
3.1.2. Optical fibres and associated equipment.....	- 58 -
3.1.3. Reinforcing fibres .....	- 60 -
3.1.4. Chemicals .....	- 60 -
3.1.5. Potting and sealing media .....	- 61 -
3.2. EXPERIMENTAL PROCEDURES .....	- 62 -
3.2.1. Thermocouple .....	- 62 -
3.2.2. Abbe refractometer .....	- 62 -
3.2.2.1. Refractive index measurement of liquid samples.....	- 65 -
3.2.2.2. Refractive index measurement of solid samples .....	- 65 -
3.2.3. Cuvette-based experiments.....	- 66 -
3.2.4. Optical fibre sensor fabrication and interrogation .....	- 68 -
3.2.4.1. Fresnel reflection sensor.....	- 68 -
3.2.4.1.1. <i>Stability of the light source</i> .....	- 71 -
3.2.4.1.2. <i>Temperature stability</i> .....	- 71 -
3.2.4.1.3. <i>Cure monitoring using a Fresnel reflection sensor</i> .....	- 72 -
3.2.4.1.4. <i>Feasibility studies using the Fresnel reflection sensor</i> .....	- 74 -
3.2.4.2. Near-infrared transmission sensor.....	- 74 -
3.2.4.3. Fibre Bragg grating sensor .....	- 77 -
3.2.5. Conventional transmission FTIR spectroscopy .....	- 78 -

<b>3.2.6. Evanescent wave spectroscopy .....</b>	<b>- 79 -</b>
3.2.6.1. Sample preparation .....	- 79 -
3.2.6.2. Light transmission .....	- 80 -
3.2.6.3. Temperature-control .....	- 81 -
3.2.6.4. Cure monitoring using evanescent wave spectroscopy .....	- 83 -
<b>3.2.7. Hyphenated techniques for monitoring cross-linking reactions .....</b>	<b>- 83 -</b>
3.2.7.1. Integration of the Fresnel reflection sensor on the Abbe refractometer .....	- 87 -
3.2.7.2. Hyphenated cure monitoring on the Abbe refractometer .....	- 88 -
3.2.7.3. Hyphenated cure monitoring on the Abbe refractometer including a fibre bundle .....	- 89 -
<b>4. RESULTS AND DISCUSSION .....</b>	<b>- 97 -</b>
4.1. ABBE REFRACTOMETER .....	- 97 -
<b>4.1.1. Refractive index measurements of liquid samples .....</b>	<b>- 97 -</b>
<b>4.1.2. Refractive index measurement of solid samples .....</b>	<b>- 103 -</b>
4.2. OPTICAL FIBRE SENSORS .....	- 105 -
<b>4.2.1. Fresnel reflection sensor .....</b>	<b>- 105 -</b>
4.2.1.1. Stability of the light source.....	- 105 -
4.2.1.2. Temperature stability.....	- 108 -
4.2.1.3. Cure monitoring using a Fresnel reflection sensor.....	- 110 -
4.2.1.3.1. <i>Sensor location and bonding conditions</i> .....	- 119 -
4.2.1.3.2. <i>Mechanically-induced vibrations</i> .....	- 120 -
4.2.1.3.3. <i>Instrumentation factors</i> .....	- 121 -
4.2.1.4. Feasibility studies using the Fresnel reflection sensor .....	- 121 -
<b>4.2.2. Transmission sensor .....</b>	<b>- 123 -</b>

4.3.	EVANESCENT WAVE SPECTROSCOPY .....	- 130 -
4.3.1.	Sample preparation .....	- 131 -
4.3.2.	Light transmission .....	- 132 -
4.3.3.	Temperature-control .....	- 134 -
4.3.4.	Cure monitoring using evanescent wave spectroscopy .....	- 137 -
4.4.	HYPHENATED TECHNIQUES FOR MONITORING CROSS- LINKING REACTIONS .....	- 142 -
4.4.1.	Heating rates associated with different experimental platforms .....	- 142 -
4.4.2.	Integration of the Fresnel reflection sensor on the Abbe refractometer ..	- 143 -
4.4.3.	Integration of a resin containment cell on the Abbe refractometer.....	- 145 -
4.4.3.1.	Temperature-control within the custom-made cell.....	- 146 -
4.4.4.	Hyphenated cure monitoring on the Abbe refractometer .....	- 148 -
4.4.5.	Hyphenated cure monitoring on the Abbe refractometer including a fibre bundle .....	- 153 -
4.4.5.1.	Evanescent wave and transmission sensors.....	- 154 -
4.4.5.2.	Fresnel reflection sensor and Abbe refractometer.....	- 157 -
4.4.5.3.	Fibre Bragg grating sensor .....	- 160 -
4.4.6.	Evaluation of the interference between sensors.....	- 165 -
5.	CONCLUSIONS.....	- 167 -
6.	RECOMMENDATIONS FOR FURTHER WORK.....	- 175 -
6.1.	ABBE REFRACTOMETER.....	- 175 -
6.1.1.	The deployment of a digital refractometer.....	- 175 -
6.1.2.	Resin film casting methods .....	- 175 -

6.2.	FRESNEL REFLECTION SENSOR.....	- 176 -
6.2.1.	Quality control.....	- 176 -
6.2.2.	Equipment.....	- 176 -
6.2.3.	Temperature .....	- 176 -
6.2.4.	Multiplexing the Fresnel reflection sensor .....	- 176 -
6.2.5.	Translation of Fresnel reflection data to refractive index values .....	- 177 -
6.3.	TRANSMISSION SENSOR .....	- 178 -
6.3.1.	Fabrication method .....	- 178 -
6.4.	EVANESCENT WAVE SPECTROSCOPY .....	- 178 -
6.4.1.	Resin system .....	- 178 -
6.4.2.	Cut-off wavelength .....	- 179 -
6.5.	HYPHENATED CONFIGURATION .....	- 179 -
6.5.1.	Instrumentation .....	- 179 -
6.5.2.	Accommodation of the fibre bundle .....	- 179 -
7.	REFERENCES .....	- 180 -
	APPENDIX A.....	- 197 -
	APPENDIX B.....	- 199 -
	APPENDIX C.....	- 205 -
	APPENDIX D.....	- 207 -
	APPENDIX E.....	- 209 -
	APPENDIX F.....	- 212 -

## LIST OF FIGURES

Figure 2-1. Structure of an epoxide group.....	- 6 -
Figure 2-2. The chemical structure of epoxy-based resin diglycidyl ether of bisphenol-A (DGEBA).....	- 8 -
Figure 2-3. The chemical structure of epoxy-based resin diglycidyl ether of bisphenol-F (DGEBF) .....	- 8 -
Figure 2-4. The chemical structure of polyoxypropylene diamine .....	- 9 -
Figure 2-5. Generalised reaction schemes illustrating: (a) the reaction between a primary amine and an epoxy group; (b) the reaction between the secondary amine and another epoxy group; (c) the etherification reaction involving the hydroxyl group (by-product of the epoxy ring-opening reaction) and an epoxy group; and (d) homopolymerisation involving multiple epoxy functional groups .....	- 10 -
Figure 2-6. Schematic illustrations of (a) total internal reflection ( $\theta_i$ ) and the critical angle ( $\theta_c$ ), and (b) Snell's Law .....	- 15 -
Figure 2-7. A schematic illustration of the evanescent wave in an optical fibre....	- 19 -
Figure 2-8. Optical fibre sensor designs for transmission spectroscopy: (a) fibres in a capillary; (b) fibres in an abraded capillary; (c) fibres aligned on a pre-cured epoxy V-groove; and (d) a fibre embedded in resin.....	- 30 -
Figure 3-1. A photograph of an Abbe 60 refractometer. ....	- 63 -
Figure 3-2. A schematic diagram of the upper and lower prisms of the Abbe refractometer, showing the path of the light beam when operated in transmission or reflection mode.....	- 64 -
Figure 3-3. An illustration of a de-mountable cuvette, with a 1 mm path-length ..	- 66 -

Figure 3-4. A schematic illustration of the temperature-controlled cuvette holder which was used to house the cuvettes ..... - 68 -

Figure 3-5. Micrographs of the stripped and cleaved end-face of a multi-mode optical fibre, showing (a) the side-view and (b) the end-on view ..... - 69 -

Figure 3-6. A schematic diagram of a typical configuration of a Fresnel reflection sensor and its interrogation system..... - 70 -

Figure 3-7. A schematic (master) diagram to show the arrangement of a thermocouple and Fresnel reflection sensor in a de-mountable cuvette..... - 72 -

Figure 3-8. An illustration of the transmission sensor. The insert shows a magnified view of the sensing region ..... - 75 -

Figure 3-9. A schematic diagram of a de-mountable cuvette containing a transmission sensor and a thermocouple ..... - 77 -

Figure 3-10. An illustration of the Bragg grating inscribed on the core of an optical fibre (FBG sensor) ..... - 78 -

Figure 3-11. A photograph of a 150 mm S-2 glass<sup>®</sup> fibre bundle, terminated with SMA connectors ..... - 80 -

Figure 3-12. Illustrations of (a) the two-part heating block, also showing the aluminium platform; and (b) the aluminium platform for the fibre bundle..... - 82 -

Figure 3-13. A schematic illustration of the custom-made cell used on the Abbe refractometer for the hyphenated experiments. The cell contains the three optical fibre sensor configurations shown in the expanded views: (a) transmission sensor, (b) Fresnel reflection sensor, and (c) FBG sensor. (d) represents the S-glass fibre bundle which was used for evanescent wave spectroscopy ..... - 85 -

Figure 3-14. An overview of the experimental set-up for the hyphenated experiments which were based on the Abbe refractometer. The equipment used for interrogating each of the sensors is also indicated ..... - 86 -

Figure 3-15. An image of the adaption to the refractometer hinge to allow accommodation of the custom-made cell ..... - 86 -

Figure 3-16. A schematic diagram showing the set-up used to establish the effect on the refractive index measurement of optical fibres infringing on the refractometer measurement prism..... - 88 -

Figure 3-17. A schematic illustration of the custom-made cell housing Fresnel reflection and transmission sensors, and thermocouple on the Abbe refractometer - 89 -

Figure 3-18. Part-coverage of the refractometer prism using high-temperature tape to simulate part-coverage by a fibre bundle on: (a) one length of the prism and (b) the perimeter of the prism..... - 90 -

Figure 3-19. A schematic illustration of a custom-made cell housing a Fresnel reflection sensor, a transmission sensor, an FBG sensor, a fibre bundle and a thermocouple on the Abbe refractometer. The expanded view shows the relative locations of the sensing regions of the optical fibre sensors ..... - 91 -

Figure 3-20. Schematic illustrations of two of the modifications made to the hyphenated technique in order to accommodate the fibre bundle, showing (a) custom-made cell adhered to a sacrificial slide and (b) custom-made metal fixture ..... - 93 -

Figure 3-21. A (a) schematic illustration and (b) photograph of a custom-made cell containing seven thermocouples to monitor temperature variations within the cell - 94 -

Figure 4-1. Refractive indices of reference oils, as given by the manufacturer and as measured on the Abbe refractometer..... - 99 -

Figure 4-2. Temperature data for the isothermal-hold periods from the refractometer and thermocouple as a function of the water bath set-temperature, during a temperature ramp-hold experiment using CVC 4 silicone oil..... - 101 -

Figure 4-3. Refractive index values measured during the temperature ramp-hold of (a) CVC 4 silicone oil and (b) reference oil 1.56..... - 102 -

Figure 4-4. Refractive indices of (a) LY3505/XB3403 and (b) EpoTek® 310M in liquid-state with increasing temperature ..... - 103 -

Figure 4-5. The transmitted optical power as a function of time, through a multi-mode optical fibre when it was connected between a light source and power meter..... - 106 -

Figure 4-6. Average values calculated from data obtained in three separate experiments on (a) the transmitted optical power, (b) the normalised Fresnel reflection, and (c) the temperature, using reference oil 1.46 ..... - 107 -

Figure 4-7. Data obtained using a thermocouple and single-mode Fresnel reflection sensor immersed in reference oil 1.57 and held at 30 °C ..... - 108 -

Figure 4-8. Temperature and Fresnel reflection data obtained during a temperature ramp-hold experiment using reference oil 1.57, where (a) shows the datasets for the duration of the experiment, and (b) shows the average values during the isothermal-hold at each temperature..... - 109 -

Figure 4-9. Fresnel reflection data during the cross-linking of LY3505/XB3403 at (a) 60 and (b) 70 °C, obtained using single- and multi-mode optical fibre sensors ... - 110 -

Figure 4-10. The response of multi-mode Fresnel reflection sensors and thermocouples during the cure process of LY3505/XB3403 at 70 °C. (a) and (b) are examples of the sensor being prone to perturbations ..... - 111 -

Figure 4-11. Typical data obtained using a Fresnel reflection sensor and thermocouple during the cross-linking of LY3505/XB3403 resin system at 50 °C..... - 113 -

Figure 4-12. Fresnel reflection data for the cure of LY3505/XB3403 resin system at 50, 60 and 70 °C, normalised: (a) to the signal at 30°C and (b) to the minimum value during heating. The inserts show the magnitude of the decrease in Fresnel reflection. Graph (c) is identical to graph (b) but the slopes are displayed ..... - 114 -

Figure 4-13. Fresnel reflection data of LY3505/XB3403 resin system for (a) three cure experiments at 50 °C, and (b) four cure experiments at 60 °C, where two pairs of experiments (1 and 2) were carried out 12 months apart ..... - 118 -

Figure 4-14. Fresnel reflection data obtained by previous researchers at 40, 50, 60 and 70 °C, where (a) shows kinks in the datasets, and (b) shows the time that the kinks appear as a function of processing temperature..... - 119 -

Figure 4-15. Fresnel reflection data obtained (a) during cure of the LY3505/XB3403 resin system at 70 °C by previous researchers and the current author, and (b) in air whilst vibrations were mechanically-induced on six separate occasions ..... - 120 -

Figure 4-16. Conventional transmission spectra of EpoTek<sup>®</sup> 310M part A (epoxy resin) and part B (amine hardener) ..... - 124 -

Figure 4-17. Typical spectra of LY3505/XB3403 resin system, obtained using conventional FTIR spectroscopy (a) at 30 °C (start of reaction) and towards the end of cure at 70 °C, and (b) the evolution of spectra of the epoxy peak at 4532 cm<sup>-1</sup> from the start to the “end” of cure..... - 126 -

Figure 4-18. Transmission sensor data showing the peak area values of epoxy, amine and C-H during the cure of LY3505/XB3403 resin system at 70 °C..... - 127 -

Figure 4-19. Comparison of the conversion data of (a) epoxy and (b) amine, during the cure of LY3505/XB3403 resin system at 70 °C, obtained using the transmission sensor and conventional FTIR spectroscopy ..... - 128 -

Figure 4-20. Comparison of the conversion data of (a) epoxy and (b) amine, during the cure of EpoTek 310M<sup>®</sup> resin system at 65 °C, obtained using the transmission sensor and conventional FTIR spectroscopy ..... - 129 -

Figure 4-21. SEM images of S-2<sup>®</sup> glass 758 fibres: (a) in the as-received state, and (b) after heat-treatment at 500 °C for 4 hours ..... - 131 -

Figure 4-22. Temperature data obtained from the centre of the temperature-regulated heating block using a thermocouple during a temperature ramp-hold experiment - 135 -

Figure 4-23. Temperature data obtained during a temperature ramp-hold experiment using five thermocouples along the length of the two-part heating block ..... - 136 -

Figure 4-24. Typical evanescent wave spectra obtained during the cross-linking of EpoTek<sup>®</sup> 310M at 65 °C..... - 137 -

Figure 4-25. Depletion of the amine peak area with time for data obtained via evanescent wave spectra at specified temperatures..... - 139 -

Figure 4-26. Data extracted from Figure 4-25, where (a) represents the initial rates of amine depletion as a function of processing temperature, and (b) shows the intersection points of the regression lines for the equilibrium state and initial depletion of amine, as a function of temperature ..... - 140 -

Figure 4-27. Amine conversion traces for data obtained during evanescent wave spectroscopy at 35, 45 and 65 °C ..... - 141 -

Figure 4-28. Typical temperature profiles for three different platforms ..... - 142 -

Figure 4-29. The response of a thermocouple and Fresnel reflection sensor on the Abbe refractometer when (a) the refractometer was maintained at ambient temperature and (b) during a series of temperature ramp-holds..... - 144 -

Figure 4-30. Fresnel reflection and refractive index data obtained for CVC 4 oil during the isothermal hold periods, as a function of the measured temperature... - 145 -

Figure 4-31. Measured refractive indices of five reference oils plotted against the manufacturer-stated values ..... - 146 -

Figure 4-32. Temperature data obtained using seven thermocouples located within the custom-made cell on the Abbe refractometer during temperature ramp-hold experiments, where (a) represents the un-insulated configuration, (b) represents the insulated configuration, and (c) shows the spread of the average values over the isothermal-holds for both configurations ..... - 148 -

Figure 4-33. Epoxy conversion and Fresnel reflection data which were obtained simultaneously during the cure of LY3505/XB3403 at (a) 50 °C, (b) 60 °C and (c) 70 °C in the custom-made cell..... - 149 -

Figure 4-34. Epoxy and amine conversion data obtained using the transmission sensor in the custom-made cell for LY3505/XB3403 resin system at 50, 60 and 70 °C . - 150 -

Figure 4-35. The cross-comparison of the measured refractive indices and the response of the Fresnel reflection sensor during the cross-linking of LY3505/XB3403 resin system at (a) 50 °C, (b) 60 °C and (c) 70 °C. The comparison of the measured refractive indices at the three temperatures is shown in (d) ..... - 151 -

Figure 4-36. Amine depletion data for the EpoTek<sup>®</sup> 310M resin system, obtained using an S-2 glass<sup>®</sup> fibre bundle and a transmission sensor at (a) 45 °C, (b) 55 °C, (c) 65 °C. The initial rates of amine depletion as a function of processing temperature for each sensor are shown in (d) ..... - 155 -

Figure 4-37. Epoxy and amine conversion data obtained using the transmission sensor at 45, 55 and 65 °C ..... - 157 -

Figure 4-38. The cross-comparison of the measured refractive indices and the response of the Fresnel reflection sensor during the cross-linking of EpoTek<sup>®</sup> 310M resin system at (a) 45 °C, (b) 55 °C and (c) 65 °C. The comparison of the measured refractive indices at the three temperatures is shown in (d) ..... - 158 -

Figure 4-39. The response of the FBG sensor in the hyphenated experiment carried out at 45 °C, where (a) shows refractive index data with corresponding times where FBG spectra were obtained and are shown in (b). (c) shows the Bragg peak wavelength values and temperature data as a function of time. (d) shows the epoxy conversion at 45 °C ..... - 162 -

## LIST OF TABLES

Table 2-1. Selected properties for specified optical fibres .....	- 13 -
Table 2-2. A summary of selected studies which used FBG sensors for strain monitoring of composites during processing .....	- 46 -
Table 3-1. A summary of the resin systems investigated .....	- 57 -
Table 3-2. A comparison of the properties and cost of the single-mode and multi-mode optical fibres used to construct the sensors.....	- 59 -
Table 3-3. A summary of the media used for potting and sealing.....	- 61 -
Table 3-4. Regime for switching the light sources of the FBG, Fresnel reflection and transmission sensors on/off to study the effect of the light transmitted by each sensor on the output of the FBG sensor.....	- 92 -
Table 3-5. A summary of heating methods used for the curing of resin systems ..	- 95 -
Table 3-6. A summary of sensor designs used to monitor cure of resin systems...	- 96 -
Table 4-1. The refractive index values of reference oils as stated by the manufacturer, and as measured on the Abbe refractometer at room temperature .....	- 98 -
Table 4-2. Refractive indices of liquids measured on the Abbe refractometer ....	- 100 -
Table 4-3. Refractive index values of resin films measured on the Abbe refractometer at room temperature.....	- 104 -
Table 4-4. Values for the rates of change in temperature and Fresnel reflection during cross-linking of LY3505/XB3403 resin system at 50, 60 and 70 °C .....	- 116 -
Table 4-5. Peak assignments for epoxy/amine resin systems, such as EpoTek <sup>®</sup> 310M, as shown in Figure 4-16 .....	- 124 -
Table 4-6. Specified properties for E-glass and S-2 glass <sup>®</sup> fibres.....	- 130 -

Table 4-7. Light transmission data of S-2 glass<sup>®</sup> 758 and 463 fibre bundles of 80, 100 and 150 mm length, connected between a white light source and an FTIR spectrometer..... - 132 -

Table 4-8. Refractive index data obtained for LY3505/XB3403: (i) before cure at 30 °C, (ii) after cure at 50, 60 and 70 °C, and (iii) after subsequent cooling to room temperature ..... - 152 -

Table 4-9. Refractive index data obtained: (i) before cure at 30 °C, (ii) after cure at 45, 55 and 65 °C, and (iii) after subsequent cooling to room temperature..... - 160 -

Table 4-10. Temperature and strain data obtained using the FBG sensor during cross-linking at 45, 55 and 65 °C..... - 163 -

# 1. INTRODUCTION

In industries such as automotive, aerospace and marine, where fibre-reinforced composite materials are used extensively, the processing schedules are important to ensure consistent and high-quality components. *In-situ* real-time monitoring of chemical and physical changes during the processing of reactive materials means that the parameters can be controlled by taking corrective actions without the need to examine the output. Therefore it is of importance in optimising the efficiency of processing and the quality of end-products. The use of optical fibre sensors is an established method for monitoring properties as they occur during the cross-linking process. Such sensors are particularly effective for use in relatively inaccessible areas such as dies and autoclaves, where elevated temperatures and pressures are used.

A primary issue when monitoring the cross-linking reaction is the cross-correlation of the various data from a range of technical disciplines, as the only universal feature is the material that is being monitored. Crosby *et al.* [1] reported on the comparison of an optical fibre-based evanescent wave spectroscopy technique with conventional transmission Fourier transform infrared (FTIR) spectroscopy during the processing of an epoxy resin system. It was shown that although both techniques were able to impart information on the cross-linking process, they were carried out separately and on individual samples of the resin system. This implies that the cross-correlation of the two sets of data will be difficult.

The current study involves the design and deployment of sensor systems to facilitate process monitoring of composite materials, and more specifically, focuses on developing low-cost techniques. An FTIR spectrometer enables the attainment of quantitative data, but is an

expensive piece of equipment. Therefore, in order to exploit the low-cost route, it is necessary to demonstrate cross-correlation between established and new techniques. Particular optical fibre sensing methods, such as Fresnel reflection, are considered low-cost because standard telecommunications fibres are used in conjunction with off-the-shelf light sources and detectors.

Although fibre-optic sensors have been demonstrated for process monitoring of fibre-reinforced composites, the diameter mismatch between the optical fibre and the reinforcing fibres is often cited as an issue. However, this matter tends to be industry-specific. For example, this is not a concern in the civil engineering and marine industries because the structures are typically large and the influence of the sensor on the properties of the component is not significant. In aerospace, where requirements are more stringent in terms of certification, the introduction of a foreign body may require the material to be re-certified. This can be a time-consuming and costly process. Therefore there is merit in developing an *in-situ* technique which gives the potential to study the interface between the reinforcing fibres and resin system [2] but is not considered an inclusion. “Self-sensing” is defined here as the case where the reinforcing fibres act as sensors to enable chemical process monitoring. Subsequently, the self-sensing composite can be used in-service to obtain information on the structural integrity of the composite.

An important feature when studying cross-linking kinetics is the temperature and environmental control. Thus, this becomes an obstacle in cross-correlation studies, irrespective of the monitoring technique used.

A key objective of this research programme was to design and develop a single experimental platform to study cross-linking reactions where the following sensors were integrated onto an Abbe refractometer: (i) Fresnel reflection sensor; (ii) near-infrared transmission sensor; (iii) fibre Bragg grating (FBG) sensor; (iv) thermocouple; and (v) reinforcing fibre bundle. A conventional Abbe refractometer was used to measure the refractive index of resins in liquid- and solid-states. A cell was designed, constructed and calibrated for use on the Abbe refractometer, to monitor changes in refractive index during the cross-linking process. A brief description of each sensor which was housed in the cell is given below:

- (i) A single-mode Fresnel reflection sensor was used as an optical fibre-based method to monitor refractive index changes at the interface of the cleaved fibre-end and the resin system. The calibration of the Fresnel reflection sensor was carried out in a temperature-controlled cuvette holder;
- (ii) An optical fibre near-infrared transmission sensor was used in conjunction with an FTIR spectrometer. The sensor was constructed from two multi-mode fibres with a cavity between the cleaved fibre-ends for the infiltration of resin. This enabled the acquisition of quantitative data via FTIR spectroscopy;
- (iii) A brief study was undertaken using FBG sensors, to quantify the residual fabrication strain of a resin system after cross-linking. FBG sensors were fabricated by inscribing gratings on the core of a photo-sensitive single-mode fibre;
- (iv) A k-type thermocouple was used to monitor the temperature within the custom-made cell;
- (v) The final challenge was to integrate a reinforcing fibre bundle for *in-situ* cure monitoring using evanescent wave spectroscopy. This also enables the comparison of transmission FTIR and evanescent wave spectroscopy.

This hyphenated approach enables direct cross-correlation between the refractive indices measured via the Abbe refractometer and the above-mentioned sensor systems. If the low-cost Fresnel reflection sensor is to be accepted by industry, it is essential that correlation be demonstrated with established process monitoring sensor systems such as FTIR spectroscopy. In the case of the data obtained using the transmission and evanescent sensors, it is desirable to investigate this area, as the bulk reactions (as inferred by transmission FTIR spectroscopy) may not necessarily mirror the interface-based reactions (obtained using evanescent wave spectroscopy). The FBG sensor offers a route to monitor the temperature and evolution of strain during the conversion of the resin system from a liquid to a solid. Hence cross-correlation can be established between the development of strain and the change in refractive index during cross-linking.

### **1.1. AIMS OF THIS STUDY**

The aims of this research programme are as follows:

- (i) To design a single platform on an Abbe refractometer to accommodate a range of sensors (Fresnel reflection, transmission, thermocouple, evanescent wave spectroscopy via the reinforcing fibre bundle, and FBG);
- (ii) To simultaneously monitor the cross-linking process using the sensors in the custom-made cell, whilst also monitoring the refractive index on the Abbe refractometer; and
- (iii) To study the cross-linking reactions associated with an epoxy/amine resin system to enable cross-correlation between the above-mentioned techniques.

## **1.2. STRUCTURE OF THIS THESIS**

This thesis is structured in the following manner:

Chapter 2 surveys the literature in the areas of cure monitoring, with a focus on the cure monitoring of thermosetting epoxy/amine resin systems using optical fibre sensors.

Chapter 3 details the experimental aspects of the project, including descriptions of the materials and instruments used, and the procedures implemented. The individual cure monitoring methods are detailed first (Fresnel reflection, transmission FTIR spectroscopy and evanescent wave spectroscopy), leading to descriptions of the hyphenated technique in the second part of the chapter.

Chapter 4 presents the results obtained using the procedures detailed in Chapter 3, and discusses the interpretation and cross-correlation of the data generated using the individual and hyphenated cure monitoring methods.

Chapter 5 summarises the conclusions drawn from this study, and Chapter 6 details recommendations for future work in this area.

## 2. LITERATURE REVIEW

### 2.1. RESINS

There are two general classes of resin systems that are commonly used in advanced fibre-reinforced composites, namely, thermoplastics and thermosets. The key difference between the two categories is that a thermosetting material undergoes an irreversible reaction during processing, whereby it is permanently hardened due to the formation of cross-links between the monomer units. Thermoplastics, however, undergo only physical changes as cross-links are not formed during processing. Therefore the changes are reversible [3]. Examples of common thermosetting resins are epoxy and polyester resins. Polypropylene and polyethylene are examples of thermoplastics. The present study is concerned with thermosetting epoxy resins and amine hardeners, and therefore the focus of this overview will only consider this class of resin system.

#### 2.1.1. Epoxy resins

Epoxy resins are defined as molecules which contain one or more epoxide groups or oxirane rings [4]. The epoxide group is composed of a planar three-membered ring [5] as shown in Figure 2-1:

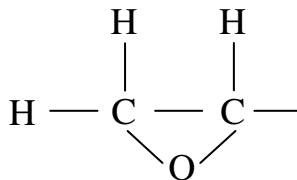


**Figure 2-1. Structure of an epoxide group.**

The chemistry of the epoxy group has been reviewed comprehensively by a number of authors [6, 7]. Such reviews contain discussions that are outside the scope of this report, but an overview of the details which are relevant to this study is presented in this chapter.

Resins with terminal epoxy groups generally have the prefix “glycidyl”. The prefix is modified by, for example, “ether”, “ester” or “amine”, according to the group attached to the third carbon atom [8]. Epoxy resins have found use in widespread applications, including adhesives, coatings, electronic applications and high-performance composites [9, 10]. They are particularly suitable as the matrix phase in fibre-reinforced composites as they produce easily-handled prepregs [11].

A combination of techniques has been used to assay, for example, the epoxy content, molecular weight and viscosity [12, 13, 14]. This topic is discussed in Section 2.3.

The following section presents an overview of the curing of epoxy resin systems.

### **2.1.2. Curing of epoxy resins**

The transformation of a resin system from a viscous liquid to a glassy solid is a result of cross-linking. As the chemical reaction progresses, there is an increase in the molecular weight, which is accompanied by an increase in the density and viscosity [8]. Eventually the system will reach gelation, whereby it is no longer able to flow easily. The formation of cross-links means that a three-dimensional network is created and therefore the material reaches vitrification, after which it becomes a rigid, glassy solid. This transformation process is known as “curing”; throughout this study, the terms “cross-linking” and “cure” are used

interchangeably to describe the process whereby a cross-linked network is developed in a material by a series of chemical reactions. The cross-linking process of epoxy-amine resin systems is described in more detail below.

The focus of this literature review is primarily, but not exclusively, upon resins based on diglycidyl ether of bisphenol-A (DGEBA). DGEBA is one of the most common commercial epoxy resins [15]. Several authors have studied the cure process of resin systems based on DGEBA using techniques such as FTIR spectroscopy [16, 17, 18] and Differential Scanning Calorimetry (DSC) [19, 20, 21, 22]. Details of the techniques used for monitoring cross-linking reactions can be found in Section 2.3. The structures of DGEBA and DGEBF epoxy resins (used in the current study) are shown in Figure 2-2 and Figure 2-3 respectively [23].

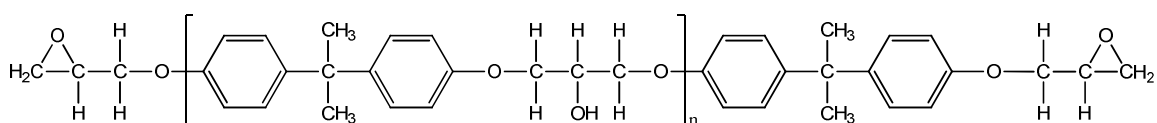


**Figure 2-2. The chemical structure of epoxy-based resin diglycidyl ether of bisphenol-A (DGEBA) [23].**

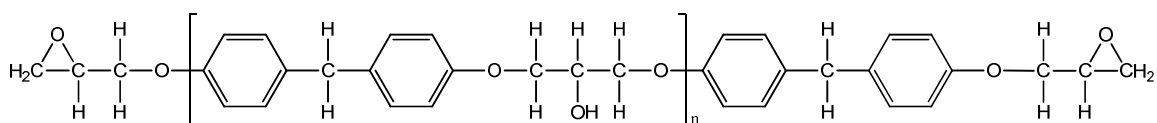


**Figure 2-3. The chemical structure of epoxy-based resin diglycidyl ether of bisphenol-F (DGEBF) [24].**

There is a wide range of curing agents which will react with epoxy resins to form cross-linked polymers. Such curing agents include aliphatic and aromatic amines, details of which can be

found in the comprehensive review by Ashcroft [25]. The structure of the amine hardener used in the current study is shown in Figure 2-4.

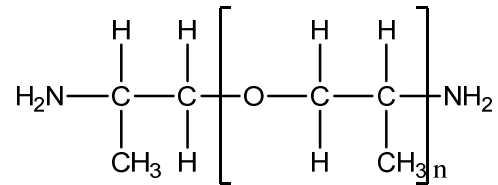
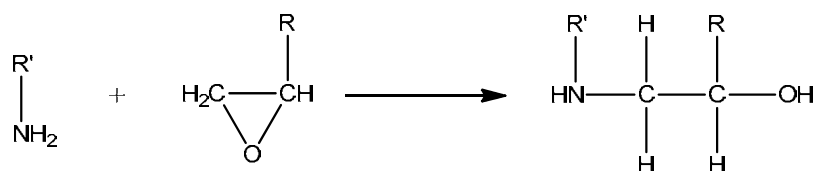


**Figure 2-4. The chemical structure of polyoxypropylene diamine [26].**

A series of generalised reaction schemes involving an epoxy resin group and amine hardener is shown in Figure 2-5 [8]. With reference to Figure 2-5a the reaction between a primary amine and an epoxy group leads to the formation of a covalent bond between the two species. The nitrogen atom on the primary amine couples to a carbon on the epoxy group. This causes the epoxy ring to open about a carbon-oxygen bond [3]. The reaction causes the conversion of the primary amine to a secondary amine, along with the formation of a new functional group, hydroxyl. This secondary amine still has a reactive hydrogen and therefore can react with another epoxy functional group to form a tertiary amine and another hydroxyl group, as in Figure 2-5b. Thus, when hardeners (amines) and resins (epoxies) with multiple functional groups are used, the above-mentioned reactions can lead to highly cross-linked structures. The molecular weight of the resin system therefore increases as the cross-linking reaction proceeds. This is accompanied by an increase in the density and refractive index of the resin system [8]. A number of side reactions can also take place, such as those illustrated in Figure 2-5c and d; under certain reaction conditions, the hydroxyl groups formed by the ring-opening addition reactions can react with epoxy groups to form ether linkages (see Figure 2-5c). However, it has been shown that this will only occur when epoxy groups are present in excess

[27, 28]. Homo-polymerisation of the epoxy functional groups is also possible under specified reaction conditions (see Figure 2-5d).

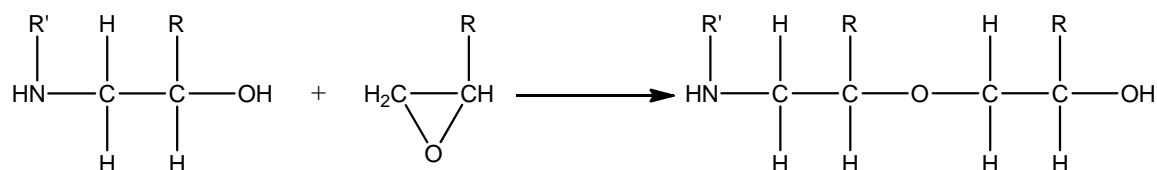
(a) Primary amine-epoxy addition:



(b) Secondary amine-epoxy addition:



(c) Hydroxyl-epoxy (etherification):



(d) Epoxy-epoxy (homopolymerisation):

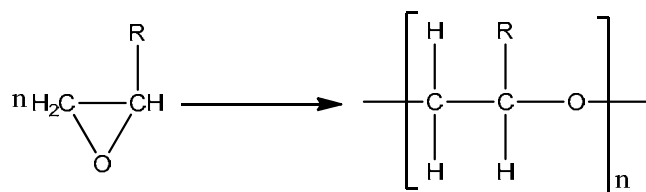


**Figure 2-5. Generalised reaction schemes illustrating: (a) the reaction between a primary amine and an epoxy group; (b) the reaction between the secondary amine and another epoxy group; (c) the etherification reaction involving the hydroxyl group (by-product of the epoxy ring-opening reaction) and an epoxy group; and (d) homopolymerisation involving two epoxy functional groups [8].**

Changes in the properties of the resin system during the cross-linking reaction can be tracked using various monitoring techniques. The following section presents a general discussion on optical fibres. Section 2.3 gives an account of conventional and optical fibre-based sensor systems for monitoring the cross-linking reaction.

## **2.2. OPTICAL FIBRES**

Optical fibres are waveguides with a cylindrical cross-section, generally made from dielectric materials. An optical fibre essentially consists of three layers – the central region, known as the core, is surrounded by a cladding, which in turn is surrounded by a protective polymeric coating. The refractive index of the core is higher than that of the cladding – the significance of this is discussed in Section 2.2.2. The refractive index ( $n$ ) of a medium is calculated by dividing the speed of light in a vacuum by the speed of light in the medium [29].

A relatively large range of optical fibres are commercially available and their applications are dictated by the material used to produce the fibres. A summary of selected optical fibre materials and their specified properties is presented in Table 2-1. Silica-based glasses and certain plastics are most commonly used, but other materials such as chalcogenide and sapphire are employed for specialised applications. The current study involves silica-based fibres, and therefore the literature review is primarily focused on this topic.

### **2.2.1. Silica-based optical fibres**

As optical fibres require a low refractive index core and a higher refractive index cladding, dopants must be added to silica to alter the refractive index. Depending on the dopant selected, typically they will increase the refractive index of the silica. Therefore they are

generally used for the fibre core, and pure silica is employed as the lower refractive index cladding. The most common core dopant is germanium [29] – it is chemically similar to silicon, has low absorption, and germania ( $\text{GeO}_2$ ), like silica, forms glass. It is not uncommon for pure silica to be used as the core material. In this case materials such as fluorine and boron are used to reduce the refractive index of the cladding. Alternatively, a pure silica core can be clad with a lower refractive index polymer [29].

Details relating to the manufacturing processes of optical fibres can be found in references [29, 30, 31].

There are two categories of optical fibre which differ in their construction and their propagation properties; single-mode and multi-mode. Single-mode fibres typically have core diameters in the range 8 to 10  $\mu\text{m}$  and a cladding diameter of 125  $\mu\text{m}$  [30]. In contrast, the core diameters of multi-mode fibres are typically between 50 and 100  $\mu\text{m}$ , with cladding diameters in the range of 125 to 140  $\mu\text{m}$  [30]; plastic optical fibres have core sizes of 120-1000  $\mu\text{m}$  [30]. In multi-mode fibres, the larger core means that light can propagate via many independent optical paths or modes. As some modes are longer than others, light comprising of several modes will ‘spread out’ as it propagates; this is known as “mode dispersion”.

<b>Property</b>	<b>Silica</b>	<b>Chalcogenide</b>	<b>Fluoride</b>	<b>Sapphire</b>	<b>Polymethyl- methacrylate (PMMA)</b>
<b>Wavelength range</b>	0.2-4 $\mu\text{m}$ 50,000-2500 $\text{cm}^{-1}$	3-10 $\mu\text{m}$ 3300-1000 $\text{cm}^{-1}$	0.5-4.3 $\mu\text{m}$ 20,000-2325 $\text{cm}^{-1}$	0.2-4 $\mu\text{m}$ 50,000-2500 $\text{cm}^{-1}$	0.4-0.8 $\mu\text{m}$ 25,000-10,000 $\text{cm}^{-1}$
<b>Attenuation</b>	0.5 dB/m @ 1500 nm	0.5 dB/m @ 6000 nm	0.02 dB/m @ 2600 nm	20 dB/m @ 3000 nm	30 dB/m @ 800 nm 0.1 dB/m @ 600 nm
<b>Refractive index (core)</b>	1.458	2.9	1.51	1.7	1.492
<b>Maximum usage temperature (<math>^{\circ}\text{C}</math>)</b>	800	300	250	>1500	80
<b>Approximate price (2009)</b>	£0.02/m	£55/m	-	£600/m	-
<b>Young's modulus (GPa)</b>	73	21	56	414	3.3
<b>Thermal expansion coefficient</b>	$0.54 \times 10^{-6} \text{ K}^{-1}$	$14 \times 10^{-6} \text{ K}^{-1}$	$18.7 \times 10^{-6} \text{ K}^{-1}$	$8.8 \times 10^{-6} \text{ K}^{-1}$	$260 \times 10^{-6} \text{ K}^{-1}$

**Table 2-1. Selected properties for specified optical fibres (data presented where available) [32].**

Multi-mode fibres can further be divided into “step-index” and “graded-index” fibres. Step-index fibres have a refractive index profile characterised by a uniform refractive index of the core and a sharp decrease in refractive index at the core/cladding interface. The change results in an abrupt internal reflection of the light rays (discussed in further detail in Section 2.2.2); for some applications this causes a distortion in the received signal because of the differences in propagation paths [33]. As a consequence graded-index fibres were introduced, where the refractive index decreases gradually over the radius of the core [34]. This causes the light rays to curve as they approach the cladding and limits their divergence. According to Gloge [33], refractive index profiles approximating a parabolic change from the core centre to the core/cladding interface reduce the dispersion by several orders of magnitude compared to the step-index profiles. In graded-index fibres, the dispersion is reduced in comparison to step-index fibres. In the current study only single-mode fibres and multi-mode step-index fibres have been employed.

### **2.2.2. Light propagation**

When an optical fibre is illuminated at its cleaved end, the light is contained within, and guided through, the core by the phenomenon of “total internal reflection” at the core/cladding interface [35]. Total internal reflection (as depicted in Figure 2-6a) refers to the case where light travelling from a medium, with a refractive index of  $n_1$ , to a different medium with refractive index  $n_2$  (where  $n_1 > n_2$ ), undergoes reflection and refraction as governed by Snell’s law (Figure 2-6b) [30]:

$$n_1 \sin \theta_i = n_2 \sin \theta_r \qquad \text{Equation 2-1}$$

where  $\theta_i$  is the angle of incidence of the light and  $\theta_r$  is the angle of refraction.

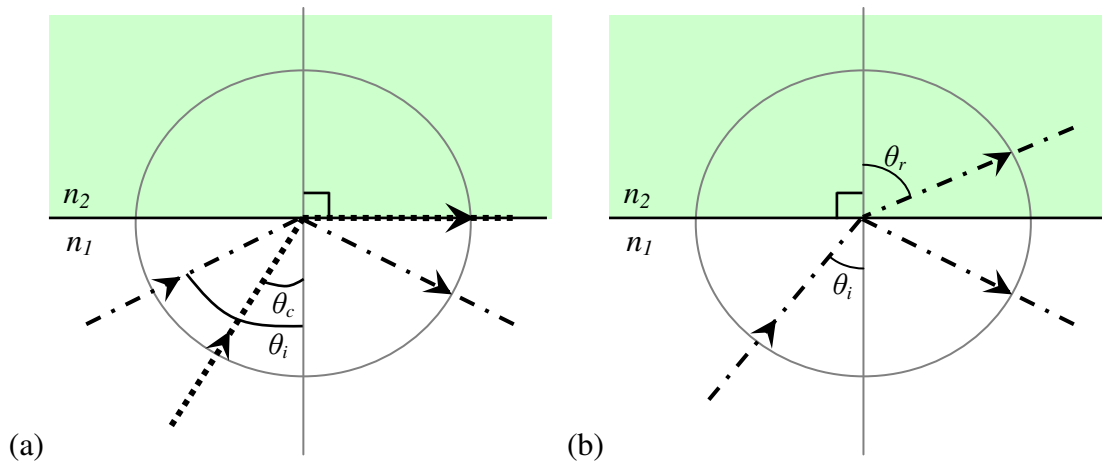


**Figure 2-6. Schematic illustrations of (a) total internal reflection ( $\theta_i$ ) and the critical angle ( $\theta_c$ ), and (b) Snell's Law [29], where  $n_1 > n_2$ .**

For a given medium, the angle of incidence for which light grazes the interface of the two media (i.e. at greater incident angles the light will be reflected) is known as the critical angle ( $\theta_c$ ). The critical angle can be calculated by [30]:

$$\sin \theta_c = \frac{n_2}{n_1} \qquad \text{Equation 2-2}$$

When  $\theta_i$  is smaller than  $\theta_c$  the light is refracted to the cladding and eventually escapes the fibre. When  $\theta_i$  is greater than  $\theta_c$  the light undergoes total internal reflection. In a fibre ( $n_1$  refers to the core and  $n_2$  is the cladding) light will be totally reflected each time it strikes the core/cladding interface and therefore will be guided along the fibre in this manner. For typical fibres used in data communication, the difference in the refractive index values between the core and cladding is stated to be 0.002-0.008 [36].

The numerical aperture (NA) of a fibre defines the acceptance angle of the fibre both above and below its axis. It refers to the maximum angle for which light impinging on the fibre end-

face can still be refracted into the fibre core and then undergo total internal reflection. It can be calculated by [23]:

$$NA = \sqrt{n_{co}^2 - n_{cl}^2} \quad \text{Equation 2-3}$$

where  $n_{co}$  and  $n_{cl}$  represent the refractive indices of the fibre core and cladding respectively. Single-mode fibres typically have a NA of approximately 0.1 and multi-mode fibres vary from 0.2-0.3 [37].

The diameter of the area in which an optical signal propagates through a single-mode fibre is known as the mode-field diameter [29]. Although a majority of the signal is confined to the core, some also travels in the cladding – this is discussed in greater detail in Section 2.2.4.

### **2.2.3. Light attenuation**

Signal strength can degrade in an optical fibre as a cumulative result of absorption, material scattering and perturbation of the optical path [29]. It therefore limits how far a signal can travel through a fibre before it becomes too weak to detect. Inefficient light coupling into the fibre-ends can also be a dominant factor in signal loss, and is commonly referred to as insertion loss. Attenuation is generally expressed as the ratio of the strength of the output signal to the input signal per unit length. It is a function of the operating wavelength, and is measured in the logarithmic unit of decibels (dB) [31]:

$$\text{Attenuation (dB)} = -10 \times \log_{10} \left( \frac{\text{power out}}{\text{power in}} \right) \quad \text{Equation 2-4}$$

With reference to Table 2-1, plastic optical fibres show a much higher loss than silica-based fibres [30] and therefore their applications are confined to shorter distance transmission.

The mechanisms that contribute to the light loss in a fibre can be categorised as either intrinsic or extrinsic [31]; absorption and scattering are considered as intrinsic losses, and perturbations of the optical path are classed as extrinsic. Intrinsic losses are those which occur within the core material, and are induced by the fundamental material properties of the fibre. Extrinsic mechanisms refer to the situation where attenuation of light occurs due to changes at the core-cladding interface, such as bending of the fibre.

Absorption losses during light propagation depend strongly on the composition of the fibre and can arise from impurities in the fibre material. The core material is composed of a variety of atomic structures; essentially the light is absorbed by specific atomic structures, which are subsequently energised and emit the energy in a different form such as heat [38]. The various atomic structures only absorb electromagnetic radiation at particular wavelengths and thus the attenuation due to absorption is wavelength-dependent.

Losses due to scattering occur when light hits the atoms and other particles in the fibre material [39]. The light is not absorbed in this instance but is re-directed; a process known as Rayleigh scattering. Scattering depends on the size of the particles relative to the wavelength of light rather than on the type of material; more scattering will occur when the wavelength and particle size are close. Optical fibres are produced using high purity materials to limit the scattering loss.

Bending the fibre changes the angle at which the light will meet the core/cladding interface; if light strikes the interface at an angle lower than the critical angle it will refract into the cladding. Bending losses can be further divided into macro- and micro-bending losses.

Macro-bends are obvious to the eye and are user-dependent [31]. They occur primarily due to handling of the fibre rather than manufacturing issues [38]. Micro-bends can take the form of ripple-like irregularities at the core/cladding boundary, caused by deformation and damage due to processing. The magnitude of these axial displacements is in the order of micrometres. In a similar manner to macro-bends, they affect the incident angle of the light.

Another light loss mechanism associated with total internal reflection is evanescent loss in the presence of an absorbing species in the cladding. Waveguide analysis has shown that the light energy in fibres is not confined completely to the core, but a fraction of the energy travels in the cladding as an evanescent wave. This phenomenon is discussed in Section 2.2.4.

#### **2.2.4. Evanescent waves**

An evanescent wave is created whenever light undergoes total internal reflection at the interface between two dielectric media [40]. In the case of optical fibres, a small percentage of the light guided within the core by total internal reflection propagates the cladding at the core/cladding interface. This evanescent wave has an exponentially decaying intensity (from the point of incidence at the interface) into the medium with lower refractive index [41]. The evanescent wave is illustrated in Figure 2-7.

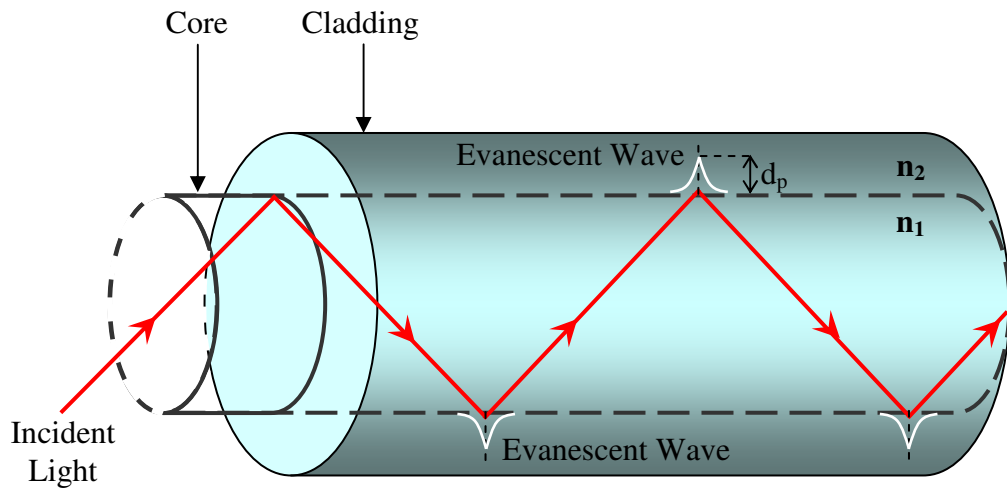


**Figure 2-7. A schematic illustration of the evanescent wave in an optical fibre ( $n_1 > n_2$ ).**

The penetration depth,  $d_p$ , of the evanescent wave is expressed as [23]:

$$d_p = \frac{\lambda}{2\pi(n_{core}^2 \sin^2 \theta - n_{cladding}^2)^{1/2}} \quad \text{Equation 2-5}$$

where  $\lambda$  and  $\theta$  are the wavelength of light and the angle of incidence at the core/cladding boundary respectively. Provided that the cladding is transparent (non-absorbing) to the guided wavelengths, the total internally reflected light does not lose its power as it travels along the length of the fibre [23]. When the cladding is not transparent to the wavelength of light, the light suffers attenuation via evanescent wave absorption as it propagates along the fibre [23].

The next section presents an overview of conventional and optical fibre-based techniques used for process monitoring.

### **2.3. PROCESS MONITORING**

Process monitoring, or cure monitoring, in the context of this thesis is a term that is used to describe techniques which are employed to facilitate the tracking of real-time changes in physical state or chemical reaction that occur during the curing process. The on-line monitoring of the cross-linking process provides information on the degree and rate of cure. The approach typically used to process resins or composites is based on the supplier's recommended schedule [42], which is generally pre-determined using off-line measurements [43]. As a result, assumptions are made about the chemical state of the material. Therefore processing conditions (temperature, time, vacuum and pressure) are fixed and allow no flexibility for factors such as batch-to-batch variation, the condition of individual samples (e.g. aging an absorbed moisture), ambient environment variations, and variable thickness across a preform. In specific end-use applications, monitoring the cure process may overcome some of these issues. This section of the literature review primarily concentrates on the range of available techniques that can be used for cure monitoring.

It is desirable to monitor the cure process to gain information on the extent and rate of reaction. This knowledge can be used to enable optimisation of the processing procedures [44, 45, 46, 47]. Cost-related benefits which stem from the ability to monitor the cure process include: (i) the reduction of power consumption due to reduced cycle times brought about by the knowledge of process completion [8]; and (ii) the potential reduction of rejection rates as wastage due to eventualities such as poor mixing, incorrect stoichiometry of the resin and hardener, and incorrect processing conditions can be avoided [48].

On examining Figure 2-5, it can be expected that several parameters will alter during the cross-linking reactions. A selection of these is listed below with brief descriptions of the reasons they are likely to change:

- (i) Refractive index – It is clear that the highly cross-linked networks which are formed as the reaction proceeds will increase the molecular weight of the resin system. This is accompanied by a concomitant increase in the density and therefore the refractive index;
- (ii) Temperature – The ring-opening addition reactions are exothermic and therefore, depending on the thermal management scheme used, a temperature rise may be detectable;
- (iii) Depletion and formation of specified functional groups – The relative concentrations of the resin and hardener will change due to their consumption during the reactions. This will be accompanied by a proportional increase in the hydroxyl concentration;
- (iv) Cure-induced strain – The formation of covalent bonds between the reagents will result in shrinkage of the resin system;
- (v) Residual fabrication strain – The differences in the thermal expansion of the fibres and the matrix will lead to the formation of residual stress when the material is cooled down to ambient from the processing temperature; and
- (vi) Other parameters such as the dielectric, acoustic and ultrasonic properties are likely to change due to the cross-linking reaction.

The chemical and physical changes in the resin system as a consequence of the cross-linking reactions can be detected using various techniques. The remainder of this chapter is divided into two parts; the first part gives an overview of conventional methods which have been

deployed for process monitoring, and the latter part introduces optical fibre-based techniques for monitoring cure.

### **2.3.1. Conventional methods of process monitoring**

Conventional methods that have commonly been used to characterise thermosetting resins include spectroscopy techniques such as infrared [17, 49, 50] and Raman [51, 52, 53], and thermal analysis techniques such as DSC [10, 54, 55], dynamic mechanical analysis (DMA) [56, 57, 58], and thermo-gravimetric analysis (TGA) [59, 60, 61].

Of these conventional techniques, this study only focussed on transmission Fourier transform near-infrared spectroscopy. The topic of infrared spectroscopy is discussed in detail below.

#### ***2.3.1.1. Infrared spectroscopy***

FTIR spectroscopy represents a desirable monitoring technique owing to the plethora of molecular-level information contained in the infrared segment of the electromagnetic spectrum [62, 63]. FTIR spectroscopy is a technique which is used to detect chemical changes in the resin system through the depletion and formation of absorbance peaks which relate to specific functional groups. It is a means of obtaining infrared spectra by first collecting an interferogram (a plot of infrared detector response as a function of optical path difference [64]) of a sample signal using an interferometer. A “Fourier transform” calculation is then performed on the interferogram by the spectrometer to convert the raw data into an infrared spectrum. The regions of the infrared spectrum can be categorised as follows [8]: (i) the far-infrared region occupies frequencies below  $650\text{ cm}^{-1}$ , (ii) the mid-infrared region spans  $650\text{-}4000\text{ cm}^{-1}$ , and (iii) frequencies from  $4000\text{-}13000\text{ cm}^{-1}$  are called near-infrared. FTIR spectroscopy is based on the vibrations of the atoms of a molecule and on the molecules

absorbing fractions of the incident infrared energy of specific frequencies which are characteristic of their structure [63]. It can provide both qualitative and quantitative information [8]; a key advantage for characterisation studies. In the context of the current research, qualitative information can identify the chemical functional groups that are present in a resin system and quantitative analysis determines the abundance of the functional groups. Cure information is typically collected *in-situ* (the spectra are collected in real-time) [16, 52, 65, 66, 67] or *ex-situ* (the resin is cured externally and samples are removed periodically for spectra to be obtained) [17, 18, 68, 69].

In a conventional FTIR spectrometer the sample is generally contained in a cuvette that is within the housing of the spectrometer. However, fibre-coupled spectrometers are also available, where the samples can be located remotely from the instrument. In this instance, optical fibre bundles (probes) are used to deliver and collect the transmitted light from the cuvette [70, 71, 72]. In this study, these configurations are defined as “conventional” techniques.

From the perspective of the present study, the principal advantages of infrared spectroscopy over the other techniques listed above are: (i) sample preparation is relatively simple, particularly for liquids where a de-mountable cell can be employed; (ii) both qualitative and quantitative information can be obtained; (iii) *in-situ* characterisation can be undertaken; and (iv) a large library of literature exists, so it can be relatively simple to interpret the spectra that are produced. It is difficult, however, to ensure efficient thermal management in conventional infrared spectroscopy assemblies as the samples are heated by conduction and radiation [8]. Therefore it is possible for a thermal gradient to exist across a sample.

Various modes of interaction between infrared radiation and thermosetting resin systems have been discussed in the literature [8, 50, 63, 73, 74, 75], including transmission, specular reflection, attenuated total reflection and diffuse reflection. The present study uses transmission as the sampling technique; this section of the review is therefore principally focused on transmission spectroscopy.

A transmission spectrum can be obtained when the infrared light beam of the FTIR spectrometer is passed through an organic material. Light of certain frequencies is absorbed while other frequencies continue to transmit, and therefore a reduction in light intensity is observed at the position(s) where the light has been absorbed [76]. The relationship between the intensity of the incident and transmitted light and the concentration of the specific functional group is dictated by the Beer-Lambert law, as shown in Equation 2-6 [8]:

$$A = \log_{10} \left( \frac{I_0}{I} \right) = \epsilon cl$$

*Equation 2-6*

where  $A$  is absorbance,  $I_0$  and  $I$  are the intensity of the incident and transmitted light respectively,  $\epsilon$  is the extinction coefficient,  $c$  is the concentration of the absorbing material in the sample, and  $l$  is the path-length.

For representative quantitative analysis, spectra should be continuously collected *in-situ* for the duration of the curing process. When the absorption peaks of interest are identified, their area can be used to observe the consumption of each reactant [23]. Conversion ( $\alpha$ ) is the term used to describe the extent of cure of a particular functional group (as a percentage of a fully cured system) at a specific time during the reaction [1]. In order to compensate for any changes in path-length an internal standard, which does not participate in the cure reaction, is

typically used; the presence of an inert peak means that the peak areas corresponding to the functional groups of interest can be normalised, effectively normalising the data for any optical path-length changes during the course of the cross-linking reaction [8]. The percentage conversion can be calculated using the following equation [8]:

$$\alpha = 1 - \frac{\left( \frac{A_x}{A_y} \right)_t}{\left( \frac{A_x}{A_y} \right)_0} \times 100 \quad \text{Equation 2-7}$$

where  $A_x$  is the area of the absorption peak of interest (e.g. epoxy or amine),  $A_y$  represents the area of the reference peak (e.g. C-H),  $t$  specifies the cure time in minutes, and 0 refers to the start of the reaction.

Several researchers have carried out mid- and near-infrared spectral analysis on epoxy resins [18, 66, 77, 78]. The strongest vibrational absorption frequencies of organic molecules that are infrared-active occur in the mid-infrared region [8]. Absorption bands in the near-infrared region are caused by the combination and overtones of the fundamental mid-infrared vibrations [66]. For epoxy-amine resin systems, the absorption bands of primary importance are due to vibrations of the C-H, O-H and N-H groups in the near-infrared region. Discrepancies between mid- and near-infrared analysis of epoxy peaks have arisen in the literature [66, 79]. Poisson *et al.* [66] and Mijović and Andjelić [79] reported a reduction of up to 35% and 16% (respectively) in the calculated epoxy conversion between the near- and mid-infrared spectra. It was established that the discrepancies arose from the mid-infrared analysis as both authors observed an unidentified absorption peak at approximately  $905 \text{ cm}^{-1}$ . This was particularly important as it overlapped the epoxy peak at  $915 \text{ cm}^{-1}$ , thereby potentially showing a premature plateau in the conversion data. This is an example of how

quantitative analysis of mid-infrared spectra can become difficult; many of the absorption bands overlap [8]. In contrast, the near-infrared region is dominated by overtones and combination bands which are broader and weaker, and thus can be isolated, allowing easier quantitative measurements [8]. For this reason near-infrared spectroscopy is generally preferred over mid-infrared spectroscopy where quantitative analysis is required [79, 80]. Moreover, the weaker absorption bands in the near-infrared region allow for longer path-lengths to be used, making sample preparation simpler than for mid-infrared analysis [49]. During the current study near-infrared spectroscopy was used for the qualitative and quantitative analysis of epoxy-amine resin systems. Therefore the remainder of this review is focused on literature based on the near-infrared region.

The aforementioned overtones occur because of asymmetrical stretching of the bonds between the atoms [23]; hence the near-infrared region is typically populated with asymmetric C-H, O-H and N-H bonds. Combination bands occur as the result of simultaneous excitation of two different fundamentals.

### **2.3.2. Optical fibre-based methods of process monitoring**

Although conventional techniques are adequate and reliable for specified applications, some are not capable of providing real-time in-situ information within the processing equipment. Sensor systems including electrical- and optical fibre-based have more recently been employed for process monitoring. Optical fibres offer a number of advantages over electrical-based sensor systems, including the following [81]:

- (i) Immunity from electromagnetic interference;
- (ii) Intrinsically safe and chemically inert (for example, silica-based optical fibres);

- (iii) A selection of optical fibre types are available (for example, silica, sapphire, PMMA) in a range of diameters (15 – 1000  $\mu\text{m}$ );
- (iv) Can be relatively low-cost if telecommunications fibres (1310 and 1550 nm) are used for fabricating the sensors;
- (v) A large number of sensors can be fabricated on a single optical fibre or multiple fibres can be used;
- (vi) Their circular cross-section makes them conducive for integration into fibre-reinforced composites;
- (vii) Data can be transmitted over long distances (kilometres) via optical fibres and therefore remote sensing and interrogation is possible;
- (viii) Ability to be used in harsh environments provided that appropriate protection is provided; and
- (ix) Multi-measurand sensors are available, and the same sensor system can be used initially for chemical process monitoring and subsequently be used for structural integrity assessment of the component or structure in-service [82].

This section will address optical fibre-based techniques which have been used to facilitate real-time cure monitoring.

#### ***2.3.2.1. Optical fibre-based infrared spectroscopy***

Some of the spectroscopic techniques referred to previously (such as near-infrared, mid-infrared and Raman) have been adapted for cure monitoring using optical fibre sensors [1, 43, 83, 84]. The focus of this section is on transmission near-infrared spectroscopy. Near-infrared spectroscopy is a convenient and cost-effective technique because of the availability of relatively low-cost optical fibres and spectrometers with the associated ancillary equipment (such as couplers and connectors), which are used in the telecommunications industry [23].

The concept for optical fibre-based transmission spectroscopy for monitoring cross-linking reactions is as follows [23]. An optical fibre is used to deliver the light from the spectrometer or an external light source to the resin, which is contained in a “reservoir” or cell. After passage through the resin system, the transmitted light is collected by a second optical fibre and is delivered to the detector of the spectrometer. Alignment of the two optical fibres is critical for this type of sensor [48].

In the remainder of this thesis, the nomenclature for the optical fibre core and cladding diameters are represented as “x/y  $\mu\text{m}$ ”. For example, a fibre with a core diameter of 8  $\mu\text{m}$  and a cladding diameter of 125  $\mu\text{m}$  will be coded as 8/125  $\mu\text{m}$ .

Mijović *et al.* [85, 86] fabricated an optical fibre near-infrared transmission sensor for monitoring the cure process of several epoxy-amine resin systems. The sensor was constructed from two large-core (600/630  $\mu\text{m}$ ) multi-mode optical fibres, which were aligned in a capillary as shown in Figure 2-8a. The cavity between the fibre-ends, where the resin was introduced, was 2-3 mm. As the cure reaction progressed, the spectra showed a decrease in the epoxy and amine absorption peak areas. Quantitative analysis was undertaken using the C-H peak as the reference. The rates of reaction were shown to increase with increasing isothermal temperature, and the extent of reaction was greater with higher cure temperatures. The authors did not offer any explanations as to why these trends were observed. Although the approach used was adaptable and relatively low-cost, it must be noted that direct coupling between the sensor and the light source/detector was not used. The experimental section of the paper details how the resin system was heated prior to being introduced into the reaction vessel, to obtain a “clear” mixture. This suggests that the cross-linking reaction had started

well in advance of the data being recorded. Moreover, the relatively large dimensions of the fibres and capillary suggest that this method would not be suitable for deployment in fibre-reinforced composite applications.

A similar sensor construction was used by Rogers *et al.* [87] but with smaller dimensions. The silica fibres (200/280  $\mu\text{m}$ ) were separated by 2 mm, and sealed in PTFE tubing (internal diameter of 300  $\mu\text{m}$ ) using nail varnish. Near-infrared spectra of an epoxy-amine resin system were obtained, and the concentrations of the epoxy and amine groups were shown to decrease as a function of time. However, no explanations offered for these observations and quantitative analysis was not performed. In the studies by Mijović *et al.* and Rogers *et al.* it has to be assumed that an interference-fit is present between the capillary and fibres in order to hold the fibre cores aligned. However, neither of them discusses the methods that were used in ensuring that the resin system being monitored entered the cavity between the fibre-ends.

Fernando *et al.* [88] adopted a similar sensor construction, but introduced a slot into the capillary to permit the ingress of the resin system. A schematic illustration of this design is shown Figure 2-8b. Two 50/125  $\mu\text{m}$  fibres were aligned in the metal capillary and near-infrared spectra of an epoxy-amine resin system were obtained during the cure process at 30, 40, 50 and 60 °C. The epoxy peak was shown to decrease as a function of time during cross-linking. Quantitative analysis was undertaken using C-H as a reference peak. It was shown that the higher isothermal cure temperatures induced a faster reaction rate and a greater extent of cure than the lower temperatures. It was reported that distortion of the capillary occurred when introducing the slot, thus there was difficulty in ensuring alignment of the fibres and

specifying the path-length of the sensor. Besides this, a metal capillary is unlikely to be attractive for integration into some end-use applications of fibre-reinforced composites [8].

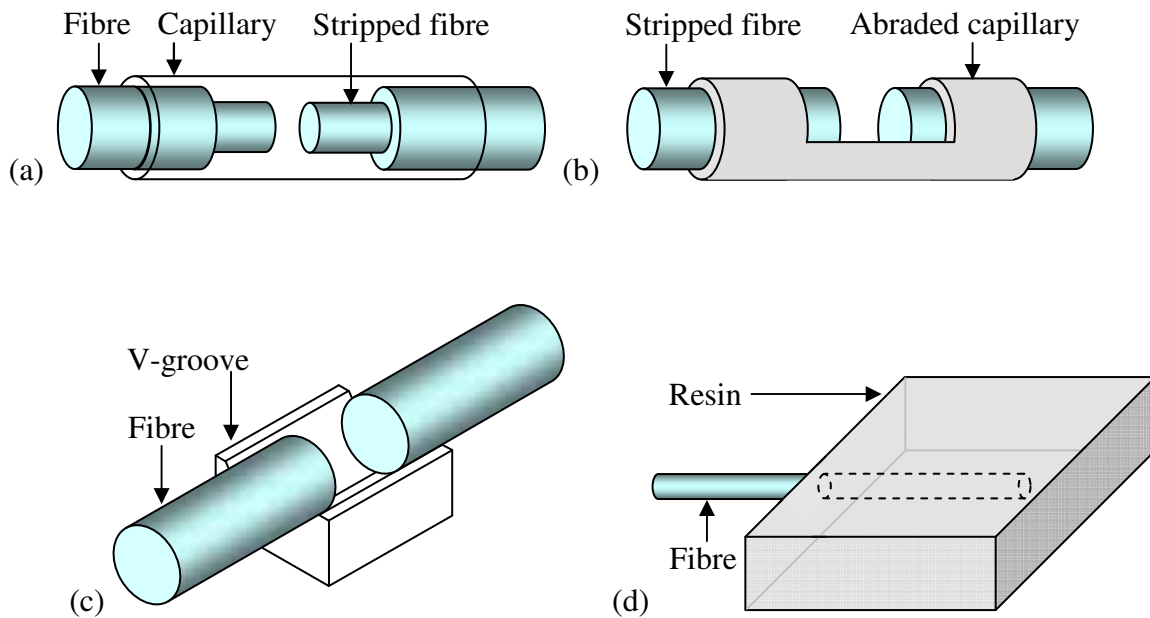


**Figure 2-8. Optical fibre sensor designs for transmission spectroscopy: (a) fibres in a capillary [85]; (b) fibres in an abraded capillary [88]; (c) fibres aligned on a pre-cured epoxy V-groove [41]; and (d) a fibre embedded in resin [91].**

In a similar method, a transmission sensor constructed by Crosby *et al.* [89] consisted of two 50/125  $\mu\text{m}$  optical fibres within a glass capillary. In this case, a section of the capillary was ground using abrasive paper to expose a 1.25 mm cavity between the fibre-ends. The resin was cured at 40 °C. The findings corresponded to the observations by the studies reported above; the epoxy and amine peaks were shown to decrease in magnitude during the cross-linking process. It was reported that the perforation of the glass capillary in such a sensor configuration can be tedious due to premature fracture [8]. An advancement of this method of sensor construction was the formation of a micro-cavity produced by laser ablation [90]. It

was demonstrated that a precise cavity could be micro-machined through the diameter of a single-mode optical fibre using a laser. Although this technique was not adapted for cure monitoring, it was suggested that the cavities could be used as the resin containment cell in optical fibre-based transmission spectroscopy. The main appeal here would be that the overall dimensions of the sensor would be no larger than the sensing fibre. However, the costs involved with laser facilities can be high.

Optical fibre near-infrared transmission spectroscopy was undertaken by Powell *et al.* [41] using two 200/240  $\mu\text{m}$  silica optical fibres aligned on a V-shaped groove. The V-groove platform was fabricated from the same resin system that was to be monitored, and was fully cured before introducing the fibres. The fibre end-faces were positioned 0.5-1.5 mm apart, between which an epoxy-amine resin system was introduced. A schematic illustration of this design is shown in Figure 2-8c. The peak area of the epoxy group was shown to decrease during the cure reaction, and quantitative data were obtained by normalising the epoxy peak values with a C-H reference peak. In accordance with the other studies reviewed here, the authors reported that epoxy groups were consumed at a faster rate under cure at higher temperatures and a higher final conversion percentage was reached at higher temperatures. The data obtained using the optical fibre sensor were found to be comparable with results obtained using conventional FTIR spectroscopy at 40, 50 and 60  $^{\circ}\text{C}$ . A discrepancy was observed at 30  $^{\circ}\text{C}$  but the authors did not speculate on the reasons for this. The use of the same material for the V-groove and cure means that the thermal expansions and chemical compatibility are the same. However, the fibres were bonded to the platform, so alignment may be an issue. The dimensions of the pre-cured platform were not reported.

A similar style was used by Mahendran *et al.* [71], where the alignment fixture was fabricated from the same resin system that was being monitored. In this study a glass capillary was first cured in the resin system to make a channel for the fibres. Once cured, a groove was cut into the resin and through the capillary; this acted as the cavity for the resin system during cure. Two fibres were cleaved and fed through the capillary to meet at the groove. A gap of 100  $\mu\text{m}$  was set between the fibre-ends. Quantitative analysis was performed using the C-H peak as a reference. The final extent of cure was shown to be comparable to data obtained using conventional transmission FTIR spectroscopy. The dimensions of the pre-cured resin fixture were large, so the applicability of this sensor in a composite is not attractive.

The approach taken by Calvert *et al.* [91] was optical fibre-based, but not an *in-situ* technique. A single optical fibre (either 600  $\mu\text{m}$  or 200  $\mu\text{m}$  in diameter) was embedded between layers of extruded epoxy-amine resin during a free-forming process on a hot plate at 100 °C. The distal end of the fibre was contained within, and approximately 2 mm from the edge of, the specimen. The sample was pre-cured overnight at 100 °C in an oven and then fully cured at either 160 °C or 170 °C. The loose end of the fibre extended 200 mm out of the specimen, as illustrated in Figure 2-8d. At intervals during the cure process the specimen was removed from the oven and the loose end of the fibre was positioned at the focus of a near-infrared spectrometer whilst an external light source was directed at the specimen, towards the embedded fibre-end. This study reported that the amine absorption peak was absent after the pre-cure, implying that total amine consumption had occurred. The authors suggested that this corresponded to gelation of the resin system. They did however observe that un-reacted epoxy was still present after the pre-cure, and thus the full-cure would allow it to react with the secondary amine groups. The sensitivity of the pre-cured sample to ambient moisture was

defined by the presence of an O-H peak in the pre-cured spectra, and its reduction after full-cure. This change was attributed to the removal of secondary amine groups during cure, which therefore reduced the number of active sites for the sorption of water. A faster rate of cross-linking was observed with the higher curing temperature, but the reasons for this were not speculated. Although not stated by the authors, in an application such as this it is critical for the fibre-end to be directly aligned with the light source [39]; for this precision, it would imply that the sample is removed from the oven for a long period for each measurement. However, it is not indicated how regular removal from the oven may have effected the cure cycle or the results. Moreover the distance of the light from the fibre will influence the coupling efficiency due to the divergence of the light beam, and coupling through air can be problematic. With an experimental set-up such as that described by Calvert *et al.*, it is likely that the light-to-fibre-to-spectrometer alignment will be difficult to repeat. Furthermore, the report proposes that a flat cleave at the sensing end-face of the fibre is not important. On the contrary, for adequate light coupling, a perpendicular cleave is essential; a poor cleave will induce significant scattering [15]. It was stated that there was discolouration of the resin specimen after both pre-curing and curing, but the reasons and the effects of this were not hypothesised.

#### ***2.3.2.2. Optical fibre-based evanescent wave spectroscopy***

Techniques for monitoring cross-linking based on evanescent wave spectroscopy have been reported by a number of authors [1, 41]. If the cladding of an optical fibre is removed, the evanescent wave can react with the medium surrounding the core [41]. As described previously, if the surrounding medium is absorbing, energy will be removed from the evanescent wave, which will result in a loss in the overall energy transmitted by the fibre. Thus, the fibre can be used to obtain an absorption spectrum of the medium.

Crosby *et al.* [1] used a 190/250  $\mu\text{m}$  multi-mode optical fibre with a core refractive index of 1.70 to fabricate an optical fibre-based evanescent wave sensor. A 300 mm long section of the polymer cladding was removed by immersing the fibre in concentrated sulphuric acid at 60 °C for 8 minutes. The fibre-ends were connected to a light source and a spectrometer. In order to evaluate the relationship between evanescent absorption and concentration, the response of the sensor was monitored while immersed in amine solutions of known concentrations; the peak area corresponding to amine absorption increased in a linear fashion with the amine concentration. For the cure studies, the sensing region was immersed in an epoxy-amine resin system. It was shown that the reduction in the amine and epoxy peak areas followed a similar trend to data obtained using conventional transmission FTIR spectroscopy.

Powell *et al.* [41] adopted a similar sensor design. They used an optical fibre with a core diameter of 120  $\mu\text{m}$  and core refractive index of 1.65, and removed a 200 mm length of the cladding using sulphuric acid at 60 °C for 8 minutes. The sensor was placed in a curved glass tube and immersed in a water bath so that the open-ends of the tube were above the water-level, and the sensing region was below. An epoxy-amine resin system was introduced into the tube, and cured at 30, 40, 50 and 60 °C. The area of the N-H absorption peak was observed to reduce with cure time, and quantitative analysis was carried out. The results were in accordance with the trends recorded using a transmission sensor (discussed in Section 2.3.2.1), whereby the cross-linking reaction is observed to proceed at a faster rate at higher isothermal temperatures. However, the 30 °C data displayed the largest scatter, which the authors attributed to the high viscosity of the resin system at the lower temperature not providing good wetting of the sensor. A faster rate of cure was consistently detected by the evanescent sensor than by the transmission sensor at each of the cure temperatures. This

observation was reported as being due to the penetration depth of the evanescent wave decreasing as the refractive index of the resin increases (according to Equation 2-5) during cure, and therefore the sensor will progressively see a smaller volume of resin.

These sensor configurations offer smaller dimensions than many of the transmission sensors discussed in Section 2.3.2.1, but still provide quantitative data on the cross-linking process. However, as it is beneficial to have a core of a high refractive index, the fibres used for fabricating the sensors are more costly than standard optical fibres. Furthermore, the removal of the cladding reduces the strength of the fibre, making it susceptible to fracture when under load. The de-clad region also exposes a large area which can be subject to surface contamination.

Other types of optical fibre sensor which have been developed to enable access to the evanescent wave include tapered fibres [8] and side-polished fibres [40]. The principle behind these sensors is that the cladding is reduced so the evanescent wave can propagate into the surrounding medium. However, the primary drawback with such devices is that it is difficult to manufacture reproducible tapers and polished profiles [8]. U-shaped fibres have also been adopted [92, 93] but are generally large in diameter and the risk of fibre-breakage is high when defining the optimum bend radius. It is possible for a laser ablation technique to be employed for creating micro-channels along the length of an optical fibre [94]. The limitations of this technique have been discussed previously.

#### *2.3.2.2.1. Reinforcing fibre-based evanescent wave spectroscopy*

A relatively new application of evanescent wave spectroscopy for process monitoring is the development of “self-sensing” composites, whereby the reinforcing glass fibres are

themselves used for sensing the cure process. The diameter mismatch between optical fibres and reinforcing fibres has been documented [23, 95, 96, 97]. Reinforcing glass fibres used in the manufacture of composites are typically 12-14  $\mu\text{m}$  in diameter [72], whereas the optical fibres used for process monitoring are at least an order of magnitude larger. Thus the optical fibre sensors can induce distortion in the orientation of the reinforcing fibres and therefore can have an adverse effect on the mechanical properties of the composite. It has been proposed that the reinforcing fibres can act as light guides over short distances, to effectively make the composite self-sensing, and enable process monitoring [2, 95, 96, 97]. In comparison to optical fibres, the light-guiding characteristics of reinforcing fibres are very poor [23]. As in the de-clad optical fibre-based evanescent wave spectroscopy sensor, the method of obtaining spectra using the self-sensing fibres is for the surrounding resin system to act as the cladding.

Wang *et al.* [72, 98] used un-sized reinforcing E-glass fibres to obtain evanescent wave spectra for the process monitoring of two epoxy-amine resin systems. The fibres were bundled and connected to a light source and spectrometer. They were immersed in the resin system and cured at known temperatures between 35 and 70  $^{\circ}\text{C}$ . It was observed that the spectra obtained using evanescent wave spectroscopy were of poorer quality than those obtained using conventional transmission FTIR. This was attributed to a comparatively low signal throughout the cure process. For one of the resin systems [72], the spectra showed a decrease in the epoxy absorption peak as a function of time during the cure process. Quantitative data were acquired by normalising the values with the reference C-H peak. It was shown that the evanescent data followed the same trend as conventional transmission data, but that the final extent of conversion was slightly lower. Moreover, there was a discrepancy observed in the rates of cure at the higher isothermal temperatures. The authors

reported the causes to be due to differences in the experimental procedures and temperature-controls. Evanescent data obtained on the second resin system [98] also showed a reduction in the epoxy peak absorption area and was normalised to the C-H peak area to provide quantitative data. However, spectra could only be obtained on the initial part of the reaction, due to the resin system reaching the same refractive index as the fibres. When compared to data acquired using conventional transmission spectroscopy, the initial reaction rate was shown to correlate well. In order to monitor the full cross-linking reaction of this resin system using evanescent wave spectroscopy, the authors used custom-made small-diameter optical fibres (18  $\mu\text{m}$ ) which had a higher refractive index than the E-glass fibres. It was shown that they were successfully able to monitor the full cure cycle using these fibres, and that a good correlation was seen with conventional transmission spectroscopy. A further study [99] demonstrated that using the E-glass reinforcing fibres as light-guides can also facilitate the detection of damage in fibre-reinforced composites. A high-speed camera was used to study the fracture of individual fibres in the bundle in real-time while under tension.

Although the deployment of reinforcing fibres as sensors for process monitoring is an elegant approach, there are limitations which need to be appreciated. For example:

- (i) It is not always possible to have access to both ends of the input and output fibres in a composite structure. Whilst this technique is suitable for laboratory-based specimens, the attenuating characteristics of E-glass fibres limit the transmission lengths to less than 100 mm [72]; and
- (ii) Like all spectral-based techniques, although quantitative information can be extracted, the costs associated with spectrometers can be prohibitive and not necessarily suited to an industrial environment.

Intensity-based techniques have also been employed [96, 97, 100] for self-sensing process monitoring but, as will be discussed in Section 2.3.2.3, such approaches may not account for drifts in the light source.

### ***2.3.2.3. Optical fibre-based refractive index monitoring***

As detailed earlier in this chapter, the refractive index of an epoxy-amine resin system increases as it undergoes cure because of the increase in the cross-link density. Several researchers have used the change in refractive index to qualitatively monitor the cure process using optical fibre-based techniques; some of these are reviewed here.

Afromowitz [101] developed an ‘epoxy optical fibre’ to monitor the cure of an epoxy resin system. A 10 mm long tapered (from 1 mm to 0.5 mm diameter), S-shaped fibre was fabricated using the same epoxy resin as that being monitored. The epoxy fibre was fully cured before it was immersed into the uncured resin, and each end was adhered to a 600  $\mu\text{m}$  core conventional optical fibre. The conventional optical fibres were connected to a light source and detector. The intensity of the light was shown to decrease as the refractive index of the resin sample reached that of the epoxy fibre. At full cure, 7% of the original light intensity was still detected; the authors suggested that this was a result of the short epoxy fibre length. That is, the light input fibre and the detecting fibre were relatively close and somewhat aligned. It is not clear why a “gentle S-bend” was included in the design or whether it was merely a product of the fabrication process. It would however serve to off-set the light source and detector. Nevertheless such a design is likely to suffer macro-bending losses (see Section 2.2.3), particularly when at least two major bends are occurring over such a short length. Moreover, it is likely that alignment of the epoxy fibre and the conventional optical fibres will be difficult. As previously alluded to, the use of a sensor which is

fabricated using the same resin system as the one being monitored is favourable. Afromowitz does not elucidate his reasons for fabricating a tapered fibre.

Afromowitz and Lam [102] furthered this study by demonstrating that the technique could be readily used as a ‘cure detector’ in epoxy-based carbon composites. The pre-cured epoxy fibre during this study was 20 mm long. It was embedded in the composite, which was cured under pressure in an oven. Essentially the findings corresponded to those of the previous study, whereby the output intensity decreased as the cure reaction progressed. Brief increases in intensity were observed during the initial temperature ramping, but were attributed to an increasing refractive index difference (between the cured and uncured epoxy resin system) as the temperature was ramped. Erratic intensity variations at the start of the cure cycle were characterised as “bedding in” of the sensor element between the carbon fibre plies of the composite.

The same intensity-based principle was adopted by several authors who used a de-clad section of an optical fibre as the sensing interface [1, 41, 103, 104].

Crosby *et al.* [1] used a 190/250  $\mu\text{m}$  optical fibre with a high refractive index (1.70) core to fabricate the sensor. This sensor was manufactured in the same manner as the evanescent wave sensor, as described in Section 2.3.2.2. However, in this case the fibre was connected to a light source and detector. The sensing region was immersed in an epoxy-amine resin system, which was cured on a hot-plate at 25, 30, 40 and 50  $^{\circ}\text{C}$ . An initial increase in the intensity of the signal was observed, which the authors attributed to a drop in the refractive index due to the initial temperature ramp (from room temperature to the isothermal cure

temperature). After this, the intensity of the detected light signal was shown to decrease with time, in accordance with the data obtained by Afromowitz [101]. The data obtained using the de-clad fibre sensor were compared with the quantitative data obtained using conventional transmission FTIR spectroscopy. It was found that they followed a close relationship in terms of the occurrence of cure initiation and completion. Although this sensor design may be susceptible to surface contamination, and access to both fibre-ends is still required, it has several advantages over the style used by Afromowitz [101, 102]. For example, the dimensions of the fibre are smaller and furthermore, the dimensions of optical fibres and their orientation in a composite can be selected to have minimal impact on the mechanical properties of the composite [105]. The diameter alone would make this sensor easier to integrate into a composite. The design also appears more practical as it is a single fibre, so there will be no weak points where the sensing region joins the input/output fibre. Therefore insertion loss will not occur at these points. However, the de-clad region generally tends to be brittle and therefore susceptible to fracture when under load.

Li *et al.* [104] demonstrated the use of this sensor design in an industrial environment by embedding the sensor in a carbon composite pre-preg, and curing it using a hot-press and an autoclave. However outputs from the sensors in the two processing environments were dissimilar. It is difficult to draw conclusions from this study because the authors did not offer any explanations for the different trends in the data when using the same resin system.

In a simpler approach, the use of a single-ended refractive index sensor has been investigated by several researchers [1, 8, 106, 107, 108], and is discussed below.

When light travels from a medium of a given refractive index into a second medium of a different refractive index, both reflection and refraction of the light may occur at the interface [39]. Based on this, it is possible to use a cleaved optical fibre as a sensor to infer changes in the refractive index of the resin system during cross-linking. As discussed in Section 2.2, the cleaved end face of an optical fibre can accept light between defined input angles, governed by the numerical aperture. The capacity of this light acceptance is dictated by the refractive indices of the core and cladding. When a perpendicularly cleaved fibre-end is in direct contact with the resin system, the intensity of the reflected light,  $R$ , at the interface is related to the refractive indices of the fibre core and the resin, according to Fresnel's law [109, 110]:

$$R = \left( \frac{n_{core} - n_{resin}}{n_{core} + n_{resin}} \right)^2 \quad \text{Equation 2-8}$$

where  $n_{core}$  and  $n_{resin}$  are the refractive indices of the core and resin respectively.

Based on this theory, Afromowitz and Lam [106] monitored the change in refractive index of an epoxy-amine resin system by immersing a cleaved fibre-end (200/240  $\mu\text{m}$ ) in an uncured sample. The sensor was connected to a light source and detector via a 2x1 coupler. The resin system was cured at 60, 90 and 130  $^{\circ}\text{C}$ . The initial temperature ramp data were not displayed or discussed. The refractive indices recorded by the sensor at the isothermal temperatures were shown to increase as a function of time and gradually plateau. However, the reasons for these changes were not deliberated.

Cusano *et al.* [107] also used a 2x1 coupler in their Fresnel reflection sensor configuration. A cleaved single-mode optical fibre was immersed in an epoxy-amine resin system during cure

at 50, 60 and 70 °C. It was observed that as cure progressed, the increase in density led to an increase in refractive index.

Crosby *et al.* [1] used a Fresnel reflection sensor (core refractive index of 1.46) to verify the results obtained using a de-clad fibre (discussed previously) during the cure of an epoxy-amine resin system. The authors reported that the responses of the sensors were the mirror image of one another, with the Fresnel reflection sensor showing an initial decrease during the temperature rise followed by an increase during the isothermal stage. They attributed the opposing responses to the refractive indices of the fibres.

The primary issue with using a 2x1 coupler in Fresnel reflection sensors is that any power drifts in the light source cannot be monitored. Vacher *et al.* [108] used a Fresnel reflection sensor for real-time cure monitoring of an epoxy resin system, but used a 2x2 coupler. Here, the second distal fibre was connected to a reference photo-diode to monitor and compensate for any power drifts of the light source. The resin system was cured isothermally at 140, 150, 160, 170, 180 and 190 °C, followed by a cooling cycle. It was reported that an increase in the temperature of the resin system induced a decrease in the density and thus showed an associated decrease in the refractive index. During the isothermal cure the density and refractive index increased, and during the cooling cycle a further increase in the refractive index of the cured resin was observed.

Wang *et al.* [98] employed a Fresnel reflection sensor with a 2x2 coupler, where both distal fibres were immersed in the resin system. An epoxy-amine resin system was cured at 40, 50, 60 and 70 °C. It was reported that the initial increase in temperature caused a decrease in the

output signal, corresponding to the refractive index of the resin system. This was due to the reduction in the density of the resin. During the isothermal stage an increase in the signal was observed, which was attributed to the cross-linking reaction causing the density and refractive index to rise. This was also said to be concomitant with an increase in the molecular weight of the resin system.

An array of fibres based on the Fresnel reflection sensor has also been used for optical time domain reflectometry measurements during the cure of an epoxy resin system [111]. This, however, is an expensive method of cure monitoring. Other applications where Fresnel reflection-based sensors have been employed include liquid-liquid flow [112, 113, 114] and biosensors [115, 116].

In conclusion, two main types of optical fibre sensors have been reviewed for monitoring the cross-linking process through changes in the refractive index of the resin system. The main issues with the de-clad sensor are: (i) access to both ends of the fibre is required; (ii) a relatively large area is subject to any contamination in the resin; (iii) the de-clad section is brittle and therefore susceptible to fracture under load/pressure; and (iv) the methods for removing the cladding are time-consuming, costly, and cannot be easily controlled. In contrast, the single-ended Fresnel reflection sensor is a simple and economic cure monitoring technique. However, quantitative data cannot be obtained using these methods.

#### ***2.3.2.4. Optical fibre-based strain monitoring***

Previous researchers have suggested that the cure process can be tracked by monitoring the development of strain as recorded by embedded FBGs [117, 118, 119]. There are uncertainties if this approach is adopted for the following reasons:

- (i) The grating will respond to temperature changes, but also any lateral forces that act on the grating. Temperature changes can also be brought about by the exothermic nature of thermosetting resin systems. Therefore de-coupling the recorded “strain” from temperature may not be straightforward;
- (ii) The two primary factors which contribute to the development of residual strain in composites are strain induced by the resin shrinking and the mismatch of the coefficients of thermal expansion between the materials in the composite [98]. This will also make de-coupling difficult in terms of analysis and interpretation;
- (iii) In the context of fibre-reinforced composite materials, waviness or undulations in the reinforcing fibres can create localised stress fields in the vicinity of the grating, thus making interpretation difficult;
- (iv) In the context of residual stresses caused by shrinkage and thermal mismatches in the various materials in the composite it is not clear as to when strain is transferred to an FBG during the cross-linking process;
- (v) In situations where parameters such as vacuum and pressure are used in the processing of composites, it is often difficult to de-convolute the response of the grating to temperature and the above-mentioned factors;
- (vi) Reinforcing fibres such as Kevlar<sup>®</sup> have a negative coefficient of thermal expansion, therefore there is a possibility that this fibre can undergo micro-buckling. This in turn can interfere with the interpretation of the Bragg signal;
- (vii) In situations where hot-presses are used when processing composite preforms, over-pressurisation can lead to significant resin loss along with undesired movement of the reinforcement. Therefore it will be difficult to assume that the relative orientation of the FBG sensor is retained.

An FBG sensor is fabricated by inscribing periodic variations in the refractive index in the core of an optical fibre [23]. The sensor will reflect particular wavelengths of light (depending on the wavelength used to inscribe the grating) and transmit all others. The grating can be inscribed using a variety of techniques such as phase-mask or point-by-point inscription. The reflected signal of the FBG sensor displays a peak at the wavelength that the grating is written. The Bragg reflection peak, centred at  $\lambda_B$ , can be expressed as [23]:

$$\lambda_B = 2\Lambda n_{eff} \quad \text{Equation 2-9}$$

where  $\Lambda$  and  $n_{eff}$  are the period of the fibre grating and the effective refractive index of the fibre core respectively. Any modulation of the grating periodicity is manifested as a change in the Bragg reflection peak wavelength [23]. In order to de-couple the effects of strain and temperature, it is essential for the temperature-sensing FBG to be isolated in a strain-free environment. A typical method for this is to house the sensing region within a sealed capillary [120]. The shift of the Bragg wavelength,  $\Delta\lambda_B$ , due to external strain,  $\epsilon$ , and temperature change,  $\Delta T$ , can be expressed as [121]:

$$[\Delta\lambda_B]_{\epsilon,T} = [\Delta\lambda_B]_{\epsilon} + [\Delta\lambda_B]_T = \alpha\Delta\epsilon + \beta\Delta T \quad \text{Equation 2-10}$$

where  $\alpha = \lambda_B(1 - \rho_e)$ ;  $\rho_e$  is the strain-optic constant of the fibre [122], and  $\beta = (\alpha_\Lambda + \alpha_n)$ ;  $\alpha_\Lambda$  and  $\alpha_n$  are the coefficients of thermal expansion and thermo-optic respectively.

Table 2-2 presents a summary of selected papers where FBG sensors were used for process monitoring of composites. However, the measurand of interest was strain and not chemical cross-linking.

Authors	Experimental approach taken	Comments
Kuang <i>et al.</i> [117]	FBG sensor embedded a series of glass fibre- and carbon fibre-reinforced composites (epoxy matrix), and fibre/metal laminates (polypropylene matrix). The FBG sensor was located centrally in relation to the width of the composite and always in the principal reinforcing fibre direction, but the adjacent layers differed in orientation. The sensor was secured with adhesive tape at the edge of the specimen.	A large compressive residual strain was observed after cooling in the fibre/metal laminates due to the mismatch in the coefficients of thermal expansion. Tensile residual strain was observed in the glass fibre- and carbon fibre-reinforced composites.
Dewynter-Marty <i>et al.</i> [118]	FBG sensor placed in a machined U-groove in a layer of foam which was sandwiched between two glass-fibre/epoxy pre-pregs. The groove was off-centre; the reasons for this were not stated. A second FBG sensor was located outside the composite to monitor	During the initial heating regime, the response of the sensor was erratic, but during the isothermal hold, the strain is observed to remain constant. On cooling, compressive residual strain was found to occur.

	temperature.	
De Oliveira <i>et al.</i> [119]	Carbon fibre/epoxy composites were cured on a series of mould materials (aluminium, steel, carbon composite and carbon foam). At the optical fibre insertion and emergence points, the sensors were inserted into PTFE tubes. Uni-directional composites were fabricated where the FBG was located centrally.	An initial decrease in strain was experienced in all of the uni-directional samples. This was attributed to the negative coefficient of thermal expansion of the pre-preg material or the bedding-in of the sensor. It was shown that higher strain values occurred for the aluminium and steel moulds in comparison to the composite and foam moulds, due to the higher thermal expansions of the metals. The specimens on the composite and foam moulds mostly underwent compressive strain during the cure cycle, which increased during cooling. This was attributed to the

		negative coefficient of thermal expansion of the carbon composite uni-directional sample.
--	--	---

**Table 2-2. A summary of selected studies which used FBG sensors for strain monitoring of composites during processing.**

### **2.3.3. Cure monitoring using an Abbe refractometer**

An Abbe refractometer is typically used to measure the refractive index of liquids or solids [121, 123] by placing the sample between two temperature-controlled prisms. Several of the optical fibre-based studies reported in Section 2.3.2 have used an Abbe refractometer to confirm the refractive indices of the resin systems in the cured and uncured states, or to measure the reinforcing fibre pre-forms [1, 72, 124]. Crosby *et al.* [1] reported refractive index values which were obtained during the cure process using an Abbe refractometer. An initial decrease in the data was observed when the resin system was heated from ambient to 50 °C, followed by a gradual increase corresponding to the isothermal cure. The data were plotted with data obtained using a de-clad optical fibre refractive index sensor; the curves showed a similar form and the reaction completion point acquired with each sensor were shown to coincide.

Fernando [125] reported on the deployment of an Abbe refractometer for *in-situ* cure monitoring of an epoxy-amine resin system. However, in this experiment, the Fresnel reflection sensor was not positioned in the refractometer but carried out in a separate

experiment. The two datasets were super-imposed and similar trends were observed, whereby both showed an increase with cure time and a plateau region when cure was near-completion.

Crosby [126] published data on the cure of an epoxy-amine resin system using an Abbe refractometer in transmission mode. The upper prism was coated with a release agent, and a resin film was formed between the two prisms. Once cured, the resin was removed from the lower prism by soaking it in a solvent. Cross-linking was carried out at 30, 40, 50 and 60 °C. The trend observed corresponded to the previously reported data [1]. It was shown that higher isothermal temperatures induced a faster rate of cure. The spread in the repeat data was attributed to sample variation and technique.

Although this is a simple technique whereby actual refractive index values can be acquired, there is a danger of damaging the refractometer prisms and prism boxes by curing the resin system directly on them. As the resin is not contained, variations caused by the operator (such as the pressure placed on the upper prism) will influence the thickness and spread of the liquid sample from experiment-to-experiment.

#### **2.3.4. Hyphenated cure monitoring techniques**

Although several studies have reported data obtained by multiple stand-alone techniques to identify the cross-linking kinetics of epoxy resin systems [1, 41, 49], the cross-comparison between the techniques is not straightforward for the following reasons [121]:

- (i) The resin can be contained in different holders or substrates, such as metal or glass. Therefore, the possibility of surface-catalysed reactions and the differences in the coefficients of thermal expansion cannot be ignored;

- (ii) A key point to note with chemical kinetics is that it is important to control and monitor the temperature of the reaction vessel. As temperature is a key controlling factor for the rate of chemical reactions, it is important to ensure an identical thermal environment when experiments are conducted using different heating methods; and
- (iii) There is also a need to differentiate between quantitative and qualitative data. For example, spectral-based techniques can give quantitative data. Where qualitative data (derived from the refractive index) are used for monitoring the cross-linking process, it is necessary to establish the cross-correlation with quantitative techniques to give confidence to end-users who may be interested in deploying intensity-based and cost-effective process monitoring techniques.

The term “hyphenated” is defined here as the simultaneous acquisition of two or more measurands in a single experiment. A primary advantage of hyphenated techniques is that the parameters of interest are monitored under identical processing conditions. Thus cross-correlation studies between the techniques can be performed with a high degree of confidence. Moreover hyphenated techniques can accrue significant cost-savings because they will not require separate individual experiments to be undertaken to obtain data on different material properties.

This area of research is growing; work in this area to-date is focused mostly on DSC/FTIR [98, 127, 128, 129], DSC/X-ray [130] and DSC/light-intensity [131, 132]. This section reviews hyphenated methods of cure monitoring using optical fibre sensors.

Giordano *et al.* [133] studied the dual functionality of a cleaved single-mode optical fibre with an FBG inscribed, to measure refractive index and residual stresses of an epoxy resin during its cure cycle. A mould was fabricated to have two cavities whereby the sensing region of the FBG and the cleaved fibre-end were within separate cavities. A thermocouple was also placed in the same cavity as the fibre-end. A 2x1 coupler directed the reflected light to a wavelength division multiplexing (WDM) coupler, which was used to discriminate between the refractive index signal (1310 nm) and the FBG signal (1550 nm). The entire assembly was placed in an oven at room temperature before being ramped to 43 °C and holding isothermally for 70 minutes. This was followed by a second heating ramp to 90 °C, with an isothermal hold of 30 minutes, before cooling back to room temperature. During the initial heating cycle from room temperature to 43 °C, a linear decrease in the refractive index was observed. During both isothermal stages there was an increase in the refractive index. The initial shift in the Bragg wavelength was attributed to the fibre thermo-optic effect and thermal expansion. The authors speculated that this was because the resin system was unable to induce strain on the fibre before gelation. During the second ramping stage (i.e. from 43 to 90 °C) the thermal sensitivity was shown to double in value. This was attributed to the mismatch in the coefficient of thermal expansion between the resin and the fibre as they were now bonded together. After cooling, the gratings were shown to be subjected to compression deformation. In some instances the discussion did not reflect the data presented in the graphs. Furthermore, the limitations of the use of FBG sensors for monitoring cure reactions, discussed in Section 2.3.2.4, are applicable here.

In a similar study, Antonucci *et al.* [134] investigated the dual functionality of a single-mode optical fibre during the cure of an epoxy-amine resin system under non-isothermal conditions.

A double-cavity mould was fabricated with a fibre channel along the length of the mould. The fibre was held in position using clay to fill the grooves. The resin system was ramped from 43 °C to 133 °C. There was an initial decrease in the Fresnel reflection signal, which was attributed to the increase in temperature and therefore reduction in resin density. The signal is then shown to progressively increase again due to the formation of cross-links. The response of the FBG sensor was used to determine the onset of gelation and was compared to the temperature profile to identify the gelation temperature. There were no values quoted for the induced strain. The studies reported by Giordano *et al.* [133] and Antonucci *et al.* [134] were brief on detail making it difficult to decipher the results obtained. In terms of the experimental set-up, the main absent points for consideration in these studies include: (i) where the thermocouple was located; (ii) where the FBG sensing region was located within the cavity [133]; (iii) whether the mould was open-topped; (iv) whether the clay used to hold the fibre in the grooves solidified and whether it contaminated the resin [134]; and (v) processing temperatures were quoted in the discussion but there was no evidence to suggest that they were used in the study [134].

Crosby *et al.* [135] considered two multi-functional sensor arrangements to facilitate temperature and chemical monitoring of epoxy-amine resin systems. The first configuration consisted of an FBG sensor housed in a silica capillary opposite a de-clad evanescent wave sensor, whose cleaved end-face was also sealed in the capillary. The light was transmitted through the FBG sensor to the evanescent wave sensor, which was in-turn connected to a spectrometer. In the second design, the evanescent wave sensor was replaced with a transmission sensor. The response of the FBG sensor to temperature displayed a linear relationship. The spectra acquired by the evanescent sensor were not clear enough to make

any definitive quantitative conclusions. The authors attributed this to the poor light coupling between the FBG and the evanescent wave sensors. When the second sensor configuration was immersed in an epoxy-amine resin system, a spectrum was obtained using the transmission sensor. The N-H and C-H peaks were identifiable. The Bragg peak wavelength was also shown in a single spectrum. Overall, the quality of the FTIR data obtained was not suitable for process monitoring. The authors suggested that a higher power light source would improve the quality of the data. However, it is still likely that the air gap between the fibre-ends of the two sensors in each arrangement will cause difficulty with light-coupling. Furthermore, the light may be attenuated due to factors such as debris, airborne particles, moisture etc. before it reaches the second fibre-end.

Mahendran *et al.* [136] developed an optical fibre multi-functional sensor based on an extrinsic fibre Fabry-Perot interferometer (EFPI). The sensor was designed to adopt a single platform to simultaneously impart real-time information on the temperature, strain, refractive index and concentration of functional groups during the cure of an epoxy-amine resin system. A conventional EFPI was fabricated to monitor strain, whereby two cleaved optical fibres were secured inside a capillary and the gap between the fibre-ends constituted a Fabry-Perot cavity. One of the fibres also had a Bragg grating which served as a temperature sensor. The end-face of the capillary was gold-coated and a series of optical fibres were secured onto the original EFPI sensor fibre, facing the reflective surface. The gap between one of the fibres and the end-face of the capillary served as the cavity for transmission/reflection infrared spectroscopy. Two other fibres served as a Fresnel reflection sensor. The epoxy peak absorption acquired using transmission/reflection spectroscopy were normalised and fitted well to conventional transmission FTIR spectroscopy data. The temperature data obtained

using the FBG sensor were shown to shift to a longer wavelength as the resin system was heated, and the return to the initial wavelength after cooling confirmed that it remained in a strain-free state. The interference fringes obtained from the EFPI sensor pre- and post-cross-linking were different due to a change in the cavity length. This was attributed to compressive strain, however the gauge length was not measured and therefore a value of compressive residual fabrication strain could not be reported. The Fresnel reflection sensor which was mounted on the EFPI sensor fibre, displayed an initial decrease in amplitude, as the resin system was heated from ambient to the isothermal temperature. The subsequent gradual increase in reflected light intensity was attributed to the increase in molecular weight. A retardation of the cross-linking rate was the cause of a stabilisation in the recorded light intensity. The trend was comparable to an independent Fresnel reflection sensor which was used in the same experiment. The independent Fresnel reflection sensor was constructed by the current author, and the experiment and data analysis were undertaken in conjunction with Mahendran. This is a versatile configuration which will enable the incorporation of several sensors other than those reported in this study. Although multiple measurands can be accessed using a multi-functional sensor such as this, the addition of extra sensors around the original fibre increases the size of the sensor considerably.

In summary, a review was undertaken on conventional and optical fibre-based techniques that are available to facilitate process monitoring of resins and preforms used in the production of fibre-reinforced composites. The review also considered published papers on hyphenated techniques where different analytical methods were combined to study cross-linking reactions using a single sample. In the current study, a new approach was developed whereby a Fresnel reflection sensor, transmission sensor, reinforcing fibre bundle (self-sensing S-glass), and

FBG sensor were integrated into an Abbe refractometer to study the cross-linking reactions of commercially available resin systems. The next chapter details the experimental approaches that were developed and implemented.

### 3. EXPERIMENTAL PROCEDURES

#### 3.1. MATERIALS

##### 3.1.1. Resin systems

The resin systems investigated in this study are detailed below and a summary of the manufacturer-recommended cure schedules is given in Table 3-1.

- (i) Araldite LY3505/XB3403 (Huntsman Advanced Materials, UK): The two main components of LY3505 epoxy resin were bisphenol-A and bisphenol-F. The XB3403 amine-based hardener was polyoxypropylene diamine. The resin and hardener were mixed thoroughly in the stoichiometric ratio of 100:35 (resin:hardener) by weight, followed by degassing in a vacuum chamber at 70 kPa for 20 minutes. The resin system was used for cure monitoring at 50, 60 and 70 °C.
- (ii) EpoTek<sup>®</sup> 310M (Promatech Ltd., UK): The resin and hardener were mixed in the stoichiometric ratio of 100:55 (resin:hardener) by weight. The resin system was degassed at 70 kPa and was used for cure monitoring at 35, 45, 55 and 65 °C.
- (iii) Norland Optical Adhesive 68 (Norland Products Inc., USA): NOA 68 is a single-part liquid photo-curable resin (composition was proprietary) whose viscosity was 5 Pascal seconds (at 25 °C). This resin system was used to secure the optical fibre sensors to the respective fixtures.
- (iv) Alchemix<sup>®</sup> PU3660 and PU3663 (Alchemie Ltd., UK): Both of these polyurethane resin systems consisted of two components, which were mixed in the stoichiometric ratios of 100:120 and 100:100 (by weight) respectively. The mixed systems were degassed in a vacuum chamber at 70 kPa, and processed at room temperature for 6 hours and 24 hours respectively. These resin systems were only used to characterise the refractometer.

- (v) HexPly<sup>®</sup> 913 (Hexcel, UK): This epoxy resin was supplied in the form of a film. It is used as the matrix in helicopter blades at AgustaWestland. Preliminary tests were carried out to demonstrate the feasibility of using a Fresnel reflection sensor to monitor the cure process of this aerospace-grade resin system.

Source	Grade	Mixing ratio (by weight) resin:hardener	Processing temperature (°C)	Cure duration (Hours)
Huntsman Advanced Materials	LY3505/ XB3403	100:35	60	8
Promatech Ltd.	EpoTek <sup>®</sup> 310M	100:55	65	2
			Room temperature	24
Alchemie Ltd.	Alchemix <sup>®</sup> PU3660	100:120	Room temperature	6
	Alchemix <sup>®</sup> PU3663	100:100	Room temperature	18-24
Norland Products Inc.	NOA 68	1-part	(photo-cure)	0.167

**Table 3-1. A summary of the resin systems investigated.**

### 3.1.2. Optical fibres and associated equipment

The optical fibre sensors used in this study were fabricated in-house. Details of the individual sensors are given below and the typical optical fibre properties (specified by the manufacturers) are summarised in Table 3-2:

- (i) Fresnel reflection sensor for optical fibre-based refractive index measurements: Two types of Fresnel reflection sensors were used. One type employed multi-mode step-index optical fibres (Aomolin Ltd., China) with core and cladding diameters of 105 and 125  $\mu\text{m}$  respectively. The second type was fabricated using SMF-28™ single-mode optical fibres (Corning® Inc., USA) with core and cladding diameters of 8.3 and 125 ( $\pm 1$ )  $\mu\text{m}$  respectively.
- (ii) Transmission sensor for the acquisition of near-infrared spectra: Sections of a fused silica precision-bore capillary (VitroCom Inc., USA) with internal and external diameters of 128 and 300  $\mu\text{m}$  respectively were used to house multi-mode step-index optical fibres (Aomolin Ltd., China).
- (iii) Fibre Bragg grating sensor for the measurement of strain: Single-mode photo-sensitive PS1250/1500 fibres (Fibercore Ltd., UK) with core and cladding diameters of 10 and 125  $\mu\text{m}$  respectively, were used.

<b>Fibre Type</b>	<b>SMF-28™</b>	<b>Aomolin 105/125</b>	<b>PS1250/1500</b>
<b>Source</b>	Corning® Inc., USA	Aomolin Ltd., China [137]	Fibercore Ltd., UK
<b>Mode of transmission</b>	Single-mode	Multi-mode	Single-mode
<b>Numerical aperture</b>	0.13	0.22	0.12 – 0.14
<b>Refractive index of the core</b>	1.4675 at 1310 nm 1.4681 at 1550 nm	1.473	1.45 at 1550 nm
<b>Core diameter (µm)</b>	8.3	105	10
<b>Cladding diameter (µm)</b>	125 (±1)	125	125 (± 1)
<b>Coating diameter (µm)</b>	245 (±5)	245	245 (± 5%)
<b>Attenuation (dB/km)</b>	≤ 0.40 at 1310 nm ≤ 0.30 at 1550 nm	5 at 850 nm	120 at 1550 nm
<b>Coating material</b>	Acrylate (CPC6®)	Acrylate	Acrylate
<b>Price per metre (£GBP)</b>	£0.02	£1.28	£4.95

**Table 3-2. A comparison of the properties and cost of the single-mode and multi-mode optical fibres used to construct the sensors.**

In preparation for sensor fabrication, the distal ends of the optical fibres were stripped using a CFS-2 optical fibre stripper (Clauss, USA), cleaned using isopropanol and lint-free tissue, and cleaved at 90° ( $\pm 0.5^\circ$ ) using a high-precision CT-30 cleaver (Fujikura Ltd., UK). For most applications, the stripped region was approximately 10 mm in length and the cleaved end-face acted as the sensing surface.

An FSM-40PM fusion splicer (Fujikura, UK) was used to extend the length of the lead-out fibres of a sensor, or to connect a sensor to one of two types of pre-prepared connectors. These are generally referred to as sub-miniature adaptor (SMA) or fibre-optic connector/physical contact (FC/PC) connectors. Core-to-core alignment was used to create a permanent continuous optical path for transmission of optical pulses from one fibre length to the other. During this study, losses due to fusion splicing were typically in the range of 0.00 to 0.05 dB for both single-mode and multi-mode fibres.

### **3.1.3. Reinforcing fibres**

The reinforcing fibres used in this study were S-2 glass<sup>®</sup> 758 ZenTron<sup>®</sup> and S-2 glass<sup>®</sup> 463 (AGY, USA). These two types of S-glass fibres had a TEX of 2200 and 2033 respectively. Neither had a twist, and both had epoxy-compatible “sizing”. The average filament diameters were 25  $\mu\text{m}$  [138] and 9  $\mu\text{m}$  [139] respectively. The softening point of S-glass is 1050 °C and the refractive index of the bulk preform was 1.520-1.525 at 589 nm and 20 °C [140].

### **3.1.4. Chemicals**

The chemicals used throughout this study are summarised below. All of the chemicals listed were used in their as-received state for the following applications:

- (i) Acetone (Sigma-Aldrich Ltd., UK): This was used primarily for cleaning glass surfaces and removing residual resin;
- (ii) Isopropanol (Sigma-Aldrich Ltd., UK): The principal use of isopropanol was to remove any debris from the optical fibres once they had been stripped;
- (iii) Monobromonaphthalene (Sigma-Aldrich Ltd., UK): This was the contact liquid that was used on the Abbe refractometer;
- (iv) Frekote<sup>®</sup> 700-NC (Loctite<sup>®</sup>, USA): This release agent was applied in a wipe-on-wipe-off method to coat glass surfaces for the easy removal of cured resins;
- (v) Refractive index oils (Cargille Labs, USA): Standard refractive index oils in the range 1.40-1.57 were used for the calibration studies; and
- (vi) CVC 4 (GBR Technology Ltd., UK): This single-component silicone fluid was used for some preliminary calibration experiments.

### 3.1.5. Potting and sealing media

Other media used throughout the study for potting and sealing are detailed in Table 3-3.

<b>Brand/Grade</b>	<b>Source</b>	<b>Function</b>
EpoTek <sup>®</sup> 314 epoxy-amine resin	Promatech Ltd., UK	Potting
Opi-tec <sup>™</sup> 5007 epoxy resin	Intertronics, UK	Potting
UV403-T UV-curable resin	Shanghai Ji Yuan Ltd., China	Sealing
Silicone rubber (494-118)	RS Components Ltd., UK	Sealing
RTV 3140 silicone rubber	Dow Corning <sup>®</sup> , UK	Sealing

**Table 3-3. A summary of the media used for potting and sealing.**

## **3.2. EXPERIMENTAL PROCEDURES**

### **3.2.1. Thermocouple**

Type-K (chromel-alumel) twin-twist fine thermocouple wire (RS Components, UK) was used to make thermocouples to measure temperature. Each of the wires was 0.2 mm in diameter and insulated with polytetrafluoroethylene (PTFE). A section of the PTFE was stripped from each wire and a junction was formed between the ends of the two wires by applying a 1-Volt current through brass electrodes for 80 milliseconds, using a custom-made precision spot welder (University of Birmingham, UK). For data acquisition, approximately 10 mm of PTFE insulation was also stripped from the distal ends and the bare wires were connected to a SCXI-1303 terminal block that was fitted to a SCXI-1000 low-noise chassis (National Instruments Corporation (UK) Ltd.). The received signal was recorded using custom-written LabVIEW software.

### **3.2.2. Abbe refractometer**

In order to assess the feasibility of using refractive index as a method to follow the cross-linking process of a thermosetting resin system, a conventional Abbe refractometer was employed.

The refractive indices of liquid (eg. uncured resin systems) and solid (eg. resin films) samples were measured using a conventional High Accuracy 60/ED Abbe refractometer (Bellingham and Stanley Ltd., UK). The Abbe refractometer, as shown in Figure 3-1, can be operated in reflection or transmission mode using a sodium lamp, which emits monochromatic light at 589 nm.

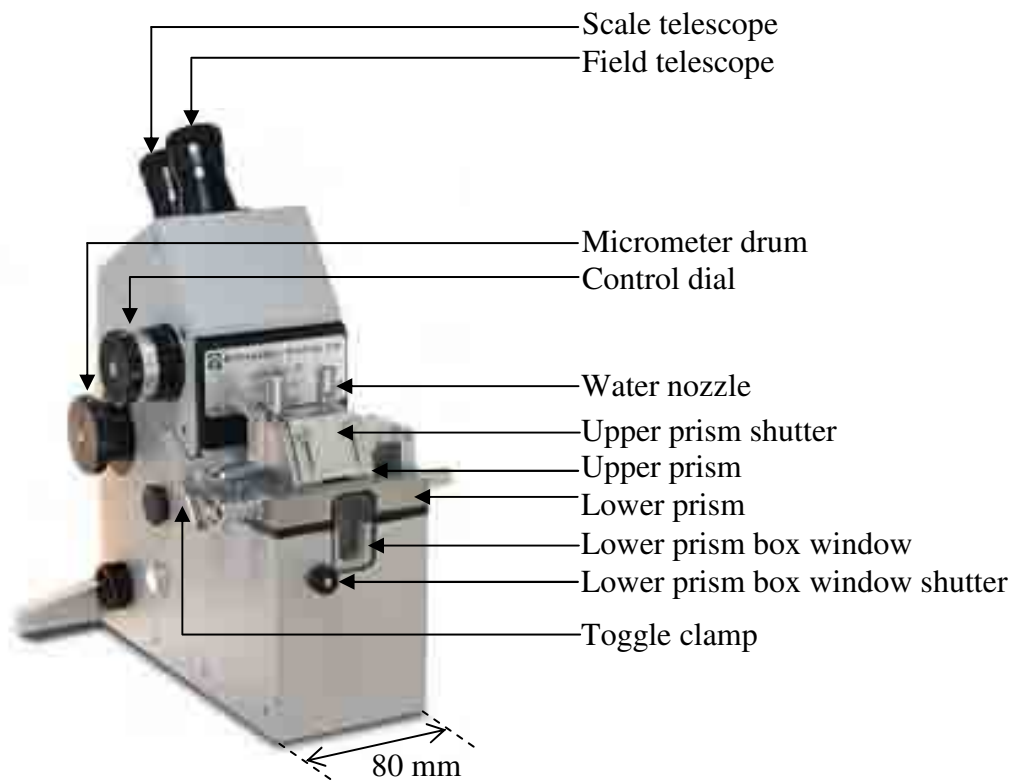


**Figure 3-1. A photograph of an Abbe 60 refractometer.**

The instrument essentially consists of an upper and a lower measurement prism, which are located within prism boxes. The refractometer was capable of measuring refractive indices in the range 1.30 to 1.74, to an accuracy of  $\pm 0.00004$  (within the temperature range of 5-75 °C with a temperature accuracy of  $\pm 0.5$  and a temperature stability of  $\pm 0.1$  [141]). In order to measure the refractive index, the samples were placed on the lower prism so that the entire prism area was covered, and the upper prism was clamped down onto the lower prism using a toggle clamp. In transmission mode, the sodium lamp was positioned such that the upper prism was illuminated, allowing light to refract through the sample into the lower prism for Abbe scale readings to be taken, as illustrated in Figure 3-2. The shutter for the lower prism box window was closed so that light only entered through the upper prism. Alternatively, in reflection mode, the sodium lamp was positioned such that the light transmitted through the

lower prism and internal reflection occurred at the interface between the lower prism and the sample (see Figure 3-2). Here, the upper prism shutter was closed so that the light only entered via the lower prism box window. During this research the refractive indices of liquid media were obtained using transmission mode, and reflection mode was used for solid samples and during the cure monitoring experiments. Measurements were made by adjusting the control dial and micrometer drum so that the borderline seen in the field telescope is aligned with the centre of the cross hairs. A reading was then obtained using a scale graticule graduated in linear divisions in the scale telescope. The refractive index value was determined from the Abbe scale reading using a calibration table. Between each measurement, the prisms of the refractometer were cleaned using isopropanol and dried using lint-free tissue.

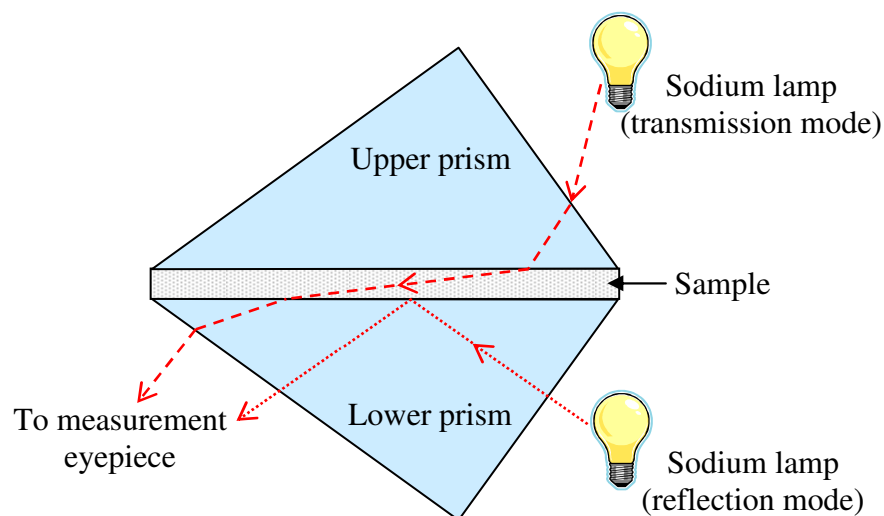


**Figure 3-2. A schematic diagram of the upper and lower prisms of the Abbe refractometer, showing the path of the light beam when operated in transmission or reflection mode.**

The Abbe refractometer was calibrated as outlined in the manual, using a precision-ground optical silica test-plate (Bellingham and Stanley Ltd., UK) and monobromonaphthalene contact liquid.

#### ***3.2.2.1. Refractive index measurement of liquid samples***

The refractive indices of the following liquids were measured using the Abbe refractometer: (i) distilled water; (ii) a series of reference refractive index oils (from here on these will be referred to as reference oils, followed by the refractive index value); (iii) the individual resin and hardener components of specified resin systems; and (iv) the mixed resin systems in the liquid-state.

The refractive indices of the CVC 4 silicone oil, reference oil 1.56, and the resin systems were evaluated as a function of temperature. Re-circulating water, from a temperature-regulated water bath (TE10D Tempette<sup>®</sup>, Techne, USA), was connected to the refractometer to maintain the prisms at the desired temperature. Polypropylene croffles were used in the water bath to reduce evaporation and heat loss. During a majority of the temperature ramp-hold experiments, the temperature was raised in 10 °C increments between room temperature (approximately 22 °C) and 70 °C, and held at each stage for a pre-determined time.

#### ***3.2.2.2. Refractive index measurement of solid samples***

Resin films were cast in order to measure the refractive indices of the resin systems after cross-linking. The films were fabricated by mixing the resin and hardener components in their stoichiometric ratio (see Table 3-1), followed by degassing in a vacuum chamber. A glass desiccator was used to hold the sample and a vacuum pump (Chas. Blatchford Ltd., UK) was connected to degas the resin system at 70 kPa for 20 minutes. The liquid mixture was then placed between two toughened glass plates which had been prepared with Frekote<sup>®</sup> release agent. The thickness of the films was controlled using four PTFE spacers of 1-2 mm

between the plates. The glass plates were then held together using miniature G-clamps. The assembly was placed vertically into a ULE 500 air-circulating oven (Mettmert GmbH, Germany) and cured according to the schedules recommended by the manufacturers, as detailed in Table 3-1. Once the resin films were fully solidified, the plates were removed and the films were cut with a blade to 4 x 2 mm samples for refractive index measurements. Monobromonaphthalene was used as the contact liquid between the resin film and the lower prism of the Abbe refractometer.

### 3.2.3. Cuvette-based experiments

Two different cuvettes were used to contain the reference oils and liquid resin. An open-ended de-mountable optical glass cuvette (Starna, UK), with dimensions of 45 mm x 12 mm and a 1 mm path-length (Figure 3-3), was used primarily for cure monitoring experiments. For calibration experiments, a PMMA cuvette (Sarstedt, Germany), with dimensions of 45 mm x 10 mm x 10 mm was used.

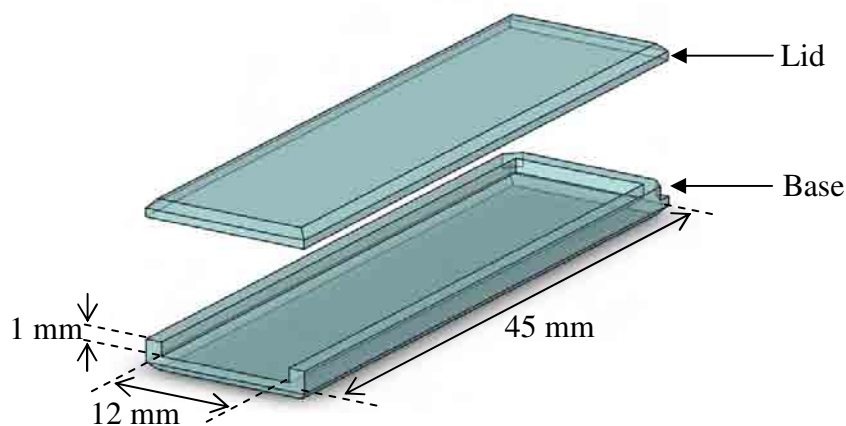


**Figure 3-3. An illustration of a de-mountable cuvette, with a 1 mm path-length.**

With respect to the de-mountable cuvette, the inner walls of the base and lid were cleaned with isopropanol and prepared with Frekote<sup>®</sup> release agent between each use, for easy

removal of the cured samples. The two components of the cuvette were sealed together along three edges using 494-118 silicone rubber, and left to set for approximately three hours. The de-mountable cuvette was used for a majority of the experiments involving fibre-optic sensors, details of which are given later in this chapter.

The PMMA and de-mountable cuvettes were housed in a TLC 50F™ fibre-optic temperature-controlled cuvette holder (Ocean Optics Inc., UK), as illustrated in Figure 3-4. The temperature of the holder was capable of being regulated to  $\pm 0.02$  °C in the range -55 to +105 °C by a thermoelectric device and a TC 125™ microprocessor-controlled Temperature Controller (Quantum Northwest Inc., USA), which was externally controlled through a PC. A water source was connected to the hose barb via tubing of 3 mm inside diameter. Water flow was provided from a submersible pump in a reservoir of distilled water. A second hose barb and tube was used for return flow. With reference to Figure 3-4, the collimating lens assembly and fibre-optic probes were used for conventional transmission FTIR spectroscopy experiments, which are discussed in Section 3.2.5.

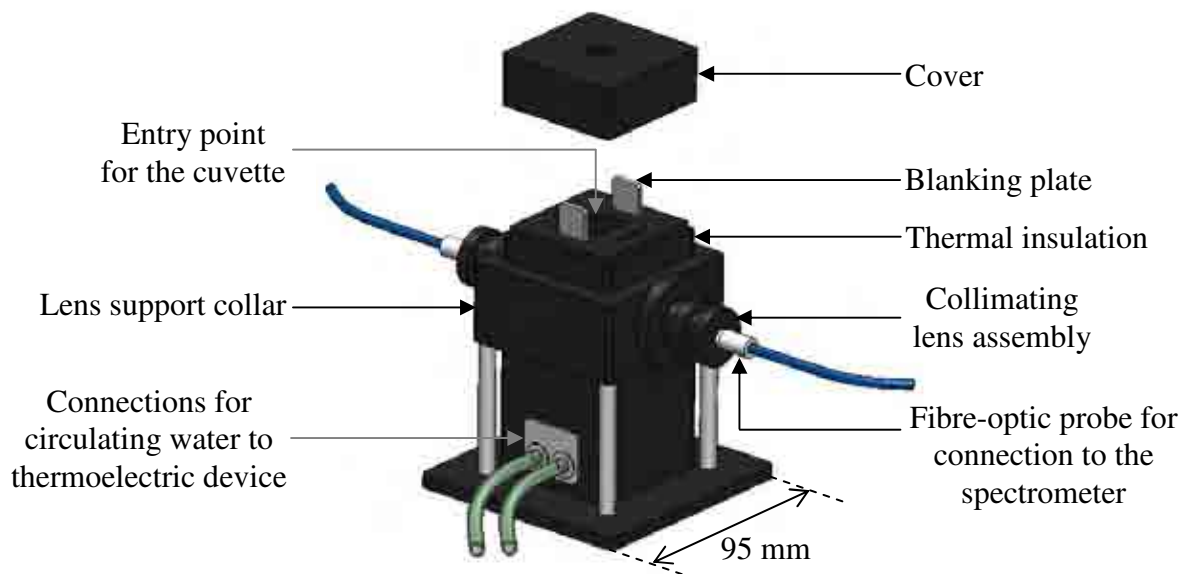


**Figure 3-4. A schematic illustration of the temperature-controlled cuvette holder which was used to house the cuvettes.**

### **3.2.4. Optical fibre sensor fabrication and interrogation**

#### **3.2.4.1. Fresnel reflection sensor**

In the context of the current work, a Fresnel reflection sensor is essentially a 2x2 fibre-optic coupler where the distal fibre-ends are perpendicularly cleaved, as illustrated in Figure 3-5 a and b. These micrographs show the quality of the cleave that was achieved, and that is required for a Fresnel reflection sensor. The fibres were stripped and cleaved as detailed in Section 3.1.2.

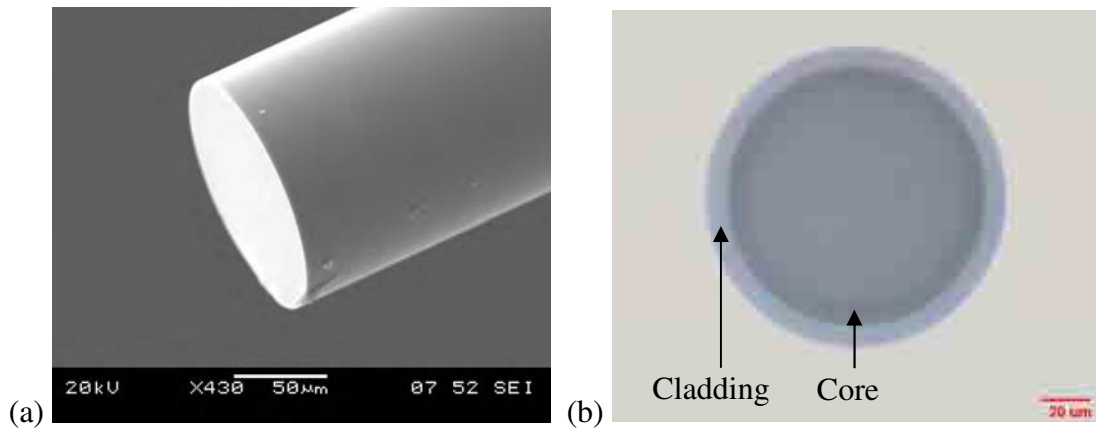


**Figure 3-5. Micrographs of the stripped and cleaved end-face of a multi-mode optical fibre, showing (a) the side-view and (b) the end-on view.**

Two types of fibres were used to construct the Fresnel reflection sensors: multi-mode step-index and single-mode. These were detailed in Table 3-2. The fibre-optic couplers were fabricated in-house using a commercially-available coupler fabrication rig (Joinwit<sup>®</sup>, China). In the multi-mode set-up, the fibre was used to transmit light from a Mikropack HL-2000 tungsten halogen light source (Ocean Optics, USA), which operated in the range 360-2000 nm. The reflected light was directed to a C5460-01 photodiode detector (Hamamatsu Photonics, Japan) through a multi-mode 2x2 coupler. The data were logged using a data acquisition system and custom-written software, as detailed in Section 3.2.1. A schematic diagram of the configuration is shown in Figure 3-6. The red and purple arrows indicate the direction of the transmitted and reflected light respectively.

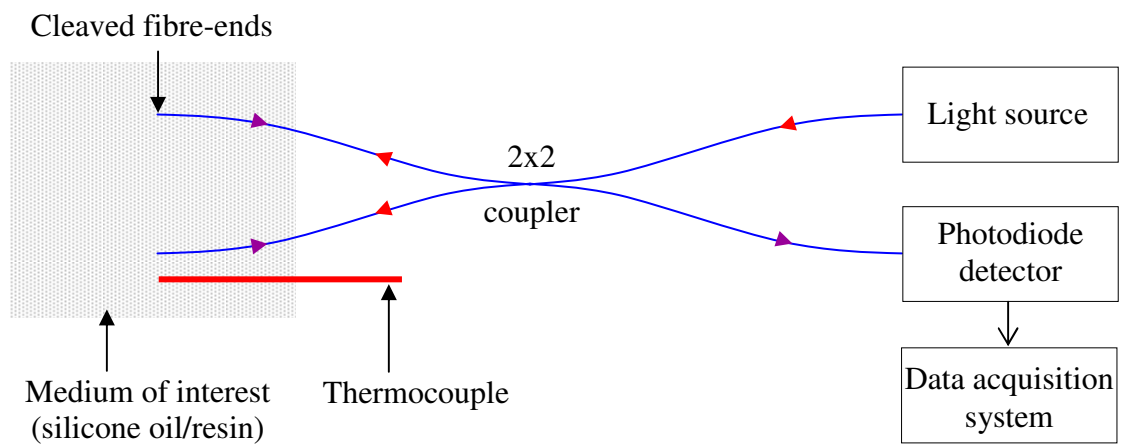


**Figure 3-6. A schematic diagram of a typical configuration of a Fresnel reflection sensor and its interrogation system.**

The experimental set-up for the single-mode Fresnel reflection sensor was the same as that illustrated in Figure 3-6. However, in this case the light source was a 1550 nm modular laser diode (ILX Lightwave, USA) and the reflected light was directed, via a single-mode 2x2 coupler, to an InGaAs photodiode detector (Thorlabs Ltd., UK). The detector was connected to a PDA 200 photodiode amplifier (Laser 2000, UK), which in turn was connected to a SR560 low-noise preamplifier (SRS, UK) to filter the high frequency noise created by the amplifier.

The light output and input fibres of the multi-mode and single-mode configurations were terminated using SMA 905 and FC/PC connectors (Thorlabs Ltd., UK) respectively. The fibres were potted in the connectors using Opi-tec™ 5007 (Intertronics, UK) epoxy resin. Once the resin was cured in the ferrule of the connectors, the fibres were polished using an SMA or FC fixture and 1 µm diamond paste on an APC-8000 automatic polisher (Senko, UK).

The distal fibres of the Fresnel reflection sensor were secured to the inner wall of the base of the de-mountable cuvette using a drop of UV-curable resin to create a bond between a section of the un-stripped region of the fibres and the glass surface. The adhesive was photo-cured using a UV75 Light (Thorlabs Ltd., UK), which operates over the range 300-425 nm.

#### *3.2.4.1.1. Stability of the light source*

The stability of the light source in a typical multi-mode Fresnel reflection set-up, as shown in Figure 3-6, was studied by connecting one of the distal fibres to a digital optical PM120 power meter (Thorlabs Ltd., UK) via an SMA connector. The power meter consisted of a S120A Silicon Sensor Power Head (Thorlabs Ltd., UK) with an SM1SMA Fibre Adaptor (Thorlabs Ltd., UK), which were mounted on a BA2 Mounting Base (Thorlabs Ltd., UK). This assembly was connected to a PM100 Display Unit (Thorlabs Ltd., UK) to give a reading of the optical power transmitted through the connected fibre. The other distal fibre and a thermocouple were suspended centrally in a PMMA cuvette, and the sensing fibre end-face and thermocouple tip were immersed in reference oil 1.46. The cuvette was placed in the temperature-controlled cuvette holder at room temperature. The temperature and intensity of the reflected Fresnel reflection signal were measured over a maximum of 15 hours.

The stability of the light source was also evaluated by connecting a fibre directly between the light source and power meter via SMA connectors.

#### *3.2.4.1.2. Temperature stability*

The stability of the temperature within the de-mountable cuvette was evaluated by using the same set-up as shown in Figure 3-6. CVC 4 silicone oil and reference oil 1.57 were used for the temperature stability experiments. Individual experiments were carried out involving either a multi-mode or single-mode Fresnel reflection sensor secured in a de-mountable

cuvette, adjacent to a thermocouple, as illustrated in Figure 3-7. The fibre-ends and tip of the thermocouple were aligned at the mid-point of the cell length; approximately 22 mm from the open-end of the cell. Two types of experiments were undertaken where the temperature and Fresnel reflection were recorded whilst: (i) the cuvette holder was maintained at one temperature for an extended period; and (ii) the temperature of the cuvette holder was increased in equal increments and held constant between stages for a minimum of 20 minutes.

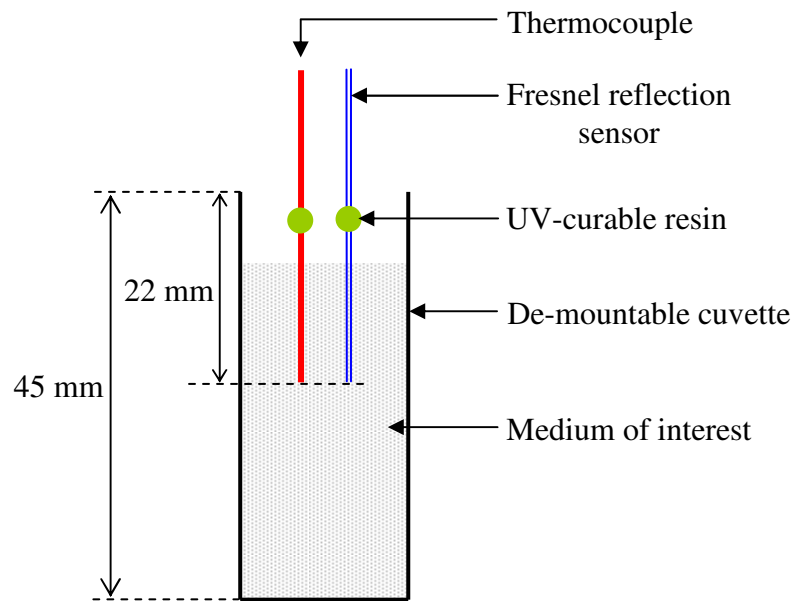


**Figure 3-7. A schematic (master) diagram to show the arrangement of a thermocouple and Fresnel reflection sensor in a de-mountable cuvette.**

A number of variations in the spatial arrangements of the sensor(s) and thermocouple were investigated. Figure 3-7 represents a master diagram and reference is made to this in the subsequent sections (to avoid repetition).

#### *3.2.4.1.3. Cure monitoring using a Fresnel reflection sensor*

For Fresnel reflection experiments involving the cross-linking of resin systems, a de-mountable cuvette was assembled in the same manner as shown in Figure 3-7. The cuvette holder was initially set to 30 °C; after the resin system had been introduced into the cuvette,

the temperature was increased to the required isothermal value. The Fresnel reflection signal and temperature data were monitored for the entire cross-linking process.

In order to compare the signals produced by the multi-mode and single-mode Fresnel reflection sensors, the sensors were employed simultaneously. The two distal fibres of each sensor were secured in a de-mountable cuvette, separated by a thermocouple; with reference to Figure 3-7, in the current case, the thermocouple was secured centrally with a Fresnel reflection sensor either side. Approximately 0.45 ml of LY3505/XB3403 resin system was injected into the cell via a syringe and needle, and the response of the sensors was evaluated during a series of isothermal cross-linking experiments at 50, 60 and 70 °C.

Research carried out by other members of the Sensors and Composites Group showed the presence of a kink periodically along the epoxy conversion curve during the cross-linking of LY3505/XB3403 resin system. The term “conversion” was defined in Section 2.3.1.1. Therefore, in order to investigate possible causes for the observed kink, the following series of experiments were undertaken:

- (i) *Sensor location and bonding conditions:* The effects of mechanical influences, such as spatial positioning, were considered by varying the location of the multi-mode Fresnel reflection sensor within the de-mountable cuvette. In these experiments, the cross-linking process of the LY3505/XB3403 resin system was monitored at 70 °C using each of the arrangements illustrated in Appendix A;
- (ii) *Mechanically-induced vibrations:* The effect of mechanically-induced vibrations on the distal fibres of a single-mode Fresnel reflection sensor was investigated to simulate accidental contact with the experimental set-up. The two distal fibres of a single-

mode Fresnel reflection sensor were fed through a hole that was drilled in a PTFE cuvette lid and secured in place using NOA 68 resin. The PTFE lid was clamped in a retort stand so that a 140 mm fibre-length was suspended centrally below the lid. The fibres were mechanically excited at six separate locations; three approximately 30 mm below the PTFE lid and at different locations around the circumference of the fibres, and three on the PTFE lid. This configuration is illustrated in Appendix A (Figure AA-1g); and

- (iii) *Instrumentation factors:* Instrumentation-related factors were assessed by making alterations to the experimental set-up such as those listed below:
- (a) The light source was altered;
  - (b) The 2x2 coupler was changed from a custom-made to a commercial device; and
  - (c) The input connection to the SCXI-1303 terminal block; was swapped in a systematic manner.

In each case, the medium used was CVC 4 oil and the temperature was maintained at 30 °C.

#### *3.2.4.1.4. Feasibility studies using the Fresnel reflection sensor*

Preliminary experiments were carried out to demonstrate the feasibility of using a Fresnel reflection sensor to characterise the cross-linking of other classes of resin. The first resin system assessed was an aerospace-grade epoxy/amine resin that is used in the manufacture of helicopter rotor blades (AgustaWestland, UK). The second resin system was a photo-curable thermoset which was selected to represent a dental resin. The experimental details associated with these feasibility studies are presented in Appendix B.

#### *3.2.4.2. Near-infrared transmission sensor*

Several methods for fabricating a transmission sensor were considered, the most suitable of which is detailed below.

The transmission sensor was fabricated in two stages. Firstly, a holding fixture was constructed from three 10 mm sections of fused silica precision-bore capillary with inner and outer diameters of 128  $\mu\text{m}$  and 300  $\mu\text{m}$  respectively. A stripped, sacrificial optical fibre was fed through two of the capillaries to align them, and the cleaved ends of the capillaries were positioned 2-3 mm apart along the fibre. The third capillary was placed against the first two in such a way as to bridge the gap. UV403-T resin was used to secure the whole assembly. In the second stage, the sacrificial fibre was removed and the fixture was used to house two multi-mode sensing fibres. The distal ends of both multi-mode fibres were stripped by approximately 11-12 mm, cleaned and cleaved at 90°. The two fibres were fed through the two aligned capillaries so that the cleaved fibre-ends were parallel, and a single-axis translation stage (Thorlabs Ltd., UK) was used to create a gap of approximately 500  $\mu\text{m}$ . This is the cavity where the resin system was introduced for transmission spectra to be obtained. The fibres were secured at their entry points into the capillaries using UV403-T resin, as illustrated in Figure 3-8.

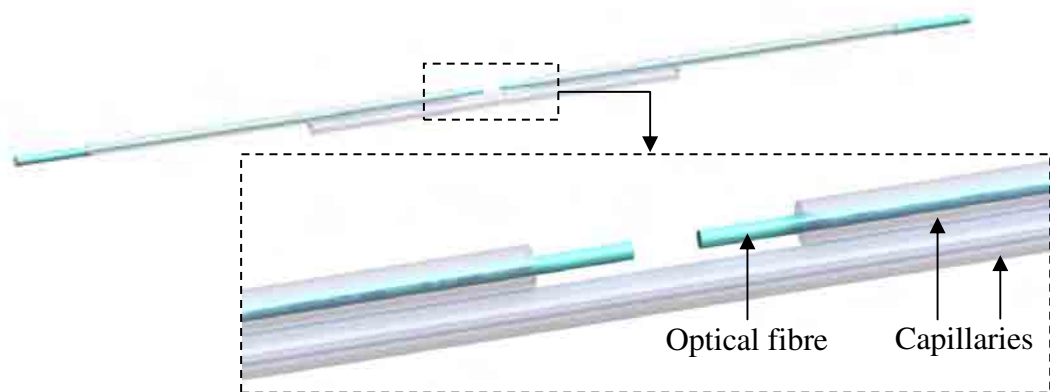


**Figure 3-8. An illustration of the transmission sensor, where two optical fibres were aligned using a fixture fabricated from three sections of capillary. The insert shows a magnified view of the sensing region.**

The distal ends of the two sensing fibres were each spliced (as detailed in Section 3.1.2) to a pre-prepared SMA connector which consisted of a multi-mode optical fibre potted using the method described in Section 3.2.4.1. The sensor was coupled to the light source and detector of a MATRIX™-F duplex FTIR spectrometer (Bruker Optics Ltd., UK). The spectrometer was programmed to operate in the near-infrared region between 11000 and 4000  $\text{cm}^{-1}$ . Spectra were collected at a resolution of 4  $\text{cm}^{-1}$  over 64 scans. A background spectrum was taken in air before the resin system was introduced.

The sensor was aligned along the side wall of a de-mountable cuvette and secured using UV-curable resin, with the stabilising capillary adjacent to the side wall. This is illustrated schematically in Figure 3-9. The resin system was injected into the cuvette and the temperature of the cuvette holder was altered accordingly. The resin systems investigated were LY3505/XB3403 and EpoTek® 310M (see Table 3-1).

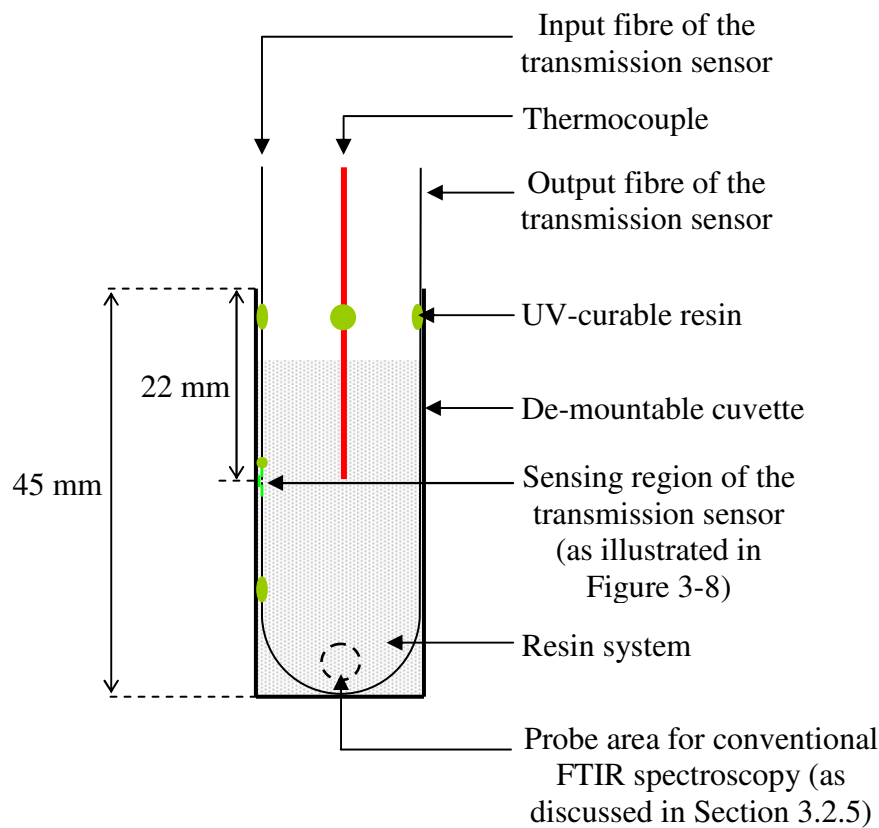


**Figure 3-9. A schematic diagram of a de-mountable cuvette containing a transmission sensor and a thermocouple.**

### ***3.2.4.3. Fibre Bragg grating sensor***

The phase-mask technique was used to inscribe the Bragg gratings for the FBG sensors used in this study. Short lengths (~300 mm) of Germania-Boron (Ge-B) co-doped single-mode photo-sensitive optical fibre (PS1250/1500) were used for the fabrication of the FBG sensors. A 20 mm section of the acrylate coating was stripped at a distance of 20-40 mm away from the fibre-end. The stripped section was magnetically clamped to a 3-axis translation stage and positioned directly beneath a 1555 nm fused silica phase-mask (QPS Photonics Inc., Canada). A 1560 nm phase-mask was also used. The incident beam from a Braggstar 500 (Coherent Inc., UK) krypton fluoride (KrF) excimer laser, operating at 248 nm, was directed

onto the phase-mask by a mirror. The gratings were produced using a pulse repetition rate of 500, with a pulse energy of 10 mJ and a pulse frequency of 20 Hertz. An illustration of an FBG sensor is shown in Figure 3-10. Typically, the mode field diameter is engineered within the photo-sensitive fibre to allow splicing to standard telecommunications fibres with minimal excess loss. Therefore, the FBG sensor was fusion spliced to a spool of SMF-28™ optical fibre, which in turn was connected to an IS7000 FBG Interrogation System (FiberPro Inc., US) via an FC/APC connector. The IS7000 Interrogation System operated with a broadband light source which had a central wavelength of 1548 nm and a 40 nm spectral bandwidth. Reflection spectra were recorded using LabVIEW software. In the current study, the FBG sensor was used for the hyphenated experiments.

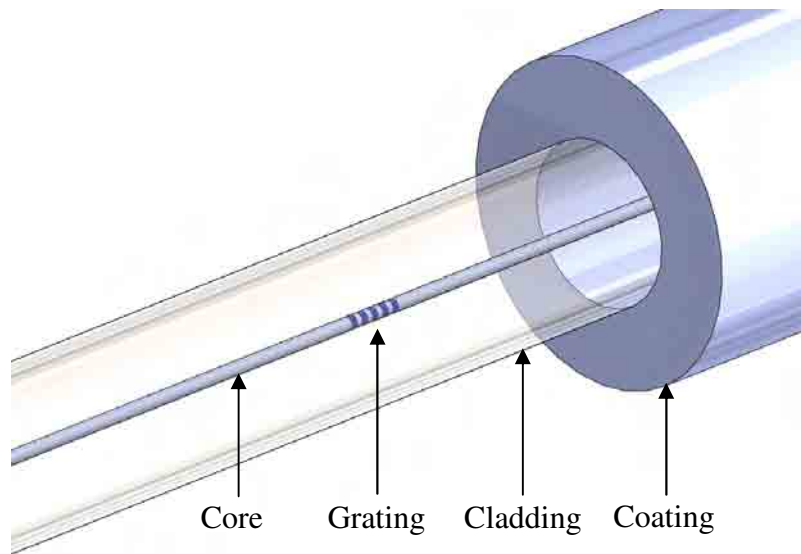


**Figure 3-10. An illustration of the Bragg grating inscribed on the core of an optical fibre (FBG sensor).**

### **3.2.5. Conventional transmission FTIR spectroscopy**

In the context of the current work, conventional transmission FTIR spectroscopy refers to the situation where spectra were obtained using a non-contact technique rather than an optical

fibre sensor. A de-mountable cuvette was placed into the cuvette holder, and the medium of interest was injected. Two SMA-terminated 600  $\mu\text{m}$ -diameter fibre-optic probes (Ocean Optics, UK) were connected to the collimating lens assembly of the holder at  $90^\circ$  to the face of the cuvette, as illustrated in Figure 3-4. The opposite ends of the probes were connected to the light source and detector ports of the FTIR spectrometer. Light was transmitted from one probe, through the 1 mm path-length of the cuvette and received by the second probe. In Figure 3-9, the position of the light beam from the probe which traverses the cuvette is indicated by a dotted circle. Spectra of the individual components of the LY3505/XB3403 and EpoTek<sup>®</sup> 310M resin systems were obtained.

### **3.2.6. Evanescent wave spectroscopy**

The chemical process monitoring of composite materials has been considered in this study through the development of evanescent wave spectroscopy. As previously alluded to, the interface between the reinforcing fibres and the resin matrix can provide quantitative information on the cross-linking kinetics.

#### ***3.2.6.1. Sample preparation***

In order to remove the sizing that was applied to the S-2 glass<sup>®</sup> fibres during the manufacturing process, fibre lengths of 200 mm were cut from the spool and heat-treated at 500 °C for four hours.

In order to enable optimum light transmission the fibre bundle was terminated with SMA connectors and polished. The bundle-ends were each inserted into an SMA connector with an inner bore of 1.4 mm, and RTV 3140 silicone rubber was used to seal the bundle and position the SMA connectors at the required sample length. The silicone rubber was applied to the

fibres at the insertion point to the SMA connectors and acted as a seal to prevent the potting resin impregnating the bulk of the sample. The silicone rubber was cured for 24 hours at room temperature. The epoxy resin and amine hardener components of EpoTek<sup>®</sup> 314 were mixed in their stoichiometric ratio (see Table 3-3) and used to pot the fibre bundle in the SMA connectors. The resin was cured at 120 °C for 3 hours. Once cured, the bonded fibre-ends were cut with a blade to approximately 2 mm from the edge of the SMA connector. The sample ends were then polished to optical quality using the APC-8000 automatic polisher. An image of a potted and polished S-2 glass<sup>®</sup> fibre bundle can be seen in Figure 3-11.

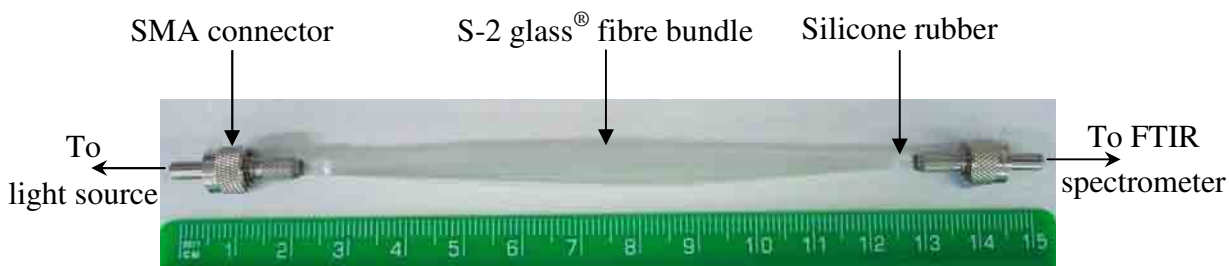


**Figure 3-11. A photograph of a 150 mm S-2 glass<sup>®</sup> fibre bundle, terminated with SMA connectors.**

### **3.2.6.2. Light transmission**

In order to estimate the intensity of light transmission through the fibre bundles, samples of 80, 100, and 150 mm in length were fabricated. Samples of each length were produced using two different types of S-glass fibres; S-2 glass<sup>®</sup> 758 ZenTron<sup>®</sup> and S-2 glass<sup>®</sup> 463, as detailed in Section 3.1.3.

The output port of a WLS100 broadband fibre-coupled white light source (Bentham Instruments Ltd., UK) was supplied with a female SMA fixture, which was positioned so that

it was longitudinally aligned with the FTIR spectrometer ports. The fibre bundle was coupled directly to the light source and FTIR spectrometer via the SMA connectors. The light source was turned on for a minimum of 30 minutes to allow it to stabilise. The signal amplitude was also allowed to stabilise once the sample was connected, and the value was then recorded. Each sample was disconnected and re-connected at both the light source and spectrometer four times to ensure consistent results.

### ***3.2.6.3. Temperature-control***

A two-part heating block was custom-made to accommodate a 150 mm long fibre bundle terminated at both ends by SMA connectors. A 20 mm wide x 5 mm deep recess along the length of the bottom part of the heating block was included in the design to accommodate the fibre bundle. An illustration of the two-part heating block is shown in Figure 3-12a. Both parts of the heating block had an inlet and outlet connection for the circulation of water via a GR150 stirred thermostatic water bath (Grant Instruments (Cambridge) Ltd., UK). Glass wool was used to insulate the outsides of the heating block, and both parts were entirely covered in adhesive-backed PTFE film.

It was found that the recess manufactured in the heating block was too deep to ensure even impregnation of the fibre bundle. To attempt to alleviate this issue, a simple platform was fabricated from a 110 x 18 x 2 mm strip of aluminium, engineered to fit into the recess. A moat was created around the perimeter of the platform using the PTFE film; the PTFE boundary was 0.73 mm deep along the length, to contain the resin, and approximately 0.24 mm deep along the width, where the fibre bundle exits the heating block. A schematic illustration of the platform is shown in Figure 3-12b.

The temperature at the centre of the heating block was measured during a temperature ramp-hold experiment using a thermocouple. The aluminium platform was placed in the recess and the thermocouple was secured to the PTFE boundary at approximately the mid-point of one of the long sides. A second thermocouple was secured outside of the heating block to monitor the external air temperature. The temperature of the water bath was raised from room temperature to 30 °C and then to 70 °C in 10 °C increments, with a dwell of around 30 minutes at each temperature.

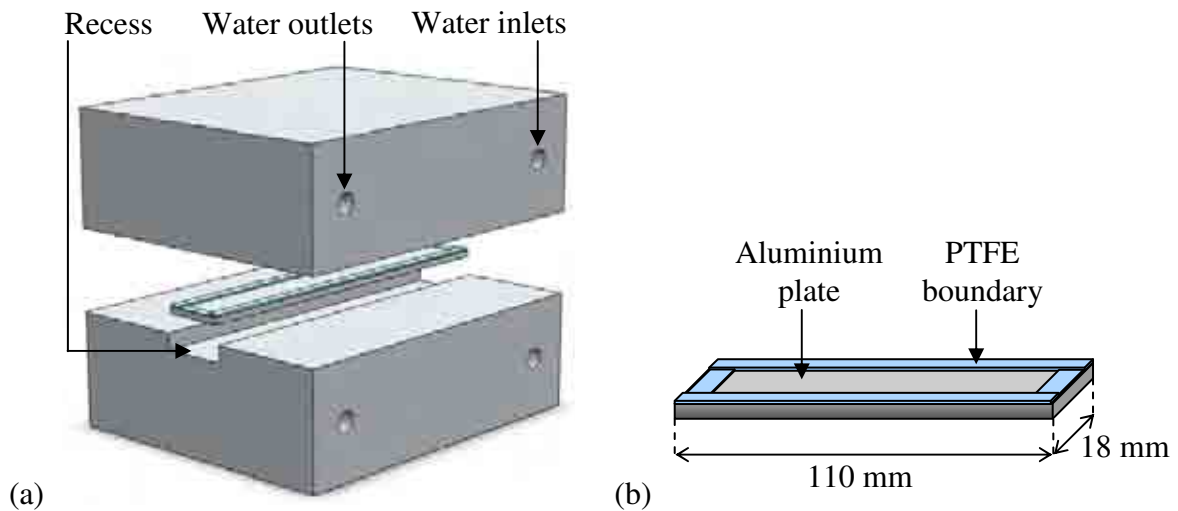


**Figure 3-12. Illustrations of (a) the two-part heating block, also showing the aluminium platform; and (b) the aluminium platform for the fibre bundle.**

To investigate the temperature variation within the heating block five thermocouples were evenly spaced along the length of the aluminium platform. One thermocouple was secured in the centre of the platform, two were positioned 3 mm from the ends, and two were approximately 23 mm from the ends. The temperature of the water bath was increased from 30 °C to 70 °C in 10 °C increments, with a dwell of 30 minutes at each stage.

#### ***3.2.6.4. Cure monitoring using evanescent wave spectroscopy***

Evanescent wave spectroscopy was undertaken using 150 mm S-2 glass<sup>®</sup> 758 fibre bundles, as shown in Figure 3-11. The fibre bundle was placed in the heating block, supported by the aluminium platform. A thermocouple was secured to the centre of the platform, and in contact with the fibres. The fibre bundle was coupled directly to the light source. The opposite end of the bundle was connected to the FTIR spectrometer via an SMA-SMA mating sleeve (Thorlabs Ltd., UK) and fibre-optic probe. The FTIR spectrometer was programmed to record spectra at a resolution of  $4\text{ cm}^{-1}$  over 128 scans. The top part of the heating block was paired to the bottom and the water bath was heated to  $30\text{ }^{\circ}\text{C}$ . A background spectrum of the sample in air at  $30\text{ }^{\circ}\text{C}$  was obtained. Degassed EpoTek<sup>®</sup> 310M resin system was then introduced to the fibre bundle, and evanescent wave spectroscopy was used to monitor the cure process at 35, 45, 55 and  $65\text{ }^{\circ}\text{C}$ .

#### **3.2.7. Hyphenated techniques for monitoring cross-linking reactions**

For hyphenated experiments which involve the Abbe refractometer it was necessary to make modifications to the refractometer to protect the prisms from the cross-linked resin system. Custom-cut SF-14 optical glass slides (Schott Jenaer Glas GmbH, Germany) of  $75.6 \times 25 \times 1$  mm were used as they had the same refractive index as the measurement prism (1.76). These glass slides were used to construct “cells” to contain the resin system; the custom-cut slide was used as one half of the cell and a standard borosilicate microscope slide (VWR International, UK) of the same dimensions was used as the other. The slides were prepared with release agent and a 1 mm spacer made of adhesive-backed PTFE film (4 mm wide) separated the two slides along both sides and across the bottom of the cell. The top remained

open as an entry point for the resin system and 494-118 silicone rubber was used to seal the cell along the three spaced sides.

Prior to discussing the integration of the various sensor systems into the custom-made cell, the relative positions of the individual sensors are illustrated in Figure 3-13. An overview of the associated interrogation systems is shown in Figure 3-14.

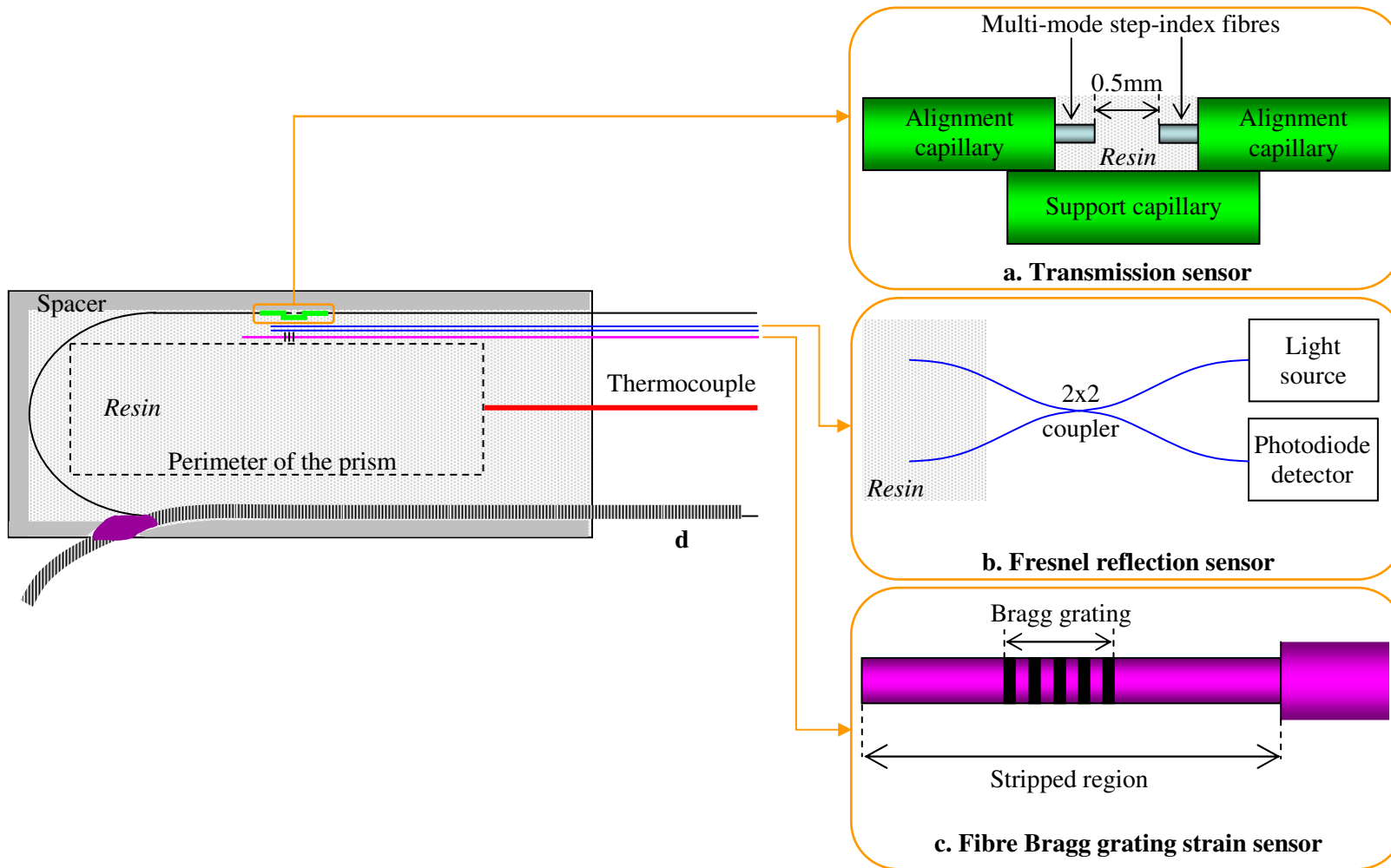


**Figure 3-13.** A schematic illustration of the custom-made cell used on the Abbe refractometer for the hyphenated experiments. The cell contains the three optical fibre sensor configurations shown in the expanded views: (a) transmission sensor, (b) Fresnel reflection sensor, and (c) FBG sensor. (d) represents the S-glass fibre bundle which was used for evanescent wave spectroscopy.

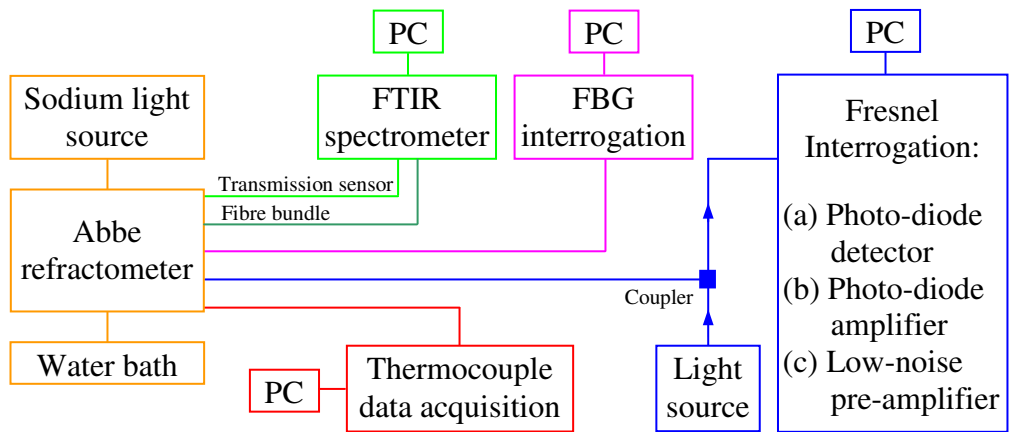


**Figure 3-14. An overview of the experimental set-up for the hyphenated experiments which were based on the Abbe refractometer. The equipment used for interrogating each of the sensors is also indicated.**

To accommodate the cell it was necessary to modify the Abbe refractometer. An adaption was made to the hinge between the upper and lower prism boxes to allow the upper prism box to close parallel to the lower prism box whilst the cell was between them. The adaption is pictured in Figure 3-15.

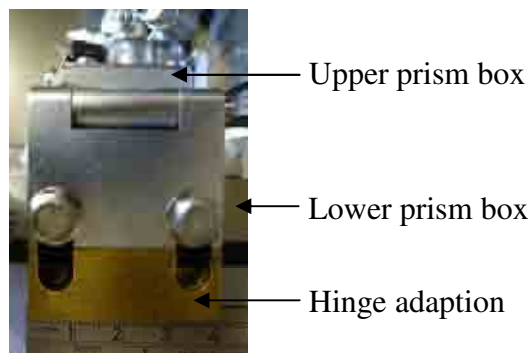


**Figure 3-15. An image of the adaption to the refractometer hinge to allow accommodation of the custom-made cell.**

In order to determine if there was any effect on the refractive index measurement when using the glass slides and release agent, three different experiments were carried out on the Abbe

refractometer. The refractive indices of five different oils were measured (i) in the conventional method, (ii) within a cell that was constructed using the method above but not prepared with release agent, and (iii) within a cell that had been prepared with release agent before construction.

#### ***3.2.7.1. Integration of the Fresnel reflection sensor on the Abbe refractometer***

A series of experiments were carried out to establish the effect on refractive index measurements of having the distal fibres of a Fresnel reflection sensor infringing on the measurement prism of the Abbe refractometer. The fibres were secured directly on the lower prism box and extended approximately 20 mm onto the lower prism, as illustrated in Figure 3-16. A thermocouple was also secured next the prism. Two drops of CVC 4 silicone oil were applied to the lower prism and the temperature of the water bath was increased from room temperature to 30 °C and subsequently to 40, 50, 60 and 70 °C. The temperature was held at each stage for an extended period. Using the Abbe refractometer, the refractive index was measured in 1-minute intervals for 10 minutes at each stage, once the temperature was stable.

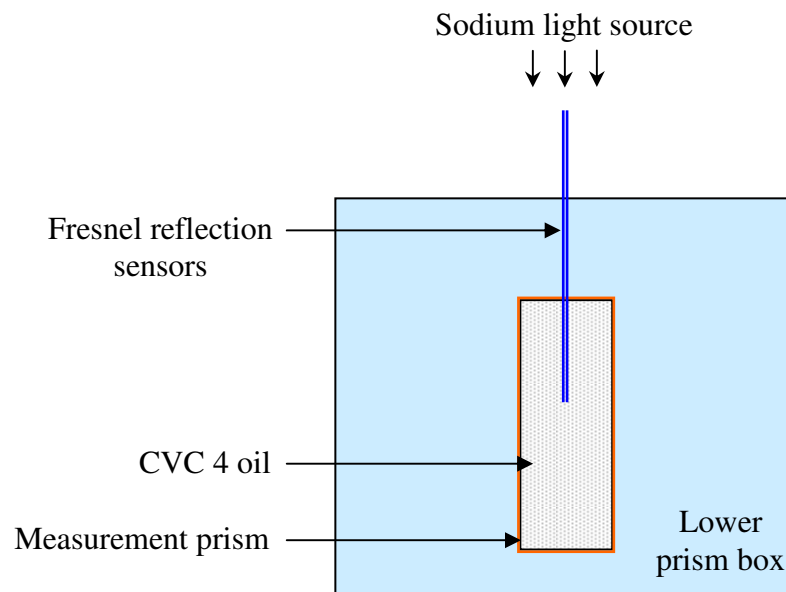


**Figure 3-16. A schematic diagram showing the set-up used to establish the effect on the refractive index measurement of optical fibres infringing on the refractometer measurement prism.**

### ***3.2.7.2. Hyphenated cure monitoring on the Abbe refractometer***

A custom-made cell was constructed according to the method described at the beginning of Section 3.2.7. A transmission sensor was aligned at the mid-point of the cell length. A single-mode Fresnel reflection sensor was secured near the opposite cell wall, with the cleaved fibre-ends aligned with the transmission sensor. As illustrated in Figure 3-17, both sensors were located outside the perimeter of the measurement prism, so that refractive index measurements could also be obtained. The LY3505/XB3403 resin system was injected into the cell and was cured at 50, 60 or 70 °C.

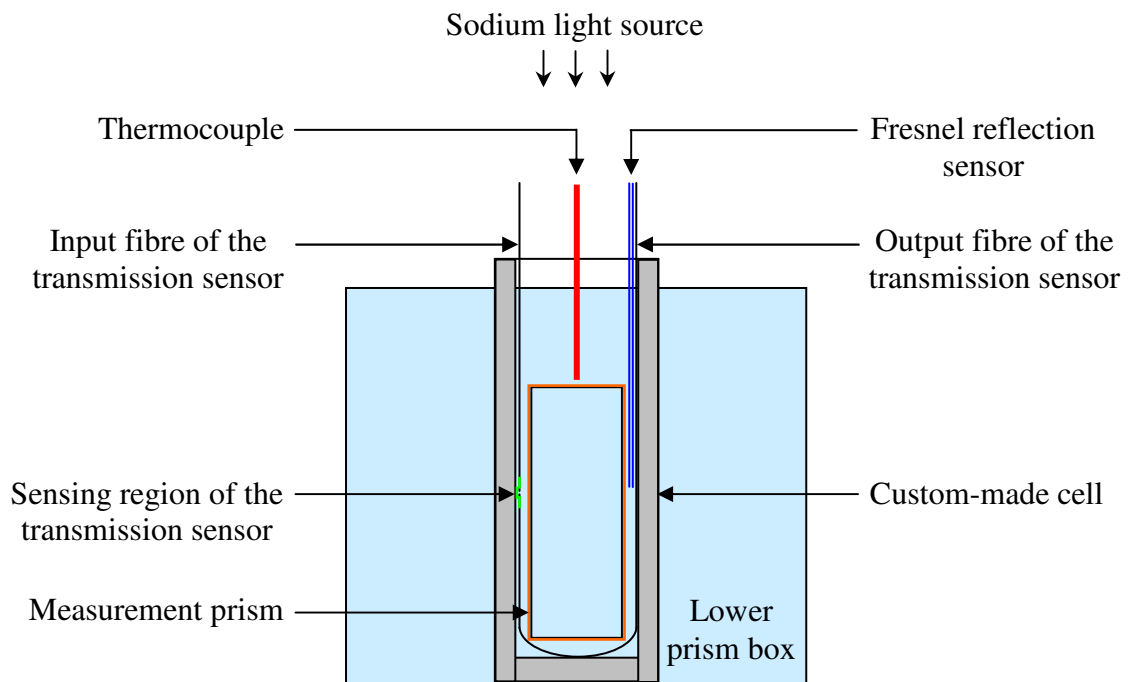


**Figure 3-17. A schematic illustration of the custom-made cell housing a Fresnel reflection sensor, a transmission sensor and a thermocouple on the Abbe refractometer.**

With reference to Figure 3-13, in this instance the S-2 glass<sup>®</sup> fibre bundle and FBG sensor were not present. Instead the space occupied by the bundle was used for the Fresnel reflection sensor, and the spacer was continuous.

### ***3.2.7.3. Hyphenated cure monitoring on the Abbe refractometer including a fibre bundle***

Experiments were initially carried out directly on the refractometer (i.e. without the custom-made cell) to establish the effect on refractive index measurements when the lower prism is partly obstructed. This was to simulate what effect part-coverage of the prism by a fibre bundle would have. Polyester high-temperature Flash FT25BS tape (Amber Composites Ltd., UK) was used to cover a 2 mm strip of the prism length; this is schematically illustrated in Figure 3-18a. Two drops of reference oil 1.57 were applied to the prism using a glass

dropper, and the refractive index was measured. In a second experiment, 2 mm of the entire perimeter of the prism was covered (Figure 3-18b), and the procedure was repeated.

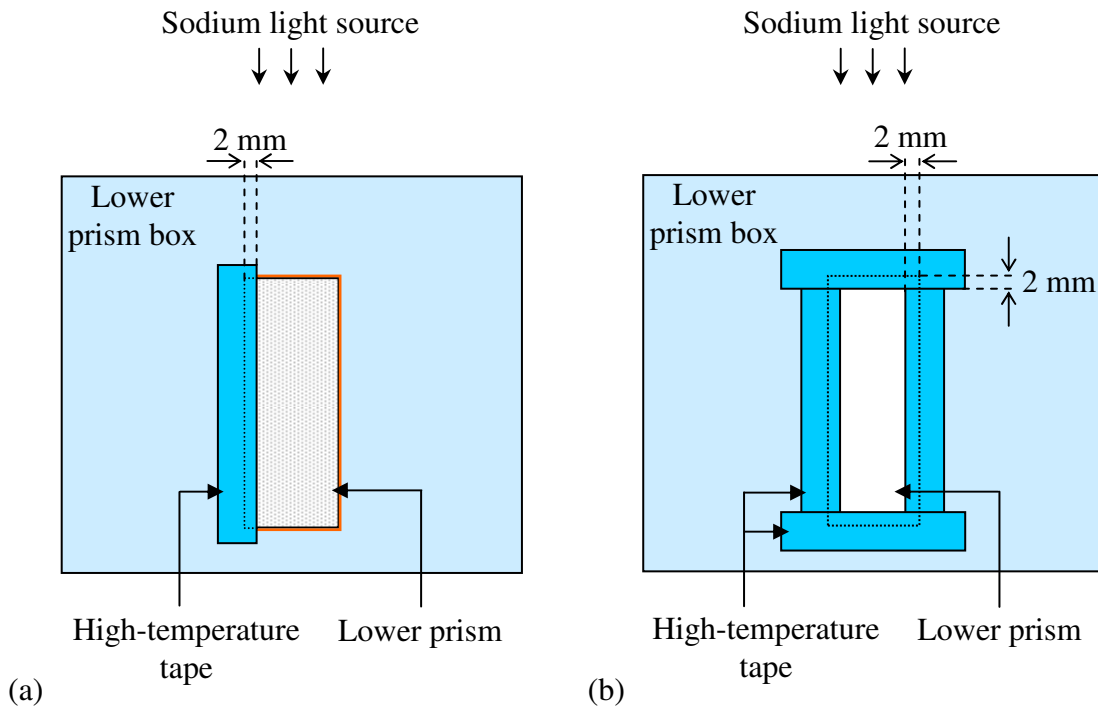


**Figure 3-18. Part-coverage of the refractometer prism using high-temperature tape to simulate part-coverage by a fibre bundle on: (a) one length of the prism and (b) the perimeter of the prism.**

In order to accommodate a series of optical fibre sensors and an SMA-terminated fibre bundle, a custom-made cell was constructed in a similar manner as described previously. The spacer in this configuration had a break approximately 20 mm from the bottom of the cell (see Figure 3-13 and Figure 3-19). The gap in the spacer was 5 mm and curved so as to exclude any arrises. This was for the fibre bundle to exit the cell so that it could be connected to a fibre-optic FTIR probe; the opposite end of the bundle exited the cell at its opening. The curvature of the gap was made very shallow so that light attenuation was affected as little as

possible, but also so that maximum bundle-length remained in the resin system. At the exit point, clear silicone rubber was used to seal the bundle and the gap to prevent resin seepage. On the opposite side of the cell a transmission sensor, Fresnel reflection sensor and FBG sensor were secured. To avoid any possible light interference between the sensors, the Fresnel reflection sensor fibre-ends were located below the receiving fibre of the transmission sensor, and the cleaved end of the FBG sensor was positioned away from the Fresnel reflection sensor fibre-ends, as illustrated in the expanded view in Figure 3-19.

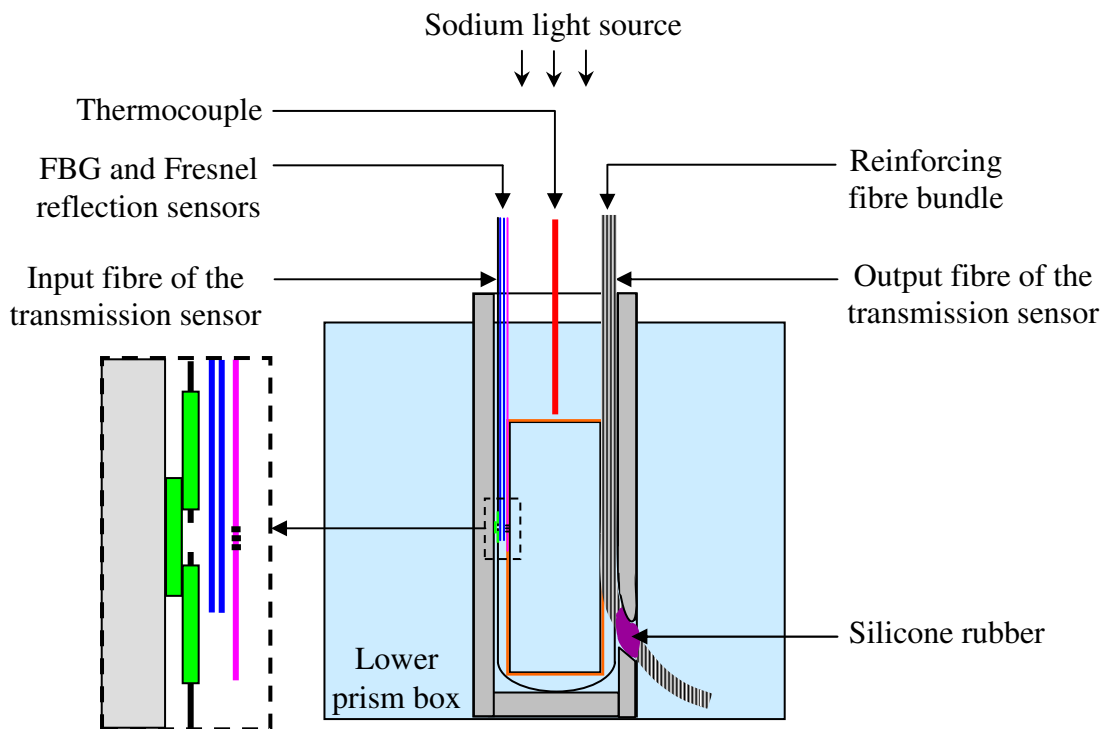


**Figure 3-19. A schematic illustration of a custom-made cell housing a Fresnel reflection sensor, a transmission sensor, an FBG sensor, a fibre bundle and a thermocouple on the Abbe refractometer. The expanded view shows the relative locations of the sensing regions of the optical fibre sensors.**

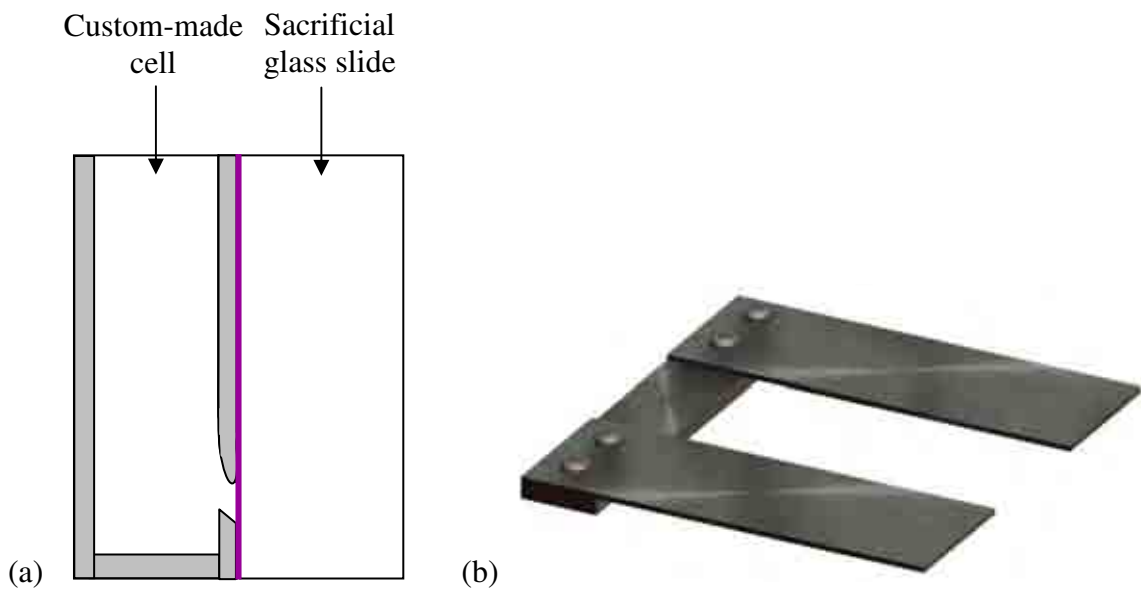
A series of experiments were undertaken to investigate if the light transmitted by the transmission sensor and Fresnel reflection sensor had an effect on the output of the FBG sensor. The cell was positioned on the refractometer and the water bath set to 30 °C. The response of the FBG in air was recorded continuously whilst the light sources of the transmission sensor and Fresnel reflection sensor were switched in the following regime, with a dwell period at each stage of approximately 5 minutes:

<b>FBG</b>	<b>Transmission</b>	<b>Fresnel</b>
Off	Off	Off
On	Off	Off
On	On	Off
On	On	On
On	Off	On
On	Off	Off

**Table 3-4. Regime for switching the light sources of the FBG, Fresnel reflection and transmission sensors on/off to study the effect of the light transmitted by each sensor on the output of the FBG sensor.**

Several modifications were made to the architecture of the experiment to protect the equipment and minimise temperature gradients. Firstly, a sacrificial glass slide was fixed adjacent to the custom-made slide of the cell with silicone rubber. This configuration is illustrated in Figure 3-20a; for clarity the sensors have not been depicted. This served the purpose of supporting the fibre bundle on its exit part-way along the cell, thereby reducing any kinks in the fibres and minimising light attenuation. It also acted to protect the

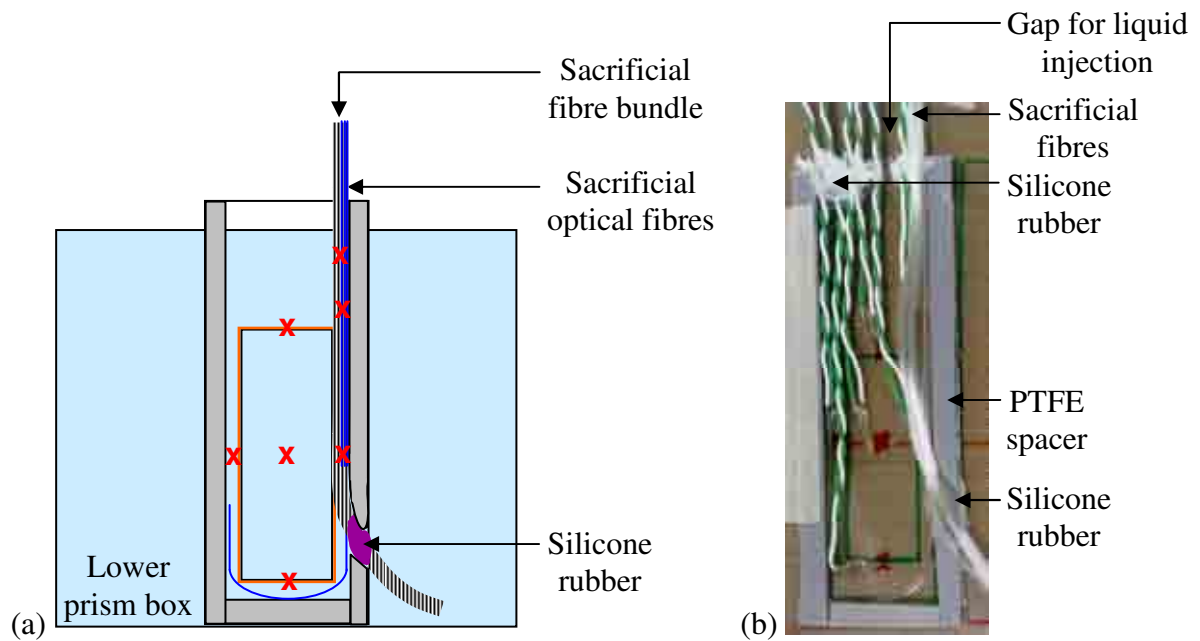
refractometer from any potential resin leakage. This assembly was succeeded by a custom-made metal fixture (shown in Figure 3-20b), which was designed to sit either side of the cell and underneath the part of the cell that was overhanging the lower prism box. It served to: (i) transfer heat to the custom-made slide; (ii) support the fibre bundle; (iii) protect the refractometer; and (iv) keep the cell centrally located over the measurement prism. The fixture and all of the metal components of the Abbe refractometer were covered with thin foil-backed polystyrene for insulation, and a floral foam block (Hobbycraft, UK) was placed over the upper prism box, which also covered the overhang of the cell/fixture.



**Figure 3-20. Schematic illustrations of two of the modifications made to the hyphenated technique in order to accommodate the fibre bundle, showing (a) a custom-made cell adhered to a sacrificial slide and (b) a custom-made metal fixture.**

The temperature variation within the custom-made cell and across the area of the measurement prism was studied by securing seven thermocouples within the cell, as illustrated in Figure 3-21a and b. Sacrificial optical fibres and a reinforcing fibre bundle were

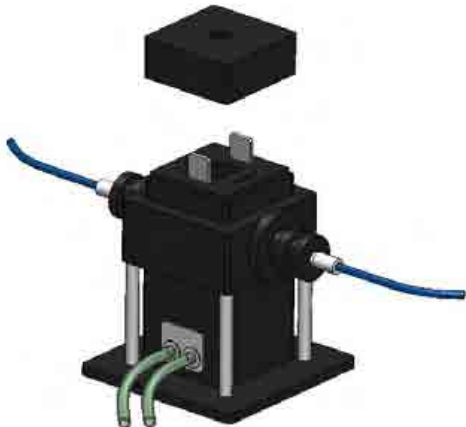
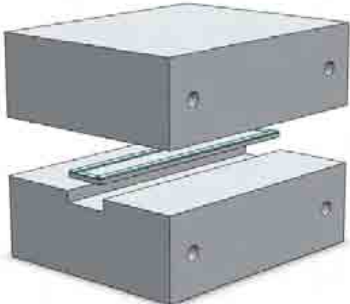
also secured in the cell to simulate the sensors used in the cure experiment. Part A of the EpoTek<sup>®</sup> 310M resin system was introduced into the cell and the temperature of the water bath was increased from 30 to 70 °C in 10 °C increments. Two separate experiments were carried out to study the temperature – firstly, whilst there were no modifications to the working architecture, and secondly whilst the metal fixture and insulation were in place.



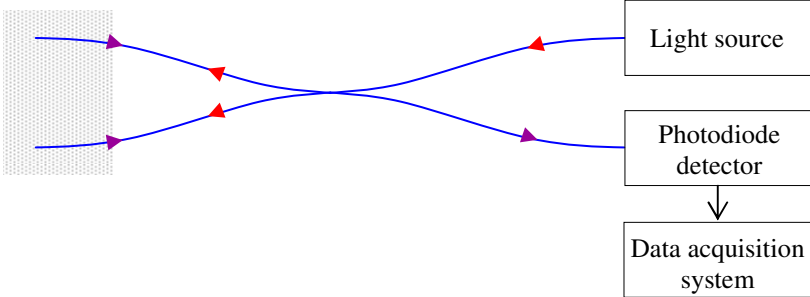
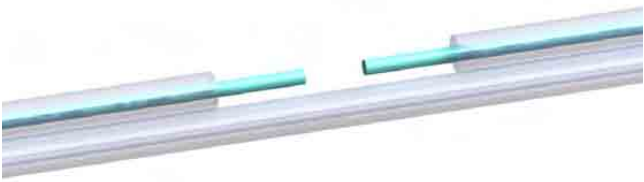
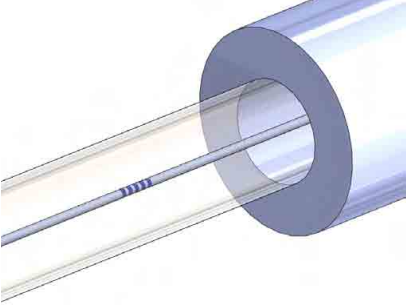
**Figure 3-21. A (a) schematic illustration and (b) photograph of a custom-made cell containing seven thermocouples (the length of the cell is 75.6 mm), to monitor the temperature variation within the cell.**

EpoTek<sup>®</sup> 310M resin system was used for the cure experiments that involved a fibre bundle as it had a lower refractive index than the LY3505/XB3403 resin. This meant that evanescent wave spectroscopy could be carried out, whereby the EpoTek<sup>®</sup> 310M resin system acted as the cladding. The resin system was injected into the cell and was cured at 45, 55 and 65 °C, followed by a cooling cycle.

Since three heating methods and four sensor designs were employed, summaries of these are presented in Table 3-5 and Table 3-6 respectively for ease of reference. A thermocouple was used in all experiments, but is not represented in Table 3-6.

Heating method	Schematic illustration/photograph
Temperature-regulated cuvette holder	
Two-part heating block	
Abbe refractometer	

**Table 3-5. A summary of the heating methods used for the curing of resin systems.**

Sensor design	Schematic illustration/photograph
Fresnel reflection sensor	
Transmission sensor	
Evanescent wave sensor	
Fibre Bragg grating sensor	

**Table 3-6. A summary of the sensor designs used to monitor the cure of resin systems.**

## 4. RESULTS AND DISCUSSION

The data in this chapter have been colour-coded to indicate the equipment or sensor design that was used. This was performed to aid the reader with visualisation, particularly when discussing the hyphenated experiments. The following coding was used:

- (i) Refractive index via the Abbe refractometer – orange;
- (ii) Thermocouple – red;
- (iii) Fresnel reflection sensor – blue;
- (iv) FTIR transmission sensor – light green;
- (v) FTIR evanescent wave sensor – dark green;
- (vi) FBG sensor – purple.

However when multiple data from the same sensor system are presented, for example when different temperatures were used, the colour-coding is indicated in the legend.

In general the calculated standard deviations are presented in parentheses after the corresponding average value for the dataset. A zero standard deviation is cited as (-).

As stated previously, the reference refractive index oils are referred to as reference oils, followed by the refractive index value.

### 4.1. ABBE REFRACTOMETER

#### 4.1.1. Refractive index measurements of liquid samples

The refractive indices of eight reference oils measured on the Abbe refractometer is summarised in Table 4-1. The measurements were carried out at room temperature and the temperature on the refractometer display module was recorded. The measured refractive

index values were temperature-corrected accordingly using Abbe Utility software (Bellingham and Stanley Ltd., UK). The data are reported to five decimal places as the accuracy of the refractometer is stated to be  $\pm 0.00004$ . The average measured refractive index values were plotted against the values given by the manufacturer for each of the oils, and are shown in Figure 4-1. The standard deviation was calculated and the error bars are included in Figure 4-1, but are negligible.

<b>Temperature during measurement (°C)</b>	<b>Oil refractive index (manufacturer)</b>	<b>Oil refractive index (measured)</b>
17.0	1.400 ( $\pm 0.0002$ )	1.40330 ( $\pm 0.00059$ )
17.0	1.420 ( $\pm 0.0002$ )	1.42341 ( $\pm 0.00022$ )
17.0	1.450 ( $\pm 0.0002$ )	1.45281 ( $\pm 0.00097$ )
17.0	1.460 ( $\pm 0.0002$ )	1.46216 ( $\pm 0.00075$ )
17.0	1.480 ( $\pm 0.0002$ )	1.48305 ( $\pm 0.00106$ )
17.0	1.510 ( $\pm 0.0002$ )	1.51281 ( $\pm 0.00008$ )
21.7	1.540 ( $\pm 0.0002$ )	1.54031 ( $\pm 0.00045$ )
21.7	1.570 ( $\pm 0.0002$ )	1.57056 ( $\pm 0.00002$ )

**Table 4-1. The refractive index values of reference oils as stated by the manufacturer, and as measured on the Abbe refractometer at room temperature.**

A linear regression line was fitted in Figure 4-1, and an excellent correlation is observed between the measured values and those reported by the manufacturer.

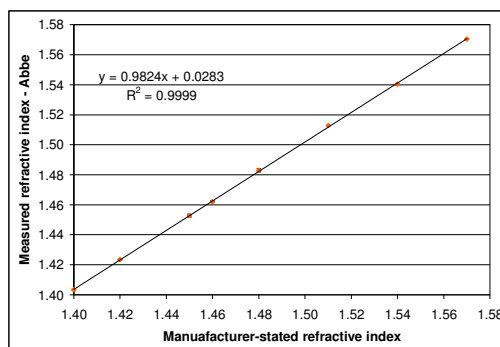


**Figure 4-1. Refractive indices of reference oils, as given by the manufacturer and as measured on the Abbe refractometer.**

The measured refractive indices of: (i) distilled water; (ii) CVC 4 silicone oil; (iii) the individual resin and hardener components of LY3505/XB3403, EpoTek<sup>®</sup> 310M and EpoTek<sup>®</sup> 314 resin systems; and (iv) the mixed resin systems of LY3505/XB3403, EpoTek<sup>®</sup> 310M and 314, and Alchemix<sup>®</sup> PU3660 and PU3663 in the liquid-state are given in Table 4-2. On average, ten repeat experiments were carried out for each medium. Although the polyurethane resin systems were not used for the study of cross-linking in the current research, they were used here in the initial screening of resin systems that could potentially be used. The selection criteria were based on: (i) the ease of casting and impregnation of the glass fibre bundles; (ii) Health and Safety protocols in terms of toxicity and COSHH requirements; and (iii) the shelf-life.

Average temperature during measurement (°C)	Medium	Measured refractive index
20.1 (-)	Distilled water	1.33302 ( $\pm 0.00002$ )
30.1 ( $\pm 0.05$ )	CVC 4 silicone oil	1.55315 ( $\pm 0.00003$ )
24.1 (-)	LY3505 resin	1.57532 ( $\pm 0.00004$ )
23.5 (-)	XB3403 hardener	1.44562 ( $\pm 0.00002$ )
23.9 (-)	EpoTek <sup>®</sup> 310M part A	1.49619 ( $\pm 0.00006$ )
23.8 (-)	EpoTek <sup>®</sup> 310M part B	1.49885 ( $\pm 0.00009$ )
24.0 (-)	EpoTek <sup>®</sup> 314 part A	1.49727 ( $\pm 0.00003$ )
23.6 (-)	EpoTek <sup>®</sup> 314 part B	1.40128 ( $\pm 0.00002$ )
30.7 (-)	LY3505/XB3403 resin system	1.53182 ( $\pm 0.00008$ )
30.6 (-)	EpoTek <sup>®</sup> 310M resin system	1.49206 ( $\pm 0.00003$ )
24.4 ( $\pm 1.02$ )	EpoTek <sup>®</sup> 314 resin system	1.49008 ( $\pm 0.00066$ )
20.4 ( $\pm 0.75$ )	Alchemix <sup>®</sup> PU3660 resin system	1.48793 ( $\pm 0.00077$ )
20.2 ( $\pm 0.54$ )	Alchemix <sup>®</sup> PU3663 resin system	1.46972 ( $\pm 0.00096$ )

**Table 4-2. Refractive indices of liquid media measured on the Abbe refractometer.**

**Standard deviation values have been quoted, where (-) represents a zero value.**

The refractive indices of EpoTek® 310M and EpoTek® 314, as stated by the manufacturer, are 1.497 (at 589 nm and 23 °C) [142] and 1.4939 (at 589.3 nm) [143] respectively. The measured data for these resin systems, as shown in Table 4-2, correlate well with these values. The refractive indices for the LY3505/XB3403, PU3360 and PU3663 resin systems were not reported by the respective manufacturers.

During a temperature ramp-hold experiment on the Abbe refractometer the values of the refractometer display module and a thermocouple located between the prism boxes were recorded. The medium used was CVC 4 silicone oil. During the hold periods (10 minutes), the average values were calculated and are plotted in Figure 4-2 as a function of the set-temperature of the water bath. Linear trend lines have been fitted to the data; the slopes of the trend lines are similar but it can be seen that the thermocouple consistently records a slightly higher value than the Abbe refractometer. The difference between the two datasets at 30 and 70 °C were 1.7 and 1.1 °C respectively. The heating rate was calculated from the thermocouple data to be 3.46 °C/minute ( $\pm 0.04$ ).

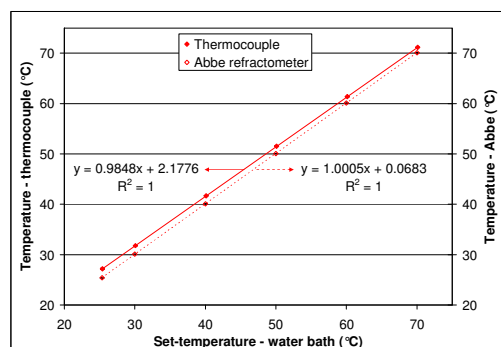


**Figure 4-2. Temperature data for the isothermal-hold periods from the refractometer and thermocouple as a function of the water bath set-temperature, during a temperature ramp-hold experiment using CVC 4 silicone oil.**

During the same experiment, the refractive index of the oil was monitored every 1-minute during the dwell at each temperature. These values were averaged and are plotted as a function of the thermocouple temperature in Figure 4-3a.

The refractive index of reference oil 1.56 was measured in the same manner at 30, 40, 50, 60 and 70 °C, and the results are presented in Figure 4-3b as a function of the set-temperature. In Figure 4-3a and b the standard deviations of the refractive index data were also calculated and error bars are plotted, but are negligible. A linear trend line was fitted to each of the data sets, and the negative slopes indicate that refractive index decreases with an increase in temperature. The equations embedded in the graphs show this relationship for these media. As described in Chapter 2, the decrease in refractive index with a rise in temperature is due to the change in the density of the liquid.

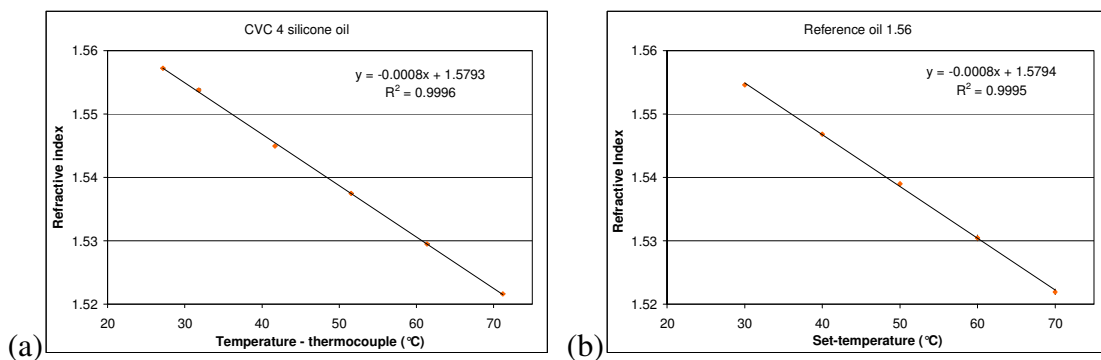


**Figure 4-3. Refractive index values measured during the temperature ramp-hold of (a) CVC 4 silicone oil and (b) reference oil 1.56.**

This experiment was repeated for LY3505 resin and EpoTek<sup>®</sup> 310M (part A), and similar trends were observed. The refractive indices of the mixed LY3505/XB3403 and EpoTek<sup>®</sup>

310M resin systems in the liquid-state were measured on the Abbe refractometer at 30, 40, 50, 60 and 70 °C. These values are presented in Figure 4-4 a and b for LY3505/XB3403 and EpoTek® 310M respectively. As with the silicone oils, the error bars have been plotted but are negligible, and linear relationships are observed between refractive index and temperature. The dwell at each temperature was in the order of one minute to ensure that the resin system did not cross-link on the refractometer prisms. However, it needs to be appreciated that some cross-linking of the resin would have been likely but it is difficult to avoid this with experiments of this nature.

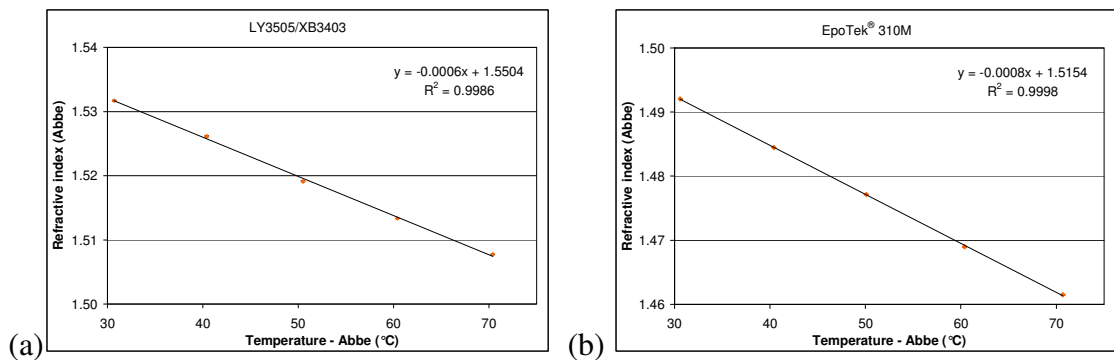


**Figure 4-4. Refractive indices of (a) LY3505/XB3403 and (b) EpoTek® 310M in liquid-state with increasing temperature.**

#### 4.1.2. Refractive index measurement of solid samples

Table 4-3 summarises the refractive indices of resin films measured on the Abbe refractometer. The far left column indicates the temperature at which the resin films were cured; all of the refractive index measurements were carried out at room temperature. On comparing the refractive indices of the resin systems before undergoing cross-linking (presented in Table 4-2) to the values of cured resin systems (Table 4-3), it can be determined that the refractive index increases when the liquid is transformed to a solid. This is due to the

increase in density of the material when the cross-linked network is formed during the reaction of the resin and hardener components (as discussed in Chapter 2).

<b>Processing temperature (°C)</b>	<b>Medium</b>	<b>Measured refractive index</b>
70	LY3505/XB3403 resin system	1.57036 ( $\pm 0.00007$ )
65	EpoTek <sup>®</sup> 310M resin system	1.52096 ( $\pm 0.00010$ )
50	Alchemix <sup>®</sup> PU3660 resin system	1.50400 ( $\pm 0.00011$ )
70	Alchemix <sup>®</sup> PU3663 resin system	1.49307 ( $\pm 0.00007$ )

**Table 4-3. Refractive index values of resin films measured on the Abbe refractometer at room temperature.**

In summary, it has been demonstrated that there is a good correlation between the refractive index values of the reference oils measured using an Abbe refractometer and the values reported by the manufacturer. The refractive indices are observed to reduce as the temperature of the liquid is increased. There was an overall increase in the refractive index of the epoxy and polyurethane resin systems from the pre- to post-cured states. The standard deviation values which have been reported demonstrate that the measurements made on the Abbe refractometer are reproducible.

The remainder of this chapter is divided into three sections consisting of: (i) optical fibre sensors; (ii) evanescent wave spectroscopy; and (iii) hyphenated techniques for monitoring

cross-linking reactions. The following section discusses the use of optical fibre sensors for measuring the refractive index of selected media, and FTIR spectra of two resin systems.

## **4.2. OPTICAL FIBRE SENSORS**

### **4.2.1. Fresnel reflection sensor**

The design used for the Fresnel reflection sensor was based on a 2x2 coupler where the distal ends were cleaved and immersed in the liquid of interest. This configuration was used in preference to the others discussed in Chapter 2 for the following reasons:

- (i) This sensor design uses standard telecommunication fibres and therefore the costs are relatively low;
- (ii) The fabrication of the sensor did not involve any complicated procedures to de-clad the fibre;
- (iii) The time taken to prepare the sensors is limited to stripping and cleaving, which are routine operations for optical fibres. The costs associated with strippers and cleavers are also low;
- (iv) Although the instrumentation used in the current study was elaborate (pre-amplifier, low-noise pre-amplifier etc.), a single unit amplifier has recently become available (Thorlabs Ltd., UK).

#### ***4.2.1.1. Stability of the light source***

As this was an intensity-based technique, it is important to establish the stability of the light source. Figure 4-5 represents the optical power transmitted through a multi-mode optical fibre when it was connected between the light source and power meter via SMA connectors. The data was recorded from when the light source was switched on, so the initial drop in the data can be attributed to the stabilisation period of the equipment. With reference to Figure

4-5 the transmitted signal of the light source was deemed stable for the duration of a typical cure experiment involving LY3505/XB3403 and EpoTek<sup>®</sup> 310M resin systems.

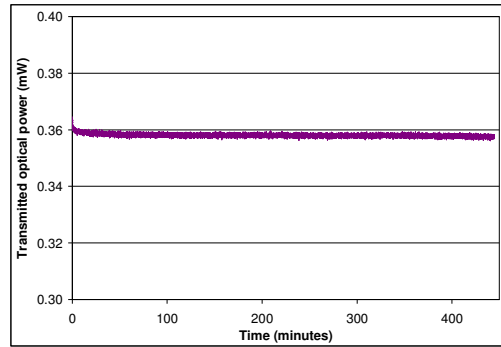


**Figure 4-5. The transmitted optical power as a function of time, through a multi-mode optical fibre when it was connected between a light source and power meter.**

Figure 4-6a-c show the data obtained during four different stability experiments where one distal arm of a multi-mode Fresnel reflection sensor was connected to the optical power metre. The other distal fibre-end and a thermocouple were immersed in reference oil 1.46 and data was collected at 1 Hz. The transmitted power, Fresnel reflection and temperature data were each averaged over the duration of the experiments and are plotted with error bars in Figure 4-6a, b and c respectively. The duration of the four experiments is specified on each of the scatter graphs.

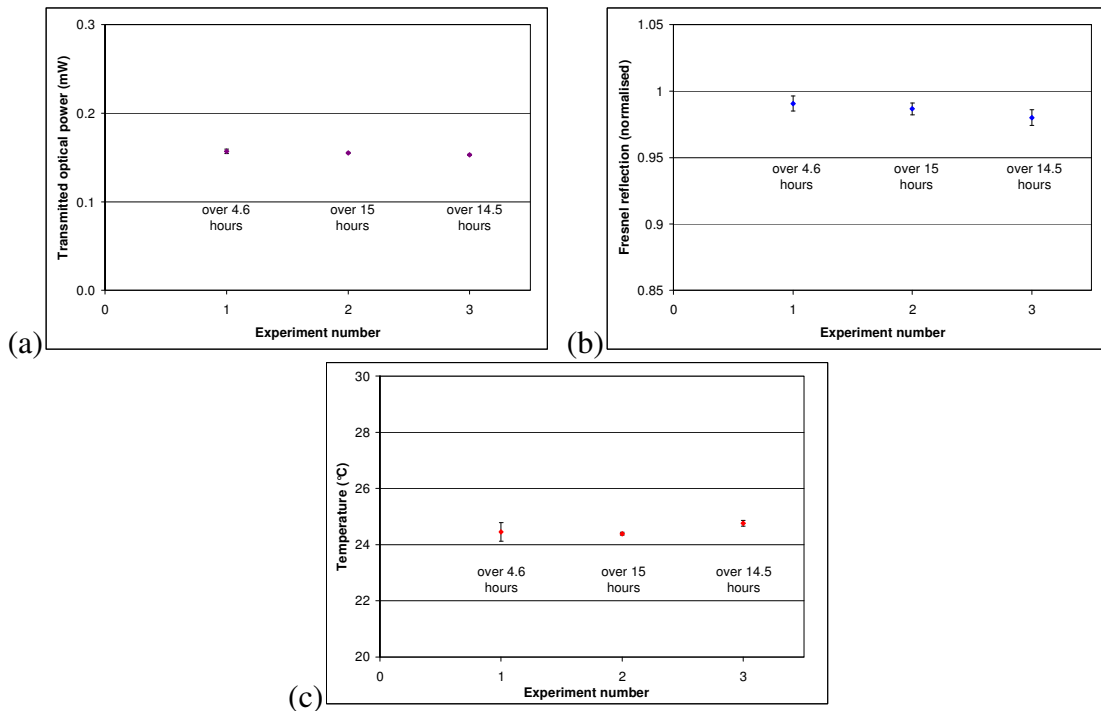


**Figure 4-6. Average values calculated from data obtained in three separate experiments on (a) the transmitted optical power, (b) the normalised Fresnel reflection, and (c) the temperature, using reference oil 1.46.**

There is a 2.5% change between the highest and the lowest transmitted optical power datasets, shown in Figure 4-6a, and a 1.7% change for the corresponding Fresnel reflection datasets. As will be seen later, the change in the Fresnel reflection signal of a resin system during cure is significantly larger than the drift observed here. Therefore, such small changes as observed in Figure 4-6b are deemed acceptable. There was an 8% change between the temperature datasets (Figure 4-6c). The reason for this is because the experiments were undertaken at ambient temperature in a room where the temperature was not controlled.

#### 4.2.1.2. Temperature stability

The stability of a single-mode Fresnel reflection sensor which was secured in a de-mountable cuvette containing reference oil 1.57 is shown in Figure 4-7. Here the experiment was controlled at 30 °C using the temperature-controlled cuvette holder.

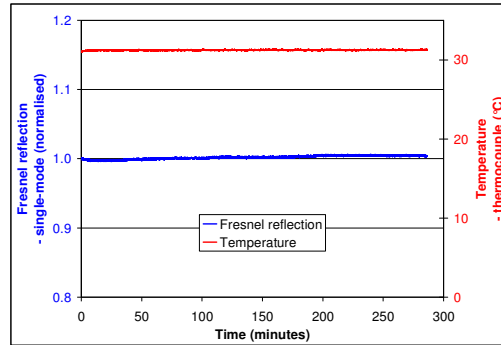


**Figure 4-7. Data obtained using a thermocouple and single-mode Fresnel reflection sensor immersed in reference oil 1.57 and held at 30 °C.**

Figure 4-8a and b present temperature and Fresnel reflection data obtained during a temperature ramp-hold experiment using reference oil 1.57. The transitions in the temperature and Fresnel reflection slopes between dwell periods, indicated by dotted lines in Figure 4-8a, were calculated to be 3.25 ( $\pm 0.072$ ) °C/minute and -0.024 ( $\pm 0.001$ ) normalised Fresnel reflection/minute respectively. Since all the slopes per dataset are near-identical, the inter-dependence of the Fresnel reflection data on the temperature is readily apparent. The data from the hold-periods at each temperature were averaged and are presented in Figure 4-8b. This linear behaviour confirms the relationship between the Fresnel reflection data and temperature.

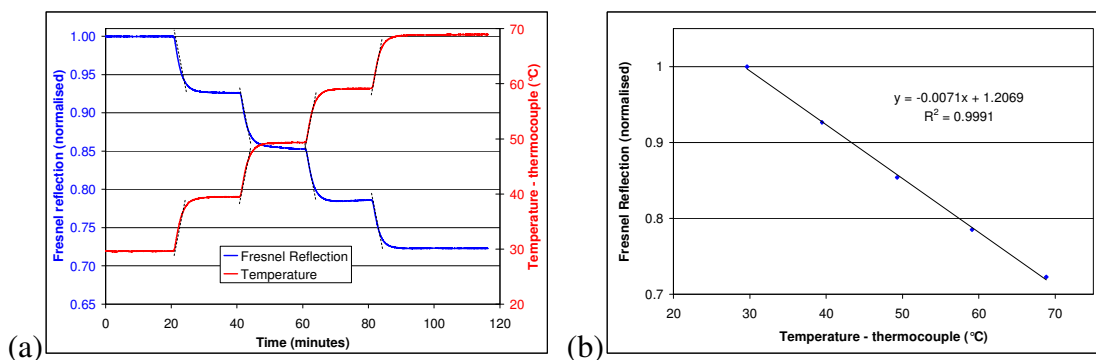


**Figure 4-8. Temperature and Fresnel reflection data obtained during a temperature ramp-hold experiment using reference oil 1.57, where (a) shows the datasets for the duration of the experiment, and (b) shows the average values during the isothermal-hold at each temperature.**

The experiment was repeated using CVC 4 silicone oil and similar results were observed. Furthermore, experiments were carried out over a 5 °C range whereby each ramp was a 1 °C change. This demonstrates clearly that the Fresnel reflection sensor and thermocouple can be used to detect small changes in temperature.

Since the cuvette holder was the mainstay of the temperature-controlled experiments, the influence of the presence/absence of the fibre-optic FTIR probe(s) on the temperature and Fresnel reflection data was briefly investigated. A temperature ramp-hold experiment was carried out and between 30 and 70 °C in increments of 10 °C, with dwell periods of approximately 60 minutes. The outcome of this brief study is presented in Appendix C. Here, it can be seen that the presence/absence of the probe(s) did not have a detectable influence on either the temperature or Fresnel reflection measured within the de-mountable cuvette.

#### 4.2.1.3. Cure monitoring using a Fresnel reflection sensor

The responses of a single-mode and a multi-mode Fresnel reflection sensor were recorded simultaneously during the cross-linking process of the LY3505/XB3403 resin system at 60 °C and 70 °C, as shown in Figure 4-9a and b respectively. The data were normalised to the initial measurement at 30 °C, and it is clear that the response of the sensors is comparable.

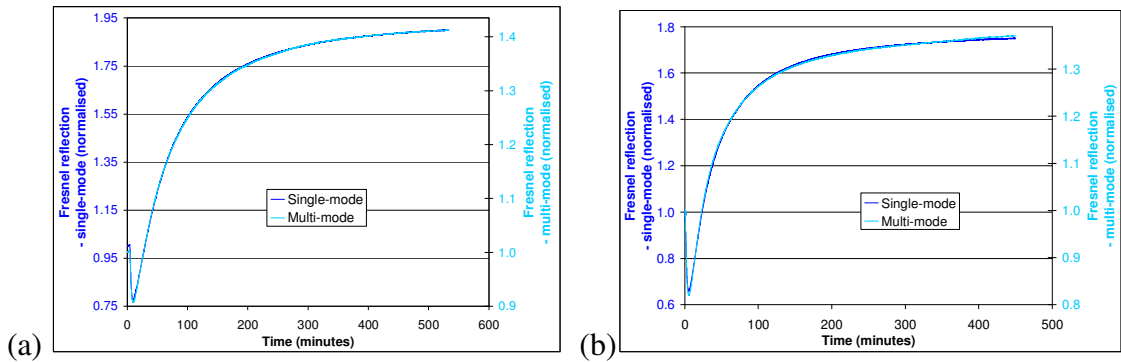


**Figure 4-9. Fresnel reflection data during the cross-linking of LY3505/XB3403 at (a) 60 °C and (b) 70 °C, obtained using single-mode and multi-mode optical fibre sensors.**

With reference to Figure 4-9a and b, the initial drop in the amplitude of the Fresnel reflection signal can be attributed to a decrease in the refractive index of the resin system as it is heated from 30 °C to the isothermal temperature (60 or 70 °C). The subsequent gradual increase in the reflected light intensity relates to the isothermal stage, whereby an increase in the density and molecular weight of the resin system due to cross-linking causes an increase in the refractive index (as discussed in Chapter 2). The subsequent stabilisation of the reflected light intensity suggests retardation of the rate of cross-linking.

It was found that, in some cases, the multi-mode Fresnel reflection sensor was more prone to environmental and mechanical perturbations. Examples of these are shown in Figure 4-10a and b.

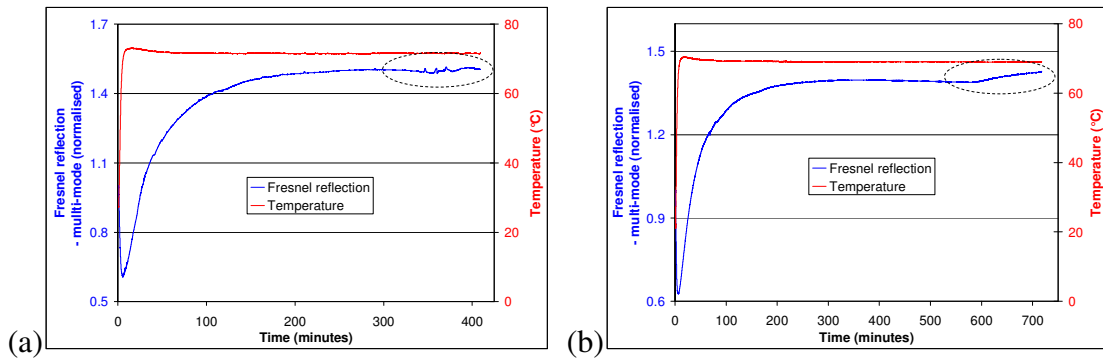


**Figure 4-10. The response of multi-mode Fresnel reflection sensors and thermocouples during the cure process of LY3505/XB3403 at 70 °C. (a) and (b) are examples of the sensor being prone to perturbations.**

A personal judgement was made that the stability and consistency of the multi-mode Fresnel reflection sensor was inferior to the single-mode sensor over the period of typical cure experiments. Therefore, all subsequent cure monitoring experiments were carried out using a single-mode Fresnel reflection sensor at 50, 60 and 70 °C. However, the data presented by Cusano *et al.* [107] using single-mode fibres also showed perturbations in the Fresnel reflection signal in the latter stages of the reaction at 50 °C, but the authors did not acknowledge or discuss it.

In Figure 4-10a and b, an overshoot in the temperature profiles is observed before the isothermal hold has been attained. This overshoot may be attributed to one or more of the following reasons: (i) the inability of the temperature-controller to retard the rate of heating

just prior to the set-temperature; (ii) the exothermic nature of the resin system; and (iii) the possibility of the cooling pump of the cuvette holder malfunctioning. The overshoot was not seen in all experiments and therefore it is difficult to attribute a specific reason. However, the magnitude of the overshoot at 70 °C typically displayed a maximum of only 1.5 °C.

The rate of heating and the rates of change in Fresnel reflection during the heating and the initial isothermal period are annotated in Figure 4-11. The rate of heating was obtained from the thermocouple data and represents the change from 30 °C to the isothermal processing temperature of 50, 60, or 70 °C, corresponding to “slope 1”. The rate of observed decrease in the Fresnel reflection signal during the heating phase is indicated by “slope a”. “Slope b” represents the initial rate of increase in the Fresnel reflection signal once the isothermal value has been reached. This method of defining the slopes is used subsequently to analyse the Fresnel reflection data.

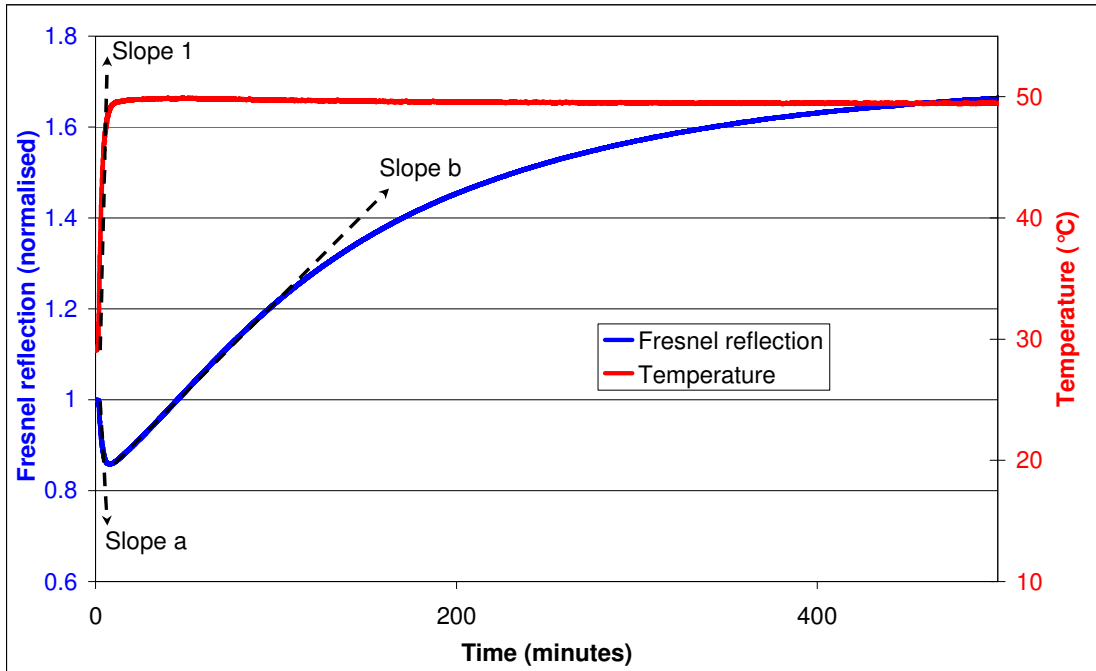


**Figure 4-11. Typical data obtained using a Fresnel reflection sensor and thermocouple during the cross-linking of LY3505/XB3403 resin system at 50 °C. Slope 1 refers to the rate of heating. Slopes a and b refer to the rate of decrease and increase in the Fresnel reflection respectively.**

Typical data obtained using single-mode Fresnel reflection sensors during the cure process of LY3505/XB3403 resin system at 50, 60 and 70 °C are shown in Figure 4-12a, b and c. It is clear that the rate of cure is faster at higher temperatures.

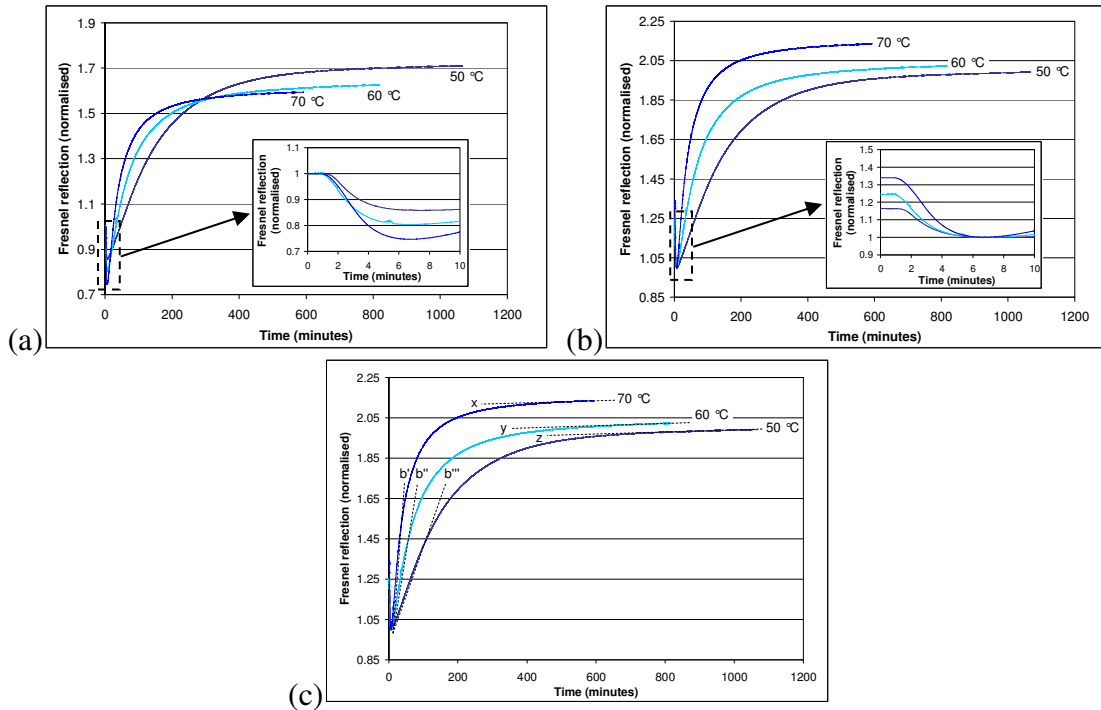


**Figure 4-12. Fresnel reflection data for the cure of LY3505/XB3403 resin system at 50, 60 and 70 °C, normalised: (a) to the signal at 30 °C and (b) to the minimum value during heating. The inserts show the magnitude of the decrease in Fresnel reflection. Graph (c) is identical to graph (b) but the slopes for the increase in the Fresnel reflection signal and the apparent equilibrium values are displayed.**

Figure 4-12a and b show the cases where two different normalisation procedures were applied to the same three Fresnel reflection datasets during cross-linking at 50, 60 and 70 °C. In Figure 4-12a the data were normalised to the Fresnel reflection signal obtained during the dwell at 30 °C prior to heating. The manifestation of this is that the increasing rank order of  $70 < 60 < 50$  °C is seen towards the end of cure. On close inspection of the initial decrease in the reflected Fresnel signal (see the insert in Figure 4-12a), the magnitude of the reductions were measured to be 0.25, 0.2 and 0.14 for the 70, 60, and 50 °C data respectively. This explains the trends in the rank order. However, when the data are normalised to the minimum

values attained from the Fresnel reflection sensor at the end of the heating phase, the rank order is  $50 < 60 < 70$  °C, which correlates with that observed in FTIR spectrometer-based experiments [41]. The insert in Figure 4-12b also reflects the magnitude of the initial drop in the Fresnel reflection signal during the initial heating phase. Both inserts clearly show the acquisition of the data at 30 °C before the temperature was ramped to the isothermal hold value. The stability of the data during the 30 °C hold-period can be used as a quality-control tool to indicate the presence or absence of any artefacts at the cleaved end-face of the optical fibres. For example, the presence of air bubbles, debris or a poor cleave may be detected during this hold period.

Slopes  $b'$ ,  $b''$  and  $b'''$  in Figure 4-12c represent the initial increase in the Fresnel reflection signal at 70, 60 and 50 °C. These slopes were calculated for the two normalisation procedures described above, and are presented in Table 4-4 which will be discussed later.

Slopes  $x$ ,  $y$  and  $z$  in Figure 4-12c relate to the apparent equilibrium states of Fresnel reflection obtained at 70, 60 and 50 °C respectively. After 450 minutes at 70 °C the change in the Fresnel reflection signal is small (slope  $x$ ). This implies that the cross-linking reaction has slowed down significantly. The same trend is observed for the 60 and 50 °C processing temperatures (slopes  $y$  and  $z$  respectively) at approximately 600 and 700 minutes respectively. Interestingly the slopes for the three datasets after the equilibrium states are attained are identical. The implication here is that the Fresnel reflection sensor can be used to determine the “end-point” of the cross-linking reaction at a specified temperature. This has advantages in industrial applications where the tendency is to adhere to a single resin system for a particular product design. Thus the Fresnel reflection sensor offers a low-cost solution to

enable the operator to decide when the cross-linking reaction is complete. It is common practice is to follow a prescribed processing schedule recommended by the supplier of the resin system.

Processing temperature (°C)	Slope 1 - Figure 4-11 (°C/minute)	Slope a - Figure 4-11 (Normalised Fresnel/minute)		Slope b - Figure 4-11 (Normalised Fresnel/minute)	
		Figure 4-12a	Figure 4-12b	Figure 4-12a	Figure 4-12b
50	7.4 (±1.05)	0.058 (±0.004)	0.067 (±0.003)	0.004 (-)	0.004 (±0.001)
60	8.5 (±0.46)	0.099 (±0.002)	0.133 (±0.005)	0.012 (±0.001)	0.016 (-)
70	12.0 (±0.38)	0.126 (±0.005)	0.163 (±0.05)	0.021 (±0.001)	0.027 (±0.009)

**Table 4-4. Values for the rates of change in temperature and Fresnel reflection during cross-linking of LY3505/XB3403 resin system at 50, 60 and 70 °C. The two columns for slopes a and b represent data which are normalised according to the method shown in either Figure 4-12a (initial point at 30 °C) or Figure 4-12b (lowest point).**

On inspecting Table 4-4 the following observations can be drawn: (i) the increase in the heating rate (slope 1) as a function of the set temperature may be attributed to the mode of operation of the heater and temperature control system where a greater power input is supplied to attain the higher set temperature; (ii) it is also likely that the exothermic nature of

the resin system contributes to the increase in the heating rate as a function of temperature; (iii) it is apparent that irrespective of the normalisation procedure, the rates of the initial decrease and the subsequent increase in Fresnel reflection (slopes a and b) show the same trend as a function of processing temperature, where  $50 < 60 < 70$  °C; and (iv) as expected, when the data are normalised to the initial Fresnel reflection point, the magnitude of the rate is lower when compared to the cases when normalisation is performed using the minimum value.

Figure 4-13a shows three datasets for the Fresnel reflection sensor during cure at 50 °C. It is apparent that the outputs from the repeat experiments are comparable. Therefore for any given processing temperature, the low-cost Fresnel reflection sensor can be used to indicate the rate of heating, rate of cross-linking and when an equilibrium value is obtained at that particular temperature. This was also the case for experiments carried out at 60 and 70 °C. However, this assumes that the chemical integrity of the resin and hardener remain constant over their shelf-life. This is illustrated in Figure 4-13b where two sets of experiments were carried out 12 months apart. The implication here is that the Fresnel reflection sensor is capable of identifying the chemical integrity of different batches of resin systems.

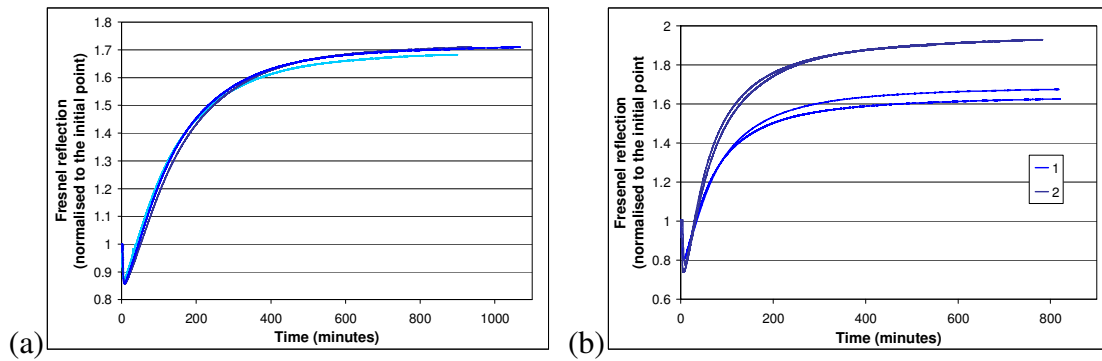


**Figure 4-13. Fresnel reflection data of LY3505/XB3403 resin system for (a) three cure experiments at 50 °C, and (b) four cure experiments at 60 °C, where two pairs of experiments (1 and 2) were carried out 12 months apart.**

The data in Figure 4-14a were generated by other members of the Sensors and Composites Group at the University of Birmingham. These traces show the presence of kinks in the multi-mode Fresnel reflection signal as the initial rate of increase begins to slow down. The locations of these kinks with respect to processing time were plotted against the processing temperature and, as seen in Figure 4-14b, a linear trend is observed. A detailed and systematic study was undertaken to ascertain the reasons for the occurrence of the kinks. This was deemed important for the following reasons:

- (i) The linear trend ( $y = -8.6x + 665.3$  with a coefficient of determination of 0.97) observed in Figure 4-14b suggests that the Fresnel reflection sensor may be used to identify the vitrification region of the resin system;
- (ii) The kink may be caused by cracking of the resin in the vicinity of the optical fibre due to constrained shrinking. For example, the author visually observed cracking after cure around the fibre-end when the Fresnel reflection sensor was contained in resin volumes greater than 1.5 ml;

- (iii) It necessary to establish whether the effect was due to the fabrication methods used. For example, the location of the cleaved fibre-end within the cell, the volume and position of the adhesive used to secure the sensor to the cuvette, and the volume of the resin system used; and
- (iv) Whether the output of the Fresnel reflection sensor was dependent on the instrumentation and sensor configuration.

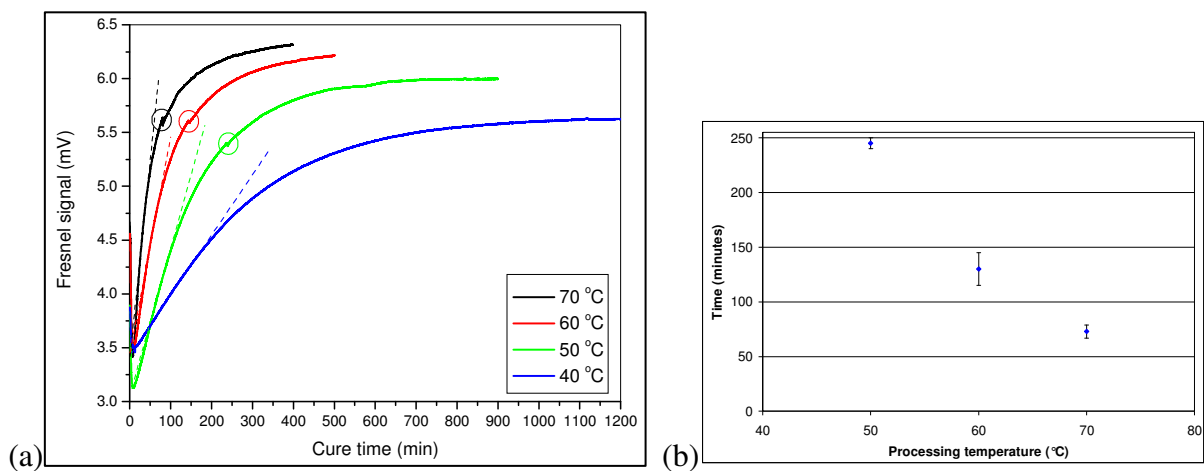


**Figure 4-14. Fresnel reflection data obtained by previous researchers (L. Wang and V. R. Machavaram) at 40, 50, 60 and 70 °C, where (a) shows kinks in the datasets, and (b) shows the time that the kinks appear as a function of processing temperature.**

#### 4.2.1.3.1. Sensor location and bonding conditions

The samples prepared by the previous researchers who observed the kink were inspected and schematic illustrations of a selection of them are presented in Appendix D, where the relative positions of the sensor and the volumes of UV-curable resin used to attach the sensor to the walls of the cuvette are shown. It can be seen that the methodology for securing the Fresnel reflection sensor was not consistent. With reference to the experimental set-up shown in Appendix D (Figure AD-1), the arrangement was reproduced by the author. The Fresnel

reflection data from the previous and current researchers are shown in Figure 4-15a. It is clear that the kink was not reproduced in the data generated by the author (boxed area in Figure 4-15a). A number of different experimental conditions, shown in Appendix A (Figures AA-1a-f) were repeated but the presence of the kinks was not consistent. Moreover their relative positions along the epoxy conversion curves, when present, were random.

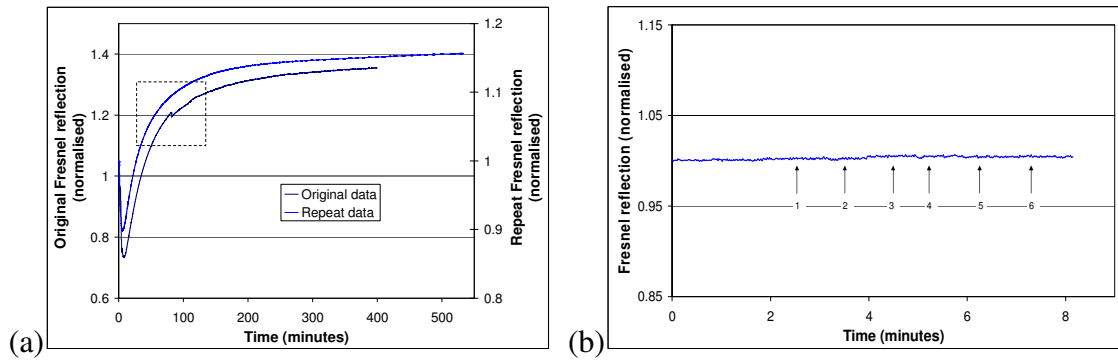


**Figure 4-15. Fresnel reflection data obtained (a) during cure of the LY3505/XB3403 resin system at 70 °C by previous researchers and the current author – these two datasets have been offset for clarity, and (b) in air whilst vibrations were mechanically-induced on six separate occasions.**

#### 4.2.1.3.2. Mechanically-induced vibrations

The effect of mechanically-induced vibrations on the output of the Fresnel reflection sensor was investigated briefly using the set-up illustrated in Appendix A (Figure AA-1f). The sensor was impacted manually as described in Section 3.2.4.1.3. The response of the sensor is shown in Figure 4-15b, where it is seen that the mechanical impulses do not influence the output signal.

#### *4.2.1.3.3. Instrumentation factors*

In the final assessment to try to understand the reasons for the kinks observed by the previous researchers in the Group, instrumentation-related issues were considered. Here, the light source, the coupler and the connections to the data acquisition system were altered, but these factors were not seen to cause the kink in the Fresnel reflection data.

Therefore, it has to be concluded that the kinks may have been caused by variations in the manner in which the sensors were prepared and secured in the cuvette. Over one hundred Fresnel reflection experiments were carried out carefully and systematically in the current study, but the kink was not observed except in the minority of cases. However, in these exceptions the discontinuity cannot be attributed to the vitrification process as their positions on the epoxy conversion curve were random.

#### *4.2.1.4. Feasibility studies using the Fresnel reflection sensor*

Having demonstrated the stability and repeatability of the performance of the Fresnel reflection sensor, a brief study was undertaken to characterise the cross-linking of other classes of resin. These were an aerospace-grade epoxy/amine resin (Hexcel 913) and a photo-curable thermoset (NOA 68). The experimental details and results of this investigation are detailed in Appendix B.

The key aspects that can be drawn from the Fresnel reflection sensor section are summarised below.

It was determined that any drift in the light source was not significant over the duration of a typical cure reaction. Furthermore the signal recorded by the Fresnel reflection sensor was found to be sensitive to the temperature of the surrounding medium.

With regard to cure monitoring, the general trend observed in the profile of the Fresnel reflection signal can be divided into three stages: (i) a rapid decrease in the reflected intensity when the temperature was ramped from the starting temperature (30 °C in the current study) to the isothermal value. This is because the density of the resin system decreases as the temperature is increased; (ii) an increase in the signal once the isothermal condition was reached. The primary reason for this is the increase in the cross-link density of the resin system, concomitant with an increase in the refractive index; and (iii) a retardation in the rate of the increase in the signal followed by the attainment of an equilibrium state. These observations are attributed to the vitrification of the resin system, after which the cross-linking reactions become diffusion-controlled.

The relative performances of the Fresnel reflection sensors fabricated using single- and multi-mode fibres were evaluated. It was shown that when the two sensors were deployed in the same experiment, their responses were similar. However, the long-term stability of the single-mode Fresnel reflection sensor was found to be superior in comparison to the multi-mode sensor.

Two methods of normalising the Fresnel reflection data were investigated in this study. In the first method, the data were normalised to the initial point where the temperature was maintained at 30 °C. In the second case, the normalisation was undertaken using the

minimum point attained. It was found that irrespective of the normalisation procedure, the rates of the change in the initial decrease and subsequent increase of the Fresnel reflection signal show the same trend as a function of processing temperature.

Previous researchers in the Group reported the presence of a kink in the Fresnel reflection data, where it was implied that this may be due to the vitrification process. Therefore a programme of work was undertaken to reproduce the kink, where the relative positions of the Fresnel reflection sensor and the method of attachment in the de-mountable cuvette were investigated in detail. A majority of the datasets did not indicate the presence of the kink and therefore this phenomenon was attributed to the method of integration of the sensors into the cuvette.

Two batches of resin systems were used, and it was demonstrated that the data from the Fresnel reflection sensor could be used to discriminate between them. Furthermore, this sensor was used to characterise two different classes of industrial resin systems.

#### **4.2.2. Transmission sensor**

The light transmitted through the resin system using transmission FTIR spectroscopy was used to perform qualitative and quantitative analysis on the epoxy-amine resin systems. Typical near-infrared transmission spectra of the two individual components of EpoTek<sup>®</sup> 310M are presented in Figure 4-16. The spectra for the LY3505/XB3403 resin system are similar and therefore are not presented here. The absorption peaks observed for the epoxy resin and amine hardener are labelled with the letters a to m; these peaks are assigned in Table 4-5.

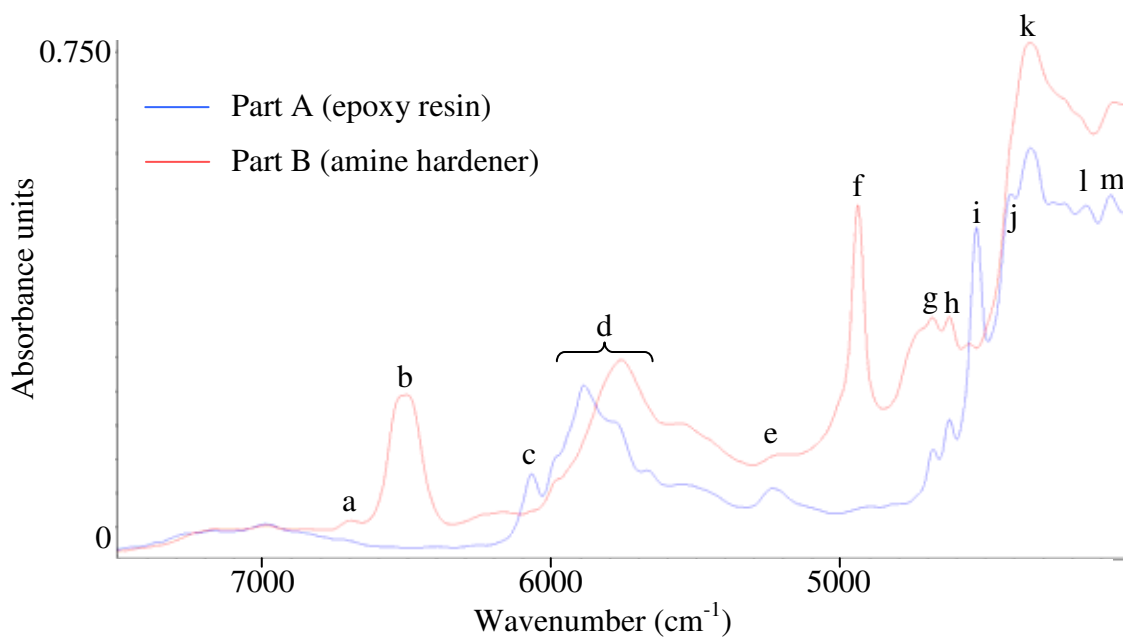


**Figure 4-16. Conventional transmission spectra of EpoTek® 310M part A (epoxy resin) and part B (amine hardener).**

Peak reference	Wavenumber (cm <sup>-1</sup> )	Peak assignment
a	6702	Primary amine 1 <sup>st</sup> overtone (N-H asymmetric stretching)
b	6527	Primary and secondary amine combined (overtone of N-H stretching)
c	6060	Terminal epoxy 1 <sup>st</sup> overtone (C-H stretching)
d	5650-5988	The series of bonds at 5650, 5767, 5882, and 5988 cm <sup>-1</sup> can all be attributed to aliphatic C-H groups
e	5249	O-H asymmetric stretching and bending

f	4939	Primary amine combination (N-H stretching and bending)
g	4680	Aromatic C-H stretching
h	4622	Aromatic C-H stretching
i	4532	Epoxy combination (C-H bending and stretching)
j	4410	Methyl overtone
k	4350	CH <sub>3</sub> , CH <sub>2</sub> and CH
l	4150	Methyl fundamental
m	4065	Aromatic ring fundamental (C-H stretching)

**Table 4-5. Peak assignments for epoxy/amine resin systems, such as EpoTek<sup>®</sup> 310M, as shown in Figure 4-16 [1, 17, 18, 51, 52, 69, 78, 85, 127, 144, 145, 146, 147, 148].**

Typical spectra of the mixed LY3505/XB3403 resin system, which were obtained by conventional spectroscopy before and after cross-linking at 70 °C are shown in Figure 4-17a. The absorption peaks of interest in Figure 4-17a have been labelled according to Table 4-5. The evolution of these spectra for the epoxy peak centred at 4532 cm<sup>-1</sup> is shown in Figure 4-17b. In Figure 4-17a and b the spectra have been translated to a common starting point on the y-axis to demonstrate the change in the peak areas as a function of cross-linking time. As the cross-linking reaction proceeds, the main observations which can be drawn from Figure 4-17a in relation to the generalised reaction scheme shown previously in Figure 2-5, are as follows:

- (i) A decrease in epoxy absorption at 6060 cm<sup>-1</sup> and 4532 cm<sup>-1</sup> (Figure 4-17b);

- (ii) A decrease in primary and secondary amine absorption at  $6527\text{ cm}^{-1}$  and a decrease in primary amine at  $4939\text{ cm}^{-1}$ ; and
- (iii) The absorption of aromatic C-H at  $4680\text{ cm}^{-1}$  and  $4622\text{ cm}^{-1}$  is seen to be relatively constant. This is because it does not take part in the cross-linking reactions.

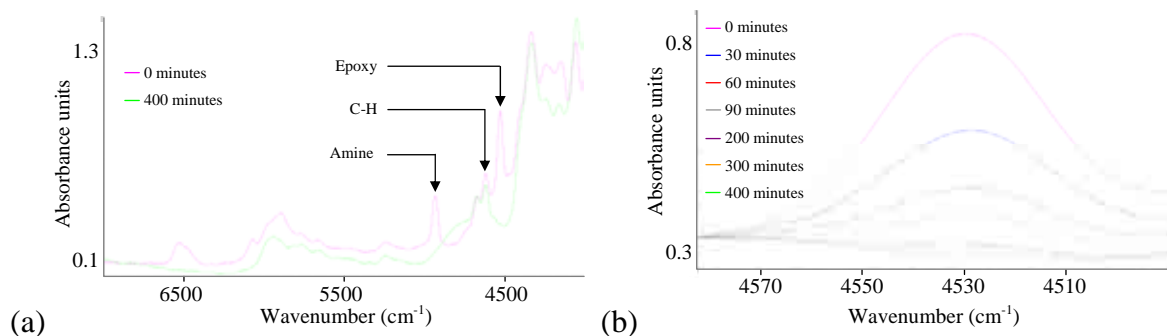


**Figure 4-17. Typical spectra of LY3505/XB3403 resin system, obtained using conventional FTIR spectroscopy (a) at  $30\text{ }^{\circ}\text{C}$  (start of reaction) and towards the end of cure at  $70\text{ }^{\circ}\text{C}$ , and (b) the evolution of spectra of the epoxy peak at  $4532\text{ cm}^{-1}$  from the start to the “end” of cure.**

To obtain quantitative information, the areas of the peaks of interest were measured as a function of cross-linking time. The epoxy peak at  $4532\text{ cm}^{-1}$  has been reported as the most suitable for quantitative analysis [17, 18, 52, 145, 149]. Accordingly, where accessible, this peak was used for quantitative analysis in the current study. The amine absorption peak at  $4939\text{ cm}^{-1}$  was also used in this study for quantitative analysis, and has been used by previous researchers [1, 78].

The peak area was calculated by first determining the appropriate positions for the baseline. The depletion in the areas of the epoxy ( $4532\text{ cm}^{-1}$ ) and primary amine ( $4939\text{ cm}^{-1}$ ) peaks as a

function of processing time, during the cure of LY3505/XB3403 resin system at 70 °C, are shown in Figure 4-18.

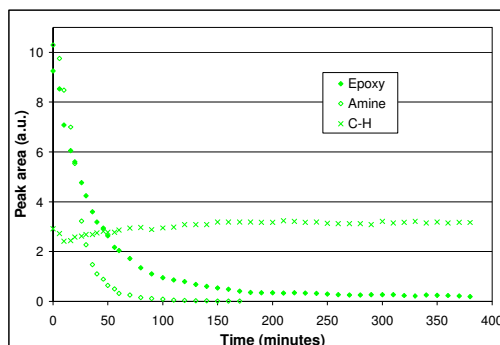


**Figure 4-18. Transmission sensor data showing the peak area values of epoxy, amine and C-H during the cure of LY3505/XB3403 resin system at 70 °C.**

The degree of conversion (extent of cure at a given time) of the epoxy and amine peaks was calculated using Equation 2-7. In order to compensate for any changes in path-length the peak area of C-H, centred at  $4622\text{ cm}^{-1}$ , was used to normalise the peak area of the reactive functional groups. The change in the peak area of C-H as a function of cross-linking time is presented in Figure 4-18, alongside the depletion data for the epoxy and amine peaks. It can be seen from Figure 4-18 that the rate of depletion in the peak area of the amine functional group is faster than that of the epoxy group; the primary amine groups appear to be consumed within approximately 100 minutes and the epoxy groups within approximately 200 minutes. The peak area of the C-H displays a dip during the early stages of the cure cycle; this is consistent with the initial temperature ramp from 30 °C to the isothermal hold of 70 °C.

The conversion data for the epoxy and amine functional groups are presented in Figure 4-19a and b respectively, and are compared with data obtained using conventional spectroscopy during the same experiment. The two datasets correlate well. The epoxy data show a steep

increase in conversion until approximately 55%, when the rate begins to retard and eventually plateaus to approximately 98%. The rate of conversion for the amine data does not decelerate until around 60%, and presents a final conversion value of 99.9%. The initial rates of increase in epoxy conversion are 1.8 %/minute for the transmission sensor and conventional FTIR spectroscopy. The amine conversion data shows initial rates of increase to be 4.1 and 4.0 %/minute for the transmission sensor and conventional FTIR spectroscopy respectively. The similarity in the rates obtained using the two techniques demonstrate that the transmission sensor can be used for remote and real-time process monitoring.

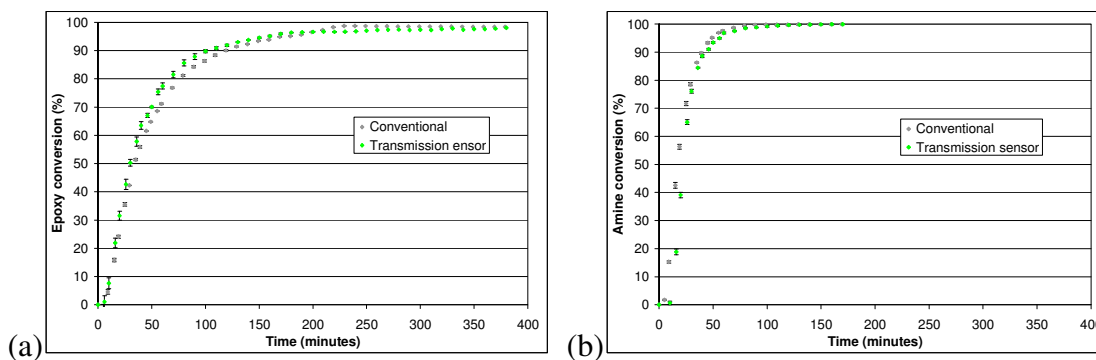


**Figure 4-19. Comparison of the conversion data of (a) epoxy and (b) amine, during the cure of LY3505/XB3403 resin system at 70 °C, obtained using the transmission sensor and conventional FTIR spectroscopy.**

The conversion traces for the epoxy and amine functional groups during the cure of EpoTek<sup>®</sup> 310M at 65 °C are shown in Figure 4-20a and b respectively, where the data were obtained using a transmission sensor and conventional FTIR spectroscopy. Although these data refer to a different resin system, the behaviour of the conversion plots show a similar trend to those observed for the LY3505/XB3403 resin system. Therefore these data are not discussed further.

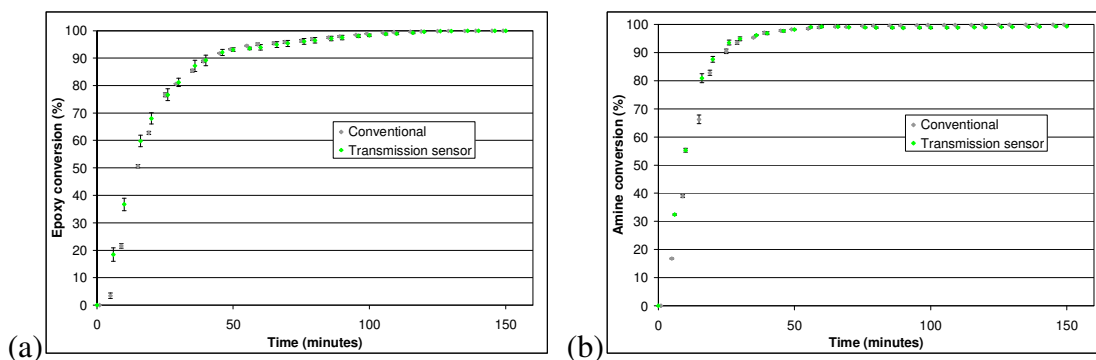


**Figure 4-20. Comparison of the conversion data of (a) epoxy and (b) amine, during the cure of EpoTek 310M<sup>®</sup> resin system at 65 °C, obtained using the transmission sensor and conventional FTIR spectroscopy.**

It is worth noting that the diameters of the sensor optical fibre core and the probe are 105  $\mu\text{m}$  and 600  $\mu\text{m}$  respectively. Although the sampling volumes are different, the data presented above suggests that this does not significantly influence the epoxy or amine conversion data.

In conclusion, transmission FTIR spectroscopy was performed using a fibre-optic transmission sensor. In addition, conventional FTIR spectroscopy was carried out simultaneously. Qualitative analysis was carried out to identify the absorption peaks in the transmission spectrum of LY3505/XB3403 and EpoTek 310M<sup>®</sup> resin systems. Two main reactive peaks were identified; epoxy at 4532  $\text{cm}^{-1}$  and primary amine at 4939  $\text{cm}^{-1}$ . The areas of these peaks were measured for the quantitative analysis of the resin systems during cure at 70 °C and 65 °C for LY3505/XB3403 and EpoTek<sup>®</sup> 310M respectively. The depletion of the peak areas indicated that the primary amine groups are consumed at a faster rate than the epoxy groups. The conversion data were obtained using the C-H peak at 4622  $\text{cm}^{-1}$  to normalise the peaks of the epoxy and amine groups. A good correlation was observed between the data attained using the transmission sensor and conventional FTIR spectroscopy.

### 4.3. EVANESCENT WAVE SPECTROSCOPY

Although significant work has been reported using E-glass fibres [72, 97, 100], at the time of writing, the author was not aware of any previous work on the deployment of S-2<sup>®</sup> glass fibres for process monitoring. S-2<sup>®</sup> glass fibres are used extensively in applications where electromagnetic transparency is required such as radomes [150], and in demanding applications such as helicopter blades, vehicle armour protection and pressure vessels [150]. The data summarised in Table 4-6 for E- and S-2<sup>®</sup> glass fibres, show that S-2<sup>®</sup> glass has a better balance of properties than E-glass. Since no information is available on the cross-linking kinetics on the surfaces of S-2<sup>®</sup> glass fibres, the primary aim of this section was to establish if evanescent wave spectroscopy could be used on this class of reinforcing fibre.

	<b>E-glass</b>	<b>S-2 glass<sup>®</sup></b>
Diameter (µm)	15 (±2) (1200 TEX)	25 (2200 TEX)
Coefficient of thermal expansion (x10 <sup>-6</sup> /°C)	5.4 (AGY)	2.9 (AGY)
Refractive index (589 nm)	1.547-1.562	1.520-1.525
Young's modulus – single filament (GPa)	69-72	86-90
Tensile strength – single filament (GPa)	1.9- 2.7	4.6-4.8
Maximum service temperature (°C)	400	760
Softening point (°C)	846	1056

**Table 4-6. Specified properties for E-glass and S-2 glass<sup>®</sup> fibres [140, 150].**

### 4.3.1. Sample preparation

Since the surface quality of the S-2<sup>®</sup> glass fibres is important to obtain evanescent wave spectra, SEM images of S-2 glass<sup>®</sup> 758 fibres were obtained before and after heat-treatment at 500 °C for four hours. The heat treatment was carried out to pyrolyse the processing aids that were applied to the fibres during manufacture. The conditions chosen for the heat-treatment were derived in consultation with the supplier of the fibres (AGY, USA). A comparison of the surfaces of the S-2<sup>®</sup> glass fibres before and after heat-treatment is presented in Figure 4-21a and b.

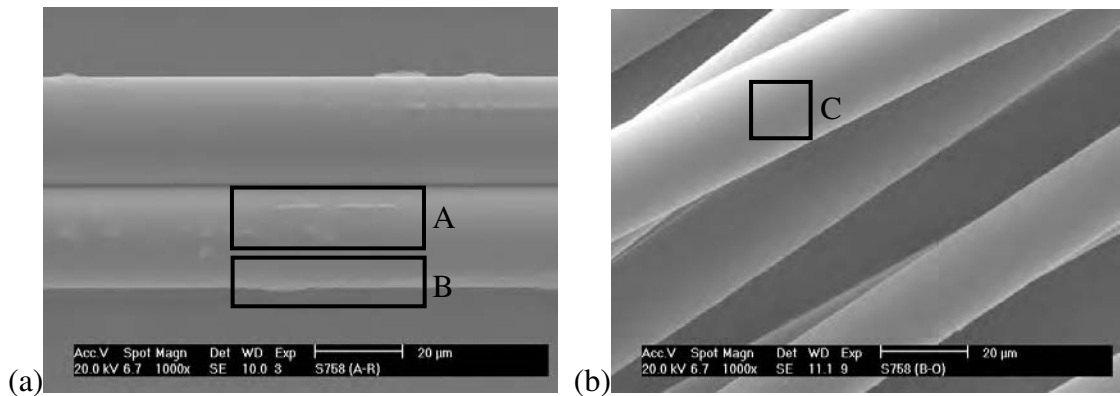


**Figure 4-21. SEM images of S-2<sup>®</sup> glass 758 fibres: (a) in the as-received state, and (b) after heat-treatment at 500 °C for 4 hours.**

It is clear from Figure 4-21a that the surface of the as-received fibres shows the presence of an uneven coating, highlighted in areas A and B. This is likely to be the epoxy-compatible sizing and other unspecified processing aids. In comparison, Figure 4-21b shows that the surfaces of the fibres are much smoother after heat-treatment. There is no obvious coating or debris remaining on the fibre, but minor specks of an unspecified contaminant are visible (C) which appear to be inherent to the fibre structure; it is unlikely to be organic in nature as it remains after being pyrolysed up to 500 °C.

In terms of ease of handling, the as-received fibres were found to be delicate and were prone to static charging. The heat-treatment regime was a careful balance between the removal of the sizing and not causing unacceptable embrittlement of the fibres during manual handling. Although due care was taken during the handling of the as-received and pyrolysed fibres (potting, polishing etc.) a few fibre-breakages were sometimes observed during the sample preparation. The number of broken fibres due to manual handling was estimated visually to be 1% of the total number of fibres.

#### 4.3.2. Light transmission

The intensity of transmitted white light through S-2 glass<sup>®</sup> 758 and 463 fibre bundles that were terminated with SMA connectors is presented in Table 4-7. Samples of three different lengths were connected between the longitudinally-aligned light source and spectrometer, and the tests were repeated four times for each sample. The average value and standard deviation of the four tests were calculated for each sample length and are recorded in Table 4-7.

	Signal amplitude (a.u.)		
	80 mm	100 mm	150 mm
<i>S-2 glass<sup>®</sup> 758</i>	2447.5 (±40.41)	644.75 (±111.16)	368.75 (±63.86)
<i>S-2 glass<sup>®</sup> 463</i>	523 (±17.38)	336.25 (±44.12)	237.75 (±63.60)

**Table 4-7. Light transmission data of S-2 glass<sup>®</sup> 758 and 463 fibre bundles of 80, 100 and 150 mm length, connected between a white light source and an FTIR spectrometer.**

As expected, for both fibre types, the transmitted light was attenuated with an increase in fibre length. These fibres are not designed as light-guides, so their transmission properties will differ greatly from optical fibres. The data shown in Table 4-7 indicate that these fibres can be manipulated as light-guides over relatively short distances and therefore may be suitable for use in obtaining evanescent wave spectra. Although the evanescent absorption will be proportional to the length of the sample, this needs to be balanced with the light attenuation characteristics. Previous research using E-glass fibres for obtaining evanescent wave spectra has shown that light can be guided through a maximum length of 80 mm [72]. The data in Table 4-7 shows that S-2 glass<sup>®</sup> fibres can transmit light through lengths up to 150 mm. Two furnaces of lengths which could accommodate 80 and 150 mm bundles were available for the cure experiments. Since sufficient signal strength was observed when using 150 mm sample lengths, this was adopted for all of the evanescent wave-based cure monitoring experiments.

A series of trials were undertaken to decide on the optimum method to attach connectors to the ends of the fibre bundle. In the first approach, heat-shrink tubing was used to compact the fibres prior to cleaving with a surgical razor blade. In a second approach, the fibre bundles were potted and polished using conventional procedures. Unlike the SMA connector technique, where the bundle-ends are fixed in relation to the light source and spectrometer, with the heat-shrink tubing method it was necessary to establish the effects of the distance between the bundle-end-face and the plane of the light source/spectrometer. Although the heat-shrink tubing method was significantly quicker, the quality of the light transmission intensity was superior with the SMA connectors. Hence all subsequent experiments involving light transmission through S-2 glass<sup>®</sup> fibre bundles were carried out using SMA connectors.

### **4.3.3. Temperature-control**

It is generally appreciated that temperature-control is a prerequisite for obtaining reliable data on the cross-linking kinetics. The temperature-regulated heating block described in Section 3.2.6.3 was used here for heating pre-impregnated S-glass fibre bundles. The temperature at the centre of the heating block was measured using a thermocouple and the data, as a function of the set-temperature, are presented in Figure 4-22. The continuous red line shows the dataset for the temperature ramp-hold experiment. The average temperature during the hold periods was calculated and is represented by individual data points as a function of the set-temperature, where a linear trend line has been fitted. These datasets clearly demonstrate that the set-temperature and measured temperature are in excellent agreement. Figure 4-22 also shows the temperature measured outside the heating block over the duration of the experiment.

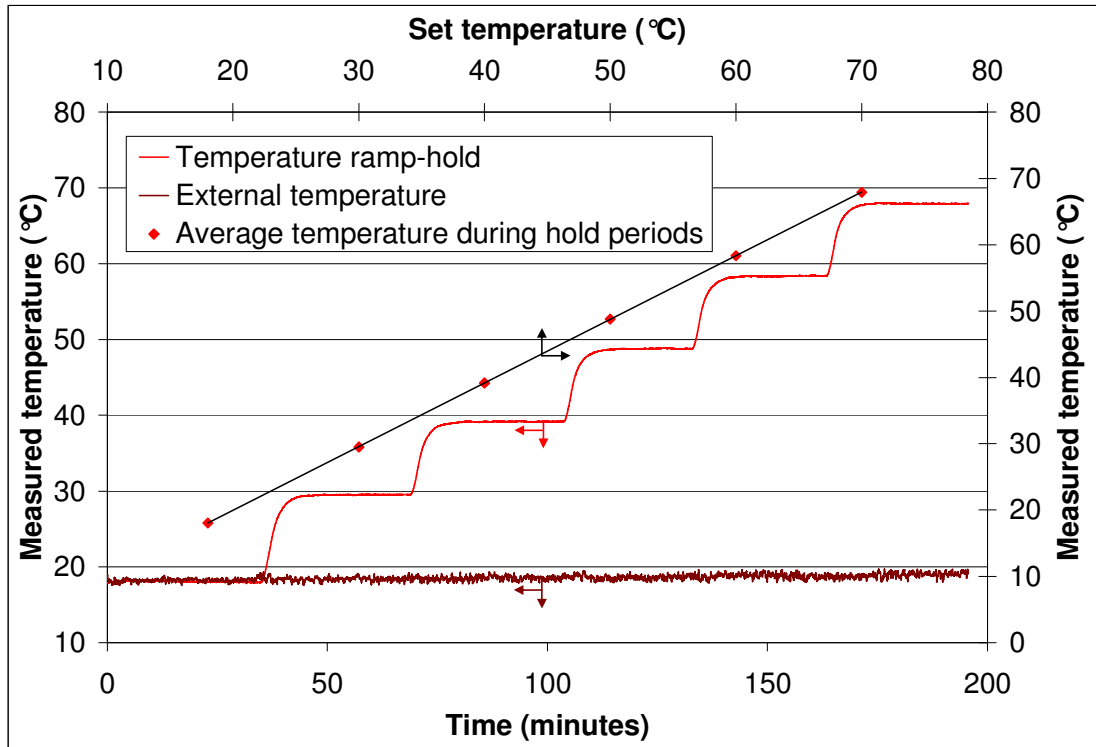


**Figure 4-22. Temperature data obtained from the centre of the temperature-regulated heating block using a thermocouple during a temperature ramp-hold experiment.**

**Three datasets are shown (see text for details).**

Since the ends of the temperature-regulated heating block were exposed to the atmosphere (optical access was required for the input and output ends of the fibre bundle), the temperature gradient along the length of the heating block was determined by positioning five thermocouples at regular intervals on the platform.

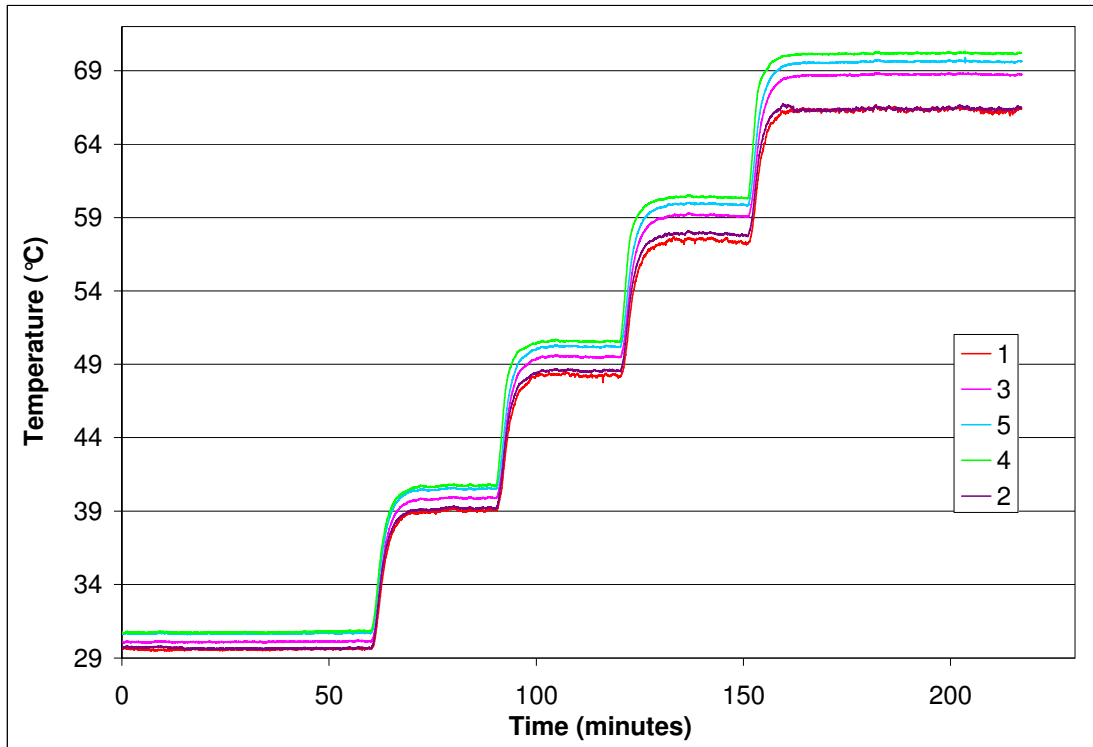


**Figure 4-23. Temperature data obtained during a temperature ramp-hold experiment using five thermocouples along the length of the two-part heating block.**

In Figure 4-23, the legend indicates the relative positions of the thermocouples along the platform, where 1 and 2 represent the open-ends of the heating block. As expected, these positions always recorded the lowest temperatures when compared to the other thermocouples. The temperature difference between thermocouples 3, 4 and 5 at 40, 50, 60 and 70 °C were 0.83, 1.05, 1.3 and 1.42 °C respectively. The data presented in Figure 4-22 and Figure 4-23 show that the measured temperature at the centre is stable to within  $\pm 0.07$  °C during the isothermal hold period. The temperature at the centre of the heating block was measured in all of the cure experiments.

#### 4.3.4. Cure monitoring using evanescent wave spectroscopy

Figure 4-24 shows typical evanescent wave spectra obtained during cross-linking at 65 °C for the EpoTek<sup>®</sup> 310M resin system. The three time-lapsed spectra were obtained at t = 0, 30, and 300 minutes. It can be seen that the signal becomes noisy after approximately 4500 cm<sup>-1</sup>. This can be attributed to the cut-off wavelength for S-2 glass<sup>®</sup> fibres which was established for the first time in the current study. Apart from the composition of the fibres, which was assumed to be uniform, this apparent cut-off wavelength and the attenuation characteristics of the fibre bundle may have been influenced by a number of factors including the following: (i) surface contamination during sample preparation, which was a multi-stage operation; (ii) the degree of fibre alignment within the bundle; (iii) the number of broken fibres; and (iv) the degree of impregnation of the fibre bundle with the resin system.

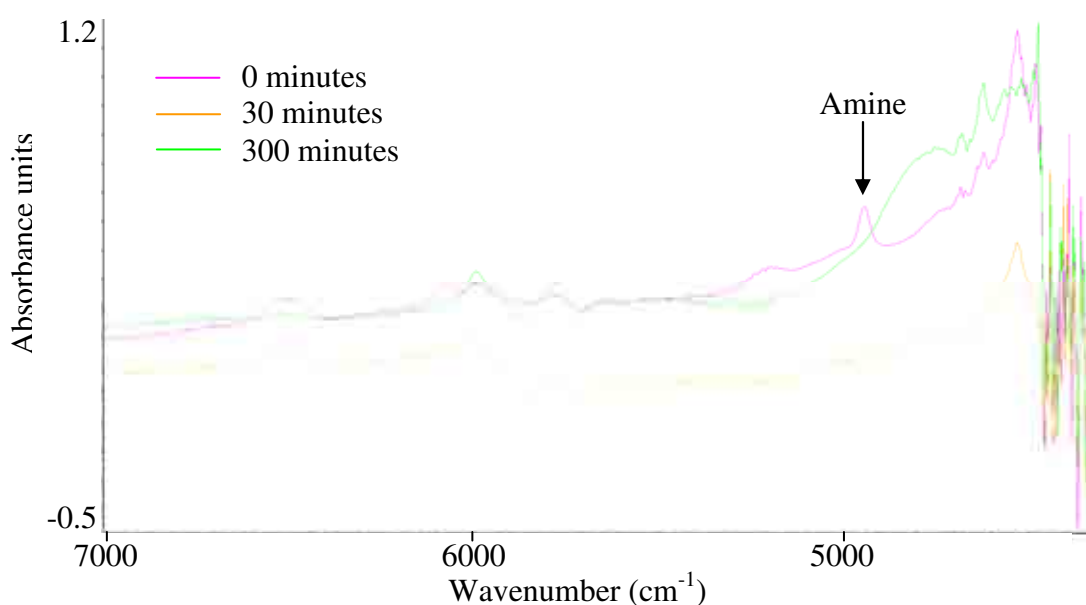


**Figure 4-24. Typical evanescent wave spectra obtained during the cross-linking of EpoTek<sup>®</sup> 310M at 65 °C.**

In Figure 4-24, when  $t = 30$  minutes the spectrum is seen to shift along the y-axis to a lower absorbance in comparison to when  $t = 0$ . This is because the resin system is heated from  $30\text{ }^{\circ}\text{C}$  to the isothermal value, and the refractive index decreases. With further processing the spectrum shows higher absorbance, as seen in the case where  $t = 300$  minutes. The reason for this is that the refractive index increases as a function of the cross-link density. The amine group used in the analysis of the cure reactions is labelled in Figure 4-24. In this series of spectra, the epoxy peak at  $4532\text{ cm}^{-1}$  is seen to be close to the cut-off wavelength. This was seen to cause issues when defining the peak area for analysis especially as the signal-to-noise was substantially low. As a consequence the analysis of the epoxy functional group was not possible.

Figure 4-25 shows the depletion of the amine peak as a function of time for data obtained at  $35$ ,  $45$ ,  $55$  and  $65\text{ }^{\circ}\text{C}$ . The general trend observed is that there is a rapid reduction in the relative concentration of the amine, followed by retardation in the rate of consumption at  $35$  and  $45\text{ }^{\circ}\text{C}$  and an apparent cessation at  $55$  and  $65\text{ }^{\circ}\text{C}$ . The amine functional group is seen to be fully consumed after approximately  $150$  minutes at  $65\text{ }^{\circ}\text{C}$ . The initial rates of depletion for the data shown in Figure 4-25 are plotted as a function of processing temperature in Figure 4-26a, where a linear trend is observed over the temperature range investigated. This suggests that evanescent wave spectroscopy can be implemented using S-2 glass<sup>®</sup> fibres to monitor the initial rate of consumption of the amine functional group at a specified temperature.

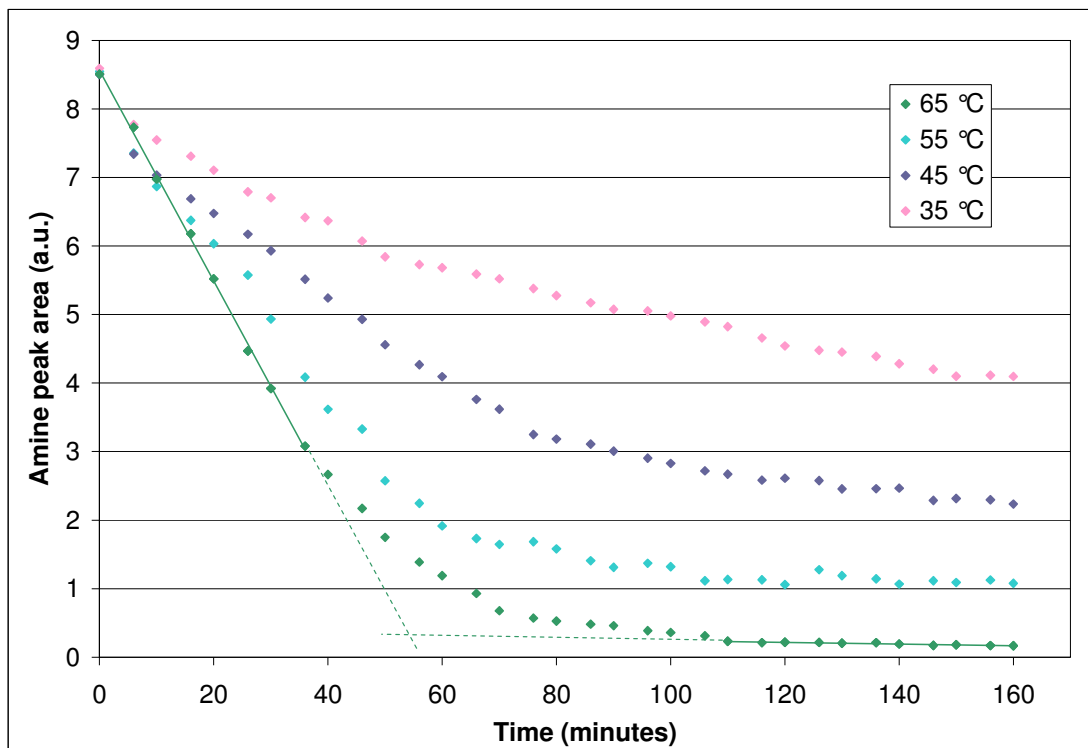


**Figure 4-25. Depletion of the amine peak area with time for data obtained via evanescent wave spectra at specified temperatures. The regression lines for the initial peak area depletion and equilibrium state are displayed for the 65 °C.**

Although the data obtained at 55°C seem to have attained an equilibrium value after approximately 180 minutes, some residual amine is still present. This behaviour is also observed for the 45 and 35 °C data. The change in slope between the initial decrease and the apparent equilibrium state towards the end of the cross-linking reaction may be attributed to the vitrification of the resin system at a specified temperature. In Figure 4-25 the regression lines were generated over the linear portion of the initial decrease and the final equilibrium state for the 65 °C data. The same approach was taken for the 55, 45 and 35 °C data, and the intersection points are shown in Figure 4-26b, where once again a linear trend is observed. The implication here is that evanescent wave spectroscopy can not only be used to infer the

initial rate of depletion of the hardener (amine), but also when the cross-linking reaction ceases at a specified isothermal processing temperature.

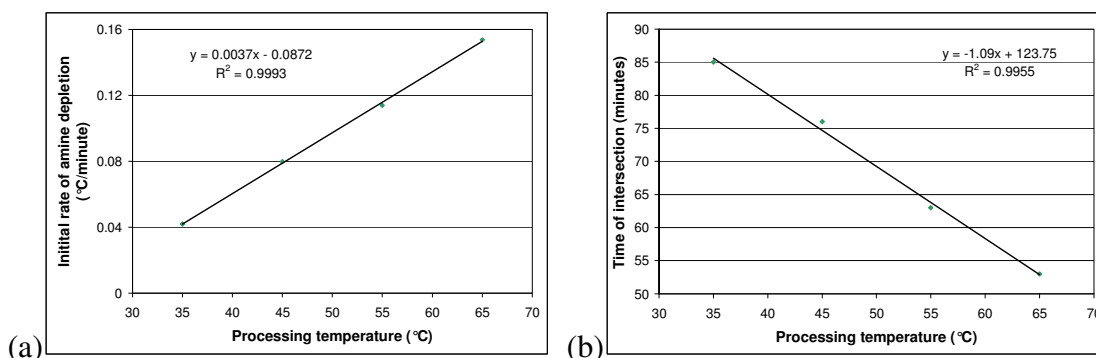


**Figure 4-26.** The data presented here have been extracted from Figure 4-25, where (a) represents the initial rates of amine depletion as a function of processing temperature, and (b) shows the intersection points of the regression lines for the equilibrium state and initial depletion of amine, as a function of temperature.

Normalisation of the amine functional group was performed using the inert C-H peak at  $4622\text{ cm}^{-1}$ , and the conversion traces are shown in Figure 4-27 for the 35, 45 and  $65\text{ }^{\circ}\text{C}$  data. As expected, the initial rate of conversion was greater at the higher temperatures, and the final conversions reached were 71, 92 and 98% when processed at 35, 45 and  $65\text{ }^{\circ}\text{C}$  respectively. In the case of the  $55\text{ }^{\circ}\text{C}$  data, two repeat experiments were carried out, but in both cases the signal-to-noise was poor. Hence it was not possible to analyse the peak area with confidence, and it is not included in Figure 4-27.

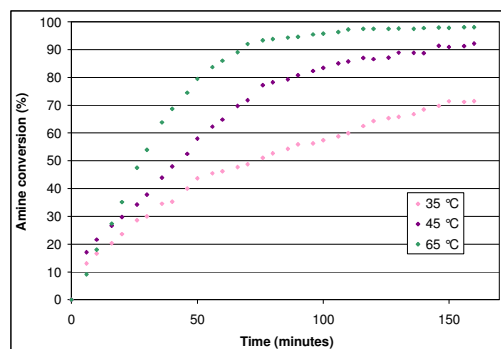


**Figure 4-27. Amine conversion traces for data obtained during evanescent wave spectroscopy at 35, 45 and 65 °C.**

In summary, it was demonstrated for the first time that S-2 glass<sup>®</sup> fibres can be used to obtain cross-linking data at the fibre/matrix interface using evanescent wave spectroscopy. It was established that S-2 glass<sup>®</sup> fibres were capable of transmitting light over a longer length than previously-reported values for E-glass. However, it was found that there was a cut-off wavelength after approximately  $4500\text{ cm}^{-1}$ , which interfered with the acquisition of the epoxy absorption band at  $4532\text{ cm}^{-1}$ .

The temperature-control of the heating block containing the impregnated fibre bundle was capable of maintaining the temperature to within  $\pm 0.045\text{ °C}$  during the isothermal period.

The rate of consumption of the amine functional group was shown to be faster at the higher temperatures. A linear behaviour was seen between this rate of depletion and the processing temperatures. Furthermore the residual amine content was found to be greater at the lower cure temperatures. Linear regression lines were generated using the initial amine depletion rate and the apparent equilibrium in the residual amine content; their intersection points at the specified processing temperatures yielded a linear behaviour.

## 4.4. HYPHENATED TECHNIQUES FOR MONITORING CROSS-LINKING REACTIONS

### 4.4.1. Heating rates associated with different experimental platforms

Figure 4-28 shows the significant differences in the rates of heating associated with three experimental platforms, when the EpoTek<sup>®</sup> 310M resin system was ramped from 30 to 65 °C. This demonstrates clearly the problems in cross-comparing data from different experimental set-ups [1, 41, 49]. Therefore, this section is concerned with the design and development of an experimental platform where the different sensor designs are integrated within one environment.

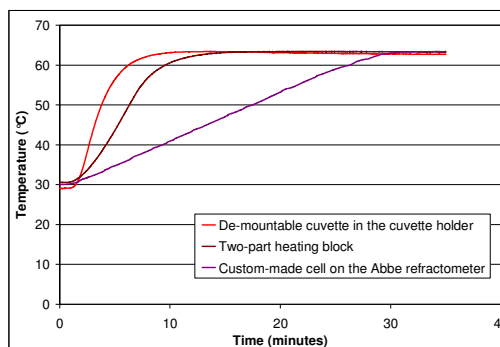


**Figure 4-28. Typical temperature profiles for three different experimental platforms.**

The three datasets represented in Figure 4-28 are as follows: (i) the fastest heating rate refers to the experiments carried out using the de-mountable cuvette in the cuvette holder; (ii) the dataset with the second fastest rate of heating refers to experiments undertaken in the two-part heating block; and (iii) the slowest rate of heating corresponds to experiments carried out using the custom-made cell on the Abbe refractometer. The heating rates for the above-mentioned conditions were 10.15, 4.66 and 1.23 °C/minute respectively

Prior to discussing the experimental data for the custom-made cell on the Abbe refractometer, as shown in Figure 4-28, independent experiments were carried out to establish whether the presence of a Fresnel reflection sensor between the prisms influenced the measured refractive index; these are discussed below.

#### **4.4.2. Integration of the Fresnel reflection sensor on the Abbe refractometer**

In the case where a Fresnel reflection sensor was positioned within the boundaries of the measurement prism, it was still possible to determine the refractive index values but the contrast of the borderline was poor. Furthermore, it is not practical or advisable to cure the resin system directly on the Abbe refractometer prisms. For these reasons, the experimental set-up for the hyphenated techniques on the Abbe refractometer should not involve coverage of the measurement prism by any sensors. Figure 4-29a shows the stability of the temperature and Fresnel reflection data when immersed in CVC 4 oil on the refractometer. Similarly, the data shown in Figure 4-29b represent a temperature ramp-hold experiment to illustrate the correlation between the temperature and Fresnel reflection. The heating rate was calculated to be  $3.46 (\pm 0.05) \text{ }^\circ\text{C/minute}$  during each of the ramp periods; this is identical to the case where the Fresnel reflection sensor was not located between the prisms (see Section 4.1.1). The temperature stability during the isothermal periods recorded by the thermocouple showed a linear relationship with the set-temperature. Once again, this result is the same as that reported for when the sensors were not located between the prisms.

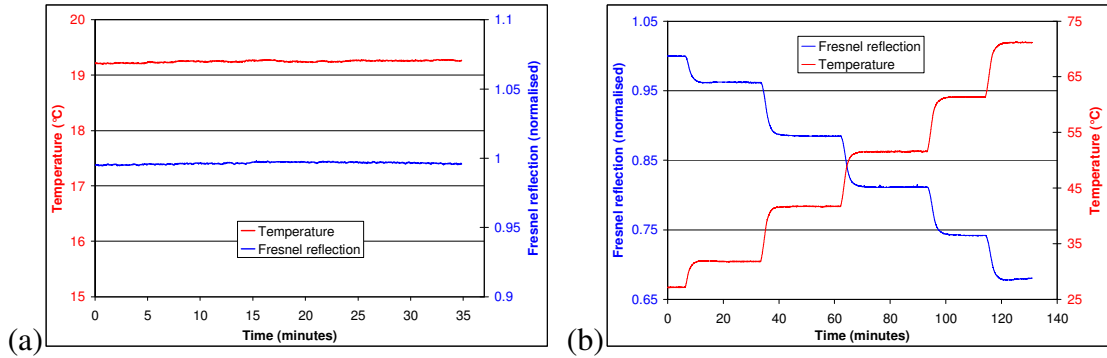


**Figure 4-29. The response of a thermocouple and Fresnel reflection sensor on the Abbe refractometer when (a) the refractometer was maintained at ambient temperature and (b) during a series of temperature ramp-holds.**

Figure 4-30 presents the average Fresnel reflection data obtained during the isothermal hold periods, and the refractive indices measured simultaneously using the Abbe refractometer. Error bars have been included for both datasets, but are negligible. A linear relationship can be seen for the data obtained by each of the techniques, and the two gradients are different by only 0.0065. This small difference may be due to the following reasons: (i) the sampling rates for the Fresnel reflection sensor and refractometer were 1 and 60 Hz respectively; (ii) the Fresnel reflection data are sensitive to localised variations in the vicinity of the cleaved fibre; and (iii) the sampling area of the Fresnel reflection sensor and the refractometer are 0.054 and 363 mm<sup>2</sup> respectively.

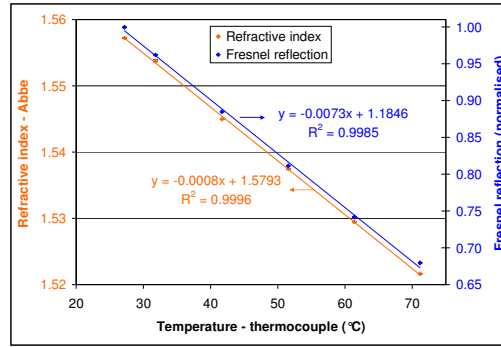


**Figure 4-30. Fresnel reflection and refractive index data obtained for CVC 4 oil during the isothermal hold periods, plotted as a function of the measured temperature.**

In summary, it has been shown that the Fresnel reflection sensor can be housed in the refractometer and refractive index data can be obtained simultaneously. The integration of the Fresnel reflection sensor was not observed to have any effect on the temperature stability of the refractometer. However, the sensor had to be positioned outside the perimeter of the measurement prism in order not to interfere with the refractive index measurements. A good correlation was observed between the refractive index data attained using both techniques.

#### **4.4.3. Integration of a resin containment cell on the Abbe refractometer**

Since the prisms of the Abbe refractometer had to be protected from the cross-linking resin system, a custom-made containment cell was designed and constructed. The cell consisted of two glass slides separated by spacers. As the measurements were taken in reflection mode, the glass slide which was in contact with the measurement prism had the same refractive index as that of the prism (1.76).

The data presented in Figure 4-31 represent the refractive indices of five different reference oils that were measured: (i) directly on the Abbe refractometer, in the conventional method

described in Section 3.2.2; (ii) in the custom-made cell where the release agent was not applied to the slides; and (iii) in the custom-made cell which had been prepared with release agent. The average values of the measured refractive indices are plotted against those stated by the manufacturer. The standard deviation was calculated and the error bars are plotted here but are negligible. A linear behaviour is observed for each of the datasets, and the difference between them is insignificant. This suggests that the use of the custom-made cell and the release agent did not have a detectable influence on the measured refractive indices on the Abbe refractometer. Hence, it can be concluded that the custom-made cell can be used as a containment device for housing resin systems during process monitoring on the Abbe refractometer. Thus the possibility of damage to the prisms does not arise.

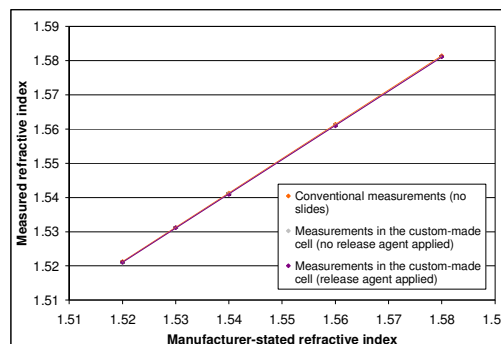


**Figure 4-31. Measured refractive indices of five reference oils plotted against the manufacturer-stated values for the three conditions cited in the legend.**

#### ***4.4.3.1. Temperature-control within the custom-made cell***

Figure 4-32a and b show the temperature data obtained using seven thermocouples during a temperature ramp-hold experiment, where the relative positions within the cell are shown in the inserts. In Figure 4-32a, the temperature difference between the thermocouples is seen to increase with the isothermal-hold. The thermocouple located in position ‘g’ was the closest to

the opening of the cell and therefore displays the lowest temperature at each hold period. The measured temperature ranges during the isothermal periods are observed to be greater with increasing temperature. The temperature difference between the thermocouples located in positions 'e' and 'g' at the 70 °C hold is 25.1 °C. This observed temperature gradient is attributed to heat-loss from the edges of the custom-made cell and the section of the cell which protruded from the refractometer. The effect of the modifications rendered to the refractometer in terms of extending the heat-sink and the insulation is seen in Figure 4-32b. Here, the temperature difference between thermocouples 'e' and 'g' at the 70 °C hold is 7.9 °C. Figure 4-32c represents the difference between the average values during the hold periods for thermocouples 'e' and 'g' as a function of set-temperature for the un-insulated and insulated configurations. This temperature range was the optimum which could be obtained within the timescale and with the resources available.

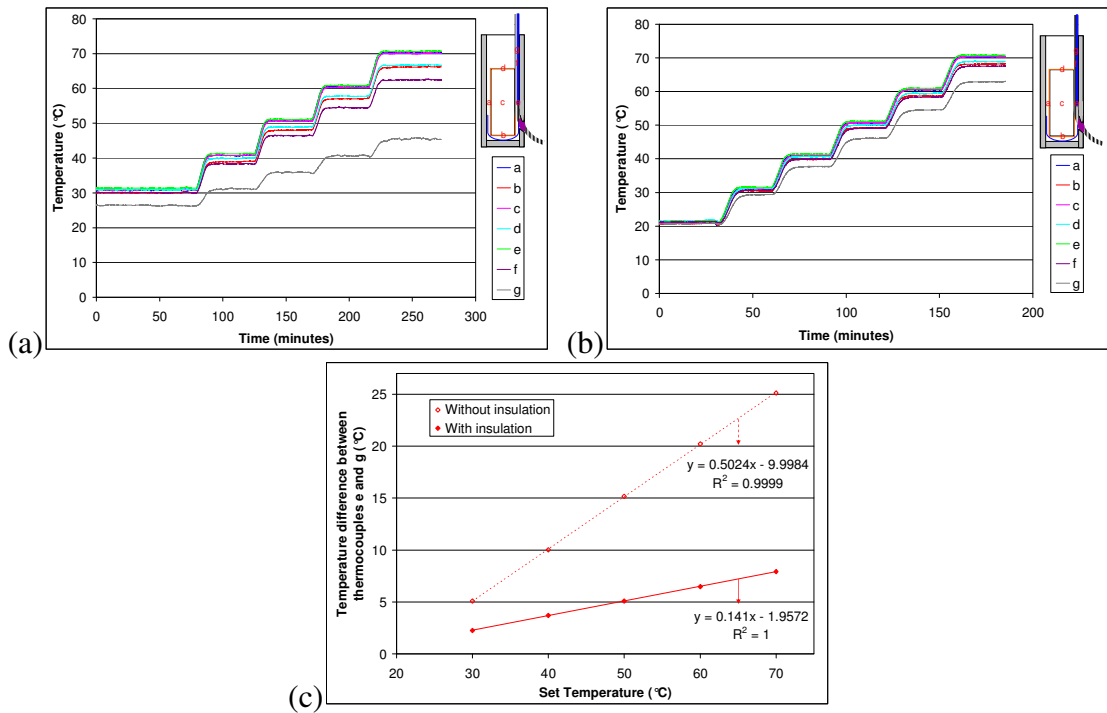


**Figure 4-32. Temperature data obtained using seven thermocouples located within the custom-made cell on the Abbe refractometer during temperature ramp-hold experiments, where (a) represents the un-insulated configuration, (b) represents the insulated configuration, and (c) shows the spread of the average values over the isothermal-holds for both configurations. The inserts show the relative positions of the thermocouples within the cell.**

#### 4.4.4. Hyphenated cure monitoring on the Abbe refractometer

A Fresnel reflection sensor and transmission sensor were secured in the custom-made cell for monitoring the cure of the LY3505/XB3403 resin system. Figure 4-33a, b and c show the excellent correlation between typical Fresnel reflection data and the epoxy conversion obtained using the transmission sensor at 50, 60 and 70 °C.

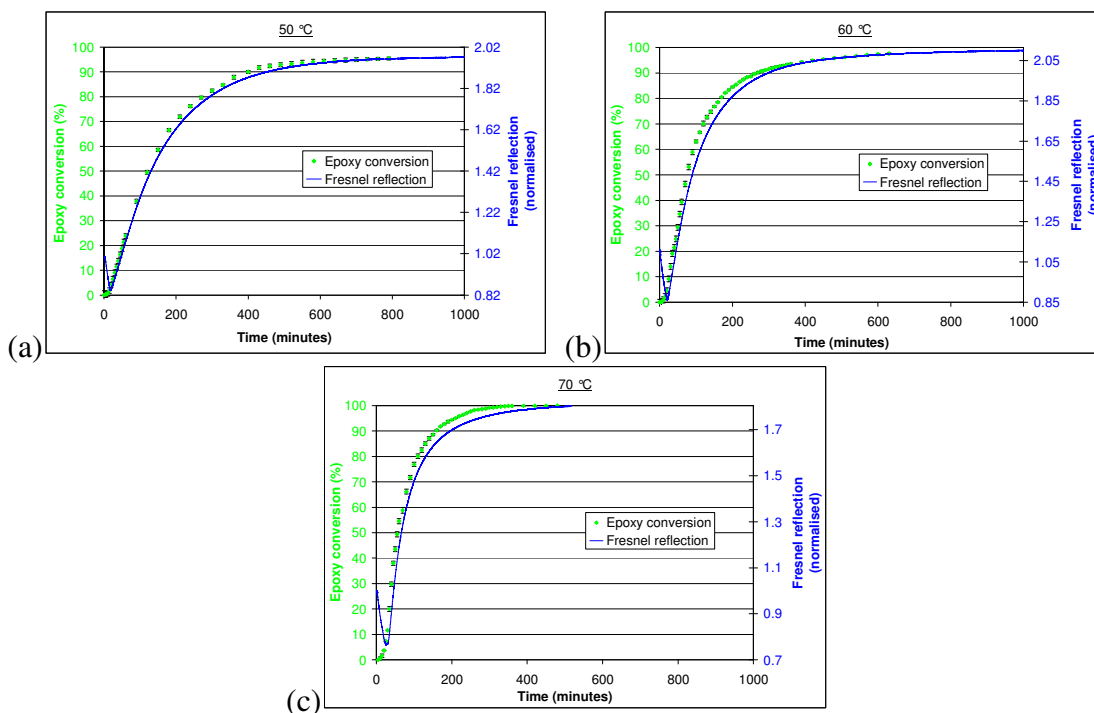


**Figure 4-33. Epoxy conversion and Fresnel reflection data which were obtained simultaneously during the cure of LY3505/XB3403 at (a) 50 °C, (b) 60 °C and (c) 70 °C in the custom-made cell.**

The rates of initial epoxy conversion at 50, 60 and 70 °C are 0.48, 0.81 and 1.32 %/minute respectively. The data obtained during cure in the de-mountable cuvette at 70 °C was 1.8 %/minute, as shown in Section 4.2.2. The rates of conversion are slower when the sensor is integrated into the hyphenated technique because the rate of heating is 1.23 °C/minute, in comparison to 10.15 °C/minute for the de-mountable cuvette.

The amine and epoxy conversion traces for the 50, 60 and 70 °C cure experiments are shown in Figure 4-34 for the first 200 minutes. The coding “A” and “E” represent the amine and epoxy traces respectively, and the numbers represent the corresponding processing temperatures. As observed previously for the transmission sensor data in the de-mountable

cuvette, the rate of amine conversion is faster than that of the epoxy for each of the temperatures. Furthermore, as noted previously, the extent of reaction is greater for the higher processing temperatures.

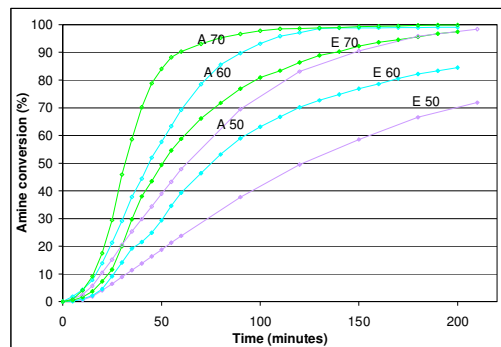


**Figure 4-34. Epoxy and amine conversion data obtained using the transmission sensor in the custom-made cell for the LY3505/XB3403 resin system at 50, 60 and 70 °C. “A” and “E” represent the amine and epoxy traces respectively, and the numbers represent the corresponding processing temperatures.**

Figure 4-35a, b, and c show the response of the Fresnel reflection sensor and the measured refractive index during cure at 50, 60 and 70 °C respectively. Both methods provide data on the refractive index; the Fresnel reflection data is a function of the refractive index of the resin system surrounding the sensor (see Equation 2-8), and the refractometer is pre-calibrated to give values of refractive index. An interesting feature in Figure 4-35a, b and c is that the proportional initial decrease in the refractometer data is significantly higher than that observed for the Fresnel reflection signals. The actual reasons for this are currently unknown but the following explanation is offered. It is possible that the prism is heated more rapidly and uniformly when compared to the sensor which is located outside the prism area and within the custom-made cell. Once the isothermal temperature has been attained in the prism

area and the cell, and the fact that the cross-linking reaction has commenced, it is reasonable to assume that the evolution of the refractive index will be similar in both cases.

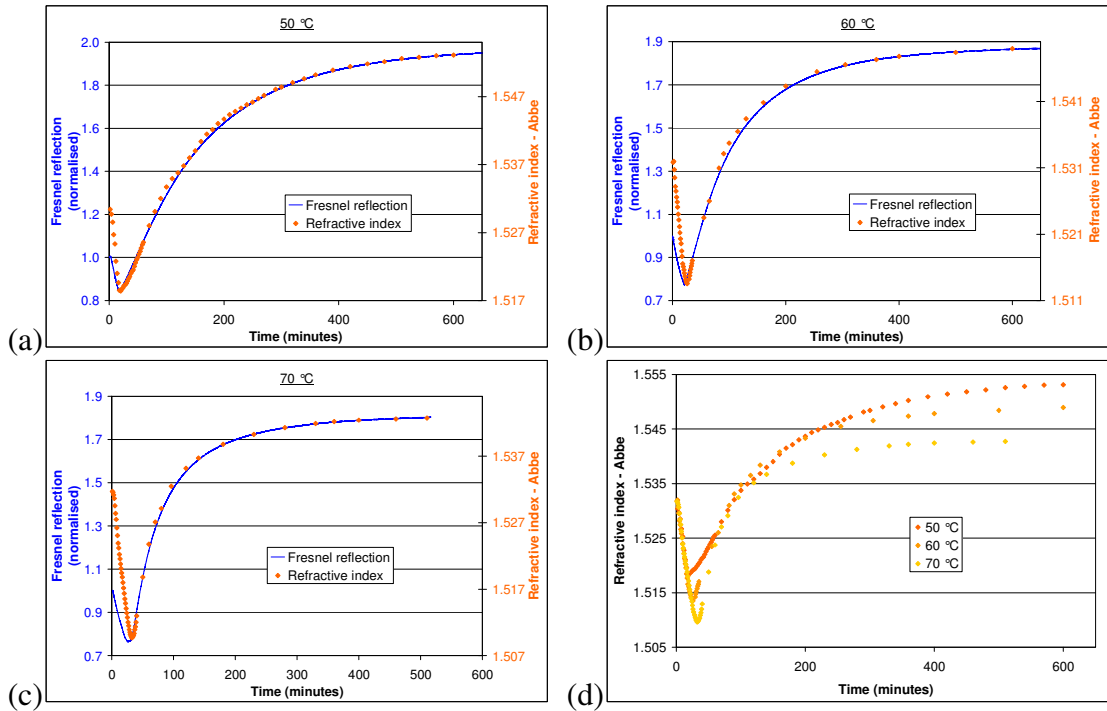


**Figure 4-35. The cross-comparison of the measured refractive indices and the response of the Fresnel reflection sensor during the cross-linking of LY3505/XB3403 resin system at (a) 50 °C, (b) 60 °C and (c) 70 °C. The comparison of the measured refractive indices at the three temperatures is shown in (d).**

Figure 4-35d shows the refractive index data for the cure process at 50, 60 and 70 °C. Here, a similar trend is observed to that for the Fresnel reflection data, where there is a rapid initial drop in the refractive index followed by a sharp increase and a subsequent attainment of a steady-state value. The reasons for this behaviour were discussed previously in the context of the initial decrease being primarily caused by temperature and the increase by the cross-link density with processing time. The initial decrease in the 70 °C data is greater than that of the

60 and 50 °C. This is expected because the refractive index is a function of temperature; during this initial stage the predominant effect is due to temperature.

Table 4-8 summarises the refractive index data obtained from the initial hold period at 30 °C, after cure at the specified processing temperatures, and after cooling back to room temperature. An increase in the refractive indices is shown after cure at the specified temperatures, and a further increase is seen after the sample is cooled. The data obtained here, after cooling, do not correspond to those reported previously for the cast resin films (see Table 4-3). This is likely to be because the cast films were manufactured using a pair of glass plates with a resin volume of approximately 150 ml. The deployment of such a large volume of resin would have resulted in a significant exotherm, where the temperature of the resin would have been higher than the set temperature of the air-circulating oven; this may account for the observed discrepancy.

	<b>Processing temperature (°C)</b>		
	50	60	70
Initial refractive index	1.53042 (at 30 °C)	1.53185 (at 30 °C)	1.53168 (at 30 °C)
Final refractive index after cure	1.5549 (at 1440 minutes)	1.54977 (at 1238 minutes)	1.54279 (at 510 minutes)
Refractive index after cooling	1.56893 (at 22.8 °C)	1.56666 (at 22.6 °C)	1.56290 (at 30 °C)

**Table 4-8. Refractive index data obtained for LY3505/XB3403: (i) before cure at 30 °C, (ii) after cure at 50, 60 and 70 °C, and (iii) after subsequent cooling to room temperature.**

#### **4.4.5. Hyphenated cure monitoring on the Abbe refractometer including a fibre bundle**

In the previous section, the custom-made cell was used on the refractometer without a fibre bundle. However, in this section a fibre bundle was introduced into the custom-made cell, and therefore the following sensors were integrated: (i) evanescent wave sensor (S-2 glass<sup>®</sup> fibre bundle); (ii) transmission sensor; (iii) Fresnel reflection sensor; (iv) FBG sensor; and (v) thermocouple. The introduction of the evanescent wave sensor dictated the need for a resin system whose refractive index is lower than that of the fibres in order to monitor the cure process. The refractive indices of the LY3505/XB3403 resin system before and after cure are 1.53 (measured at 30 °C) and 1.57 (processed at 50 °C and measured at 22.8 °C) respectively. The refractive index of the S-2 glass<sup>®</sup> fibres, however, is 1.520-1.525. Therefore this resin system cannot be used for evanescent wave spectroscopy using S-2 glass<sup>®</sup> fibres. Consequently the EpoTek<sup>®</sup> 310M resin system, whose uncured and cured refractive indices are 1.49 and 1.52 respectively (see Table 4-2 and Table 4-3), was used for the hyphenated experiments involving the fibre bundle.

In the case when the perimeter of the prism was reduced to simulate coverage by a fibre bundle, it was still possible to determine the refractive index values but the contrast of the borderline was poor.

As shown previously in Figure 4-24, the cut-off wavelength did not permit analysis of the epoxy peak. Moreover, because of the low signal-to-noise in the C-H absorption wavelength range, access to this peak was limited. As a result, the analysis in the current section is concentrated on the depletion of the amine functional group. The recommended minimum

cure schedule for the EpoTek<sup>®</sup> 310M resin system is two hours at 65 °C. This is the reason for the difference in the isothermal cure regimes for the two resin systems. In the current study the general trend observed was that the epoxy and the amine functional groups were not fully depleted after the recommended cure schedule. Therefore, the processing time was increased.

#### ***4.4.5.1. Evanescent wave and transmission sensors***

Figure 4-36a, b and c show the cross-linking behaviour of the EpoTek<sup>®</sup> 310M resin system using the evanescent wave and transmission sensors at 45, 55, and 65 °C respectively. In the former case the cure kinetics are obtained at the fibre-matrix interface, whereas in the latter case it can be considered to be representative of bulk transmission spectroscopy. On inspecting these figures it is clear that the consumption of the amine functional group obtained using these two techniques shows a good agreement. Linear regression lines were fitted to the initial portion of the amine depletion curves obtained using each sensor, and these slope values are plotted as a function of processing temperature in Figure 4-36d. The initial rates of amine depletion as a function of processing temperature are shown to be equivalent for the two sensors. Therefore from Figure 4-36d a single equation can be used to approximate the initial rate of depletion of the amine functional group.

Linear regression lines were also calculated for the equilibrium state towards the end of the reaction. The intersection points between the initial and the final depletion trend lines were calculated for each processing temperature and their relationship was found to be:  $y = -0.95x + 102.58$ , with a coefficient of determination of 0.9991.

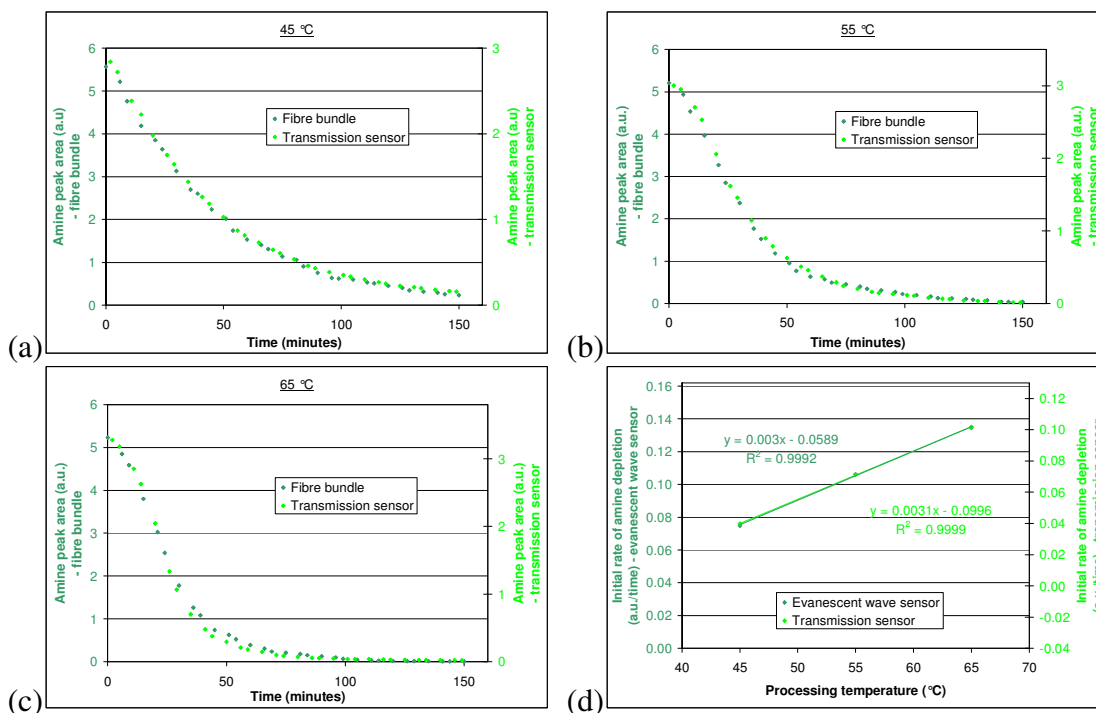


**Figure 4-36. Amine depletion data for the EpoTek® 310M resin system, obtained using an S-2 glass® fibre bundle and a transmission sensor at (a) 45 °C, (b) 55 °C, (c) 65 °C. The initial rates of amine depletion as a function of processing temperature for each sensor are shown in (d).**

The similarity between the two datasets means that the cross-linking kinetics can be accessed and correlated using evanescent wave spectroscopy where the sensing region is over the impregnated area of the fibre bundle, and between a pair of cleaved optical fibres with a path-length of 500  $\mu\text{m}$ .

When comparing the individual experiments carried out in the two-part heating block (as discussed in Section 4.3.4) and the hyphenated experiment discussed in this section, it was found that the following factors could influence the evanescent wave spectroscopic data: (i) in the hyphenated experiment, the fibre bundle was effectively immersed in the resin system,

whereas in the two-part heating block, the resin was introduced on the top-surface of the bundle. Therefore, the volume fraction of the resin is likely to be variable throughout the thickness of the bundle, with a greater concentration at the bottom; (ii) the degree of impregnation of the fibre bundle was found to be influenced by the mode of introduction of the resin system. In the hyphenated configuration, the resin was injected via a syringe from the bottom of the cell whilst the cell was in a vertical position. This enabled the air to be displaced from the cell and ensured thorough impregnation of the fibre bundle. However, this was not the case with the two-part heating block; (iii) any potential loss of the amine through evaporation is likely to have been slower in the hyphenated case because it was a semi-sealed system. However, the potential for the loss of amine in the two-part heating block may have been higher because the containment was open-ended; and (iv) the heating rates in the hyphenated and heating block methods were 1.23 and 4.66 °C/minute respectively. Therefore it can be assumed that a more uniform temperature was experienced in the fibre bundle in the former case.

Although the epoxy spectra was not accessible for the evanescent wave sensor due to the cut-off wavelength of S-2 glass<sup>®</sup>, the epoxy conversion data obtained using the transmission sensor are shown in Figure 4-37 with the amine conversion data at 45, 55 and 65 °C. The following observations can be drawn from Figure 4-37: (i) the rate of amine conversion is faster than that of the epoxy for each of the temperatures. This was also observed for the LY3505/XB3403 resin system (see Figure 4-34); (ii) the extent of conversion for the 55 and 65 °C datasets attain near-completion within approximately 150 minutes. However, this is not the case for the 45 °C data, where residual epoxy and amine are still present after 200 minutes; and (iii) the conversion trends up to approximately 25 % appear indistinguishable,

but the expanded insert shows distinctly that the rate of conversion increases with processing temperature. Only the epoxy data points in the insert have been joined for clarity.

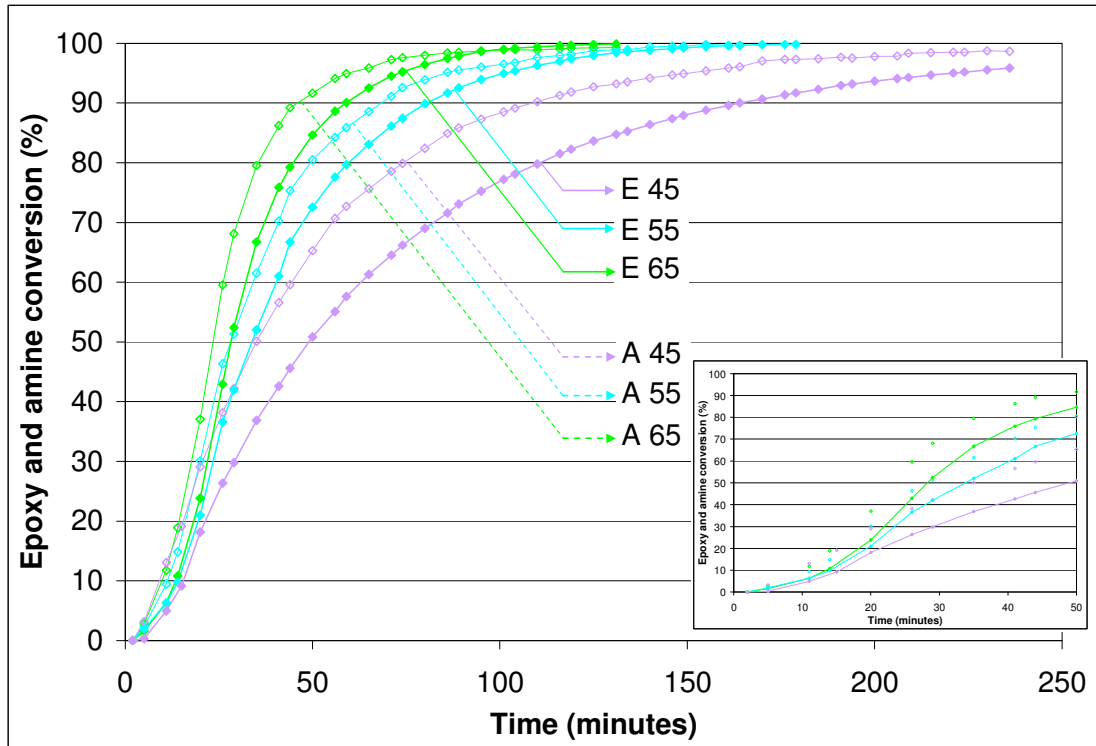


**Figure 4-37. Epoxy and amine conversion data obtained using the transmission sensor at 45, 55 and 65 °C. The insert displays the initial rates of increase in conversion, where only the epoxy data points are joined for clarity. “E” and “A” represent the epoxy and amine traces respectively, and the numbers represent the corresponding processing temperatures.**

#### ***4.4.5.2. Fresnel reflection sensor and Abbe refractometer***

Figure 4-38a, b, and c show the response of the Fresnel reflection sensor and the measured refractive index during cure at 45, 55 and 65 °C respectively. It can be seen that after the initial decrease in the data, for both of the measurement systems the increases in the refractive index show an identical behaviour. This is expected since: (i) the measurements were

obtained from the same sample under identical processing environments, and (ii) both datasets are a function of the refractive index. However, with reference to the 55 °C dataset, after approximately 250 minutes the Fresnel reflection data deviates from the refractometer measurements. Although the reasons for this are unknown the following explanation is offered. According to Figure 4-37, at 250 minutes, the extent of epoxy conversion is near completion. Therefore, it is highly unlikely that this can be attributed to the formation of air bubbles at the fibre-matrix interface. It is unlikely, but cannot be disregarded, that the transmitted light intensity was compromised by accidental human intervention (these experiments were carried out in a multi-user laboratory). This was the only instance when the single-mode Fresnel reflection sensor displayed this uncharacteristic behaviour.

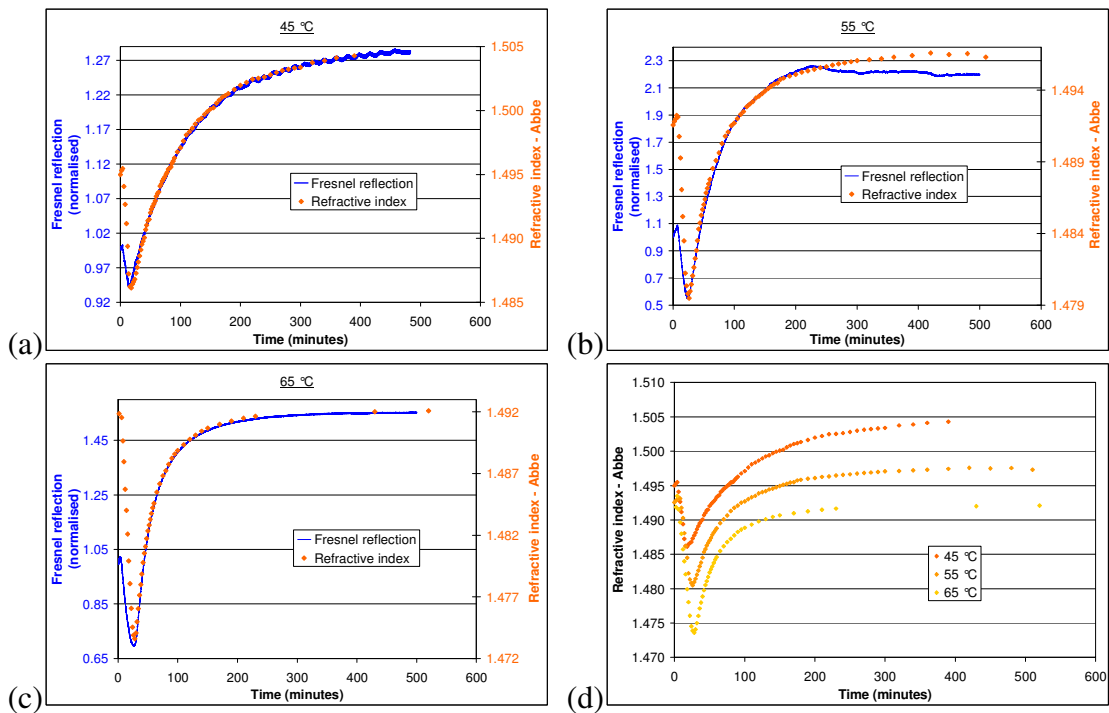


**Figure 4-38. The cross-comparison of the measured refractive indices and the response of the Fresnel reflection sensor during the cross-linking of EpoTek<sup>®</sup> 310M resin system at (a) 45 °C, (b) 55 °C and (c) 65 °C. The comparison of the measured refractive indices at the three temperatures is shown in (d).**

On closer inspection of the Fresnel reflection data obtained at 45 °C, it can be seen that minor periodic oscillations occur. Although the overall trend of the data are similar to the refractive index data, the following observations were recorded in the author's laboratory journal when the experiment was undertaken: (i) the presence of minute bubbles in the vicinity of the cleaved fibre-ends; (ii) the fibre cleaver was logged as malfunctioning during this period and was subsequently dispatched for repair. Therefore it is possible that the cleave quality was not at the required standard. It is also possible that there may have been poor connections at the connectors with the light source and detector, which may count for the periodic fluctuations (interference fringes).

As observed in Section 4.4.4, the initial decrease in the refractometer data is significantly higher than that observed for the Fresnel reflection signals. The possible reason for this was discussed previously.

The general trends in the data seen in Figure 4-38d were also observed in Figure 4-35d for the LY3505/XB3403 resin system, where explanations were offered to account for the profiles of the traces.

Table 4-9 provides a summary of refractive index data obtained from the initial hold period at 30 °C, after cure at the specified processing temperatures, and after cooling back to room temperature. It can be deduced that the uncured (at 30 °C) and cured (at 45, 55 and 65 °C) values are similar. However, on cooling to room temperature, the refractive indices for the samples cured at 45, 55 and 65 °C are 1.52020, 1.51887 and 1.50863 respectively.

	Processing temperature (°C)		
	45	55	65
Initial refractive index	1.49500 (at 30 °C)	1.49256 (at 30 °C)	1.49184 (at 30 °C)
Final refractive index after cure	1.50749 (at 1452 minutes)	1.49682 (at 1110 minutes)	1.49208 (at 520 minutes)
Refractive index after cooling	1.52020 (at 24 °C)	1.51887 (at 23.5 °C)	1.51563 (at 22.6 °C)

**Table 4-9. Refractive index data obtained: (i) before cure at 30 °C, (ii) after cure at 45, 55 and 65 °C, and (iii) after subsequent cooling to room temperature.**

#### ***4.4.5.3. Fibre Bragg grating sensor***

An FBG sensor was introduced into the hyphenated configuration to quantify the magnitude of the residual strain after cross-linking and cooling. The response of the FBG sensor during the cross-linking reaction can be attributed to two factors – strain induced by the shrinkage of the resin system and temperature variation. One of the primary reasons for the development of residual strain in thermosetting resins during the cross-linking reactions is the formation of covalent bonds between the resin and hardener components. Bragg reflection spectra were acquired at one minute intervals for the duration of the experiments. The refractive index data shown in Figure 4-39a were presented previously in Figure 4-38a; it has been reproduced here to indicate the relationship between the evolution of the refractive index and the strain development in the cross-linking resin system. Points A, B, C and D shown in Figure 4-39a represent the following stages: (A) the start-point of the experiment at ~30 °C; (B) the point where the lowest refractive index value was attained (i.e. approximately when the isothermal

temperature is reached); (C) the end of the cure reaction at ~45 °C; and (D) after cooling back to ~30 °C. Figure 4-39b shows the Bragg reflection spectra obtained at points A, B, C and D, where the following observations can be made: (A) the initial peak is centred at 1555.9 nm; (B) during the heating phase the peak shifts towards a longer wavelength as the fibre expands, with a concomitant expansion in the periodicity of the grating. When considering the change in refractive index from point A to B, it is reasonable to assume that the grating does not register a strain because the resin system is a liquid; (C) during the isothermal period, the peak has shifted to a shorter wavelength, but the shift in peak position from B to C is minimal (0.004 nm). This can be attributed to the fact that the isothermal temperature has been attained and the contribution of strain due to shrinkage is small. The thermo-optic and strain-optic coefficients for the photo-sensitive fibres used in this study are  $6 \times 10^{-6}/^{\circ}\text{C}$  and  $0.77 \times 10^{-6}/\mu\text{e}$  respectively [151]. Therefore it is seen that the response of the grating to temperature is significantly larger than to strain. With reference to the refractive index at point C, it can be seen that the equilibrium state has been attained with regard to the cross-link density (at 45 °C); and (D) after cooling back to the original starting temperature, the peak has shifted to a wavelength which is shorter than the original position (A). The reason for this is that the shrinkage of the resin system results in compressive residual strain, where the temperature is no longer a major contributing factor. In the case of the refractive index data, at point D the value is greater than that at C because the temperature is lower.

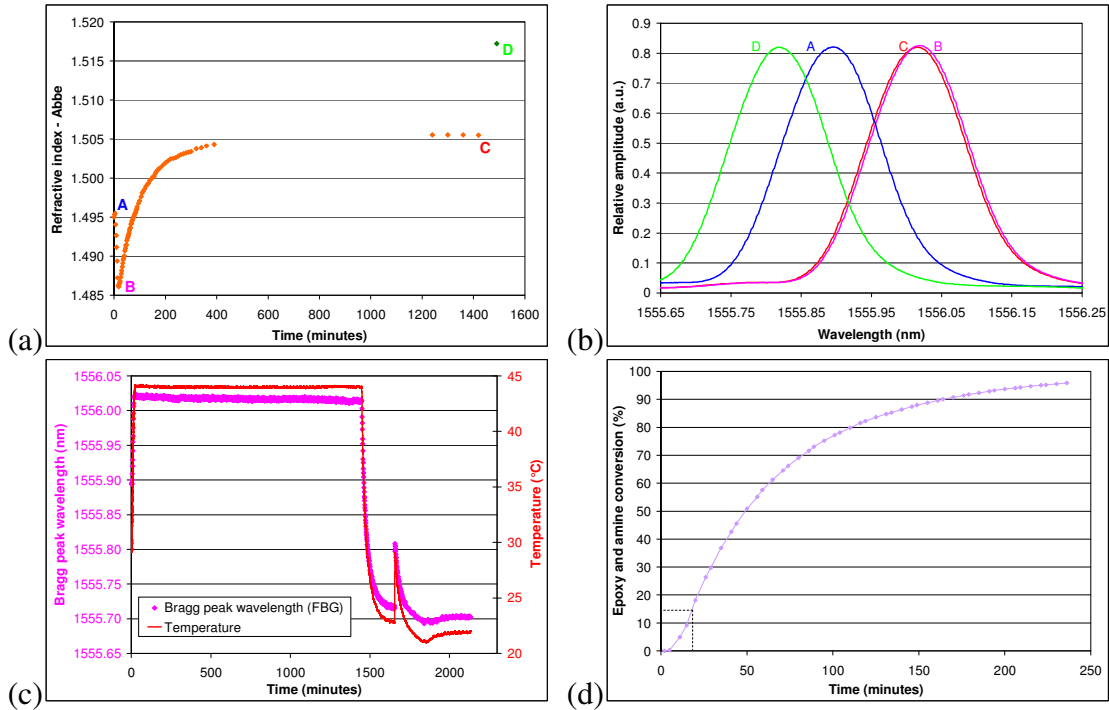


**Figure 4-39. The response of the FBG sensor in the hyphenated experiment carried out at 45 °C, where (a) shows refractive index data with corresponding times where FBG spectra were obtained and are shown in (b). (c) shows the Bragg peak wavelength values and temperature data as a function of time. (d) shows the epoxy conversion at 45 °C (see text for the explanation of the dotted lines).**

The Bragg peak wavelength values for the entire curing/cooling regime were plotted as a function of time and are shown in Figure 4-39c. Here, the resin was heated from 30 °C to 45 °C and held for 24 hours before cooling back down to room temperature. Initially, the increase in temperature from 30 °C to 45 °C induces a shift in the Bragg reflection peak of 0.123 nm towards a longer wavelength. With reference to Equation 2-10 (see Section 2.3.2.4), the strain-optic constant of the Ge-B co-doped fibre ( $\rho_e$ ) was taken to be  $0.77 \times 10^{-6}/\mu\epsilon$  [151]. Using the initial heating phase (where the FBG was assumed to be virtually strain-free) shown in Figure 4-39c, the temperature sensitivity was calculated to be 9 pm/°C for a

temperature change of 13°C. This value falls within the range reported by other researchers [117, 121, 152]. During the cool-down phase, the temperature sensitivity was 13 pm/°C over a temperature change of 7 °C. The residual compressive strain at a temperature of 21.9 °C after cooling was calculated to be 110  $\mu\epsilon$ . The same analysis was performed for the data obtained during cure at 55 and 65 °C, and a summary of the results is presented in Table 4-10.

	<b>Processing temperature</b>		
	45 °C	55 °C	65 °C
Wavelength when in the resin at the start point (nm)	1555.90 (at 29.5 °C)	1555.49 (at 30.04 °C)	1549.42 (at 30.0 °C)
Wavelength at the initial isothermal point (nm)	1556.02	1555.68	1549.72
Wavelength at the end of cure (nm)	1556.01	1555.67	1549.71
Wavelength after cooling back to the start temperature (nm)	1555.82 (at 29.5 °C)	1555.37 (at 30.02 °C)	1549.29 (at 29.9 °C)
Wavelength after cooling to room temp (nm)	1555.70 (at 21.9 °C)	1555.25 (at 19.6 °C)	1549.20 (at 22.9 °C)
Residual compressive strain after cooling to room temperature ( $\mu\epsilon$ )	110 (at 21.9 °C)	122 (at 19.6 °C)	131 (at 22.9 °C)

**Table 4-10. Temperature and strain data obtained using the FBG sensor during cross-linking at 45, 55 and 65 °C.**

In Figure 4-39c, the spike in the data after approximately 1650 minutes was caused inadvertently by switching on the re-circulating water pump which had not yet cooled to the required temperature. This is unlikely to have influenced the cross-link density because the temperature excursion was only 5 °C. The water bath was switched off when this mistake was realised.

Figure 4-39d shows the epoxy conversion data at 45 °C, as previously presented in Figure 4-37. Dotted lines have been drawn to indicate the time when the refractive index attained its minimum value (17 minutes) and the corresponding percentage conversion of the epoxy functional group (13%). The shift in the Bragg reflection peak at 17 minutes displayed the longest wavelength attained at this temperature. From this point onwards the peak values shifted to shorter wavelengths but, as stated previously, this only amounted to 0.004 nm. There has been significant interest in the literature to identify the points when strain develops in the resin system during the cross-linking reaction [117, 118, 119]. In the current study, the data suggests that the Bragg grating detects the development of cure-induced strain at as little as 13% epoxy conversion. However, the following issues need to be considered when interpreting Bragg reflection spectra: (i) FBG sensors are sensitive to temperature and strain (axial, lateral and radial). Therefore it is difficult to de-couple these contributing factors; (ii) in the hyphenated technique, one end of the cell is open and unrestrained shrinkage is possible along this plane; (iii) since the spacing between the cell walls was 1 mm but the sensor was not located centrally, the effects of constrained shrinking cannot be disregarded; (iv) whilst every effort was made to control the orientation of the FBG sensor during its integration into the cell, the retention of orientation cannot be guaranteed during the cure process. The issues discussed above dictate the need for further detailed research to understand and de-couple the

various factors that can influence the response of fibre Bragg gratings. This preliminary study, however, has shown that it is possible to integrate FBG sensors onto a platform in tandem with other sensor systems to enable the cross-correlation between the rates of depletion of specified functional groups, the evolution of the refractive index and the development of cure-induced strain in thermosetting resin systems.

#### **4.4.6. Evaluation of the interference between sensors**

This section is concerned with establishing if there was any interaction between the different instrument and sensor designs when the experiments were carried out in the hyphenated configuration on the Abbe refractometer.

All of the sensors were located outside the perimeter of the refractometer measurement prism and therefore there was no possibility of their interference with the refractive index data obtained via the Abbe refractometer. A series of experiments were carried out to investigate if the light source of the refractometer interfered with the Fresnel and transmission sensors. The sodium light source was switched on and off periodically; the data recorded by the Fresnel and transmission sensors were logged but no interference was observed. Since the fibre Bragg grating sensor was single-ended, and the fact that near-infrared illumination was used, the possibility of localised heating of the other sensors was investigated. Once again, no interference was observed between the sensors when their respective light sources were switched on and off in a systematic fashion, as described in Section 3.2.7.3. Great care was taken to position each of the sensors to minimise the possibility of stray-light coupling between the sensors. The detail of the relative positions of the sensors was detailed in Section 3.2.7.3. Therefore, on the basis of the numerous experiments that were carried out using the

hyphenated platform, it is concluded that no detectable interference was observed between the Fresnel, FBG, evanescent wave and transmission sensors.

## 5. CONCLUSIONS

The key focus of this study was to develop a single platform to enable different classes of sensors to be evaluated under near-identical processing conditions. The platform selected was a conventional Abbe refractometer where a custom-designed cell was placed between the prisms. The cell was constructed from two glass slides, separated by spacers around three edges. The slide which was in contact with the lower prism had a refractive index of 1.76 to match that of the prism.

Prior to undertaking the hyphenated experiments, a systematic study was carried out to establish the stability and output characteristics of the individual sensor systems and their associated instruments. The sensor systems used in this research programme were: (i) Fresnel reflection sensor; (ii) optical fibre transmission sensor; (iii) FBG sensor; and (iv) evanescent wave sensor based on an S-2 glass<sup>®</sup> fibre bundle.

The structure of this chapter mirrors the order of the topics covered in Chapter 4.

*Abbe refractometer:* The Abbe refractometer was used to characterise a series of reference refractive index oils and resin systems. This information was subsequently used to determine if refractive index measurements were adversely influenced by the presence of the sensors or the custom-made cell. It was concluded that the custom-made cell, when located between the prisms, did not exhibit a detectable effect on the operation of the refractometer. The integration of the sensors within the perimeter of the prism area also did not influence the data obtained, but the ease of measurement was compromised.

*Fresnel reflection sensor:* The active element of a fibre-optic Fresnel reflection sensor is its cleaved end. This can be classified as a low-cost sensor system because standard telecommunications fibres and off-the-shelf instrumentation are used. The stability of this assembly was assessed as a function of temperature and time. It was found that any drifts were insignificant over the temperature range and duration of typical cure experiments undertaken in this study.

When the Fresnel reflection sensor was used for cure monitoring in a de-mountable cuvette contained within a temperature-regulated holder, the output data displayed a unique signature consisting of three stages. In the first phase, a rapid decrease in the signal was seen as the resin system was heated from a set-temperature to the isothermal value; this was due to the decrease in the density of the liquid. In the second stage, an increase in the reflection data was observed once the isothermal conditions had been reached. This relates to the formation of cross-links and the concomitant increase in the density. Finally, an apparent equilibrium state was attained which represents the cessation of the cure reaction for a specified temperature. The magnitude of the initial decrease and the subsequent increase were a function of the processing temperature, where the trend observed was  $70 > 60 > 50$  °C for the LY3505/XB3403 resin system.

Normalisation of the Fresnel reflection data was necessary as this is an intensity-based system and therefore a number of factors can influence the output signal. For example, the quality of the cleaved end-face may vary from experiment-to-experiment, the intensity of the incident light may not be identical in each case due to micro-bend losses, the volume of dissolved gases in the resin system may be different, and the homogeneity of the mixed resin system

may also be variable. Normalising the data may compensate for these issues to some extent. The Fresnel reflection data were normalised using two methods. In the first case the normalisation was carried out using the initial value of the Fresnel reflection signal at 30 °C. In the second instance, the minimum value attained was used. Irrespective of the normalisation procedure used, the trends in the rates of change of the initial decrease and subsequent increase were the same as a function of processing temperature.

Fresnel reflection sensors were fabricated using single-mode and multi-mode fibres, and the profiles of the output signal were identical. However the long-term stability of the single-mode fibre was found to be superior.

Previous researchers in the Group reported that a discontinuity in the Fresnel reflection signal was observed during cure. They speculated that this may be congruous with vitrification. Therefore the author undertook a detailed study to assess if the “kink” was caused by vitrification. However, it was not reproducible and thus was attributed to the variations in the sensor preparation methods used by the previous researchers.

It was demonstrated conclusively that the Fresnel reflection sensor can be used to identify the heating cycle, the formation of cross-links, and when the cure reaction is near-completion. Therefore in an industrial context, given the relatively low cost of the sensor and the associated instrumentation, the Fresnel reflection sensor can be used to determine when cross-linking is complete. This is important because it is customary in industry to use pre-determined processing schedules irrespective of the chemical integrity of the resin and batch-to-batch variations. Therefore the deployment of the Fresnel reflection sensor will enable the

processing equipment to be switched off once the desired extent of reaction has been attained. This can potentially lead to significant cost-savings in power consumption and increases in productivity. Furthermore, it can also serve as a quality-control tool to certify that approved processing schedules were used. Experiments carried out in this study also demonstrated that the Fresnel reflection sensor system can be used to distinguish between age-dependent batch-to-batch variations.

The feasibility of using the Fresnel reflection sensor to monitor the cure of an aerospace-grade resin and a photo-curable resin was demonstrated.

*Transmission sensor:* A near-infrared transmission sensor was constructed using two multi-mode optical fibres aligned and secured within a precision-bore capillary fixture. The gap between the fibre-ends was 500  $\mu\text{m}$ , and this was used as the transmission cell to acquire FTIR spectra. Two resin systems were characterised when contained in the de-mountable cuvette, and a majority of the absorption bands were identified. The spectral data obtained using the optical fibre sensor was compared to conventional FTIR spectra. The epoxy and amine functional groups at 4532 and 4939  $\text{cm}^{-1}$  respectively were used to compute the extent of conversion. The inert C-H peak at 4622  $\text{cm}^{-1}$  was used to normalise the absorbance of these two reactive functional groups. The rates of initial conversion were shown to be faster at higher processing temperatures for both resin systems. The extent of reaction was also greater at the higher cure temperatures. Excellent correlation was observed for the conversion of the epoxy and amine functional groups when the optical fibre-based and conventional techniques were compared. Thus, it can be concluded that the transmission sensor can be used for remote process monitoring.

*Evanescent wave spectroscopy:* S-2 glass<sup>®</sup> fibre bundles were terminated with SMA connectors and used as light-guides. However, it was necessary to remove the binder that was applied at the time of manufacture in order to enable light transmission. Here, the fibres were heat-treated at 500 °C for four hours to pyrolise the organic coating.

The light attenuation characteristics of the fibre bundles were assessed as a function of length, and it was determined that a sample length of 150 mm could be used for spectral-based cure monitoring. A custom-made two-part heating block was used to contain the impregnated fibre bundle during the cure experiments. It was shown that the temperature-control at the centre of the heating block was maintained to within  $\pm 0.07$  °C. Since this was an open-ended heating device the temperature at the extremities was consistently lower than at the centre.

The advantage of the evanescent wave sensor is that the cross-linking reactions that occur at the surface of the fibres can be monitored. The cut-off wavelength for this fibre-type was established in this study for the first time, and was found to be around  $4500\text{ cm}^{-1}$ . Unfortunately this cut-off region interfered with the acquisition of the epoxy peak. Therefore the analysis of the cross-linking reaction was limited to the depletion and conversion of the amine functional group. The rate of consumption of the amine functional group was found to be faster at the higher processing temperatures.

At the time of writing, the author was not aware of any previous publications where S-2 glass<sup>®</sup> fibres were used to obtain evanescent wave spectra of a curing thermosetting resin system. The industrial relevance of this is that the effect of specified surface treatments, for

example the silanation of reinforcing fibres, can be studied using evanescent wave spectroscopy. Moreover, the effect of surface treatments on the cross-linking kinetics can also be investigated.

*Hyphenated techniques for cure monitoring:* Having established the relative performances and merits of the individual measurement and sensing techniques, the final challenge was to integrate them onto a common platform. This is necessary because it is difficult to cross-compare cross-linking kinetic data obtained using multiple techniques where the environment, the heat transfer and the rates of heating are not necessarily the same.

The Abbe refractometer was chosen as the reference base to accommodate a custom-made cell since it also permitted the refractive index to be measured. In other words, this experimental platform facilitated the simultaneous acquisition of the following, under a temperature-controlled regime: (i) refractive index; (ii) Fresnel reflection signal; (iii) transmission FTIR spectra; (iv) evanescent wave spectra; (v) residual fabrication strain values; and (vi) temperature data. Since the sensors could not be located over the prism area, they had to be located outside the perimeter, where the space available within the cell to house the sensors either side of the prism was approximately 3.5 mm. Therefore great care and attention was required to position and secure the individual sensors in such a manner that: (i) they did not interfere with each other; (ii) the relative orientation of the sensors was retained during their integration into the cell, and on introduction of the resin system; and (iii) the spatial alignment of the sensors was similar for each experiment. This was achieved by using a transparent film template.

In order to integrate the custom-made cell onto the Abbe refractometer, a number of modifications had to be made to the refractometer. These included a hinge adaption, an extension of the lower prism box, and insulation.

LY3505/XB3403 is a common resin system that is used extensively in industry for manufacturing techniques such as filament winding. The custom-made cell was used in conjunction with the Abbe refractometer, a thermocouple, a Fresnel reflection sensor and a transmission sensor to monitor the cross-linking process. Good correlation was observed between the Fresnel reflection sensor data and epoxy conversion values obtained using the transmission sensor for three processing temperatures. Furthermore, excellent correlation was seen between the Fresnel reflection sensor data and the refractive index values obtained using the Abbe refractometer.

The refractive indices of S-glass and the cured LY3505/XB3403 resin system are approximately 1.52 and 1.57 respectively. Therefore, in order to accommodate the fibre bundle in the custom-made cell with a view to obtaining evanescent wave spectra, it was necessary to select a resin system with a lower refractive index. A number of resin systems were evaluated and EpoTek 310M<sup>®</sup> was selected for the evanescent wave-based cure monitoring studies. For the first time, six individual measurement systems were employed simultaneously to monitor the cure process of an epoxy/amine resin system. In addition to those specified above, a fibre bundle and an FBG sensor were integrated into the custom-made cell. As with the experiments involving the LY3505/XB3403 resin system, in the current case, a good correlation was also observed between the Fresnel reflection and refractive index data. In the case of the EpoTek 310M<sup>®</sup> resin system, the trends in the amine

depletion for the transmission and evanescent wave sensors were seen to superimpose. Moreover, the evolution of the shrinkage strain in the resin system during cure was compared with specific points along the refractive index profile. The Bragg peak wavelengths at these specific points were used to calculate residual fabrication strain. Within the hyphenated experiments, it can be concluded that the following trends are a function of the processing temperature: (i) the initial decreases in the refractive index and Fresnel reflection signal; (ii) the rates of amine depletion obtained using the transmission and evanescent wave sensors; and (iii) the magnitude of the residual fabrication strain.

The deployment of the hyphenated platform developed and demonstrated in this study has shown conclusively for the first time that the data from the Fresnel reflection sensor can be cross-correlated directly to data obtained from the Abbe refractometer, the transmission FTIR sensor, the FBG sensor, and the evanescent wave sensor. On comparing the relative costs of FTIR spectrometers and FBG interrogation equipment with the light source and detector used in the Fresnel reflection sensor assembly, it can be concluded that the Fresnel reflection sensor can offer a cost-effective solution to process monitoring.

## **6. RECOMMENDATIONS FOR FURTHER WORK**

A number of the techniques used in the current study had to be developed over the course of the research programme. As this was an evolutionary process, any problems were overcome as they were encountered. Areas that could be improved are summarised below.

### **6.1. ABBE REFRACTOMETER**

#### **6.1.1. The deployment of a digital refractometer**

The current manual technique for obtaining refractive index data is time-consuming, but this can be semi-automated if a digital refractometer is used. This will also enable the data to be acquired and temperature-corrected using a computer-based data acquisition system. This will negate the need to access calibration tables manually per refractive index reading. Some digital refractometers were inspected but these were not appropriate for the following reasons: (i) the housing for the sample was concaved and therefore could not accommodate the integration of optical fibre sensors; (ii) in general, they could only accommodate small volumes of liquids; (iii) it would not have been possible to cure and remove the samples easily.

#### **6.1.2. Resin film casting methods**

The technique used for casting resin films should be reconsidered because of the magnitude of the exotherm when large volumes of mixed resins are used. In the current study, the resin is cast between glass plates and cured in an air-circulating oven without any cooling facilities for heat-management during cure. The implication here is that the actual cure temperature may be significantly higher than the set-temperature and therefore the cross-link density (and refractive index) may be higher than that anticipated.

## **6.2. FRESNEL REFLECTION SENSOR**

### **6.2.1. Quality control**

Although due care and attention was given to inspecting the quality of the cleaved fibre-ends using a microscope, a portable CCD camera-based inspection technique would be more time efficient. This will also minimise the possibility of contaminating the cleaved end-face. A CCD camera with an appropriate level of magnification will also enable the presence of air bubbles to be detected.

### **6.2.2. Equipment**

The current ensemble of equipment amounted to four individual items. This can be reduced by employing a detector with a built-in amplifier and light source.

### **6.2.3. Temperature**

It has been conclusively demonstrated in previous work and in the current study that temperature has a major influence on the measured refractive index. Therefore any practical Fresnel reflection-based system should have an integrated temperature-monitoring capability. One such sensor design has been presented in Appendix E, and this should be pursued further as it offers a practical means of monitoring temperature.

### **6.2.4. Multiplexing the Fresnel reflection sensor**

The feasibility of multiplexing was investigated briefly and the proof-of-concept has been presented in Appendix F. Aspects that can be improved are: (i) simpler instrumentation using built-in amplifiers and detectors; (ii) a more efficient light-switching unit where the performance of each channel is identical; and (iii) faster switching times between the channel selector.

### **6.2.5. Translation of Fresnel reflection data to refractive index values**

At present, the output from the Fresnel reflection sensor is in Volts. However, it is required that the output be converted to refractive index values as it is of greater practical value. This can be done by calibrating the Fresnel reflection sensor using standard refractive index oils at a known temperature. However, the following factors would need to be fully understood and controlled: (i) instrumental drift(s); (ii) light source fluctuations; (iii) undesired nucleation of bubbles in the vicinity of the cleaved fibre-end; (iv) localised heating by infrared radiation; (v) the quality of the cleave; (vi) the orientation of the fibre-end with respect to the side-walls of the containment device; (vii) gain settings of the instruments; (viii) resins free of particulate contamination; (ix) gross diurnal fluctuations; (x) coupling of stray light. Although desirable, these issues are not necessarily practical or possible. Moreover, when thermosetting resins are used, the calibration using reference oils can lead to erroneous conclusions due to the exothermic nature of this class of material. In other words, the magnitude of the exotherm is a function of the volume of resin deployed and the heat-management of the system.

Other researchers have proposed schemes to convert the electrical signals from the Fresnel reflection sensor to refractive indices. However, these approaches were not adopted in the current study for the reasons stated above, and also because it was not possible in the timescale available to de-couple the relative contributions from each variable. Future work should be directed at investigating this further.

### **6.3. TRANSMISSION SENSOR**

#### **6.3.1. Fabrication method**

The method of fabrication used for aligning the two fibres was time-consuming, and great care and attention was required to avoid premature fracture of the sensor before deployment in the containment device. A minimum volume of UV-curable adhesive was required to control the overall dimension of the sensor. The implementation of micro-resin delivery apparatus would increase the productivity and consistency of sensor fabrication. The criteria for selecting the UV-curable resin needs to be defined based on the processing conditions of the resin system to be monitored. The author carried out a series of brief feasibility studies to develop a faster and more practical method of aligning the cleaved fibres. These included: (i) CO<sub>2</sub> laser inscribing; (ii) line scribing using a precision engraving pin; (iii) manual scribing using fibre-optic pen cleavers; and (iv) micro-moulding of U-grooves. One or more of these approaches should be pursued to determine whether these techniques offer a more practical and time-efficient route for the construction of the optical fibre transmission sensor.

### **6.4. EVANESCENT WAVE SPECTROSCOPY**

#### **6.4.1. Resin system**

The current study was limited to the analysis of one resin system. Further research into the synthesis of high-performance resin systems with a lower refractive index than S-2 glass fibres<sup>®</sup> should be undertaken. This will facilitate the development of a wide range of self-sensing composites for a number of industrial sectors such as aerospace, marine, military and automotive.

#### **6.4.2. Cut-off wavelength**

A wide range of reinforcing glass fibres is commercially available. It will be valuable to establish the correlation between the composition of the glass and the cut-off wavelengths.

### **6.5. HYPHENATED CONFIGURATION**

#### **6.5.1. Instrumentation**

The systems as used here required manual intervention to switch on/off each item. Software and hardware should be developed to enable the synchronisation of the operation of the various apparatus.

#### **6.5.2. Accommodation of the fibre bundle**

The design features of the Abbe refractometer should be inspected to decide if provision can be made to increase the curvature of the fibre bundle as it exits the custom-made cell. This will thereby increase the light throughput and hence the signal strength of the evanescent wave spectra.

## 7. REFERENCES

- 
- <sup>1</sup> Crosby, P. A., Powell, G. R., Frenando, G. F., France, C. M., Spooncer, R. C., Waters, D. N. "In situ cure monitoring of epoxy resins using optical fibre sensors", *Smart Materials and Structures*, 5 (4), 415-428. (1996).
- <sup>2</sup> Harris, D., Mahendran, R. S., Brooks, D., Al-Khodairi, F. A. A., Machavaram, V. R., Reynolds, P., Wang, L., Pandita, S. D., Paget, M., Wedderburn, J., Malik, S. A., Ojo, S. O., Kukureka, S. N., Fernando, G. F. "Self-sensing, self-healing and crack-arrestor composites", 16<sup>th</sup> Annual International Symposium Smart Structures/NDE. Proceedings of SPIE, Vol. 7293, 729204. San Diego, CA, USA. (2009).
- <sup>3</sup> Billmeyer Jr., F. W. *Textbook of Polymer Science*, 3<sup>rd</sup> Edition. John Wiley and Sons Inc., USA. (1984).
- <sup>4</sup> Tanaka, Y. "Synthesis and characteristics of epoxides", Chapter 2 in *Epoxy Resins: Chemistry and Technology*, 2<sup>nd</sup> Edition, 9-284. May, C. A. (Editor). Marcel Dekker Inc., New York, USA. (1988).
- <sup>5</sup> Hamerton, I. "Recent Developments in Epoxy Resins" in *Rapra Review Report 91*, 8 (7). (1996).
- <sup>6</sup> May, C. A. *Epoxy Resins: Chemistry and Technology*, 2<sup>nd</sup> Edition. May, C. A. (Editor). Marcel Dekker Inc., New York, USA. (1988).
- <sup>7</sup> Lewars, E. G. *Comprehensive Heterocyclic Chemistry: the structure, reactions, synthesis and uses of heterocyclic compounds*, Volume 7. Katritzky, A. R., Rees, C. W. (Editors). Pergamon Press, Oxford, UK. (1984).
- <sup>8</sup> Fernando, G. F., Degamber, B. "Process monitoring of fibre reinforced composites using optical fibre sensors", *International Materials Reviews*, 51 (2), 65-106. (2006).

- 
- <sup>9</sup> May, C. A. "Introduction to Epoxy Resins", Chapter 1 in Epoxy Resins: Chemistry and Technology, 2<sup>nd</sup> Edition, 1-8. May, C. A. (Editor). Marcel Dekker Inc., New York, USA. (1988).
- <sup>10</sup> Kroutilová, I., Matějka, L., Sikora, A., Souček, K., Staš, L. "Curing of epoxy systems at sub-glass transition temperature", Journal of Applied Polymer Science, 99 (6), 3669-3676. (2006).
- <sup>11</sup> Greenfield, D. C. L. "The cure characteristics and physical properties of glycidyl ether epoxy resins", PhD Thesis, Brunel University. (1986).
- <sup>12</sup> Hodd, K. A. "Epoxy resins" in Rapra Review Reports, 4 (2), 1-115. (1990).
- <sup>13</sup> Dobinson, B., Hofmann, W., Stark, B. P. The Determination of Epoxide Groups. Pergamon Press, Oxford, UK. (1969).
- <sup>14</sup> Kim, S. C., Ko, M. B., Jo, W. H. "Effect of the viscosity of epoxy prepolymer on the generated morphology in rubber-toughened epoxy resin", Polymer, 36 (11), 2189-2195. (1995).
- <sup>15</sup> Crosby, P. A., Fernando, G. F. "The application of optical fiber sensors in advanced fiber reinforced composites. Part 2. Cure monitoring", Chapter 3 in Optical Fiber Sensor Technology - Volume 3: Applications and Systems, 57-86. Grattan, K. T. V., Meggitt, B. T. (Editors). Kluwer Academic Publishers, The Netherlands. (1999).
- <sup>16</sup> Kozielski, K. A., George, G. A., St. John, N. A., Billingham, N. C. "Kinetic studies by FT-NIR of the curing reactions of two glycidyl ether epoxy resins mixed with stoichiometric quantities of 4,4'-DDS", High Performance Polymers, 6 (3), 263-286. (1994).
- <sup>17</sup> Min, B.-G., Stachurski, Z. H., Hodgkin, J.H., Heath, G. R. "Quantitative analysis of the cure reaction of DGEBA/DDS epoxy resins without and with thermoplastic polysulfone modifier using near infra-red spectroscopy", Polymer, 34 (17), 3620-3627. (1993).

- 
- <sup>18</sup> Strehmel, V., Scherzer, T. “Structural investigation of epoxy amine networks by mid- and near-infrared spectroscopy”, *European Polymer Journal*, 30 (3), 361-368. (1994).
- <sup>19</sup> Ellis, B., Found, M. S., Bell, J. R. “Effects of cure treatment on glass transition temperatures for a BADGE-DDM epoxy resin”, *Journal of Applied Polymer Science*, 59 (10), 1493-1505. (1996).
- <sup>20</sup> Macan, J., Brnardić, I., Ivanković, M., Mencer, H. J. “DSC study of cure kinetics of DGEBA-based epoxy resin with poly(oxypropylene) diamine”, *Journal of Thermal Analysis and Calorimetry*, 81 (2), 369-373. (2005).
- <sup>21</sup> Zvetkov, V. L. “Comparative DSC kinetics of the reaction of DGEBA with aromatic diamines: I. Non-isothermal kinetic study of the reaction of DGEBA with *m*-phenylene diamine”, *Polymer*, 42 (16), 6687-6697. (2001).
- <sup>22</sup> Zvetkov, V. L. “Comparative DSC kinetics of the reaction of DGEBA with aromatic diamines: II. Isothermal kinetic study of the reaction of DGEBA with *m*-phenylene diamine”, *Polymer*, 43 (4), 1069-1080. (2002).
- <sup>23</sup> Harris, D., Machavaram, V. R., Fernando, G. F. “Process monitoring and damage detection using optical fibre sensors”, Chapter 14 in *Management, Recycling and Reuse of Waste Composites*, 369-424. Goodship, V. (Editor). Woodhead Publishing Ltd., Cambridge, UK. (2010).
- <sup>24</sup> May, C. A. “Epoxy Resins” in *Engineered Materials Handbook, Volume 1: Composites*. ASM International, USA. (1987).
- <sup>25</sup> Ashcroft, W. R. in *Chemistry and Technology of Epoxy Resins*, 37-71. Ellis, B. (Editor). Blackie Academic and Professional, Glasgow, UK. (1993).

- 
- <sup>26</sup> Machavaram, V. R., Wang, L., Harris, D., Hellman, S., Mahendran, R. S., Biddlestone, F., Fernando, G. F. “Multiplexed Fresnel reflection sensing for monitoring cross-linking reactions” – to be submitted to Journal of Near Infrared Spectroscopy.
- <sup>27</sup> Shechter, L., Wynstra, J., Kurkijy, R. P. “Glycidyl ether reactions with amines”, Industrial and Engineering Chemistry, 48 (1), 94-97. (1956).
- <sup>28</sup> Dusek, K., Bleha, M., Lunak, S. “Curing of epoxide resins: Model reactions of curing with amines”, Journal of Polymer Science: Polymer Chemistry Edition, 15 (10), 2393-2400. (1977).
- <sup>29</sup> Hecht, J. Understanding Fiber Optics, 5<sup>th</sup> Edition. Pearson Education Inc., New Jersey, USA. (2006).
- <sup>30</sup> DeCusatis, C. M., DeCusatis, C. J. S. Fiber Optic Essentials. Elsevier Inc., Oxford, UK. (2006).
- <sup>31</sup> Buck, J. A. Fundamentals of Optical Fibers, 2<sup>nd</sup> Edition. John Wiley and Sons Inc., New Jersey, USA. (2004).
- <sup>32</sup> Commercially-available data from specified suppliers.
- <sup>33</sup> Gloge, D. “The typical fibre as a transmission medium”, Reports on Progress in Physics, 42 (11), 1778-1824. (1979).
- <sup>34</sup> Miller, S. E. “Light propagation in generalized lens-like media”, Bell System Technical Journal, 44 (9), 2017-2064. (1965). In: Gloge, D. “The typical fibre as a transmission medium”, Reports on Progress in Physics, 42 (11), 1778-1824. (1979).
- <sup>35</sup> Senior, J. M. Optical Fiber Communications: Principles and Practice, 3<sup>rd</sup> Edition. Prentice Hall International, UK. (2009).

- 
- <sup>36</sup> Österberg, U. L. “Optical Fiber, Cable and Connectors”, Chapter 1 in Handbook of Fiber Optic Data Communication, 2<sup>nd</sup> Edition, 3-38. DeCustias, C. (Editor). Academic Press, Ca, USA. (2002).
- <sup>37</sup> Jacobs, I. “Optical Fiber Communication Technology and System Overview”, Chapter 9 in Handbook of Optics, Volume V: Atmospheric Optics, Modulators, Fiber Optics, X-Ray and Neutron Optics. Bass, M. (Editor) *et al.*. McGraw-Hill. (2010).
- <sup>38</sup> Gilmore, M., Elliott, B. Fiber Optic Cabling, 2<sup>nd</sup> Edition. Newnes, Oxford, UK. (2002).
- <sup>39</sup> Crisp, J. Introduction to Fiber Optics, 2<sup>nd</sup> Edition. Newnes, Oxford, UK. (2001).
- <sup>40</sup> Stewart, G., Johnstone, W. “Evanescently Coupled Components”, Chapter 3 in Optical Fiber Sensors: Components and Subsystems, Volume 3. Culshaw, B., Dakin, J. (Editors). Artech House Inc., USA. (1996).
- <sup>41</sup> Powell, G. R., Crosby, P. A., Waters, D. N., France, C. M., Spooncer, R. C., Fernando, G. F. “*In-situ* cure monitoring using optical fibre sensors – a comparative study”, Smart Materials and Structures, 7 (4), 557-568. (1998).
- <sup>42</sup> Lodeiro, M., Mulligan, D. R. Measurement Good Practice Guide No. 75: Good Practice Guide to Cure Monitoring. Crown Copyright, Middlesex, UK. (2005).
- <sup>43</sup> Farquharson, S., Smith, W., Rigas, E., Granville, D. “Characterization of polymer composites during autoclave manufacturing by Fourier transform Raman spectroscopy”, Optical Methods for Industrial Processes, 4201, 103-111. (2001)
- <sup>44</sup> LeGrand, M., Bellenger, V. “The cure optimisation of carbon/epoxy prepregs”, Composites Science and Technology, 58 (5), 639-644. (1998).
- <sup>45</sup> Hodges, J., Yates, B., Darby, M. I., Wostenholm, G. H., Clemment, J. F., Keates, T. F. “Residual stresses and the optimum cure cycle for an epoxy resin”, Journal of Materials Science, 24 (6), 1984-1990. (1989).

- 
- <sup>46</sup> White, S. R., Hahn, H. T. “Cure cycle optimisation for the reduction of processing-induced residual stresses in composite materials”, *Journal of Composite Materials*, 27 (14), 1352-1378. (1993).
- <sup>47</sup> Hojjati, M., Hoa, S. V. “Curing simulation of thick thermosetting composites”, *Composites Manufacturing*, 5 (3), 159-169. (1994).
- <sup>48</sup> Mulligan, D. R. “Cure Monitoring for Composites and Adhesives” in *Rapra Review Report* 164, 14 (8). (2003).
- <sup>49</sup> St. John, N. A., George, G. A. “Cure kinetics and mechanisms of a tetraglycidyl-4,4'-diaminodiphenylmethane/diaminodiphenylsulphone epoxy resin using near i.r. spectroscopy”, *Polymer*, 33 (13), 2679-2687. (1992).
- <sup>50</sup> Occhiello, E., Garbassi, F., Morra, M., Nicolais, L. “Spectroscopic characterization of interfaces in polymer composites”, *Composites Science and Technology*, 36 (2), 133-151. (1989).
- <sup>51</sup> DeBakker, C. J., George, G. A., St. John, N. A., Fredericks, P. M. “The kinetics of the cure of an advanced epoxy resin by Fourier transform Raman and near-IR spectroscopy”, *Spectrochimica Acta*, 49A (5/6), 739-752. (1993).
- <sup>52</sup> Chike, K. E., Myrick, M. L., Lyon, R. E., Angel, S. M. “Raman and near-infrared studies of an epoxy resin”, *Applied Spectroscopy*, 47 (10), 1631-1635. (1993).
- <sup>53</sup> Younes, M., Wartewig, S., Lellinger, D., Strehmel, B., Strehmel, V. “The curing of epoxy resins as studied by various methods”, *Polymer*, 35 (24), 5269-5278. (1994).
- <sup>54</sup> Toussaint, A., Cuypers, P., D'Hont, L. “DSC and TMA analysis of the curing of a liquid epoxy resin with diamines”, *Journal of Coatings Technology*, 57 (728), 71-82. (1985).
- <sup>55</sup> Du, S., Guo, Z.-S., Zhang, B., Wu, Z. “Cure kinetics of epoxy resin used for advanced composites”, *Polymer International*, 53 (9), 1343-1347. (2004).

- 
- <sup>56</sup> Frey, T., Große-Brinkhaus, K.-H., Rökrath, U. “Cure monitoring of thermoset coatings”, *Progress in Organic Coatings*, 27 (1-4), 59-66. (1996).
- <sup>57</sup> Eloundou, J. P., Feve, M., Gerard, J. F., Harran, D., Pascault, J. P. “Temperature dependence of the behaviour of an epoxy-amine system near the gel point through viscoelastic study. 1. Low-Tg epoxy-amine system”, *Macromolecules*, 29 (21), 6907-6916. (1996).
- <sup>58</sup> White, S. R., Mather, P. T., Smith, M. J. “Characterization of the cure-state of DGEBA-DDS epoxy using ultrasonic, dynamic mechanical, and thermal probes”, *Polymer Engineering and Science*, 42 (1), 51-67. (2002).
- <sup>59</sup> Su, C.-T., Lin, K.-Y., Lee, T.-J., Liang, M. “Preparation, characterization and curing properties of epoxy-terminated poly (alkyl-phenylene oxide)s”, *European Polymer Journal*, 46 (7), 1488-1497. (2010).
- <sup>60</sup> Soni, H. K., Patel, V. S., Patel, R. G. “Effect of fortifier on the cure kinetics and thermal stability of N,N,N',N'-tetraglycidyl ether of 4,4'-diaminodiphenyl methane using amines as curing agents”, *Thermochimica Acta*, 196 (2), 327-337. (1992).
- <sup>61</sup> Liaw, D. J., Shen, W. C. “Curing of acrylated epoxy-resin based on bisphenol-S”, *Polymer Engineering and Science*, 34 (16), 1297-1303. (1994).
- <sup>62</sup> Griffiths, P. R., de Haseth, J. A. *Fourier Transform Infrared Spectrometry*, 2<sup>nd</sup> Edition. John Wiley and Sons, New Jersey, USA. (2007).
- <sup>63</sup> Stuart, B. *Infrared Spectroscopy: Fundamentals and Applications*. John Wiley and Sons, Chichester, UK. (2004).
- <sup>64</sup> Newport FT-IR Spectroscopy manual. “Definitions of Characteristics”, Newport Corporation, California, USA.
- <sup>65</sup> Xu, L., Fu, J. H., Schlup, J. R. “In situ near-infrared spectroscopic investigation of the kinetics and mechanisms of reactions between phenyl glycidyl ether (PGE) and

---

multifunctional aromatic amines”, *Industrial and Engineering Chemistry Research*, 35 (3), 963-972. (1996).

<sup>66</sup> Poisson, N., Lachenal, G., Sautereau, H. “Near- and mid- infrared spectroscopy studies of an epoxy reactive system”, *Vibrational Spectroscopy*, 12 (2), 237-247. (1996).

<sup>67</sup> Mijović, J., Andjelić, S. “A study of reaction kinetics by near-infrared spectroscopy. 1. Comprehensive analysis of a model epoxy-amine system”, *Macromolecules*, 28 (8), 2787-2796. (1995).

<sup>68</sup> Morgan, R. J., Shin, E. E., Rosenberg, B., Jurek, A. “Characterization of the cure reactions of bismaleimide composite matrices”, *Polymer*, 38 (3), 639-646. (1997).

<sup>69</sup> Varley, R. J., Heath, G. R., Hawthorne, D. G., Hodgkin, J. H., Simon, G. P. “Toughening of a trifunctional epoxy system: 1. Near infra-red spectroscopy of homopolymer cure”, *Polymer*, 36 (7), 1347-1355. (1995).

<sup>70</sup> Degamber, B., Fernando, G. F. “Process monitoring of a thermosetting resin using optical-fiber sensors in a microwave environment”, *IEEE Sensors Journal*, 4 (6), 713-721. (2004).

<sup>71</sup> Mahendran, R. S., Wang, L., Machavaram, V. R., Pandita, S. D., Chen, R., Kukureka, S. N., Fernando, G. F. “Fiber-optic sensor design for chemical process and environmental monitoring”, *Optics and Lasers*, 47 (10), 1069-1076. (2009).

<sup>72</sup> Wang, L., Pandita, S., Machavaram, V. R., Malik, S., Harris, D., Fernando, G. F. “Characterisation of the cross-linking process in an E-glass fibre-epoxy composite using evanescent wave spectroscopy”, *Composites Science and Technology*, 69 (13), 2069-2074. (2009).

<sup>73</sup> Mirabella, F. M. “Introduction”, Chapter 1 in *Modern Techniques in Applied Molecular Spectroscopy: Techniques in Analytical Chemistry*. Mirabella, F. M. (Editor). John Wiley and Sons Inc., New York, USA. (1998).

- 
- <sup>74</sup> Koenig, J. L. *Spectroscopy of Polymers*, Second Edition. Elsevier, New York, USA. (1999).
- <sup>75</sup> Xu, L., Fu, J. H., Schlup, J. R. "In situ near-infrared spectroscopic investigation of epoxy resin-aromatic amine cure mechanisms", *Journal of the American Chemical Society*, 116 (7), 2821-2826. (1994).
- <sup>76</sup> Kemp, W. *Organic Spectroscopy*, Third Edition. Palgrave Macmillan, UK. (1991). In: Degamber, B. "Microwave curing and process monitoring of thermosets", PhD Thesis, Cranfield University. (2003).
- <sup>77</sup> Li, L., Wu, Q., Li, S., Wu, P. "Study of the infrared spectral features of an epoxy curing mechanism", *Applied Spectroscopy*, 62 (10), 1129-1136. (2008).
- <sup>78</sup> Rigail-Cedeño, A., Sung, C. S. P. "Fluorescence and IR characterisation of epoxy cured with aliphatic amines", *Polymer*, 46 (22), 9378-9384. (2005).
- <sup>79</sup> Mijović, J., Andjelić, S. "Monitoring of reactive processing by remote mid infra-red spectroscopy", *Polymer*, 37 (8), 1295-1303. (1996).
- <sup>80</sup> George, G., Hynard, N., Cash, G., Rintoul, L., O'Shea, M. "Spectroscopic probes for real-time monitoring of polymer modification and degradation reactions", *Comptes Rendus Chimie*, 9 (11-12), 1433-1443. (2006).
- <sup>81</sup> Fernando, G. F., Hameed, A., Winter, D., Tetlow, J., Leng, J., Barnes, R., Mays, G., Kister, G. "Structural health monitoring of concrete structures via optical fiber sensors: sensor protection systems", *Journal of Structural Health Monitoring*, 2 (2), 123-135. (2003).
- <sup>82</sup> Measures, R. M. *Structural Monitoring with Fiber Optic Technology*. Academic Press, London, UK. (2001).
- <sup>83</sup> Aust, J. F., Booksh, K. S., Myrick, M. L. "Novel in-situ probe for monitoring polymer curing", *Applied Spectroscopy*, 50 (3), 382-387 (1996).

- 
- <sup>84</sup> Aust, J. F., Booksh, K. S., Stellman, C. M., Parnas, R. S., Myrick, M. L. “Precise determination of percent cure of epoxide polymers and composites via fibre-optic Raman spectroscopy and multivariate analysis”, *Applied Spectroscopy*, 51 (2), 247-252 (1997).
- <sup>85</sup> Mijović, J., Andjelić, S., Kenny, J. “In-situ real-time monitoring of epoxy/amine kinetics by remote near infrared spectroscopy”, *Polymers for Advanced Technologies*, 7 (1), 1-16. (1996).
- <sup>86</sup> Mijović, J., Andjelić, S. “In-situ real-time monitoring of reactive systems by remote fibre-optic near-infrared spectroscopy”, *Polymer*, 36 (19), 3783-3786. (1995).
- <sup>87</sup> Rogers, D., Marand, E., Hill, D. J. T., George, G. A. “Anomalies between microwave and thermal cure kinetics of epoxy-amine resin systems”, *High Performance Polymers*, 11 (1), 27-39. (1999).
- <sup>88</sup> Fernando, G. F., Liu, T., Crosby, P., Doyle, C., Martin, A., Brooks, D., Ralph, B., Badcock, R. “A multi-purpose optical fibre sensor design for fibre reinforced composite materials”, *Measurement Science and Technology*, 8 (10), 1065-1079. (1999).
- <sup>89</sup> Crosby, P. A., Connolley, M., Fernando, G. F. “Cure monitoring of advanced fibre reinforced composites using an optical fibre sensor”, 7<sup>th</sup> International Conference on Fibre Reinforced Composites, 128-135. Newcastle, UK. (1998).
- <sup>90</sup> Machavaram, V. R., Badcock, R. A., Fernando, G. F. “Fabrication of intrinsic fibre Fabry-Perot cavities in silica optical fibres via F<sub>2</sub>-laser ablation”, *Measurement Science and Technology*, 18 (3), 928-934. (2007).
- <sup>91</sup> Calvert, P., George, G., Rintoul, L. “Monitoring of cure and water uptake in a freeformed epoxy resin by an embedded optical fibre”, *Chemistry in Materials*, 8 (6), 1298-1301. (1996).
- <sup>92</sup> Khijwania, S. K., Gupta, B. D. “Fiber optic evanescent field absorption sensor with high sensitivity and linear dynamic range” *Optics Communications*, 152 (4-6), 259-262. (1998).

- 
- <sup>93</sup> Elosua, C., Matias, I. R., Barriain, C., Arregui, F. J. “Volatile organic compound optical fiber sensors”, *Sensors*, 6, 1440-1465. (2006).
- <sup>94</sup> Machavaram, V. R. “Micro-machining Techniques for the fabrication of Fibre Fabry-Perot sensors”, PhD Thesis, Cranfield University. (2006).
- <sup>95</sup> Harris, D., Mahendran, R. S., Brooks, D., Al-Khodairi, F. A. A., Machavaram, V. R., Reynolds, P., Wang, L., Pandita, S. D., Paget, M., Wedderburn, J., Malik, S. A., Ojo, S. O., Kukureka, S. N., Fernando, G. F. “Self-sensing, self-healing and crack-arrestor composites”, 16<sup>th</sup> Annual International Symposium Smart Structures/NDE. Proceedings of SPIE, Volume 7293, 729324. San Diego, CA. USA. (2009).
- <sup>96</sup> Hayes, S., Liu, T., Brooks, D., Monteith, S., Ralph, B., Vickers, S., Fernando, G. F. “*In situ* self-sensing fibre reinforced composites”, *Smart Materials and Structures*, 6 (4), 432-440. (1997).
- <sup>97</sup> Zolfaghar, K., Khan, N., Brooks, D., Hayes, S., Liu, T., Roca, J., Lander, J., Fernando, G. F. “Quartz and E-glass fibre self-sensing composites”, Proceedings of SPIE, Volume 3321, 314-328. (1996).
- <sup>98</sup> Wang, L., Machavaram, V. R., Mahendran, R., Harris, D., Pandita, S. D., Tomlin, A., Redmore, E., Malik, S. A., Fernando, G. F. “A comparison of cure monitoring techniques”, Proceedings of SPIE, Volume 7292, 729213. San Diego, CA. USA. (2009).
- <sup>99</sup> Malik, S. A., Wang, L., Mahendran, R. S., Harris, D., Ojo, S. O., Collins, D., Paget, M., Pandita, S. D., Machavaram, V. R., Fernando, G. F. "In-situ damage detection using self-sensing composites", 16<sup>th</sup> Annual International Symposium Smart Structures/NDE. Proceedings of SPIE, Vol. 7292, 729204. San Diego, CA. USA. (2009).
- <sup>100</sup> Kister, G., Wang, L., Ralph, B., Fernando, G. F. “Self-sensing E-glass fibres”, *Optical Materials*, 2 (4), 13-727. (2003).

- 
- <sup>101</sup> Afromowitz, M. A. “Fiber optic polymer cure sensor”, *Journal of Lightwave Technology*, 6 (10), 1591-1594. (1988).
- <sup>102</sup> Afromowitz, M. A., Lam, K. Y. “Fiber optic cure sensor for thermoset composites”, *Proceedings of SPIE*, Volume 986, 135-139. (1988). In: Roberts, S. S. J., Davidson, R. “Cure and fabrication monitoring of composite materials with fibre-optics sensors”, *Composites Science and Technology*, 49 (3), 265-276. (1993).
- <sup>103</sup> Lekakou, C., Cook, S., Deng, Y., Ang, T. W., Reed, G. T. “Optical fibre sensor for monitoring flow and resin curing in composites manufacturing”, *Composites: Part A*, 37 (6), 934-938. (2006).
- <sup>104</sup> Li, C., Cao, M., Wang, R., Wang, Z., Qiao, Y., Wan, L., Tian, Q., Liu, H., Zhang, D., Liang, T., Tang, C. “Fiber-optic composite cure sensor: monitoring the curing process of composite material based on intensity modulation”, *Composites Science and Technology*, 63 (12), 1749-1758. (2003).
- <sup>105</sup> Badcock, R. A., Fernando, G. F. “Fatigue damage detection in carbon-fiber-reinforced composites using an intensity-based optical fiber sensor”, *Proc. SPIE*, 2444, 422. 422-431. (1995).
- <sup>106</sup> Afromowitz, M. A., Lam, K. Y. “The optical properties of curing epoxies and applications to the fiber-optic epoxy cure sensor”, *Sensors and Actuators*, A21-A23, 1107-1110. (1990).
- <sup>107</sup> Cusano, A., Cutolo, A., Giordano, M., Nicolais, L. “An optoelectronic sensor for cure monitoring in thermoset-based composites”, *Sensors and Actuators*, 84 (3), 270-275. (2000).
- <sup>108</sup> Vacher, S., Molimard, J., Gagnaire, H., Vautrin, A. “A Fresnel’s reflection optical fibre sensor for thermoset polymer cure monitoring”, *Polymers and Polymer Composites*, 12 (4), 269-276. (2004).
- <sup>109</sup> Klein, M. V., Furtak, T. E. *Optics*, 2<sup>nd</sup> edition. John Wiley & Sons, London, UK. (1986).

- 
- <sup>110</sup> Cusano, A., Cutolo, A., Giordano, M., Nicolais, L. “Optoelectronic refractive index measurements: application to smart processing”, *IEEE Sensors Journal*, 3 (6), 781-787. (2003).
- <sup>111</sup> Liu, Y. M., Ganesh, C., Steele, J. P. H., Jones, J. E. “Fiber optic sensor development for real-time in-situ epoxy cure monitoring”, *Journal of Composite Materials*, 31 (1), 87-102. (1997).
- <sup>112</sup> Hamad, F. A., Imberton, F., Bruun, H. H. “An optical probe for measurements in liquid-liquid two-phase flow”, *Measurement Science and Technology*, 8 (10), 1122-1132. (1997).
- <sup>113</sup> Hamad, F. A., Imberton, F., Bruun, H. H. “A dual optical probe for volume fraction, drop velocity and drop size measurements in liquid-liquid two-phase flow”, *Measurement Science and Technology*, 11 (9), 1307-1318. (2000).
- <sup>114</sup> Fordham, E. J., Holmes, A., Ramos, R. T., Simonian, S., Huang, S-M., Lenn, C. P. “Multi-phase-fluid discrimination with local fibre-optical probes: I. Liquid/liquid flows”, *Measurement Science and Technology*, 10 (12). 1329-1337. (1999).
- <sup>115</sup> Bosch, M. E., Sánchez, A. J. R., Rojas, F. S., Ojeda, C. B. “Recent development in optical fiber biosensors”, *Sensors*, 7, 797-859. (2007).
- <sup>116</sup> Skivesen, N., Horvath, R., Pedersen, H. C. “Optimization of metal-clad waveguide sensors”, *Sensors and Actuators B*, 106 (2), 668-676. (2005).
- <sup>117</sup> Kuang, K. S. C., Kenny, R., Whelan, M. P., Cantwell, W. J., Chalker, P. R. “Embedded fibre Bragg grating sensors in advanced composite materials”, *Composites Science and Technology*, 61 (10), 1379-1387. (2001).
- <sup>118</sup> Dewynter-Marty, V., Ferdinand, P., Bocherens, E., Carbone, R., Beranger, H., Bourasseau, S., Dupont, M., Balageas, D. “Embedded fiber Bragg grating sensors for industrial composite

---

cure monitoring”, *Journal of Intelligent Material Systems and Structures*, 9 (10), 785-787. (1998).

<sup>119</sup> De Oliveira, R., Lavanchy, S., Chatton, R., Constantini, D., Michaud, V., Salathé, R., Månson, J.-A. E. “Experimental investigation of the effect of the mould thermal expansion on the development of internal stresses during carbon fibre composite processing”, *Composites Part A*, 39 (7), 1083-1090. (2008).

<sup>120</sup> Gebremichael, Y. M., Li, W., Boyle, W. J. O., Meggitt, B. T., Grattan, K. T. V., McKinley, B., Fernando, G. F., Kister, G., Winter, D., Canning, L., Luke, S. “Integration and assessment of fibre Bragg grating sensors in an all-fibre reinforced polymer composite road bridge”, *Sensors and Actuators A*, 118 (1), 78-85. (2005).

<sup>121</sup> Harris, D., Fernando, G. F. “Simultaneous acquisition of data on refractive index, strain, temperature and cross-linking kinetics”, 17<sup>th</sup> International Conference on Composite Materials: ICCM-17. Edinburgh, UK. (2009).

<sup>122</sup> Kersey, A. D., Davis, M. A., Patrick, H. J., LeBlanc, M., Koo, K. P., Askins, C. G., Putnam, M. A., Friebele, E. J. “Fiber grating sensors”, *Journal of Lightwave Technology*, 15 (8), 1442-1463. (1997).

<sup>123</sup> Rheims, J., Koser, J., Wriedt, T. “Refractive-index measurements in the near-IR using an Abbe refractometer”, *Measurement Science and Technology*, 8 (6), 601-605. (1997).

<sup>124</sup> Chailleux, E., Salvia, M., Jaffrezic-Renault, N., Matejec, V., Kasik, I. “In situ study of the epoxy cure process using a fibre-optic sensor”, *Smart Materials and Structures*, 10 (2), 194-202. (2001).

<sup>125</sup> Fernando, G. F. “Fibre optic sensor systems for monitoring composite structures”, *Reinforced Plastics*, 49 (11), 41-49. (2005).

- 
- <sup>126</sup> Crosby, P. “In-situ cure monitoring of epoxy resin systems”, PhD Thesis, Brunel University. (1997).
- <sup>127</sup> DeBakker, C. J., St John, N. A., George, G. A. “Simultaneous differential scanning calorimetry and near-infra-red analysis of the curing of tetraglycidyl-diaminodiphenylmethane with diaminodiphenylsulphone”, *Polymer*, 34 (4), 716-725. (1993).
- <sup>128</sup> Dumitrescu, O. R. “Simultaneous Differential Scanning Calorimetry-Fourier Transform Infrared Spectroscopy”, PhD Thesis, Cranfield University. (2003).
- <sup>129</sup> Degamber, B., Winter, D., Tetlow, J., Teagle, M., Fernando, G. F. “Simultaneous DSC/FTIRS/TMA”, *Measurement Science and Technology*, 15 (9), L5-L10. (2004).
- <sup>130</sup> Yoshida, H., Kinoshita, R., Teramoto, Y. “Development of the simultaneous thermal analysis/X-ray scattering measurement system”, *Thermochimica Acta*, 264 (1-2), 173-183. (1995).
- <sup>131</sup> Haines, P. J., Skinner, G. A. “Simultaneous differential scanning calorimetry and reflected light intensity measurement”, *Thermochimica Acta*, 59 (3), 343-359. (1982).
- <sup>132</sup> Haines, P. J., Skinner, G. A. “Simultaneous differential scanning calorimetry and reflected light intensity measurements in polymer studies”, *Thermochimica Acta*, 134, 201-206. (1988).
- <sup>133</sup> Giordano, M., Laudati, A., Russo, M., Nasser, J., Persiano, G. V., Cusano, A. “Advanced cure monitoring by optoelectronic multifunction sensing system”, *Thin Solid Films*, 450 (1), 190-194. (2004).
- <sup>134</sup> Antonucci, V., Giordano, M., Cusano, A., Nasser, J., Nicolais, L. “Real-time monitoring of cure and gelification of a thermoset matrix”, *Composites Science and Technology*, 66 (16), 3273-3280. (2006).

- 
- <sup>135</sup> Crsoby, P. A., Doyle, C., Tuck, C., Singh, M., Fernando, G. F. “Multi-functional fiber optic sensors for cure and temperature monitoring”, Proceedings of SPIE, Volume 3670, 144-153. Newport Beach, CA., USA. (1999).
- <sup>136</sup> Mahendran, R. S., Machavaram, V. R., Wang, L., Burns, J. M., Harris, D., Kukureka, S. N., Fernando, G. F. “A novel multi-functional fibre optic sensor”, 16<sup>th</sup> Annual International Symposium Smart Structures/NDE. Proceedings of SPIE, Volume 7293, 729204. San Diego, CA., USA. (2009).
- <sup>137</sup> Data obtained through private communication with Aomolin Ltd.
- <sup>138</sup> AGY datasheet, LIT-2004-081 R3.
- <sup>139</sup> AGY datasheet, LIT-2004-061.
- <sup>140</sup> AGY datasheet, LIT-2009-351 R1(1/09).
- <sup>141</sup> Abbe 60 Refractometer User Guide, Issue 4.0. (2002)
- <sup>142</sup> EpoTek<sup>®</sup> 310M Technical Datasheet, 2005.
- <sup>143</sup> EpoTek<sup>®</sup> 314 Datasheet, 1997.
- <sup>144</sup> Bruker Infrared Spectroscopy Guide, BOPT-090401
- <sup>145</sup> Scherzer, T., “Characterization of diol modified epoxy resins by near- and mid-infrared spectroscopy”, Journal of Applied Polymer Science, 51 (3), 491-502. (1994).
- <sup>146</sup> Tosi, C., Pinto, A. “Near-infrared spectroscopy of hydrocarbon functional groups”, Spectrochimica Acta, 28A (3), 585-597. (1972).
- <sup>147</sup> Xu, L., Schlup, J. R. “Etherification versus amine addition during epoxy resin/amine cure: An *in situ* study using near-infrared spectroscopy”, Journal of Applied Polymer Science, 67 (5), 895-901. (1998).
- <sup>148</sup> Workman, J., Weyer, L. Practical Guide to Interpretative Near-infrared Spectroscopy. CRC Press, USA. (2007).

---

<sup>149</sup> Dannenberg, H. “Determination of functional groups in epoxy resins by near-infrared spectroscopy”, SPE Transactions, January, 78-88. (1963).

<sup>150</sup> www.agy.com; LIT-2004-341 (03/04).

<sup>151</sup> Yoon, H.-J., Constantini, D. M., Limberger, H. G., Salathé, R. P., Kim, C.-G., Michaud, V. “In situ strain and temperature monitoring of adaptive composite materials”, Journal of Intelligent Material Systems and Structures, 17 (12), 1059-1067. (2006).

<sup>152</sup> Pal, S., Mandal, J., Sun, T., Grattan, K. T. V., Fokine, M., Carlsson, F., Fonjallaz, R. Y., Wade, S. A., Collins, S. F. “Characteristics of potential fibre Bragg grating sensor-based devices at elevated temperatures”, Measurements Science and Technology, 14 (7), 1131-1136. (2003).

## **APPENDIX A**

### **FRESNEL REFLECTION SENSOR LOCATION AND BONDING**

Figure AA-1a represents the master diagram, which was shown previously in Chapter 3. The variations in position and bonding of the Fresnel reflection sensors are as follows: (b) the distal fibres were split and separated by the thermocouple; (c) the distal fibres were together and secured using UV-resin over a length of approximately 15 mm, but ensuring the resin was at least 5 mm from the fibre-ends; (d) the distal fibres were together and located close to the side-wall of the cuvette; and (e) the distal fibres were together and secured close to the side-wall of the cuvette with UV-curable resin over a length of approximately 15 mm but at least 5 mm from the fibre-ends. In cases b, d and e, the thermocouple was located centrally. As indicated in a, the fibre-ends and the tip of the thermocouple were aligned at the mid-point of the cell length; approximately 22 mm from the open-end of the cell. Figure AA-1f shows the configuration of the cell when two Fresnel reflection sensors were employed.

Figure AA-1g shows the experimental set-up where the fibres were cantilevered and mechanical vibrations were induced at six separate locations, as shown by the numbers 1-6.

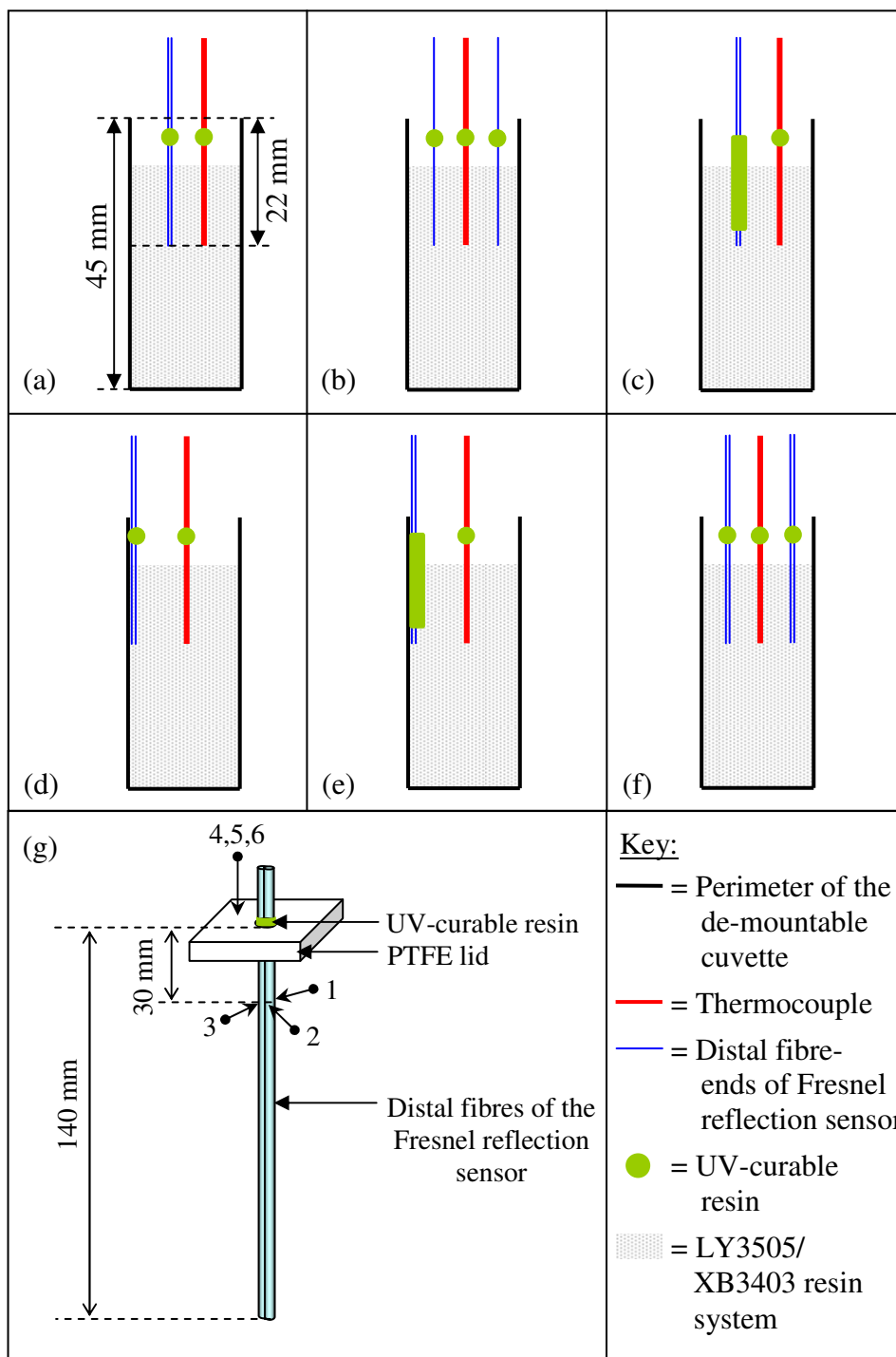


**Figure AA-1. Schematic illustrations to show: (a to f) variable positions of the Fresnel reflection sensor and volumes of UV-curable resin used to attach the sensors in a de-mountable cuvette, and (g) the locations of six mechanically-induced vibrations (labelled**

**1-6).**

## **APPENDIX B**

### **FEASIBILITY STUDIES USING THE FRESNEL REFLECTION SENSOR**

#### **AB1 Introduction**

A brief study was undertaken to characterise the cross-linking of two classes of resins: (i) an aerospace-grade epoxy/amine resin (Hexcel 913); and (ii) a photo-curable thermoset (NOA 68), using a single-mode Fresnel reflection sensor.

#### **AB2 Hexcel 913**

##### *AB2.1 Experimental procedure*

The Hexcel 913 resin was in the form of a film and was stored at -18 °C. A sample of the film was compacted at room temperature and de-gassed. A Fresnel reflection sensor and a thermocouple were secured in a de-mountable cuvette. The compacted sample was placed in the cuvette on top of the sensor and thermocouple, as illustrated in Figure AB2-1. The cell was then sealed using silicone rubber, and the assembly was placed in the temperature-regulated cuvette holder at room temperature. After ten minutes the temperature was increased to 30°C and held for 25 minutes. Finally, the temperature was increased to 70°C and held overnight.

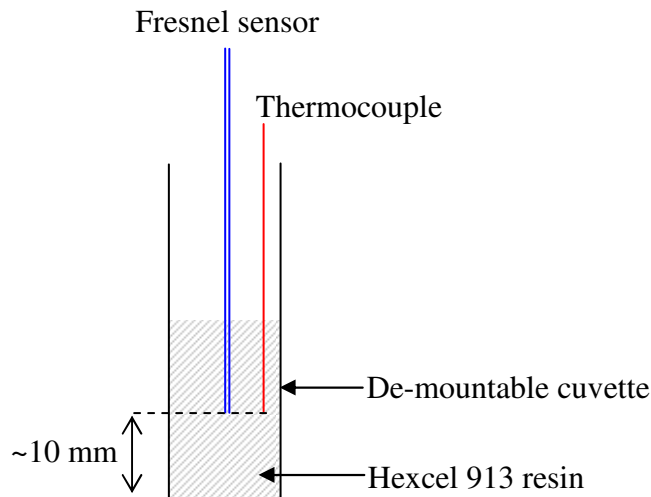


**Figure AB2-1. A schematic illustration of the locations of the Fresnel reflection sensor and thermocouple within the de-mountable cuvette, containing the Hexcel 913 resin.**

#### *AB2.2 Results and discussion*

Figure AB2-2a shows the responses of the Fresnel reflection sensor and thermocouple during the processing of the Hexcel 913 resin system. As noted with the LY3505/XB3403 resin system, there is a decrease in the Fresnel reflection signal as the temperature is increased. Once the isothermal hold of 70 °C has been attained, a steady increase in the Fresnel reflection is observed up to approximately 700 minutes, after which point retardation of the rate of increase occurs. At around 1200 minutes, the Fresnel reflection signal represents the maximum extent of reaction that can be achieved at 70 °C.

The “noise” in the Fresnel reflection signal between 30 and 450 minutes is likely to be due to the wetting of the cleaved end-face by the resin system as the viscosity drops. Furthermore, the entrapment of air bubbles in the resin due to the compaction process may also be a contributing factor to the observed noise.

A repeat experiment was undertaken and the results are shown in Figure AB2-2b, along with the above-mentioned data, for ease of comparison. It is readily apparent that the datasets are similar. This gives confidence that the low-cost Fresnel reflection sensor can be used to monitor the cure process of a high-performance resin system which is used in the manufacture of helicopter rotor blades.

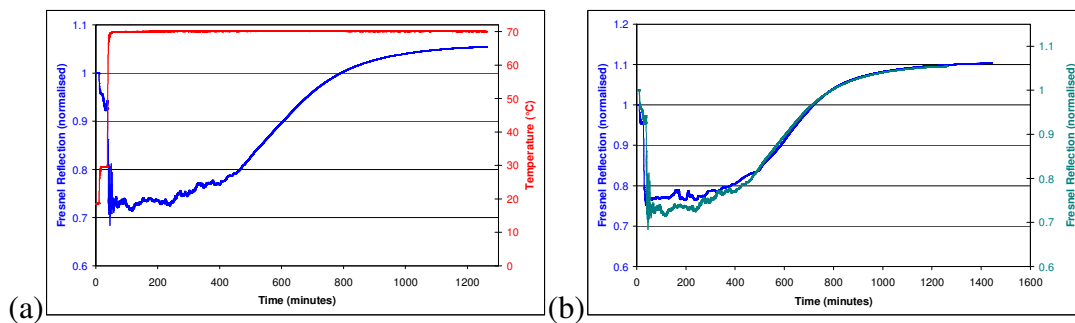


**Figure AB2-2. (a) The responses of the Fresnel reflection sensor and thermocouple during the cure of Hexcel 913 resin at 70 °C; (b) Fresnel reflection sensor repeat data during cure at 70 °C.**

### **AB3 NOA 68**

#### *AB3.1 Experimental*

NOA 68 resin is a photo-curable medium which is used in the optoelectronics industry. The experimental set-up used here is illustrated in Figure AB3-1, where the Fresnel reflection sensor was secured on a microscope slide. A UV light source was positioned directly above the fibre-ends, at a distance of 20 mm. A drop of NOA 68 resin was introduced onto the cleaved fibre-ends and the Fresnel reflection signal was recorded. After 20 seconds the UV light source was switched on; the light source switched off automatically after 60 seconds.

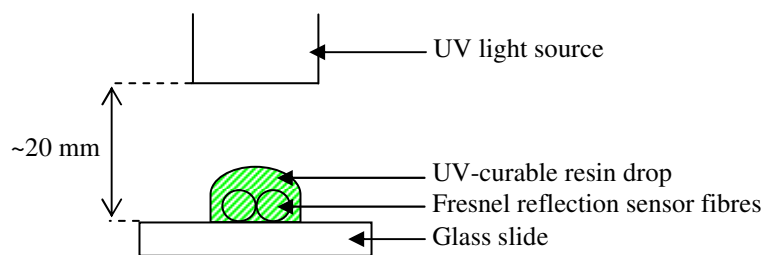


**Figure AB3-1. A schematic illustration of a drop of NOA 68 resin on the Fresnel reflection sensor fibre-ends, with the UV light source 20 mm directly above.**

### *AB3.2 Results and discussion*

A stable signal is observed up to 20 seconds for when the Fresnel reflection sensor is immersed in NOA 68 resin. Once the UV light source is switched on, a rapid increase in the signal can be seen. After 60 seconds the light source switched off automatically, and a step change occurred in the sensor output because the heat source is removed. As a result, the sample cools and a concomitant increase in the refractive index is experienced. The rates of increase in the Fresnel reflection signal when the UV light is on and when it has turned off, are indicated in Figure AB3-2. It can also be seen that an equilibrium state is attained after approximately 5 minutes indicating that the cure reaction has ceased.

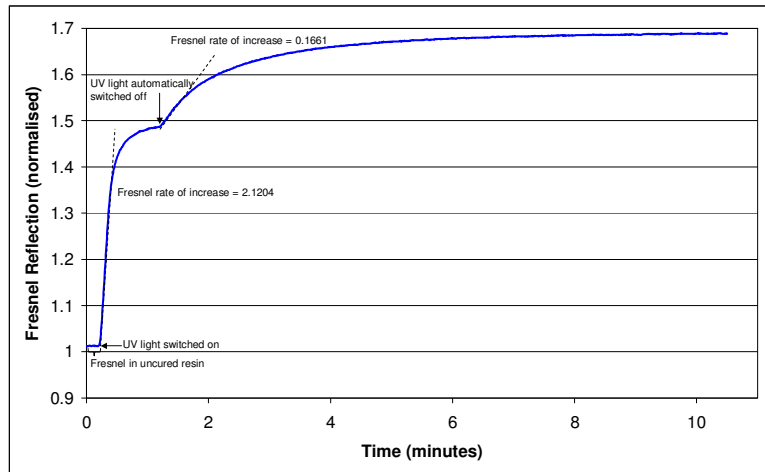


**Figure AB3-2. The response of the Fresnel reflection sensor when immersed in NOA 68 resin and exposed to UV light.**

A separate study was undertaken to quantify the magnitude of the heat generated by the UV light source as a function of distance from the surface of the sample. It was found that when the light source was located at a distance of 20 mm from the sample, a temperature rise of approximately 50 °C was recorded.

In order to investigate the temperature effect further, and to establish if the resin continued to cure after repeat exposure to UV light, the sample was subjected to a series of periodic UV exposures for 60 seconds at a time. The effect of this is shown in Figure AB3-3, where a rapid decrease in the signal was observed each time the UV light was switched on. This was followed by a rapid increase once the light source was switched off. These trends are indicative of the temperature change discussed previously. However, the magnitude of the rise was seen to increase with each exposure up to five sequential exposures (labelled 1-5 in Figure AB3-3). The implication here is that the resin system still has residual monomer capable of curing.

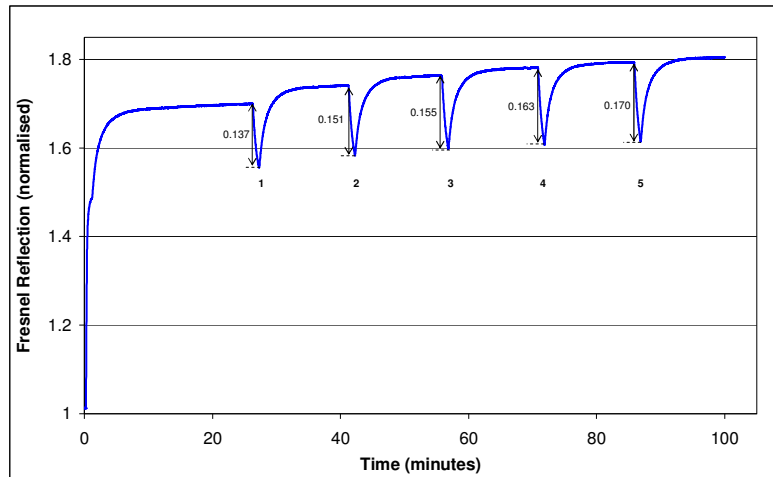


**Figure AB3-3. The response of the Fresnel reflection sensor when embedded in UV-cured resin and re-exposed to UV light on five separate occasions.**

#### **AB4 Conclusions**

It has been demonstrated that the Fresnel reflection sensor is versatile. Here, cure monitoring of an aerospace-grade resin system and a photo-curable adhesive was successfully undertaken.

## APPENDIX C

### INFLUENCE OF PROBE POSITION ON TEMPERATURE AND FRESNEL REFLECTION

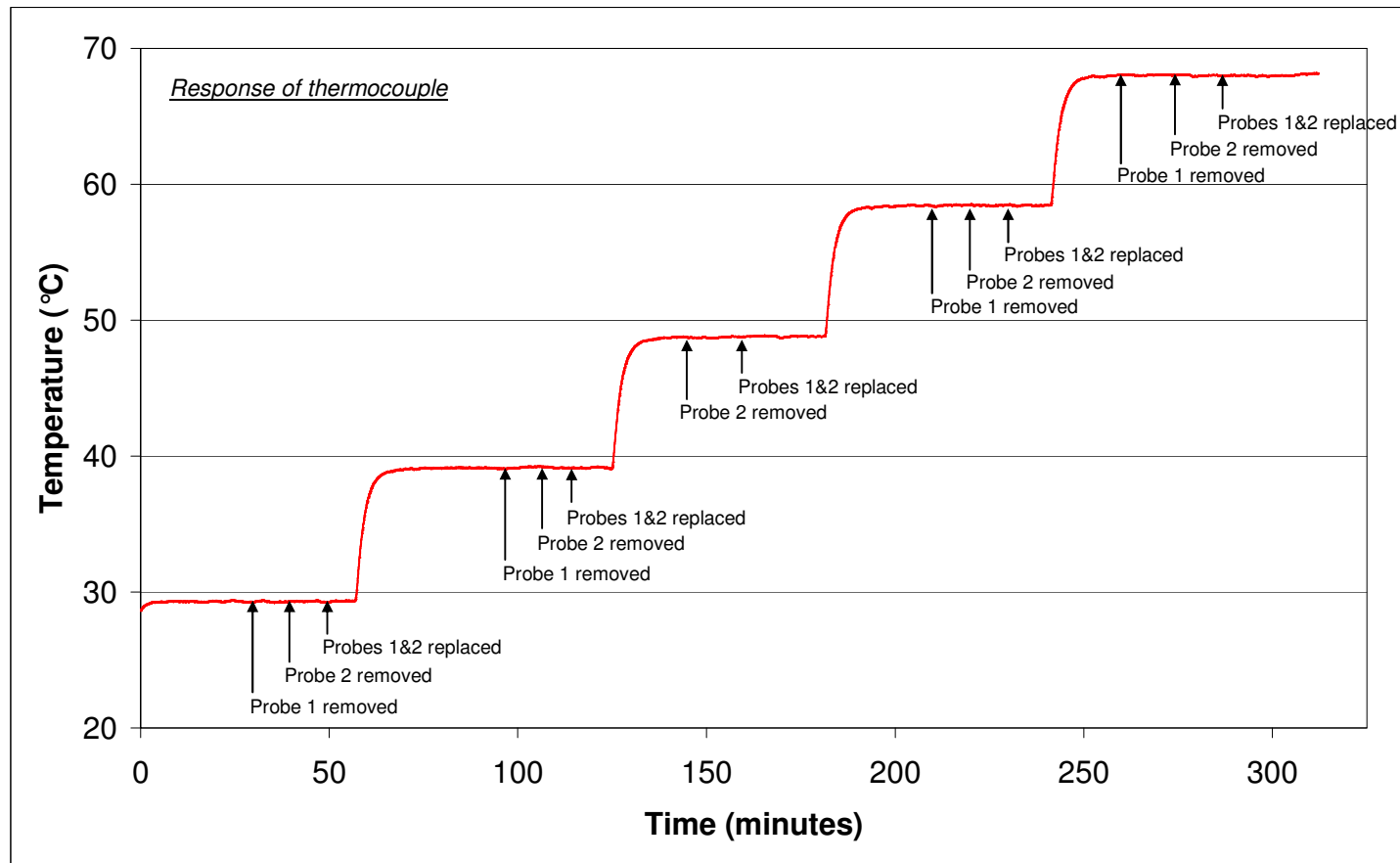
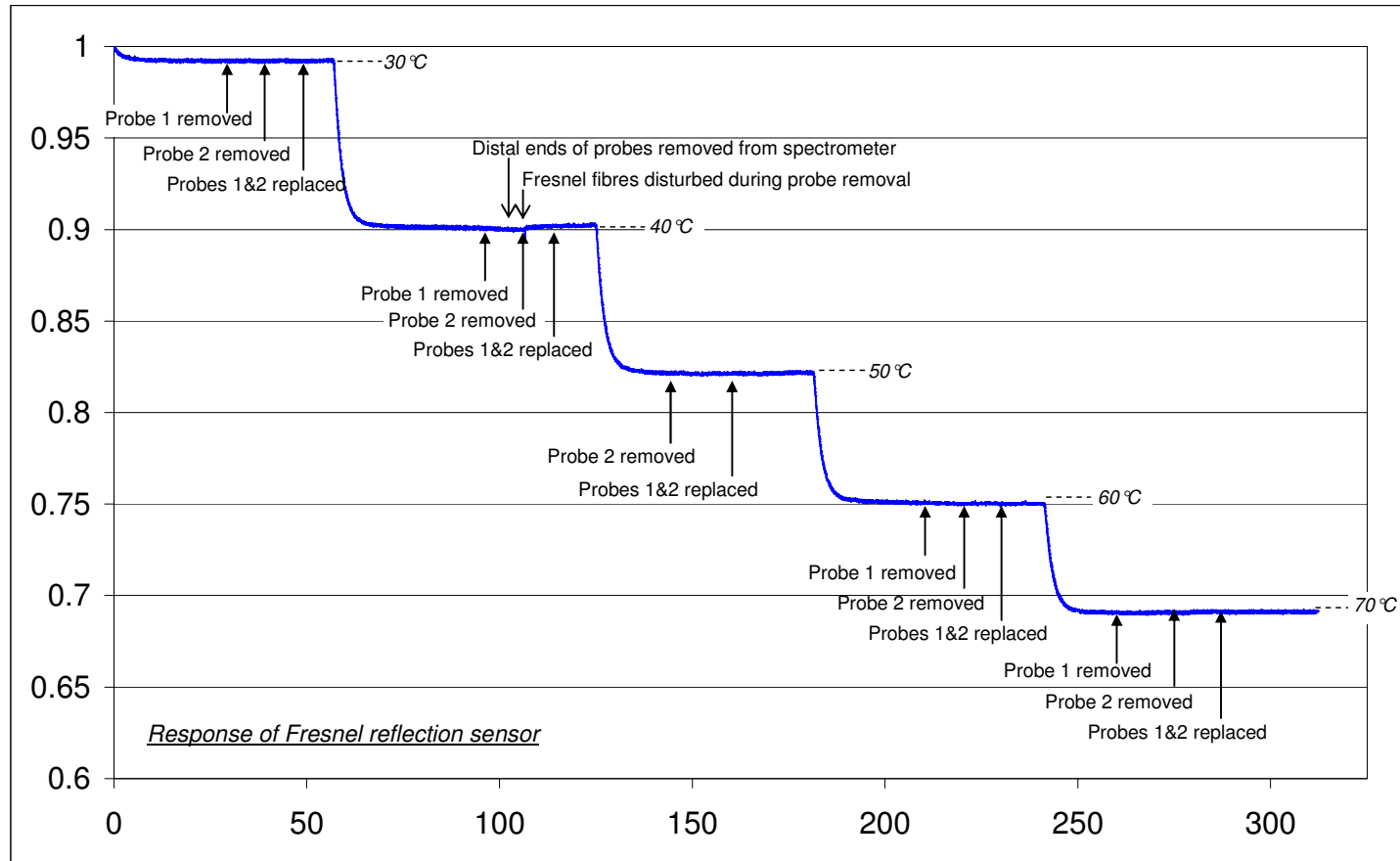


Figure AC-1. The response of the thermocouple during a temperature ramp-hold experiment whilst the fibre-optic probes of the cuvette holder were removed and replaced systematically.



**Figure AC-2. The response of the Fresnel reflection sensor during a temperature ramp-hold experiment whilst the fibre-optic probes of the cuvette holder were removed and replaced systematically.**

## **APPENDIX D**

### **INSPECTION OF CURED FRESNEL REFLECTION SAMPLES**

#### **PRODUCED BY PREVIOUS RESEARCHERS**

Previous researchers in the Group observed a “kink” in the Fresnel reflection data during the cure of the LY3505/XB3403 resin system. The cured samples which had been prepared by them were inspected in an attempt to deduce the cause of the discontinuity in the signal. Figure AD1-1 depicts schematic illustrations of four of the cured samples.

The sensor arrangement shown in Figure AD1-1 was reproduced by the author, but the kink was not observed.

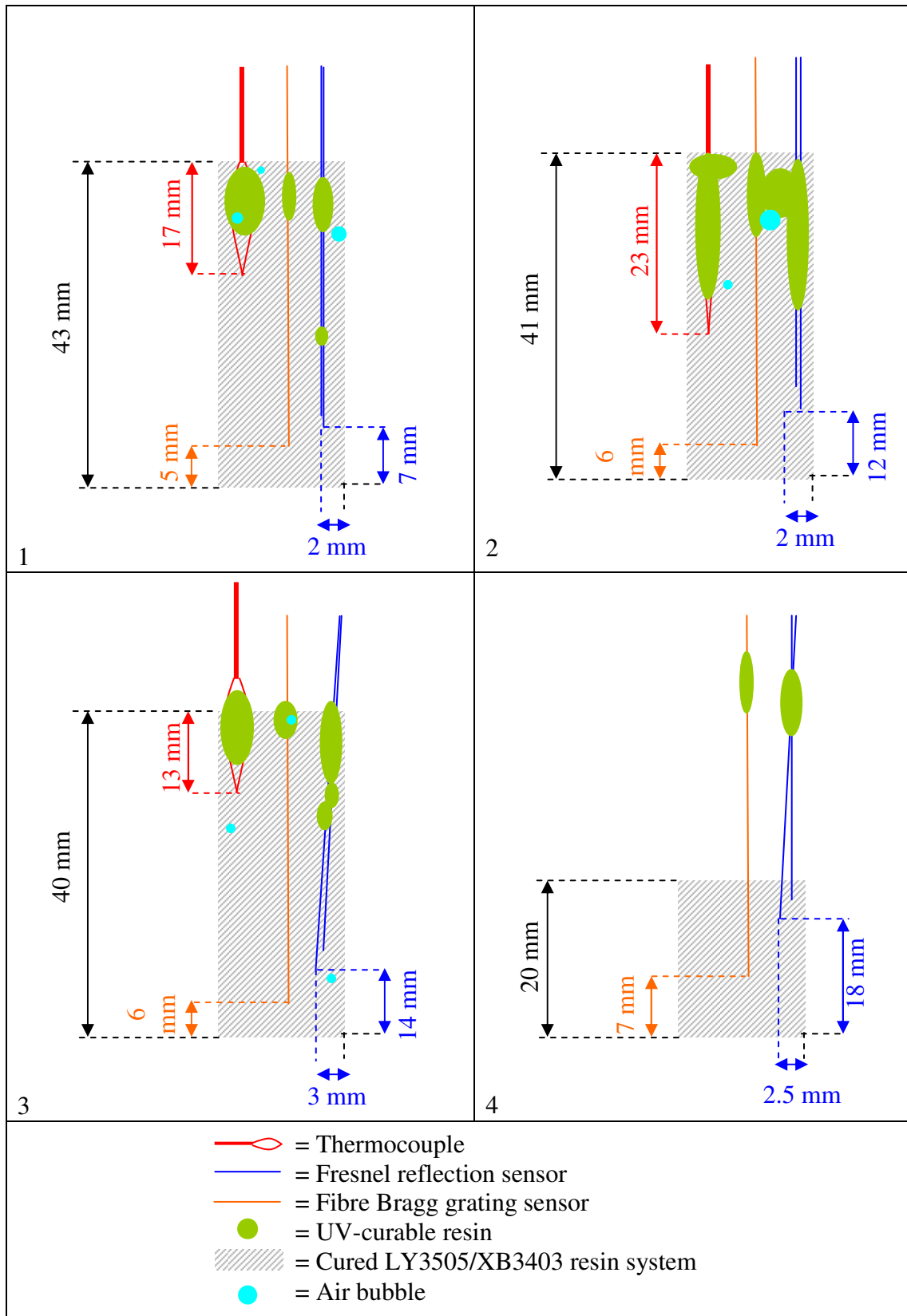


**Figure AD1-1. Schematic illustrations of the cured samples which were prepared by the previous researchers who observed kinks in the Fresnel reflection data during cure.**

## **APPENDIX E**

### **FIBRE-OPTIC TEMPERATURE SENSOR**

#### **AE1 Introduction**

The strong dependence of the refractive index on temperature was emphasised and demonstrated previously. Therefore, the option of modifying the Fresnel reflection sensor design to serve as a temperature sensor was undertaken.

#### **AE2 Experimental procedures**

A schematic illustration of the technique that was used to construct the temperature sensor is illustrated in Figure AE2-1a. In keeping with the low-cost philosophy adopted in this research programme, the temperature sensor was fabricated by holding a cleaved single-mode optical fibre vertically, and introducing a drop of NOA 68 photo-curable resin at the tip of the fibre. This assembly was lowered onto the glass slide such that the adhesive was brought into contact with the glass slide. Since the glass slide had been prepared with release agent, the adhesive did not wet or bond to it. The resin was cured using the UV75 light source from an angle above the slide for 120 seconds, and then de-mounted from the glass slide. The glass slide was used because it provided a simple method to create an “optically flat” surface, see Figure AE2-1b. The cleaved optical fibre with the cured adhesive was connected to the FBG Interrogation unit.

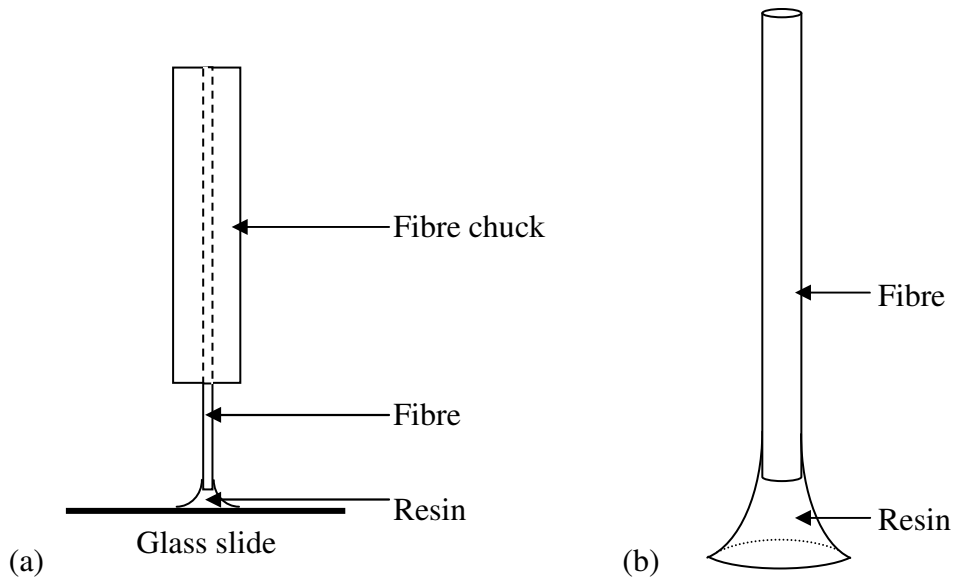


**Figure AE2-1. Schematic illustrations to show (a) the method used to fabricate the temperature sensor, and (b) the temperature sensor.**

### AE3 Results

The output spectra from the new temperature sensor design is shown in Figure AE3-1, where interference fringes with a high fringe visibility is apparent.

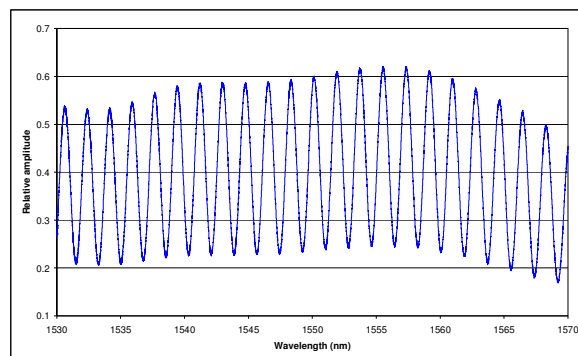


**Figure AE3-1. The output of the temperature sensor when connected to the FBG Interrogation unit.**

The interpretation of the interference fringes shown in Figure A3-1 is illustrated schematically in Figure AE3-2, alongside the temperature sensor, where “d” is the distance between the cleaved fibre end-face and the flat surface of the cured resin. When the fibre/cured resin assembly is subjected to a temperature rise, the two components will expand. Hence an increase in “d” can be computed using Equation AE3-1:

$$d = \frac{n\lambda_1\lambda_2}{2000(\Delta\lambda)} \mu m$$

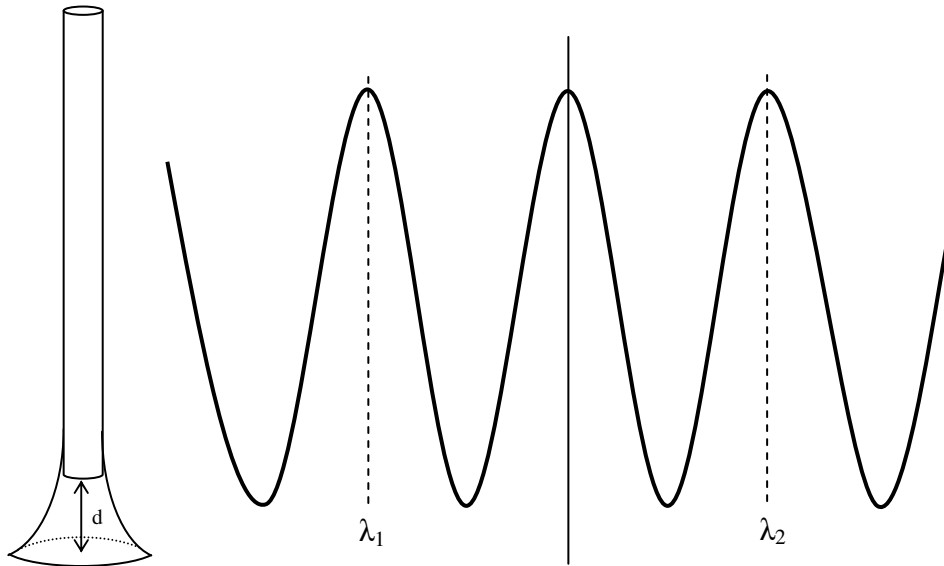


**Figure AE3-2. The temperature sensor, where “d” is the distance between the cleaved fibre end-face and the flat surface of the cured resin.**

The author carried out a brief study to manufacture this sensor by using a PTFE tube to contain the adhesive. After the resin was photo-cured, the PTFE tube was removed carefully. The intention was to insert this bonded resin rod into a capillary to isolate it from the surrounding fluid. However, due to time constraints, this was not pursued.

## **APPENDIX F**

### **MULTIPLEXED FRESNEL REFLECTION SENSORS**

#### **AF1 Introduction**

The versatility and simplicity of the Fresnel reflection sensor was discussed at length in the preceding sections of this thesis. In the context of processing composite preforms in industry, multi-point monitoring of the cross-linking reactions will be advantageous. This is because the structures tend to be large and with a variable cross-section and thickness. Therefore, the temperature profile or the heat-transfer may not be uniform. The availability of a cost-effective and disposable sensor system will enable multi-point sensing of the cross-linking reactions at specified locations within the preform.

#### **AF2 Experimental procedures**

The demonstration of multiplexing the Fresnel reflection sensor in this study was undertaken using reference silicone oil with a refractive index of 1.55. A glass cuvette (45 x 10 x 10 mm) was used to contain the oil, and the PTFE lid of the cuvette was drilled to accommodate a thermocouple and six optical fibres (see Figures AF2-1a and b).

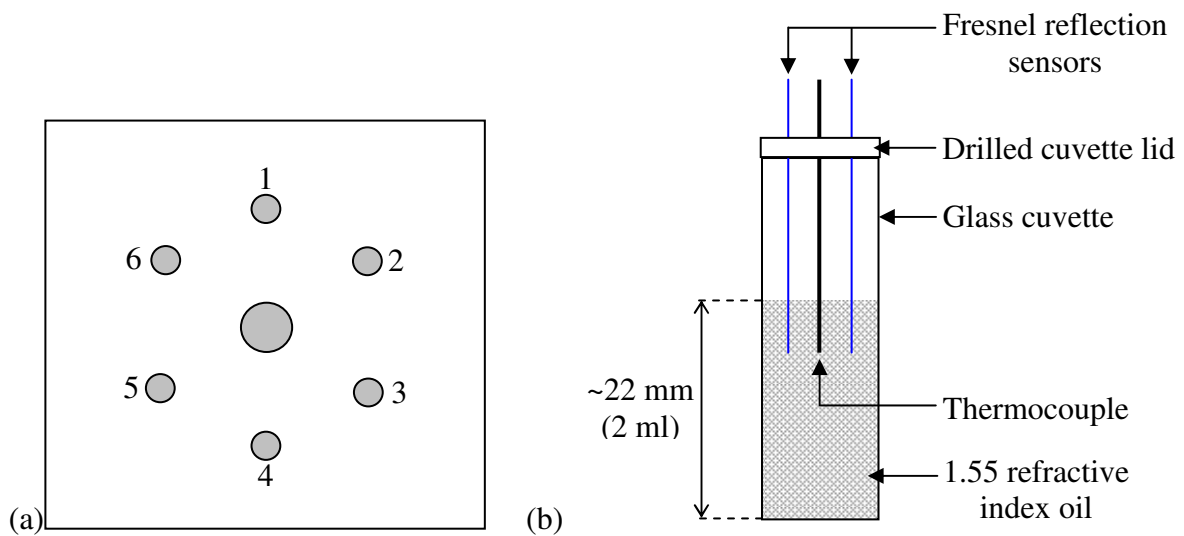


**Figure AF2-1. (a) The PTFE cuvette lid which was drilled to accommodate a thermocouple at the centre, surrounded by six optical fibres; (b) a side-view of the cuvette, where the fibres and thermocouple are secured to the PTFE lid.**

In this case, the reflections were measured using single-ended sensors, rather than the two distal fibres discussed in earlier chapters. The experimental configuration is illustrated in Figure AF2-2, where one distal fibre-end was immersed in refractive index-matching gel and the other was connected to a switcher unit. The incident light from this fibre is rotated between six channels. Six potted and polished fibres were connected to the channels of the switcher unit to receive the light, and the distal ends of these fibres were secured in the holes of the PTFE lid. There was a delay of approximately 8 seconds between each channel during switching.

The cuvette was placed in the temperature-regulated cuvette holder and subject to a series of temperature ramp-hold sequences between 30 and 70 °C in 10 °C increments.

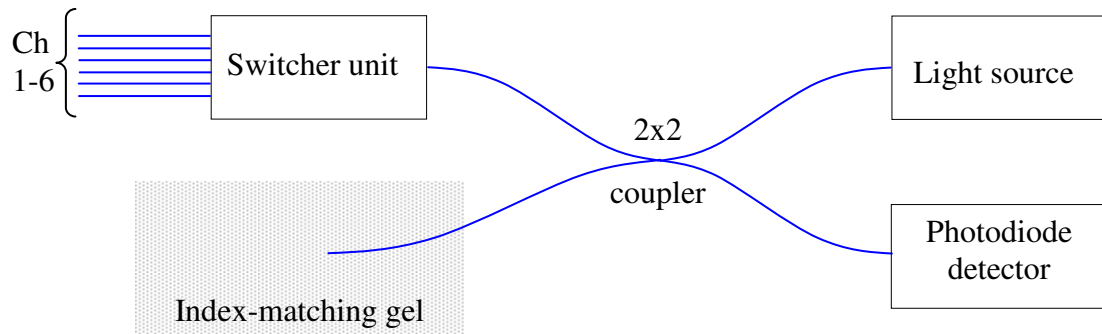


**Figure AF2-2. The arrangement of the multiplexed Fresnel reflection sensor configuration.**

### **AF3 Results and discussion**

Figure AF3-1 shows the output from the six independent Fresnel reflection sensors that were located within the cuvette. The data in Figure AF3-1 were normalised to the initial Fresnel signal at 0 minutes and 30 °C. A notable feature in Figure AF3-1 is that all six of the sensors show a similar trend with respect to ramp-hold cycles. It can be observed that for some of the sensors there is a small increase in the signal during the hold periods. At the time of writing, the reasons for this were unknown. However, this preliminary study has shown that it is possible for the Fresnel reflection sensor to be multiplexed.

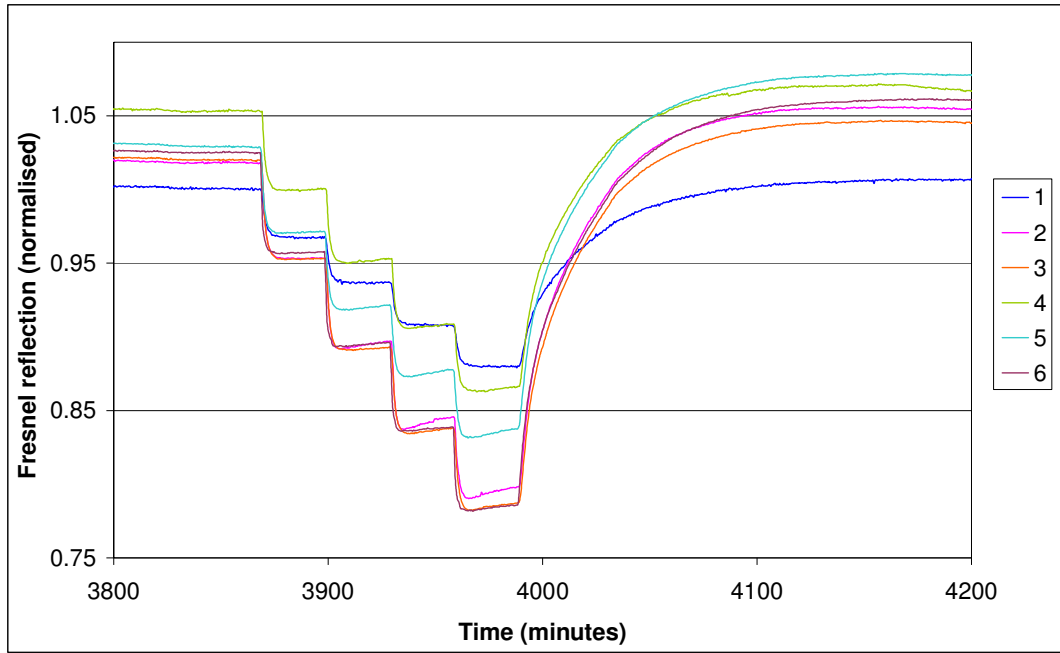


**Figure AF3-1. The response of the multiplexed Fresnel reflection sensors during a ramp-hold cycle.**